Oligonucleotide-based biosensors for the detection of prostate cancer biomarkers

Jolly, Pawan

Award date:
2016

Awarding institution:
University of Bath

Oligonucleotide-based biosensors for the detection of prostate cancer biomarkers

Pawan Jolly

A thesis submitted for the degree of Doctor of Philosophy

University of Bath

Department of Electronic and Electrical Engineering

April 2016

COPYRIGHT

Table of contents

Acknowledgements

During the course of writing this dissertation, I received so much help and advice from many people. My gratitude is beyond words. Any attempt to list the people and opportunities with which my life has been richly blessed would be futile. Yet among these stand some individuals whose profound impact deserves special acknowledgement.

I would like to thank Marie Curie Initial Training Network- PROSENSE for the funding. Following, with a deep sense of veneration and obligation, I avail this opportunity to express my thanks to Dr. Pedro Estrela and Prof. Chris. Frost for giving me the opportunity to undergo my Ph.D. at the University of Bath. I will always be indebted to the time I spent preparing my report under their supervision. They have given me sustained guidance, patience, and encouragement throughout my research. I would also like to thank Dr. Jan Tkac, Dr. Jaroslav Katrlik, Dr. Virginia Chu, Prof. Joao Pedro Conde, Dr. Chris Allender, Prof. Sven Ingebrandt, Dr. Matthew D. Lloyd, Dr. Paul Ko Ferrigno, Dr. Sandro Carrara from the PROSENSE network for all the collaborations and letting me spend time in their laboratory in their respective institutes to complete a part of my Ph.D. study. As Newton wrote, "if I see further, it is because I stand upon the shoulder of giants." This is what I feel when I think of my supervisors. With special regards to Dr. Pedro Estrela, for being my supervisor and supporting me in a friendly way every time I had a question.

I would like to extend my sincerest thanks to all the laboratory members from the University of Bath for their comprehensive and most instructive collaborations, discussions and support. I would also thank the PROSENSE team for all the good times, collaborations and healthy discussions. All my friends Dr. Anna Miodek, Nikhil Bhalla, Nello Formisano, Caleb Wong, Pavel Zhurauski, Dr. Ed Regan, Sunil Arya, Marina Batistuti, Joshua Rainbow, Pavel Damborsky, Dr. Narayanan Srinivasan, Vibha Tamboli for their constant support and shared moments.

Lastly, thanks to all the people who have helped me directly or indirectly for the day to day affairs. Words seem inadequate to express the immense contribution of my parents who have stood by me in all my endeavours, and have always encouraged me.

List of Publications

- **Jolly, P.,** Batistuti, M.R., Miodek, A., Zhurauski, P., Mulato, M., Lindsay, M.A., and Estrela, P., 2016. Highly sensitive dual mode electrochemical platform for MicroRNAs detection. Submitted to *Scientific Reports* (Nature Publishing Group).
- **Jolly, P.,** Miodek, A., Lloyd, M.D., Yang, D.K., Chen, L.C., and Estrela, P., 2016. Electro-engineered polymeric films for the development of sensitive aptasensors for prostate cancer marker detection. Submitted to *ACS Sensors*.
- Tamboli, V., Bhalla, N., **Jolly, P.,** Allender, C.J., & Bowen, J.L., and Estrela, P., 2016. Apta-MIP hybrid receptors on MOSFET devices for cancer biomarker detection in human serum. Submitted to *Analytical Chemistry*. **(Equal first author contribution)**
- Aliakbarinodehi, N., **Jolly, P.,** Bhalla, N., Miodek, A., Micheli, G.D., Estrela, P., and Carrara, S., 2016. Label free AptaFET biosensor for drug monitoring in human serum. Submitted to *Scientific Reports* (Nature Publishing Group).
- **Jolly, P.,** Zhurauski, P., Miodek, A., Liébana, S., Bertok, T., Drago, G-A., Tkac, J., and Estrela, P., 2016. Self-assembled aptamer modified redox activated gold nanoparticles for cancer biomarker detection. In preparation.
- Rani, D., **Jolly, P.,** Pachauri, V., Estrela, P., and Ingebrandt, S., 2016. A new Si NW FET array based aptasensor for electronic and optical detection for PSA. In preparation.
- Lu, X., Miodek, A., **Jolly, P.,** Pachauri, V., Estrela, P., and Ingebrandt, S., 2016. Reduced graphene-oxide thin-film transducers as in-line impedimetric biosensors. In preparation.
- Gaiji, H., **Jolly, P.,** Abderrabba, M., Estrella, P., and Frost, C., 2016. Investigation of ferrocene intercalator for PNA/DNA duplex. In preparation.
- Tzouvadaki, I., **Jolly, P.,** Lu, X., Ingebrandt, S., Estrela, P., Micheli, G.D., and Carrara, S., 2016. Label-free ultrasensitive memristive aptasensor. *Nano Letters*, 16 (7), 4472–4476. **(Equal first author contribution)**
- Formisano, N., Bhalla, N., Heeran, M., Martinez, J. R., Sarkar, A., Laabei, M., **Jolly, P.,** Bowen, C. R., Taylor, J. T., Flitsch, S. L., and Estrela, P., 2016. Inexpensive and fast pathogenic bacteria screening using field-effect transistors. *Biosensors and Bioelectronics*, 85, 103-109.

- **Jolly, P.,** Estrela, P., and Ladomery, M., 2016. Oligonucleotide-based Systems: DNA, MicroRNAs, DNA/RNA Aptamers, in "Biosensor Technologies for Detection of Biomolecules", *Essays in Biochemistry*, 60, 27-35.
- Bhalla, N., **Jolly, P.,** Formisano, N., and Estrela, P., 2016. Introduction to biosensors. *Essays in Biochemistry*, 60, 1-8.
- **Jolly, P.,** Damborsky, P., Madaboosi, N., Soares, R.R., Chu, V., Conde, J.P., Katrlik, J., and Estrela, P., 2016. DNA aptamer-based sandwich microfluidic assays for dual quantification and multi-glycan profiling of cancer biomarkers. *Biosensors and Bioelectronics*, 79, 313-319.
- **Jolly, P.,** Tamboli, V., Harniman, R.L., Estrela, P., Allender, C.J., and Bowen, J.L., 2016. Aptamer–MIP hybrid receptor for highly sensitive electrochemical detection of prostate specific antigen. *Biosensors and Bioelectronics*, 75, 188-195.
- **Jolly, P.,** Wong, L.C., Miodek, A., Lindsay, M.A., and Estrela, P., 2015, November. A simple and highly sensitive electrochemical platform for detection of MicroRNAs. SENSORS, *2015 IEEE* (1-4). IEEE.
- Formisano, N., **Jolly, P.,** Bhalla, N., Cromhout, M., Flanagan, S.P., Fogel, R., Limson, J.L., and Estrela, P., 2015. Optimisation of an electrochemical impedance spectroscopy aptasensor by exploiting quartz crystal microbalance with dissipation signals. *Sensors and Actuators B: Chemical*, 22-, 369-375
- **Jolly, P.,** Formisano, N., Tkáč, J., Kasák, P., Frost, C. G., and Estrela, P., 2015. Label-free impedimetric aptasensor with antifouling surface chemistry: A prostate specific antigen case study. *Sensors and Actuators B: Chemical*, 209, 306-312.
- **Jolly, P.,** Formisano, N., and Estrela, P., 2015. DNA aptamer-based detection of prostate cancer. *Chemical Papers*, 69(1), 77-89.
- Huck, C., **Jolly, P.,** Wagner, P., Poghossian, A., and Schöning, M.J., 2011. One-chip integrated dual amperometric/field-effect sensor for the detection of dissolved hydrogen. *Procedia Engineering*, 25, 1161-1164.

Research Grant

- **Jolly, P.,** Estrela, P., and Lindsey, M., 2015. An electrochemical biosensor platform for the sensitive detection of miRNAs specific for prostate cancer. *Seed Corn Funding* from Cancer Research at Bath (CR@B)

Abstract

The introduction of prostate-specific antigen (PSA) testing about 3 decades ago led to the possibility of early detection of prostate cancer (PCa). Although PSA testing reduced the mortality rate, it is also associated with high risk of over diagnosis in patients with and without PCa. Despite the current drawbacks, it would be a challenge to replace PSA testing entirely. Instead, there is a need to develop parallel testing of other potential biomarkers that can complement the results from PSA tests. To address alternative biomarker sensing, this thesis highlights on the development of oligonucleotide-based biosensors for the detection of different biomarkers of PCa.

Using PSA as a gold standard, the first study of this dissertation investigates the use of DNA aptamers to detect PSA using electrochemical impedance spectroscopy (EIS). The study compares 6-mercapto 1-hexanol chemistry with sulfo-betaine chemistry for the development of PSA aptasensor in terms of performance and selectivity. The second study focuses on glycoprofiling in order to complement PSA quantification as an additional information for reliable PCa diagnosis. This strategy was developed in a microfluidic channel with an optical read out using chemiluminescence. This study addresses one of the major problems of cross-reactivity with lectins in glycoprofiling, which can be solved using DNA aptamers. A third study concentrates on the development of an aptasensor for Alpha-Methylacyl-CoA Racemase (AMACR). AMACR has been reported for its high specificity and sensitivity to PCa. For the fabrication of the biosensor, a new strategy using polyethylene glycol was developed by electrochemical grafting it to a polypyrrole film. Since PCa diagnosis can be improved by looking at different biomarkers, an electrochemical platform for miRNA/DNA detection using a gold nanoparticle amplification strategy was also investigated. The sensor was fabricated using peptide nucleic acids (PNA) probes on gold electrodes. The study presents non-Faradaic EIS and amperometric techniques in order to exploit the inherent charges of nucleic acids.

In conclusion, this thesis wants to serve as a potential orientation for overcoming the shortcomings of the current PCa testing and contribute towards the development of oligonucleotide-based biosensors for PCa biomarker detection and hopefully enhance the diagnosis and prognosis of PCa.

Nomenclature

A	Area
c	Concentration
C	Capacitance
d	Distance
D	Diffusion constant
D_O	Diffusion coefficient
e	Electron charge
V	Electrode potential
$V^{0'}$	Formal potential
f	Frequency
F	Faraday constant
i	Current
I	Ionic strength
J	Flux
k	Rate constant
k_B	Boltzmann constant
K_d	Dissociation constant
n	Number of electrons transferred
N_A	Avogadro number
Q	Charge
R_{ct}	Charge transfer resistance
s_{bl}	Standard deviation of blank
S	Scan rate
t	Time
T	Temperature
V	Voltage
W	Warburg impedance element
x	Direction
Y_o	Magnitude of the CPE admittance at $\omega = 1\ rad/s$
z	Ion valence
Z	Impedance
α	Anodic transfer coefficient
Γ	Amount of species adsorbed
ε_0	Permittivity of free space
ε_r	Relative permittivity

η	Overpotential
θ	Phase
κ	Debye inverse length
λ	Conductance
λ_D	Debye length
σ	Surface charge
Φ	Electrostatic potential
ω	Angular frequency

List of abbreviations

ACT	alpha chymotrypsin
A2M	α2-microglobulin
AMACR	α-Methylacyl-CoA racemase
ANTA	Nα,Nα-Bis(carboxymethyl)-L-lysine hydrate
ANXA3	Annexin A3
ATR	Attenuated total reflection
A.U.	Arbiturary units
AuNP	Gold nanoparticle
BPH	Benign prostatic hyperplasia
BSA	Bovine Serum Albumin
Cav-1	Caveolin 1
CE	Counter electrode
CNT	Carbon nanotube
CPE	Constant phase element
CV	Cyclic voltammetry
Cy3	Cyanine 3
DL	Double layer
DNA	Deoxyribonucleic acid
DPV	Differential pulse voltammetry
DRE	Digital rectal examination
DWL	Direct write lithography
EDC	1-ethyl-3-(3-dimethylaminopropyl)carbodiimide
EIS	Electrochemical impedance spectroscopy
ELISA	Enzyme-linked immunosorbent assay
ELAA	Enzyme-linked aptamer assay
EN-2	Engrailed 2

EPCA	Early prostate cancer antigen
Fc	6-(ferrocenyl)hexanethiol
FET	Field effect transistor
fPSA	Free PSA
FRA	Frequency-response analyser
FT-IR	Fourier transform infrared spectroscopy
GCE	Glassy carbon electrode
GOPTS	3-Glycidyloxypropyl)trimethoxysilane
hK2	Human Kallikrein 2
HSA	Human serum albumin
IHP	Inner Helmholtz plane
LNA	Locked nucleic acid
LOD	Limit of detection
LOQ	Limit of quantitation
MAA	*Maackia amurensis*
MCH	6-mercapto-1-hexanol
miRNA	Micro RNA
MOSFET	Metal–oxide–semiconductor field-effect transistor
MS	Mass spectrometry
MUA	11-Mercaptoundecanoic acid
OCP	Open circuit potential
OHP	Outer Helmholtz plane
PBS	Phosphate buffer saline
PCa	Prostate Cancer
PDMS	Polydimethylsiloxane
PEG	Polyethylene-glycol
PEI	Poly-(ethylenimine)
phi	Prostate health index
PL	Photoluminescence
PNA	Peptide nucleic acid
PoC	Point of Care
PPy	Polypyrrole
PSA	Prostate specific antigen
PSGR	Prostate specific G protein coupled receptor
PSMA	Prostate specific membrane antigen
QCM	Quartz crystal microbalance
QCM-D	Quartz crystal microbalance with dissipation mode

RE	Reference electrode
RIU	Refractive index unit
RMS	Root mean square
RT-PCR	Reverse transcription polymerase chain reaction
SAM	Self assembled monolayer
SELEX	Systematic evolution of ligands by exponential enrichment
SEM	Scanning electron microscopy
SiNW FET	Silicon nanowire field effect transistors
SNA	*Sambucus nigra*
SPR	Surface plasmon resonance
Sulfo-NHS	Sulfo-N-Hydroxysulfosuccinimide
SWV	Square wave voltammetry
TNA	Therose nucleic acid
tPSA	Total PSA
TRUS	Transrectal ultrasound
USPSTF	US preventative services task force
UTR	Untranslated region
WE	Working electrode

Chapter 1. Introduction

The work in this thesis aims at developing oligonucleotide-based biosensors for the detection of different biomarkers for prostate cancer (PCa). In order to fabricate such a biosensor, it is imperative to understand the prostate and the physiological processes associated with it in patients with PCa. This Chapter will describe PCa, its current diagnosis status, and the potential PCa biomarkers. It will also introduce electrochemical biosensors and oligonucleotide-based recognition layers which have been used as the foundation for different types of biosensors mentioned in this thesis.

Part of the work presented in thesis is published in Jolly *et al*. (Jolly *et al.* 2015a).

1.1 Prostate cancer

Cancer is a disease state developed due to an error in the cell division cycle leading to abnormal cell growth. There are many factors that can cause this un-programmed cell death such as carcinogens, genetic factors, and environmental factors. These factors introduce mutations in the genes (p53) which are responsible for programmed cell death (Lilja *et al*. 1987). PCa is a type of cancer associated with the prostate gland. The prostate gland is a male reproductive organ that weighs between 7 to 16 grams depending on the person (Leissner and Tisell 1979). It is located just below the bladder and surrounds the urethra which carries urine from the bladder to the penis (Figure 1.1).

Its primary function is to produce fluid that forms the part of semen (Lilja *et al.* 1987). The prostate gland squeezes this fluid which combines with the sperm into the urethra

during ejaculation. The fluid produced by the prostate functions by nourishing and protecting the sperms. Since the prostate is well connected to numerous lymph nodes, it is easier for the cancer cells to escape from its primary site of origin into the lymph nodes. From lymph nodes, the cancerous cells enter the blood vessels and migrate to secondary sites making the spread of PCa very easy. Some of the most common sites of PCa metastatic process are found in bones (Chou and Simons 1997).

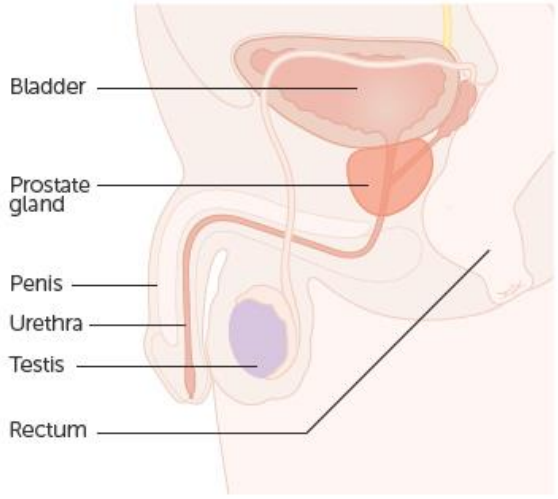

Figure 1.1 Prostate gland. Source internet: Cancer Research UK.

1.1.1 Current status and detection techniques

PCa often develops very slowly and the lack of symptoms during the early stages of the disease leads to a late diagnosis of the tumour. Moreover, the current detection techniques used in central labs are also surrounded by controversies of being reliable. Like any other cancer, if PCa is diagnosed in a late stage, no effective treatments can be provided, which leads to patients death. It is due to such reasons that PCa is considered as the leading cause of cancer-related mortality among men worldwide (Greenlee *et al.* 2000; Jolly *et al.* 2015a). PCa accounts for around 7% of all cancer-related deaths making it the 4th most common cause of cancer-related death in the UK (2011). It has also been reported that one man deceases from PCa every one hour making it more than 10,000 every year. It has been also projected that PCa will be the most common cancer by 2030 (Jolly *et al.* 2015a; Cancer Research UK (2012)).

There has been a steady increase in the number of cases diagnosed all over in the UK from 1993 to 2010. This increase could be a result of the adoption of prostate specific antigen (PSA) testing in men during the same period. Over 41,000 cases were diagnosed in the UK (2010), of which 85% were from England. It has also been reported that PCa is predominant in older men above the age of 50 (Kirk *et al.* 1997; Hoffman *et al.* 2011). Looking at the trend of mortality statistics, there is a significant need for better diagnostic tools to facilitate early and accurate diagnosis of PCa.

Currently, there is not a self-reliant detection technique to diagnose PCa. However, there are three techniques which are most commonly practiced worldwide . One of these methods is called digital rectal examination (DRE), where the doctor examines the irregularities in terms of bumps of the prostate gland by inserting a sterilised gloved finger through the rectum (Carvalhal *et al.* 1999). The second technique is the transrectal ultrasound (TRUS) and involves an ultrasound probe being inserted into the rectum to image the prostate gland, in order to examine the pathology of the tumour. TRUS is also used for biopsy by gliding a needle for sampling tissues (Hara *et al.* 2008). However, the most common test for PCa screening is a blood test where the altered levels of PSA are measured (Walter *et al.* 2006). If the levels of PSA exceeds 4 ng/mL, biopsy procedures may be considered (Catalona *et al.* 1991). All these tests have advantages and disadvantages which make them controversial in nature. For instance, DRE test is just 59% accurate in diagnosing PCa, which could be further increased when combined with biopsy and PSA tests (Basler and Thompson 1998, Uzzo *et al.* 1995). In the case of biopsy, many samples are required which is quite painful for the patients and could result in a higher risk of critical infections (Loeb *et al.* 2013). Also, PSA levels might be increased due to other factors or conditions such as benign prostatic hyperplasia (BPH) and prostatitis. For such reasons patients with PCa either escape early diagnosis or have a late diagnosis, both adding to the mortality rate (Carter *et al.* 1992). In October 2011, the US Preventative Services Task Force (USPSTF) recommended against PSA screening in all men (Brett and Ablin 2011). This emphasized the need for superior biomarkers for the diagnosis of PCa.

1.1.2 Candidate biomarkers for PCa

The shortcomings of current detection techniques put a significant need on developing a more definitive technique for PCa detection. Presently, a dynamic area of importance involves non-invasive or minimally invasive techniques to detect PCa. Researchers are looking into potential biomarkers that could detect PCa at an early stage with high sensitivity and reliability. According to the National Institutes of Health Biomarkers Definitions Working Group, a biomarker is "a characteristic that is objectively measured and evaluated as an indicator of normal biological processes, or pharmacologic responses to a therapeutic intervention"(Colburn *et al.* 2001). Table 1.1 lists some of the candidate biomarkers for PCa that have the potential and are clinically persuasive for further investigation to be developed as a potential biomarker for diagnostics or prognostics. The list is quite exhaustive, however, this thesis will focus mainly on four biomarkers (PSA, glycosylation pattern of PSA, AMACR and miRNA) based on their importance and feasibility to be detected using oligonucleotide-based approaches.

1.1.2.1 Prostate specific antigen

In the year 1971, the most important PCa biomarker, prostate specific antigen (PSA) was discovered, becoming the foundation and gold standard of PCa detection and monitoring (Balk *et al.* 2003; Hara *et al.* 1971). PSA belongs to the family of kallikrein proteins which are from a class of serine proteases. There are about 15 kallikrein proteins with PSA (hK3) being the only kallikrein specific to prostate (Balk *et al.* 2003).

PSA is synthesised as a 244 amino acid long protein and is called pro-PSA; it serves as an inactive form of PSA and has no enzymatic activity (Figure 1.2). Human Kallikrein 2 (hK2) enzyme cleaves the pro-PSA in the prostate from the N terminus resulting in active PSA which is 237 amino acids long (Takayama *et al.* 1997). The active PSA which is a 30 KDa protein is found in both semen and serum of men.

Table 1.1 List of potential biomarkers for PCa

Biomarker	Source	Description	Differentiates BHP from PCa	Reference
Prostate specific antigen (PSA)	Serum/ Urine	A Kallikrein protease, 30 KDa which proteolysis semenogelin proteins of seminal fluids. Undergoes glycosylation. Sensitivity: 24%, Specificity: 93%; Cut off level: 4 ng/ml in serum	No	Catalona *et al.* 1991; Thompson *et al.* 2004; Özen and Sözen 2006; Gilgunn et al. 2013b
α-Methylacyl-CoA racemase (AMACR)	Serum/ Urine/ Tissue	Racemase enzyme involved in stereo-isomerization, bile acid synthesis and β oxidation of branched fatty acids. Sensitivity: 97%, Specificity: 92%	yes	Jiang *et al.* 2004b; Sreekumar *et al.* 2004; Rogers *et al.* 2004
Prostate Specific Membrane Antigen (PSMA)	Serum/ Tissue/ circulating PCa cells	Type II Integral membrane protein with cell surface carboxy-peptidase function. It translocate to plasma membrane in PCa cells while, remain in the cytosol in normal prostate cells.	Yes	Hara *et al.* 1971; Madu and Lu 2010
Human Kallikrein 2 (hK2)	Serum	Kallikrein protein with trypsin like activity. It cleaves pro-PSA to active PSA and truncated forms of PSA.	Yes (if combined with %fPSA)	Diamandis and Yousef 2002; Rittenhouse *et al.* 1998
Early Prostate Cancer Antigen (EPCA)	Serum	Nuclear matrix protein linked to PCa development. Sensitivity: 92%, Specificity: 94%	Yes	Madu and Lu 2010; Paul *et al.* 2005
Caveolin-1 (Cav-1)	Serum	Integral membrane protein with structural/regulatory function.	Yes	Madu and Lu 2010; Tahir *et al.* 2008
Engrailed-2 (EN-2)	Urine	A transcription factor which has regulatory functions. Sensitivity: 66% Specificity: 88.2%, Cur off level: 42.5 ng/ml	Yes	Morgan *et al.* 2011; Pandha *et al.* 2012
prostate-specific G-protein-coupled receptor (PSGR)	Tissue	An olfactory receptor which has been reported to be highly expressed in prostate epithelial cells. An increased expression has been reported in PCa patients		Xu *et al.* 2006; Launay *et al.* 2012
Annexin A3 (ANXA3)	Urine	A calcium binding protein involved in broad range of cellular and molecular processes. It has decreased levels in PCa patients. Sensitivity: 50% Specificity: 90%	Yes	Schostak *et al.* 2009; Liu *et al.* 2009; Roobol *et al.* 2011
Circulating Micro RNAs (miRNAs)	Serum/ Tissue/ Urine	Small (22 nucleotides) non-coding RNAs involved in regulation of expression of proteins. It acts like fingerprints to tumour formation and metastasis. These are either upregulated or downregulated in a particular disease.	Yes	Yeh *et al.* 2008; Catto *et al.* 2011; Ilic *et al.* 2013

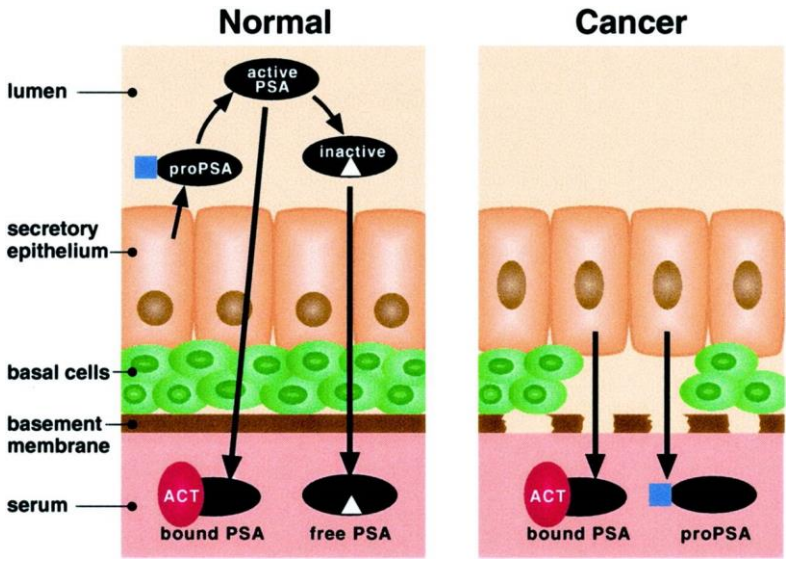

Figure 1.2 Model of PSA biosynthesis in normal and cancer prostate gland (Balk et al. 2003).

The physiological role of PSA, which is present in the range of 0.5 – 2 mg/mL in semen, is to de-coagulate semen by breaking down the proteins semenogelin I and II (Lilja *et al.* 1987; Lövgren *et al*. 1999).

In semen, about 30% of PSA is enzymatically active, while only 5% of PSA is complexed to protein inhibitors. The remaining PSA is made inactive by internal cleavages catalysed by hK proteases. Some of the active PSA escapes into the blood stream where it is rapidly inactivated by protein inhibitors such as alpha chymotrypsin (ACT) and α2-microglobulin (A2M) (Hara *et al.* 1971). However, in PCa, both active PSA and pro-PSA escapes into the blood due to rupture of the basal membrane of the prostate. Internally cleaved forms of PSA (with no enzymatic activity) also enter the blood stream and remain un-complexed and are taken into free PSA (fPSA) count. fPSA together with complexed PSA is termed as total PSA (tPSA) (Takayama *et al.* 1997).

With the introduction of PSA testing, which is more accepted than DRE, there has been an increase in the early detection of PCa (Balducci *et al.* 1997). Although PSA testing reduced the mortality rate, it is still associated with high risk of over-diagnosis in patients without PCa (Andriole *et al.* 2009). For instance, if PSA levels are higher

than the cut-off levels, biopsy procedures are considered (Catalona *et al.* 1991). However, the levels of PSA in blood in ageing men can also be raised due to other factors like benign prostatic hyperplasia (BPH) and prostatitis leading to over diagnosis in men (Carter *et al.* 1992). Due to faulty diagnosis, patients undergo biopsy surgery which is painful and also makes patients vulnerable to severe infections. Such controversies led to refinements in PSA testing. One of the methods to uncover the reason behind the high PSA levels was to quantify independently fPSA and tPSA. Lower levels of fPSA have been reported in patients with PCa compared to patients with BPH making it a potential indicator of the aggressiveness of the cancer (Christensson *et al.* 1993). However, the amount of fPSA might be higher in patients with larger prostate volume, making this method unreliable (Catalona *et al.* 1998). Nonetheless, the combined results of ratio of fPSA to tPSA with tPSA increased the confidence of the diagnosis (Velonas *et al.* 2013). Some other refinements include measurement of immunologically detectable forms of PSA on an equimolar basis (the equimolar tPSA assay) in order to avoid preferential detection of fPSA (Wians *et al.* 2002), and the prostate health index (phi) which can be calculated from a combination of tPSA, fPSA and truncated forms of PSA (Filella and Giménez 2013). Such assay refinements have driven the PSA tests, especially in the 'gray zone' (4-10 ng/mL), to somewhat more effective PCa diagnosis and treatment.

1.1.2.2 Glycosylation

Rapid and robust screening of biomarkers for diagnostic purposes has also led to the investigation of glycosylation patterns on protein biomarkers. In order to understand the phenomenon of glycosylation, it is important to first define the glycome. Glycome represents the complete set of sugar chains (glycans and glycan conjugates) that are synthesised by a cell under specific conditions. Glycomics is a study of glycomes (Varki *et al.* 2009) while, glycosylation is a phenomenon where carbohydrate moieties are covalently attached to proteins, lipids, ceramide, etc. This phenomenon is one of the most abundant and structurally diverse post-translational modifications of proteins occurring in the human body (An *et al.* 2009). It is involved in numerous physiological regulatory processes including protein folding (Shental-Bechor and Levy 2009), cell-

cell or cell-matrix interactions (Rudd *et al.* 1999) and the immune response (Rudd *et al.* 2001). Such modifications can dramatically change due to alterations in the cellular environment. Due to such reasons, glycosylation is associated with pathological states of many diseases such as cancer (Christiansen *et al.* 2014; Gilgunn *et al.* 2013), AIDS (Go *et al.* 2011), rheumatoid arthritis (Axford 1999), neurodegenerative diseases (Hwang *et al.* 2010) and autoimmune disorders (Goulabchand *et al.* 2014). Since glycosylation is a hallmark of disease states, altered glyco-forms may serve as viable candidate biomarkers for early-stage cancer diagnosis (Christiansen *et al*. 2014; Gilgunn *et al*. 2013). The entire process of alterations in glycan structures usually arise from disturbances in the expression and activity levels of various enzymes including glycotransferases and glycosidases resulting in protein structural modifications associated with cell-specific glycan expression patterns (Bosques *et al.* 2006; Kuzmanov *et al.* 2013). Although the molecular sub-forms of PSA have enabled better utility of PSA testing for PCa detection; but, it still lacks the specificity to differentiate between indolent and aggressive cancer. On the other hand, altered glyco-forms might serve as applicable candidate biomarkers for early-stage PCa diagnosis and improve the specificity of existing PCa biomarkers (Adamczyk *et al.* 2011; Pihíková *et al.* 2015).

PSA is a glycoprotein with various glycoforms. Thus, the determination of cancer-associated glycoforms of PSA may help to improve early-stage clinical diagnosis of PCa (Meany and Chan 2011). There are plenty of studies showing that altered glycosylation patterns allow the possibility of distinguishing patients with PCa from those with BPH. For example, the differential binding of PSA in serum to *Maackia amurensis* lectin (MAA). MAA is a lectin that recognises terminal α-2,3 sialylation, and binds at a greater concentration to PSA in men with PCa (Ohyama *et al.* 2004). The *Sambucus nigra* lectin (SNA) detects α-2,6-linked sialic, commonly present in healthy men (Saldova *et al.* 2011). Furthermore, glycoproteins constitute the majority of FDA-approved cancer markers and glycosylation patterns are now being widely accepted as characteristics of various cancers (Meany and Chan 2011). The measurement of such cancer-related glycans of PSA has already been demonstrated to improve the specificity of PSA (Peracaula *et al.* 2003).

1.1.2.3 α-methylacyl coenzyme A racemase (P504S)

Advancements in molecular biological techniques have helped researchers worldwide to investigate and discover novel biomarkers for numerous diseases including PCa. One of the discoveries that hold great promise is α-methylacyl CoA racemase (AMACR), also known as P504S which is an enzyme consisting of 382 amino acids. AMACR belongs to the family of racemases and epimerases involved in the synthesis and oxidative metabolism of branched-chain fatty acids. AMACR catalyses the reaction where (2R)-methylacyl-CoA esters are converted to their (2S)-methylacyl-CoA epimers (Jiang *et al.* 2004a; Lloyd *et al.* 2008). Studies have shown high expression levels of the AMACR gene at the mRNA and protein levels in PCa, making it a potential candidate biomarker with high specificity for diagnosis (Jiang *et al.* 2002; Jiang *et al.* 2004b; Rubin *et al.* 2002). Furthermore, immune-histochemical staining studies have demonstrated that AMACR can distinguish benign prostate tissue from cancerous prostate tissue with a diagnostic sensitivity of 97% and specificity of 92% (Jiang *et al.* 2004b). Such findings have encouraged many researchers to investigate if AMACR is also present in body fluids. Rogers *et al.* in 2004 detected AMACR in urine samples using Western blot analysis (Rogers *et al.* 2004). More recently, Zehentner *et al.* in 2012 detected the presence of AMACR transcripts in blood and urine samples using real-time reverse transcription polymerase chain reaction (RT-PCR) (Zehentner *et al.* 2006).

Although AMACR is highly sensitive to detect PCa, it also comes with some limitations. For example, in certain other cancers in patients suffering from autoimmune disorders, there is a possibility of production of endogenous AMACR antibody and humoral response (Tricoli *et al.* 2004). Nevertheless, the diagnostic efficiency for characterizing PCa stages was increased by combining the AMACR test with PSA testing (Cardillo *et al.* 2005).

1.1.2.4 MicroRNAs

The progression of PCa also has an impact on the expression levels of microRNAs (miRNAs). miRNAs are small (~22 nucleotides) non-coding RNAs that are involved in gene regulation. miRNAs bind to their complementary sequences in the 3'-untranslated region (UTR) of target RNAs and regulate the gene expression (Bartel 2004). miRNAs play a crucial role in regulating various metabolic and biological processes including oncogene processes (Meister 2007). The levels of these miRNAs are affected during a disease state such as cancer (Mitchell *et al.* 2008). miRNAs can be potentially detected in body fluids such as serum, plasma, circulating cancer cells and therefore makes them a potential diagnostic biomarker (Kuner *et al.* 2013). Consequently, abnormal levels of some miRNAs have been suggested to act like fingerprints for prostate tumorigenesis (Brase *et al.* 2010). miRNAs have therefore become an emerging field for their role in both diagnostics and therapeutics (Bader *et al.* 2011). There are several miRNAs which have been reported to be linked with PCa (Gordanpour *et al.* 2012). For instance, miR-21 which is upregulated in different tumours including cancer might enhance the processes of metastasis (White *et al.* 2011). On the contrary, miR-16-1 and miR-15a which are involved in controlling cell proliferation and transformation are downregulated in PCa (Bonci *et al.* 2008). In 2013, Larne *et al.* reported a miRNA index quote (miQ); ((miR-96-5p × miR-183-5p)/(miR-145-5p × miR221-5p)) which is a ratio of four distinct miRNAs with increased discrimination of PCa (Larne *et al.* 2013). It is worth mentioning that not a single miRNA has been successfully validated as a biomarker and therefore detection of a panel of miRNAs is needed in order to provide some valuable data to help diagnosis of PCa. Recently, several studies demonstrated the tumour-suppression characteristic of mir145 which is down-regulated in many cancers like colon cancer, ovarian cancer, breast cancer, bladder cancer and PCa (Akao *et al.* 2007; Ichimi *et al.* 2009; Nam *et al.* 2008; Spizzo *et al.* 2010; Wang *et al.* 2015). We used mir145 as an example of a target sequence to construct an electrochemical platform which will be described in Chapter 6.

1.2 Electrochemical biosensor

Analytical tools have widely exploited biomarkers to investigate biological parameters for therapeutics. Such an investigation has further extended the development of new therapies (Rolan 1997). In recent years, there is an unprecedented demand on the healthcare sector for early and reliable detection of biomarkers. One of the most promising technologies to face this challenge is a biosensor.

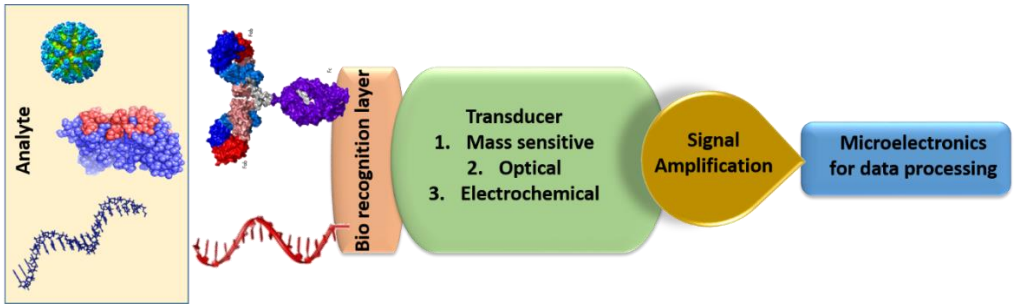

Figure 1.3 Schematic of a biosensor. Typically, a recognition layer is coated on a transducer. When a specific analyte is captured by the recognition system, a change in the properties of the recognition layer occurs. The transducer transforms the change because of the binding event into an electrical signal which is in turn amplified and processed into a readable signal by the output device.

A biosensor is an analytical device that can be used for detection of an analyte (pollutant, viral DNA, antigen or protein), by combining a biological component (e.g. enzyme, DNA, antibody, aptamer) that acts as a probe and binds to the target. Such a binding event gives rise to a signal which is detected by a transducer (mass sensitive (Janshoff *et al.* 2000), optical (Haes and Van Duyne 2002) or electrochemical (Cass *et al.* 1984)). The transducer signal is then converted into an electrical signal which is amplified and converted into an output easily read by a user (Figure 1.3) (Lowe 1984).

Biosensors are nowadays ubiquitous in biomedical diagnosis as well as a wide range of other areas such as point-of-care (PoC) monitoring of treatment and disease progression, environmental monitoring, food control, drug discovery, forensics and biomedical research. A wide range of techniques can be used for the development of biosensors. Their coupling with high-affinity biomolecules allows the sensitive and selective detection of a range of analytes. Biosensors are not only characterised by

their specificity and selectivity towards their targets, but also by important parameters such as dynamic and linear range of detection, limit of detection and sensitivity (Figure 1.4) (Jaffrezic-Renault 2013). The dynamic range is defined as the range of concentrations of analyte where a variation of the signal is observed. This range is also characterised by a linear part. The slope of the curve plotted in the linear range corresponds to the sensitivity of the biosensor. The lower value measured corresponds to the limit of quantification (LOQ) and by extrapolation of this curve the detection limit (LOD) can be calculated according to various methods described in analytical techniques. The most commonly used method in biosensors devices takes into account signal to noise ratio, where LOD is obtained by the equation:

$$LOD = \frac{\alpha_0 + 3s_{bl}}{\alpha_1} \quad (1.1)$$

Where s_{bl} is the standard deviation of blank, α_o is the measurement obtained with blank test and α_1 is the sensitivity obtained by the slope of the linear part of the calibration curve.

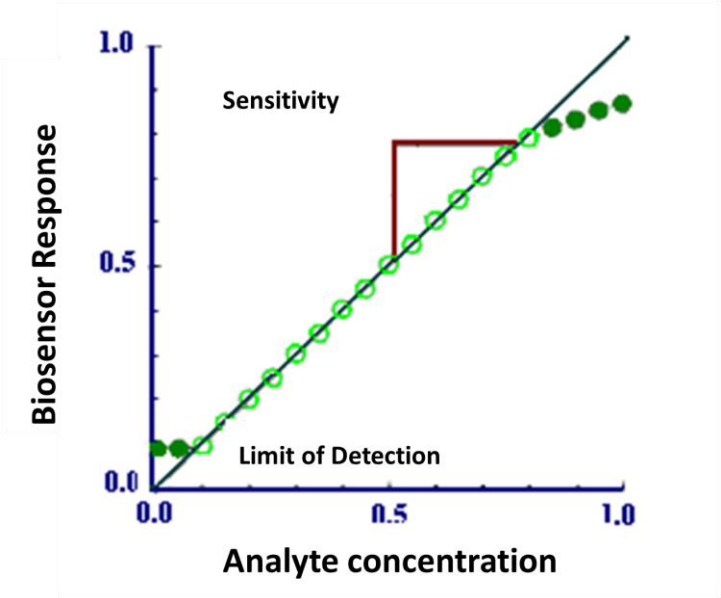

Figure 1.4 Presentation of parameters which characterize biosensors.

An electrochemical biosensor is a type of biosensor that involves an electrode surface functionalised with a bio-recognition element exploiting a physical/chemical process.

Most electrochemical setups typically consist of a cell with a three electrode configuration: a working electrode (WE), reference electrode (RE) and a counter electrode (CE) placed in an electrochemical solution. Potentials are set between the WE and the RE, while the current is measured between the WE and the CE (Figure 1.5). In measurements involving for example in Amperometric, the CE helps to maintain a stable voltage between the WE and the RE. Such a setup minimises the workload of RE. As a result, such a configuration allows the establishment of the potential of the WE against a known RE without compromising RE stability by passing a current through it (Wang 2006).

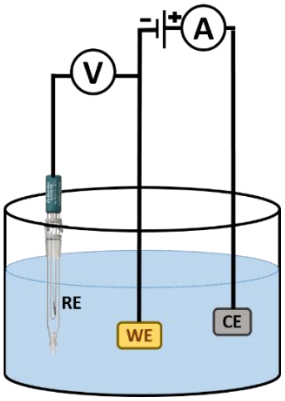

Figure 1.5 Electrochemical cell with three electrode configuration.

In order to monitor a measurable signal of the recognition event occurring on the interface of a WE, redox marker molecules can be used. Redox markers are indicators which can undergo a redox reaction. A redox process is a chemical reaction (reduction and oxidation), where molecules with redox activity are capable of exchanging electrons with the WE and as a result, a measurable current can be detected.

The signal that is gathered at the WE consists of two phenomena, namely electron transfer and mass transfer. In a solution, mass transfer is explained by the movement of the redox molecules towards the electrode surface from the bulk electrolyte solution. Mass transfer follows the theory of diffusion which is a phenomenon that involves the movement of mass down a concentration gradient. Once the redox marker molecule comes close to the electrode surface within the nanometer (nm) scale, the

next phenomenon predominates, which is electron transfer. The consequence of electron transfer results in detection of a measurable current. The region where the electron transfer takes place is called a double layer (DL, also called an electrical double layer) region.

Binding of analyte to the recognition element results in an electrical change which can be measured in the form of current transfer (amperometric, chronocoulometric), voltage (potentiometric and field effect transistors), impedance (impedimetric), conductivity (conductometric) or ion charge across the electrode (Thévenot *et al*. 2001).

The scope of this thesis with respect to detection techniques is limited to impedimetric and amperometric. These techniques will be described in detail in Chapter 2 along with other characterisation techniques used.

1.3 Oligonucleotide-based recognition layer

Over the last few decades, there is an increasing number of applications that have been developed for oligonucleotide-based biosensing systems in genetics and biomedicine. Oligonucleotide-based sensors consist of the use of oligonucleotides (DNA, RNA or synthetic analogue to naturally occurring nucleic acids) as a recognition layer. Oligonucleotides are short sequences of repeated nucleotide units. These nucleotides are linked together via phosphodiester bonds with the backbone being composed of alternating phosphate and sugar (deoxyribose in DNA and ribose in RNA) residues (Cohen 1989). Oligonucleotides are unmodified or chemically modified polymers (DNA or RNA) that are relatively small (12-25-mer) introducing an expanded range of applications in molecular genetics research and in forensics. The suffix “mer” is often used (derived from the Greek for “part”) to denote the length of an oligonucleotide. In the natural world, oligonucleotides exist mainly as small noncoding RNAs (e.g. miRNAs). Such oligonucleotides are commonly synthesised using solid phase chemistry. Chemical modifications of the sugar-phosphate backbone or the bases are often used to increase the stability and half-life of the oligonucleotides. In general, oligonucleotides work by hybridising to their complementary sequences.

They are used in many different ways including as “primers” in polymerase chain reaction (PCR), as “probes” in microarray analysis or in situ hybridisation, and in biosensing applications. The explosion of knowledge about gene expression and gene regulation mechanisms has led to many new opportunities to develop oligonucleotide-based technologies. In recent years, there is hardly a field in biology in which the potential of using synthetic oligonucleotides has not been explored. The reason for such a turnover is mainly due to the emergence of different molecular cloning techniques along with the simultaneous development of varied methods for efficient oligonucleotide synthesis. The primary motivations behind these developments for the biochemists have been not only the huge biological potential but also immense demand for synthetic oligonucleotides. Synthetic oligonucleotides or nucleic acid analogues are compounds which are structurally similar to naturally occurring RNA or DNA. Some of the artificial nucleic acids include peptide nucleic acids (PNA), locked nucleic acids (LNA), glycol nucleic acids (GNA) and threose nucleic acids (TNA), which differ from naturally occurring RNA or DNA in the backbone structure of the molecule. Consequently, availability of these synthetic oligonucleotides has led to a revolution in solving molecular biology problems along with promising applications in biosensing. This section will focus on DNA aptamers and PNA for biosensing applications.

1.3.1 DNA aptamers

DNA or RNA aptamers are short single-strand oligonucleotides, which have gained immense interest as bioreceptors in biosensors (aptasensors) or medical therapy (Hianik and Wang 2009; Iliuk *et al.* 2011). Their specificity is akin or higher than those of antibodies, with dissociation constants (K_d) in the range from nanomolar (nM) to picomolar (pM) levels. An important advantage of their use in biosensor devices is their high affinity to proteins and other molecules with low molecular weight, for example, toxins (Castillo *et al.* 2012; Evtugyn *et al.* 2009). Aptamers have several advantages over antibodies because of varied advantages, for instance, aptamers are much more stable than antibodies, making them suitable for applications in special conditions such as high temperature or extreme pH.

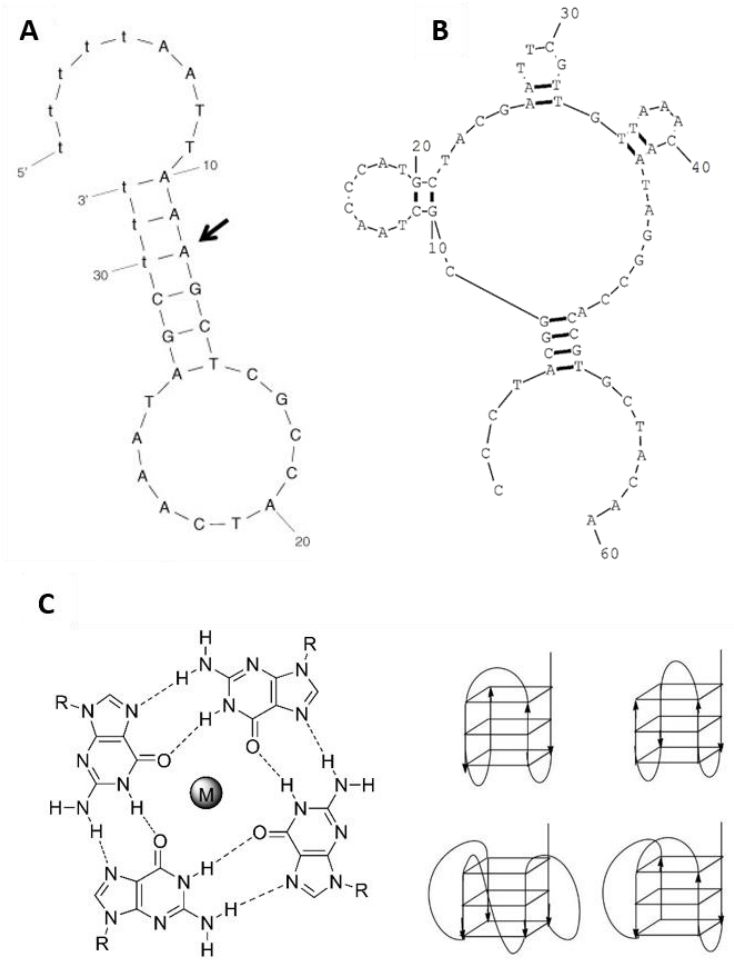

Figure 1.6 Example of aptamer structures: (A) Two-dimensional stem-loop structure of anti-PSA DNA aptamer (Savory et al. 2010); (B) multiple stem-loop structure of anti-AMACR DNA aptamer (Yang et al. 2014); (C) Crystal structure representing quadruplex conformation of anti-thrombin DNA aptamer (Macaya et al. 1993).

Another advantage is that aptamer-based biosensors can be regenerated without loss of integrity and selectivity (Mairal *et al.* 2008; Tombelli *et al.* 2005). One very interesting property of an aptamer is the conformational change that it undergoes once bound to its target, this property has been widely utilised within biosensing applications (Jolly *et al.* 2015b; Radi *et al.* 2006). The aptamers are known to form loops, stems, hairpins, triplexes or quadruplex structures. Figures 1.6A and 1.6B show an anti-PSA DNA aptamer in its stable loop configuration and an anti-AMACR DNA aptamer with multiple loop structures (Savory *et al.* 2010; Yang *et al*. 2014). The formation of loops is due to the specific interactions between nucleotides, adenine, and thymine or guanine and cytosine present in DNA aptamer chains. Quadruplexes

are nucleic acid sequences that are rich in guanine and are able to form a four-stranded structure (Figure 1.6C). The quadruplex structure is further stabilised by the presence of a cation, especially potassium, which sits in a central channel between each pair of tetrads.

Aptamers can be easily chemically modified by various functional groups, such as thiol, amine or azide as well as biotin groups. This modification allows the immobilisation of aptamers to various solid supports. For example modification of aptamers with thiols allows their association on the gold surface using Au-S interactions (Jolly *et al.* 2015b) or modification with azido groups via click chemistry (Hayat *et al*. 2013). In another case, one end of DNA or RNA aptamers can be modified with biotin and binding of these biomolecules through solid support is realized via avidin, streptavidin or neutravidin bridges (Cavic and Thompson 2002; Centi *et al.* 2007; Liss *et al.* 2002; Ostatná *et al.* 2008).

Aptamers were introduced in 1990 by two independent research groups: Turek *et al*. used the term SELEX (generalised scheme of systematic evolution of ligands by exponential enrichment) for selecting RNA ligands against T4 DNA polymerase; and Ellington et al. coined the term *in-vitro* selection (Ellington and Szostak 1990; Robertson and Joyce 1990; Tuerk and Gold 1990). In contrast to antibodies that are obtained by molecular biology techniques, aptamers are prepared by a synthetic method using an *in-vitro* selection procedure. Once an aptamer sequence is identified, it can be synthesised with high purity, reproducibility, and relatively low cost. Although aptamers have a greater advantage over antibodies, they still possess a number of limitations, for example, degradation by nucleases (DNAse and RNAse) or protein fouling in serum due to DNA binding proteins (Keum and Bermudez 2009; Sylvia *et al.* 1975). The SELEX approach starts with a random library containing 10^{13}-10^{16} ssDNA or RNA sequences (Iliuk *et al.* 2011; Song *et al.* 2008). The library is incubated with a target to initiate the first cycle of selection. This is typically followed by iterative cycles of absorption, recovery of bound DNA/RNA, and amplification. Isolation of the bound DNA/RNA is the most critical step to ensure purity and selectivity. For example, the aptamer-target complex can be separated by filtration through nitrocellulose or by affinity chromatography from the unbound DNA/RNA

sequences. The bound aptamers are then eluted and amplified by RT-PCR (for RNA libraries) or PCR (for DNA libraries) to generate new pools for the next selection cycle. An ideal aptamer selection procedure requires around 10-15 cycles. A generalised SELEX method is presented in Figure 1.7.

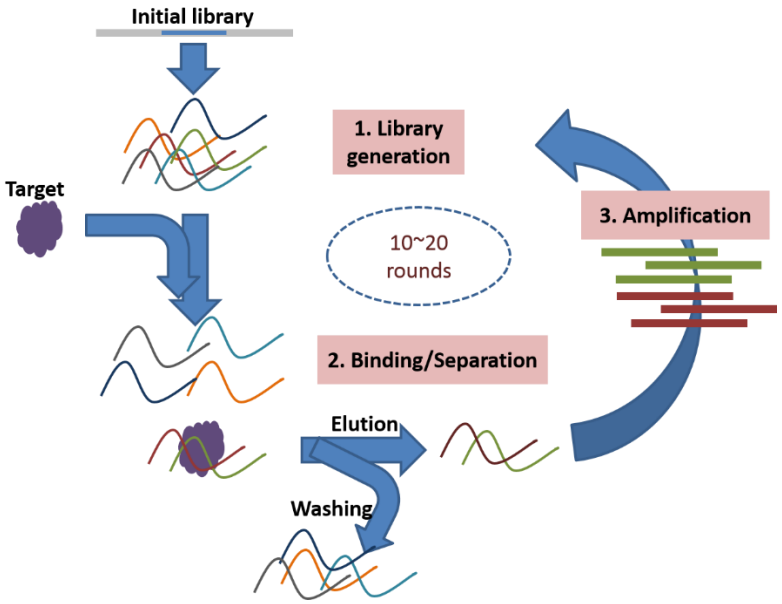

Figure 1.7 Generalised scheme of systematic evolution of ligands by exponential enrichment (SELEX). Adapted from Song et al. (Song et al. 2008).

The high specificity of aptamers and the possibility of developing aptamers against different binding sites of target analyte offer high variability of assay configuration (Figure 1.8) (Hianik and Wang 2009; Song *et al.* 2008). The first simple assay consists of the attachment of aptamers onto a support and the interactions of aptamer/target can be directly monitored (Figure 1.8A) (Formisano *et al.* 2015). Sandwich assay consists of capturing the target by specific aptamer method followed by interactions with another aptamer or antibody (Figure 1.8B, 1.8C, and 1.8D). Similar to immunosensing assays, these aptamers can be modified with nanoparticles (Pavlov *et al.* 2004) or electrochemical markers (Kang *et al.* 2008) which enhance the electric signal or allow amplification of the aptamer mass.

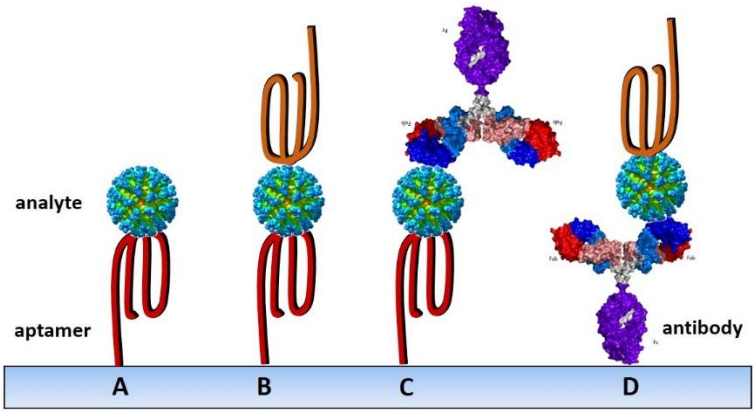

Figure 1.8 Examples of different assays based on aptamers. (A) Capture of analyte by immobilised aptamers. (B) Sandwich type assay with aptamers using two aptamers specific to two different sites of the analyte. (C) Capture of the analyte by the immobilised aptamers while a secondary antibody is used to detect in a modified ELISA format. (D) Capture of analyte by an immobilised antibody while aptamer is used as a secondary probe in a modified ELISA format.

1.3.2 Peptide nucleic acids

Emerging molecular biology and biochemistry techniques have pushed the field of biology towards usage of synthetic oligonucleotides. Such synthetic oligonucleotides are nucleic acid analogue compounds which are structurally similar to natural DNA/RNA nucleic acids. PNA is a synthetic polymer which is similar to DNA/RNA, first synthesised by Nielsen *et al.* in 1991 (Nielsen *et al.* 1991). The backbone of a PNA molecule consists of a repeat of units of N-(2-aminoethyl) glycine units linked via an amide bond (Figure 1.9). Such a modification changes the negative charges of the DNA sugar-phosphate backbone to a neutral charge of the peptide-like backbone. PNA sequences, like any peptide sequence, is depicted with an N-terminus and a C-terminus. In a PNA, the four naturally occurring nucleobases namely adenine, cytosine, guanine, and thymine are connected to the central amine of the peptide backbone via a methylene bridge and a carbonyl group (Hyrup and Nielsen 1996).

PNA has several advantages over DNA due to its neutral charge and proper base-pairing. PNA can bind to its complementary target oligonucleotide with higher affinity and specificity by following the rules of Watson-Crick base-pairing (Egholm *et al.* 1993). As a consequence, PNA/DNA duplex demonstrates higher thermal stability and there is no dependency of PNA/DNA duplex stability on the ionic strength of the solution in which hybridisation is performed (Hyrup and Nielsen 1996; Wang 1998).

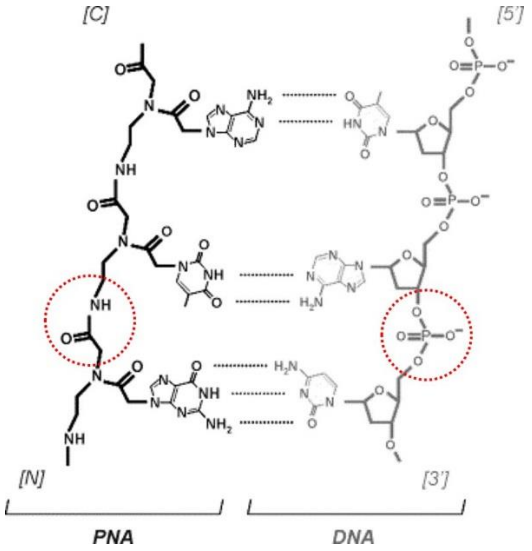

Figure 1.9 Chemical structure model of PNA (sequence N-GTA-C) hybridised with its complementary DNA (sequence 5'-TAC-3')(Nielsen et al. 1991).

Because of its unique physicochemical and biochemical properties, PNA as a bio-receptor opens up many applications (biological and diagnostic) which would not be achievable with naturally occurring oligonucleotides. Wang *et al.* in 1996 first demonstrated the use of PNA for biosensing applications with a detection limit of 10 pM (Wang *et al.* 1996). In this approach, PNA probes were adsorbed on the carbon paste electrodes and hybridised with the complementary strand. The hybridisation was detected using a $Co(phen)^{3+}_3$ redox indicator via the chronopotentiometry technique (Wang *et al.* 1996). Since then, there has been many a report on the use of PNA as probes for the development of electrochemical sensors (Cai *et al.* 2015; Du *et al.* 2013; Raoof *et al.* 2011; Zhang *et al.* 2008). Keighley *et al.* in 2008 fabricated a label-free PNA-based electrochemical impedance based sensor (Keighley *et al.* 2008). This work demonstrated how the inherent neutral charges of PNA can be exploited on an impedimetric platform. The same methodology forms the foundation of the biosensor development for DNA/miRNA detection which is presented in Chapter 6.

1.4 General overview of the project

This particular thesis is based on a project entitled "Cancer Diagnosis- Parallel Sensing of Prostate Cancer Biomarkers" which is one of the sub-projects within the Marie Curie Initial Training Network-PROSENSE focussing on the diagnosis of PCa. The principal aspect of the current work is to study biomarkers, probe immobilisation, and development of detection techniques. The core aim of the project is the development of oligonucleotide-based electrochemical platforms. This thesis draws light into four PCa biomarkers that could be detected with oligonucleotide-based electrochemical platforms. In parallel, this thesis will also detail different surface chemistries that have been employed for the development of biosensors for their potential clinical application. As a whole, the objectives can be broadly divided into different stages, namely: selection of biomarkers, characterising specific probes for detection of biomarkers, optimization of immobilisation techniques, and finally electrochemical sensing.

This particular thesis highlights the following points:

1 Characterisation of oligonucleotide-based probes when restricted to the electrode surface.
2 Different strategies for the development of oligonucleotide-based biosensors using different surface chemistries.
3 Use of electrochemical techniques (impedimetric and amperometric) for the development of highly sensitive transduction techniques for sensing.
4 Evaluation of sensor performance for its selectivity properties.

1.4.1 Outline of thesis

In order to develop biosensors for diagnosis of PCa, it is essential to understand the physiology of PCa and biomarkers associated with it. Until now Chapter 1 discussed the potential biomarkers for PCa along with a short introduction to biosensors. Since the main focus is on oligonucleotide-based biosensing, Chapter 1 could not close without introducing DNA aptamers and PNA as recognition layers for biosensor fabrication.

Chapter 2 details oligonucleotide-based approaches to fabricate biosensors, more specifically sensors for cancer diagnosis. For fabrication of a reliable and sensitive aptasensor, surface chemistry plays a crucial role. Therefore, the Chapter extends into different surface chemistries that have been employed in the reported work. Electrochemical detection techniques are further explained with different electrochemistry principles and specific detection techniques used in the study.

The oligonucleotide probes for sensor development have been characterised using different techniques. Chapter 2 will also present characterisation techniques other than electrochemical, like surface plasmon resonance (SPR) and Fourier transform infrared spectroscopy (FT-IR) that have been used in the course of the development of the biosensors.

The outcome from independently developed systems is summarised at the end of each relative Chapter. Since PSA has been widely used for PCa screening, it is a good case study to start oligonucleotide-based electrochemical detection, which is presented in Chapter 3. An anti-PSA DNA aptamer was used as a probe to capture PSA and was detected using the electrochemical impedance spectroscopy (EIS) technique. It highlights the importance of surface chemistry in terms of surface coverage by DNA aptamers in order to enhance binding efficiency. Following that, spacer molecules such as 6- mercapto 1-hexanol (MCH) and thiol terminated sulfo-betaine were investigated for their effect on sensitivity and selectivity of the aptasensor.

Chapter 4 presents a study of glycoprofiling that was performed to compensate some of the limitations of PSA testing. Such a study was performed in a microfluidic channel where DNA aptamers were immobilised to capture PSA. Finally, a secondary antibody or a lectin was used for quantification and glycoprofiling of PSA, respectively.

In Chapter 5, AMACR is used as the biomarker. Again, DNA aptamer based biosensors were constructed for AMACR detection. Two different DNA aptamer sequences were characterised for their binding efficiency for the development of a biosensor. In order to implement polyethylene glycol (PEG) based surface chemistry, a new strategy was developed. It employed the use of poly(pyrrole) films which were electrochemically modified with PEG via a one-step process. Such a surface was then

used to attach an anti-AMACR DNA aptamer for subsequent detection of AMACR using an amperometric technique.

After witnessing the anti-fouling efficiency of PEG on the surface of the electrode, detection of miRNAs was performed using PEG linkers, as described in Chapter 6. The study investigates the use of PNA probes to selectively capture synthetic RNA as a proof of concept. A non-Faradaic EIS approach was utilised using positively charged gold nanoparticles (AuNPs) as a simple amplification strategy. The sensitive detection with EIS was validated on the same platform by using thiolated ferrocene molecules. The current peaks of ferrocene were monitored using an amperometric technique.

References

Adamczyk, B., Tharmalingam, T. and Rudd, P.M., 2012. Glycans as cancer biomarkers. *Biochimica et Biophysica Acta (BBA)-General Subjects*, 1820(9), pp.1347-1353.

Akao, Y., Nakagawa, Y., and Naoe, T., 2007. MicroRNA-143 and-145 in colon cancer. *DNA and Cell Biology*, 26(5), 311-320.

An, H.J., Kronewitter, S.R., de Leoz, M.L.A., and Lebrilla, C.B., 2009. Glycomics and disease markers. *Current Opinion in Chemical Biology*, 13(5), 601-607.

Andriole, G.L., Crawford, E.D., Grubb III, R.L., Buys, S.S., Chia, D., Church, T.R., Fouad, M.N., Gelmann, E.P., Kvale, P.A., and Reding, D.J., 2009. Mortality results from a randomized prostate-cancer screening trial. *New England Journal of Medicine*, 360(13), 1310-1319.

Axford, J.S., 1999. Glycosylation and rheumatic disease. *Biochimica et Biophysica Acta (BBA) - Molecular Basis of Disease*, 1455(2–3), 219-229.

Bader, A., Brown, D., Stoudemire, J., and Lammers, P., 2011. Developing therapeutic microRNAs for cancer. *Gene Therapy*, 18(12), 1121-1126.

Balducci, L., Pow-Sang, J., Friedland, J., and Diaz, J.I., 1997. Prostate cancer. *Clinics in Geriatric Medicine*, 13(2), 283-306.

Balk, S.P., Ko, Y.-J., and Bubley, G.J., 2003. Biology of prostate-specific antigen. *Journal of Clinical Oncology*, 21(2), 383-391.

Bartel, D.P., 2004. MicroRNAs: genomics, biogenesis, mechanism, and function. *Cell*, 116(2), 281-297.

Basler, J.W., and Thompson, I.M., 1998. Lest we abandon digital rectal examination as a screening test for prostate cancer. *Journal of the National Cancer Institute*, 90(23), 1761-1763.

Bonci, D., Coppola, V., Musumeci, M., Addario, A., Giuffrida, R., Memeo, L., D'Urso, L., Pagliuca, A., Biffoni, M., and Labbaye, C., 2008. The miR-15a–miR-16-

1 cluster controls prostate cancer by targeting multiple oncogenic activities. *Nature Medicine,* 14(11), 1271-1277.

Bosques, C.J., Raguram, S., and Sasisekharan, R., 2006. The sweet side of biomarker discovery. *Nature Biotechnology,* 24(9), 1100-1101.

Brase, J.C., Wuttig, D., Kuner, R., and Sultmann, H., 2010. Serum microRNAs as non-invasive biomarkers for cancer. *Molecular Cancer,* 9(9), 306.

Brett, A.S., and Ablin, R.J., 2011. Prostate-cancer screening—what the US Preventive Services Task Force left out. *New England Journal of Medicine,* 365(21), 1949-1951.

Cai, B., Huang, L., Zhang, H., Sun, Z., Zhang, Z., and Zhang, G.-J., 2015. Gold nanoparticles-decorated graphene field-effect transistor biosensor for femtomolar MicroRNA detection. *Biosensors and Bioelectronics,* 74, 329-334.

Cardillo, M.R., Gentile, V., Ciccariello, M., Giacomelli, L., Messinetti, S., and Di Silverio, F., 2005. Can p503s, p504s and p510s gene expression in peripheral-blood be useful as a marker of prostatic cancer. *BMC Cancer,* 5(1), 111.

Carter, H.B., Pearson, J.D., Metter, E.J., Brant, L.J., Chan, D.W., Andres, R., Fozard, J.L., and Walsh, P.C., 1992. Longitudinal evaluation of prostate-specific antigen levels in men with and without prostate disease. *Jama,* 267(16), 2215.

Carvalhal, G.F., Smith, D.S., Mager, D.E., Ramos, C., and Catalona, W.J., 1999. Digital rectal examination for detecting prostate cancer at prostate specific antigen levels of 4 ng./ml. or less. *The Journal of Urology,* 161(3), 835-839.

Cass, A.E., Davis, G., Francis, G.D., Hill, H.A.O., Aston, W.J., Higgins, I.J., Plotkin, E.V., Scott, L.D., and Turner, A.P., 1984. Ferrocene-mediated enzyme electrode for amperometric determination of glucose. *Analytical Chemistry,* 56(4), 667-671.

Castillo, G., Trnkova, L., Hrdy, R., and Hianik, T., 2012. Impedimetric aptasensor for thrombin recognition based on CD support. *Electroanalysis,* 24(5), 1079-1087.

Catalona, W.J., Partin, A.W., Slawin, K.M., Brawer, M.K., Flanigan, R.C., Patel, A., Richie, J.P., Walsh, P.C., Scardino, P.T., and Lange, P.H., 1998. Use of the percentage of free prostate-specific antigen to enhance differentiation of prostate cancer from

benign prostatic disease: a prospective multicenter clinical trial. *Jama*, 279(19), 1542-1547.

Catalona, W.J., Smith, D.S., Ratliff, T.L., Dodds, K.M., Coplen, D.E., Yuan, J.J., Petros, J.A., and Andriole, G.L., 1991. Measurement of prostate-specific antigen in serum as a screening test for prostate cancer. *New England Journal of Medicine*, 324(17), 1156-1161.

Catto, J.W., Alcaraz, A., Bjartell, A.S., White, R.D.V., Evans, C.P., Fussel, S., Hamdy, F.C., Kallioniemi, O., Mengual, L., and Schlomm, T., 2011. MicroRNA in prostate, bladder, and kidney cancer: a systematic review. *European Urology*, 59(5), 671-681.

Cavic, B.A., and Thompson, M., 2002. Interfacial nucleic acid chemistry studied by acoustic shear wave propagation. *Analytica Chimica Acta*, 469(1), 101-113.

Centi, S., Tombelli, S., Minunni, M., and Mascini, M., 2007. Aptamer-based detection of plasma proteins by an electrochemical assay coupled to magnetic beads. *Analytical Chemistry*, 79(4), 1466-1473.

Chou, E., and Simons, J.W., 1997. The molecular biology of prostate cancer morbidity and mortality: Accelerated death from ejaculate poisoning, *Urologic Oncology*: *Seminars and Original Investigations*, pp. 79-84. Elsevier.

Christensson, A., Björk, T., Nilsson, O., Dahlén, U., Matikainen, M., Cockett, A., Abrahamsson, P., and Lilja, H., 1993. Serum prostate specific antigen complexed to alpha 1-antichymotrypsin as an indicator of prostate cancer. *The Journal of Urology*, 150(1), 100-105.

Christiansen, M.N., Chik, J., Lee, L., Anugraham, M., Abrahams, J.L., and Packer, N.H., 2014. Cell surface protein glycosylation in cancer. *Proteomics*, 14(4-5), 525-546.

Cohen, J.S., 1989. *Oligodeoxynucleotides: antisense inhibitors of gene expression*. CRC Press Inc.

Colburn, W., DeGruttola, V.G., DeMets, D.L., Downing, G.J., Hoth, D.F., Oates, J.A., Peck, C.C., Schooley, R.T., Spilker, B.A., and Woodcock, J., 2001. Biomarkers and

surrogate endpoints: Preferred definitions and conceptual framework. *Biomarkers Definitions Working Group. Clinical Pharmacol & Therapeutic*s, 69, 89-95.

Diamandis, E.P., and Yousef, G.M., 2002. Human tissue kallikreins: a family of new cancer biomarkers. *Clinical Chemistry*, 48(8), 1198-1205.

Du, D., Guo, S., Tang, L., Ning, Y., Yao, Q., and Zhang, G.-J., 2013. Graphene-modified electrode for DNA detection via PNA–DNA hybridisation. *Sensors and Actuators B: Chemical*, 186, 563-570.

Egholm, M., Buchardt, O., Christensen, L., Behrens, C., Freier, S.M., Driver, D.A., Berg, R.H., Kim, S.K., Norden, B., and Nielsen, P.E., 1993. PNA hybridizes to complementary oligonucleotides obeying the Watson Crick hydrogen-bonding rules. *Nature*, 365, 566-568.

Ellington, A.D., and Szostak, J.W., 1990. In vitro selection of RNA molecules that bind specific ligands. *Nature*, 346(6287), 818-822.

Evtugyn, G., Porfireva, A., Ivanov, A., Konovalova, O., and Hianik, T., 2009. Molecularly imprinted polymerized Methylene Green as a platform for electrochemical sensing of aptamer–thrombin interactions. *Electroanalysis*, 21(11), 1272-1277.

Filella, X., and Giménez, N., 2013. Evaluation of [−2] proPSA and Prostate Health Index (phi) for the detection of prostate cancer: A systematic review and meta-analysis. *Clinical Chemistry and Laboratory Medicine*, 51(4), 729-739.

Formisano, N., Jolly, P., Bhalla, N., Cromhout, M., Flanagan, S.P., Fogel, R., Limson, J.L. and Estrela, P., 2015. Optimisation of an electrochemical impedance spectroscopy aptasensor by exploiting quartz crystal microbalance with dissipation signals. *Sensors and Actuators B: Chemical*, 220, 369-375.

Gilgunn, S., Conroy, P.J., Saldova, R., Rudd, P.M., and O'Kennedy, R.J., 2013. Aberrant PSA glycosylation--a sweet predictor of prostate cancer. *Nature Reviews Urology* ,10(2), 99-107.

Go, E.P., Hewawasam, G., Liao, H.-X., Chen, H., Ping, L.-H., Anderson, J.A., Hua, D.C., Haynes, B.F., and Desaire, H., 2011. Characterization of Glycosylation Profiles of HIV-1 Transmitted/Founder Envelopes by Mass Spectrometry. *Journal of Virology,* 85(16), 8270-8284.

Gordanpour, A., Nam, R., Sugar, L., and Seth, A., 2012. MicroRNAs in prostate cancer: from biomarkers to molecularly-based therapeutics. *Prostate Cancer and Prostatic Diseases,* 15(4), 314-319.

Goulabchand, R., Vincent, T., Batteux, F., Eliaou, J.F., and Guilpain, P., 2014. Impact of autoantibody glycosylation in autoimmune diseases. *Autoimmunity Reviews*, 13(7), 742-750.

Greenlee, R.T., Murray, T., Bolden, S., and Wingo, P.A., 2000. Cancer statistics, 2000. *CA: a cancer journal for clinicians,* 50(1), 7-33.

Gu, Z., Thomas, G., Yamashiro, J., Shintaku, I., Dorey, F., Raitano, A., Witte, O., Said, J., Loda, M., and Reiter, R., 2000. Prostate stem cell antigen (PSCA) expression increases with high gleason score, advanced stage and bone metastasis in prostate cancer. *Oncogene,* 19(10), 1288-1296.

Haes, A.J., and Van Duyne, R.P., 2002. A nanoscale optical biosensor: sensitivity and selectivity of an approach based on the localized surface plasmon resonance spectroscopy of triangular silver nanoparticles. *Journal of the American Chemical Society,* 124(35), 10596-10604.

Hara, M., Koyanagi, Y., Inoue, T., and Fukuyama, T., 1971. Some physico-chemical characteristics of"-seminoprotein", an antigenic component specific for human seminal plasma. Forensic immunological study of body fluids and secretion. VII. *Nihon hōigaku zasshi= The Japanese journal of legal medicine,* 25(4), 322.

Hara, N., Kasahara, T., Kawasaki, T., Bilim, V., Obara, K., Takahashi, K., and Tomita, Y., 2002. Reverse Transcription-Polymerase Chain Reaction Detection of Prostate-specific Antigen, Prostate-specific Membrane Antigen, and Prostate Stem Cell Antigen in One Milliliter of Peripheral Blood Value for the Staging of Prostate Cancer. *Clinical Cancer Research,* 8(6), 1794-1799.

Hara, R., Jo, Y., Fujii, T., Kondo, N., Yokoyoma, T., Miyaji, Y., and Nagai, A., 2008. Optimal approach for prostate cancer detection as initial biopsy: prospective randomized study comparing transperineal versus transrectal systematic 12-core biopsy. *Urology,* 71(2), 191-195.

Hayat, A., Sassolas, A., Marty, J.-L., and Radi, A.-E., 2013. Highly sensitive ochratoxin A impedimetric aptasensor based on the immobilisation of azido-aptamer onto electrografted binary film via click chemistry. *Talanta,* 103, 14-19.

Hianik, T., and Wang, J., 2009. Electrochemical aptasensors–recent achievements and perspectives. *Electroanalysis,* 21(11), 1223-1235.

Hoffman, R. M., 2011. Screening for prostate cancer. *New England Journal of Medicine, 365*(21), 2013-2019. DOI: 10.1056/NEJMcp1103642

Hwang, H., Zhang, J., Chung, K.A., Leverenz, J.B., Zabetian, C.P., Peskind, E.R., Jankovic, J., Su, Z., Hancock, A.M., Pan, C., Montine, T.J., Pan, S., Nutt, J., Albin, R., Gearing, M., Beyer, R.P., Shi, M., and Zhang, J., 2010. Glycoproteomics in neurodegenerative diseases. *Mass Spectrometry Reviews,* 29(1), 79-125.

Hyrup, B., and Nielsen, P.E., 1996. Peptide nucleic acids (PNA): synthesis, properties and potential applications. *Bioorganic & Medicinal Chemistry,* 4(1), 5-23.

Ichimi, T., Enokida, H., Okuno, Y., Kunimoto, R., Chiyomaru, T., Kawamoto, K., Kawahara, K., Toki, K., Kawakami, K., and Nishiyama, K., 2009. Identification of novel microRNA targets based on microRNA signatures in bladder cancer. *International Journal of Cancer,* 125(2), 345-352.

Ilic, D., Neuberger, M.M., Djulbegovic, M., and Dahm, P., 2013. Screening for prostate cancer. *Cochrane Database Syst Rev* 1.

Iliuk, A.B., Hu, L., and Tao, W.A., 2011. Aptamer in bioanalytical applications. *Analytical Chemistry,* 83(12), 4440-4452.

Jaffrezic-Renault, N., 2013. Label-Free Affinity Biosensors Based on Electrochemical Impedance Spectroscopy. *Microelectrode Biosensors,* 80, 295-318.

Janshoff, A., Galla, H.-J., and Steinem, C., 2000. Piezoelectric Mass-Sensing Devices as Biosensors-An Alternative to Optical Biosensors? *Angewandte Chemie International Edition,* 39, 4004-4032.

Jiang, Z., Woda, B.A., Wu, C.-L., and Yang, X.J., 2004. Discovery and clinical application of a novel prostate cancer marker α-methylacyl CoA Racemase (P504S). *American Journal of Clinical Pathology,* 122(2), 275-289.

Jiang, Z., Wu, C-L., Woda, B.A., Dresser, K., Xu, J., Fanger, G.R., and Yang, X.J., 2002. P504S/α-methylacyl-CoA racemase: a useful marker for diagnosis of small foci of prostatic carcinoma on needle biopsy. *The American Journal of Surgical Pathology,* 26(9), 1169-1174.

Jiang, Z., Wu, C-L., Woda, B., Iczkowski, K., Chu, P., Tretiakova, M., Young, R., Weiss, L., Blute, R., and Brendler, C., 2004. Alpha-methylacyl-CoA racemase: a multi-institutional study of a new prostate cancer marker. *Histopathology,* 45(3), 218-225.

Jolly, P., Formisano, N., and Estrela, P., 2015a. DNA aptamer-based detection of prostate cancer. *Chemical Papers,* 69(1), 77-89.

Jolly, P., Formisano, N., Tkáč, J., Kasák, P., Frost, C.G., and Estrela, P., 2015b. Label-free impedimetric aptasensor with antifouling surface chemistry: A prostate specific antigen case study. *Sensors and Actuators B: Chemical,* 209, 306-312.

Kang, Y., Feng, K-J., Chen, J-W., Jiang, J-H., Shen, G.-L., and Yu, R-Q., 2008. Electrochemical detection of thrombin by sandwich approach using antibody and aptamer. *Bioelectrochemistry*, 73(1), 76-81.

Keighley, S.D., Estrela, P., Li, P., and Migliorato, P., 2008. Optimization of label-free DNA detection with electrochemical impedance spectroscopy using PNA probes. *Biosensors and Bioelectronics,* 24(4), 906-911.

Keum, J.-W., and Bermudez, H., 2009. Enhanced resistance of DNA nanostructures to enzymatic digestion. *Chemical Communications,* (45), 7036-7038.

Kirk, D., 1997. MRC study: when to commence treatment in advanced prostate cancer. *Prostate Cancer & Prostatic Diseases, 1*(1), 11-15

Kuner, R., Brase, J.C., Sültmann, H., and Wuttig, D., 2013. microRNA biomarkers in body fluids of prostate cancer patients. *Methods,* 59(1), 132-137.

Kuzmanov, U., Kosanam, H., and Diamandis, E., 2013. The sweet and sour of serological glycoprotein tumor biomarker quantification. *BMC Medicine,* 11(1), 31.

Larne, O., Martens-Uzunova, E., Hagman, Z., Edsjö, A., Lippolis, G., den Berg, M.S., Bjartell, A., Jenster, G., and Ceder, Y., 2013. miQ—a novel microRNA based diagnostic and prognostic tool for prostate cancer. *International Journal of Cancer,* 132(12), 2867-2875.

Launay, G., Téletchéa, S., Wade, F., Pajot-Augy, E., Gibrat, J.-F., and Sanz, G., 2012. Automatic modeling of mammalian olfactory receptors and docking of odorants. *Protein Engineering Design and Selection,* 25(8), 377-386.

Leissner, K.-H., and Tisell, L.-E., 1979. The weight of the human prostate. *Scandinavian Journal of Urology and Nephrology*, 13(2), 137-142.

Lilja, H., Oldbring, J., Rannevik, G., and Laurell, C., 1987. Seminal vesicle-secreted proteins and their reactions during gelation and liquefaction of human semen. *Journal of Clinical Investigation*, 80(2), 281.

Liss, M., Petersen, B., Wolf, H., and Prohaska, E., 2002. An aptamer-based quartz crystal protein biosensor. *Analytical Chemistry,* 74(17), 4488-4495.

Liu, Y., Xiao, Z., Li, M., Li, M., Zhang, P., Li, C., Li, F., Chen, Y., Yi, H., and Yao, H., 2009. Quantitative proteome analysis reveals annexin A3 as a novel biomarker in lung adenocarcinoma. *The Journal of Pathology*, 217(1), 54-64.

Lloyd, M.D., Darley, D.J., Wierzbicki, A.S., and Threadgill, M.D., 2008. α-Methylacyl-CoA racemase–an 'obscure'metabolic enzyme takes centre stage. *FEBS journal,* 275(6), 1089-1102.

Loeb, S., Vellekoop, A., Ahmed, H.U., Catto, J., Emberton, M., Nam, R., Rosario, D.J., Scattoni, V., Lotan, Y., 2013. Systematic review of complications of prostate biopsy. *European Urology,* 64(6), 876-892.

Lövgren, J., VALTONEN-ANDRÉ, C., Marsal, K., LIUA, H., and Lundwall, Å., 1999. Measurement of Prostate-Specific Antigen and Human Glandular Kallikrein 2 in Different Body Fluids. *Journal of Andrology,* 20(3), 348-355.

Lowe, C.R., 1984. Biosensors. *Trends in Biotechnology,* 2(3), 59-65.

Macaya, R.F., Schultze, P., Smith, F.W., Roe, J.A., and Feigon, J., 1993. Thrombin-binding DNA aptamer forms a unimolecular quadruplex structure in solution. *Proceedings of the National Academy of Sciences,* 90(8), 3745-3749.

Madu, C.O., and Lu, Y., 2010. Novel diagnostic biomarkers for prostate cancer. *Journal of Cancer,* 1, 150.

Mairal, T., Özalp, V.C., Sánchez, P.L., Mir, M., Katakis, I., and O'Sullivan, C.K., 2008. Aptamers: molecular tools for analytical applications. *Analytical and Bioanalytical Chemistr*y, 390(4), 989-1007.

Meany, D., and Chan, D., 2011. Aberrant glycosylation associated with enzymes as cancer biomarkers. *Clinical Proteomics,* 8(1), 7.

Meister, G., 2007. miRNAs get an early start on translational silencing. *Cell*, 131(1), 25-28.

Mitchell, P.S., Parkin, R.K., Kroh, E.M., Fritz, B.R., Wyman, S.K., Pogosova-Agadjanyan, E.L., Peterson, A., Noteboom, J., O'Briant, K.C., and Allen, A., 2008. Circulating microRNAs as stable blood-based markers for cancer detection. *Proceedings of the National Academy of Sciences,* 105(30), 10513-10518.

Morgan, R., Boxall, A., Bhatt, A., Bailey, M., Hindley, R., Langley, S., Whitaker, H.C., Neal, D.E., Ismail, M., and Whitaker, H., 2011. Engrailed-2 (EN2): a tumor specific urinary biomarker for the early diagnosis of prostate cancer. *Clinical Cancer Research,* 17(5), 1090-1098.

Nam, E.J., Yoon, H., Kim, S.W., Kim, H., Kim, Y.T., Kim, J.H., Kim, J.W., and Kim, S., 2008. MicroRNA expression profiles in serous ovarian carcinoma. *Clinical Cancer Research,* 14(9), 2690-2695.

Nielsen, P.E., Egholm, M., Berg, R.H., and Buchardt, O., 1991. Sequence-selective recognition of DNA by strand displacement with a thymine-substituted polyamide. *Science,* 254(5037), 1497-1500.

Ohyama, C., Hosono, M., Nitta, K., Oh-eda, M., Yoshikawa, K., Habuchi, T., Arai, Y., and Fukuda, M., 2004. Carbohydrate structure and differential binding of prostate specific antigen to Maackia amurensis lectin between prostate cancer and benign prostate hypertrophy. *Glycobiology,* 14(8), 671-679.

Ostatná, V., Vaisocherová, H., Homola, J., and Hianik, T., 2008. Effect of the immobilisation of DNA aptamers on the detection of thrombin by means of surface plasmon resonance. *Analytical and Bioanalytical Chemistry,* 391(5), 1861-1869.

Özen, H., and Sözen, S., 2006. PSA isoforms in prostate cancer detection. *European Urology Supplements,* 5(6), 495-499.

Pandha, H., Sorensen, K.D., Orntoft, T.F., Langley, S., Hoyer, S., Borre, M., and Morgan, R., 2012. Urinary engrailed-2 (EN2) levels predict tumour volume in men undergoing radical prostatectomy for prostate cancer. *BJU international,* 110(6b), E287-E292.

Paul, B., Dhir, R., Landsittel, D., Hitchens, M.R., and Getzenberg, R.H., 2005. Detection of prostate cancer with a blood-based assay for early prostate cancer antigen. *Cancer Research,* 65(10), 4097-4100.

Pavlov, V., Xiao, Y., Shlyahovsky, B., and Willner, I., 2004. Aptamer-functionalised Au nanoparticles for the amplified optical detection of thrombin. *Journal of the American Chemical Society,* 126(38), 11768-11769.

Peracaula, R., Tabarés, G., Royle, L., Harvey, D.J., Dwek, R.A., Rudd, P.M., and de Llorens, R., 2003. Altered glycosylation pattern allows the distinction between

prostate-specific antigen (PSA) from normal and tumor origins. *Glycobiology*, 13(6), 457-470.

Pihíková, D., Kasák, P., and Tkac, J., 2015. Glycoprofiling of cancer biomarkers: Label-free electrochemical lectin-based biosensors. *Open Chemistry,* 13, 636–655.

Radi, A.-E., Acero Sánchez, J.L., Baldrich, E., and O'Sullivan, C.K., 2006. Reagentless, reusable, ultrasensitive electrochemical molecular beacon aptasensor. *Journal of the American Chemical Society,* 128(1), 117-124.

Raoof, J.B., Ojani, R., Golabi, S.M., Hamidi-Asl, E., and Hejazi, M.S., 2011. Preparation of an electrochemical PNA biosensor for detection of target DNA sequence and single nucleotide mutation on p53 tumor suppressor gene corresponding oligonucleotide. *Sensors and Actuators B: Chemical,* 157(1), 195-201.

Rittenhouse, H.G., Finlay, J.A., Mikolajczyk, S.D., and Partin, A.W., 1998. Human kallikrein 2 (hK2) and prostate-specific antigen (PSA): two closely related, but distinct, kallikreins in the prostate. *Critical Reviews in Clinical Laboratory Sciences,* 35(4), 275-368.

Robertson, D.L., and Joyce, G.F., 1990. Selection in vitro of an RNA enzyme that specifically cleaves single-stranded DNA. *Nature,* 344(6265), 467-468.

Rogers, C.G., Yan, G., Zha, S., Gonzalgo, M.L., Isaacs, W.B., Luo, J., De Marzo, A.M., Nelson, W.G., and Pavlovich, C.P., 2004. Prostate cancer detection on urinalysis for α methylacyl coenzyme a racemase protein. *The Journal of Urology,* 172(4), 1501-1503.

Rolan, P., 1997. The contribution of clinical pharmacology surrogates and models to drug development—a critical appraisal. *British Journal of Clinical Pharmacology,* 44(3), 219-225.

Roobol, M.J., Haese, A., and Bjartell, A., 2011. Tumour markers in prostate cancer III: biomarkers in urine. *Acta Oncologica,* 50(S1), 85-89.

Rubin, M.A., Zhou, M., Dhanasekaran, S.M., Varambally, S., Barrette, T.R., Sanda, M.G., Pienta, K.J., Ghosh, D., and Chinnaiyan, A.M., 2002. α-Methylacyl coenzyme A racemase as a tissue biomarker for prostate cancer. *Jama*, 287(13), 1662-1670.

Rudd, P.M., Elliott, T., Cresswell, P., Wilson, I.A., and Dwek, R.A., 2001. Glycosylation and the immune system. *Science*, 291(5512), 2370-2376.

Rudd, P.M., Wormald, M.R., Stanfield, R.L., Huang, M., Mattsson, N., Speir, J.A., DiGennaro, J.A., Fetrow, J.S., Dwek, R.A., and Wilson, I.A., 1999. Roles for glycosylation of cell surface receptors involved in cellular immune recognition. *Journal of Molecular Biology*, 293(2), 351-366.

Saldova, R., Fan, Y., Fitzpatrick, J.M., Watson, R.W.G., and Rudd, P.M., 2011. Core fucosylation and α2-3 sialylation in serum N-glycome is significantly increased in prostate cancer comparing to benign prostate hyperplasia. *Glycobiology*, 21(2), 195-205.

Savory, N., Abe, K., Sode, K., and Ikebukuro, K., 2010. Selection of DNA aptamer against prostate specific antigen using a genetic algorithm and application to sensing. *Biosensors and Bioelectronics*, 26(4), 1386-1391.

Schostak, M., Schwall, G.P., Poznanović, S., Groebe, K., Müller, M., Messinger, D., Miller, K., Krause, H., Pelzer, A., and Horninger, W., 2009. Annexin A3 in urine: a highly specific noninvasive marker for prostate cancer early detection. *The Journal of Urology*, 181(1), 343-353.

Shental-Bechor, D., and Levy, Y., 2009. Folding of glycoproteins: toward understanding the biophysics of the glycosylation code. *Current Opinion in Structural Biology*, 19(5), 524-533.

Source internet cancer research UK website: URL: http://www.cancerresearchuk.org/cancer-help/type/prostate-cancer/, URL: http://prostatecanceruk.org/information/prostate-cancer-facts-and-Figures, accessed on 2012.

Song, S., Wang, L., Li, J., Fan, C., and Zhao, J., 2008. Aptamer-based biosensors. TrAC *Trends in Analytical Chemistry*, 27(2), 108-117.

Spizzo, R., Nicoloso, M., Lupini, L., Lu, Y., Fogarty, J., Rossi, S., Zagatti, B., Fabbri, M., Veronese, A., and Liu, X., 2010. miR-145 participates with TP53 in a death-promoting regulatory loop and targets estrogen receptor-α in human breast cancer cells. *Cell Death & Differentiation*, 17(2), 246-254.

Sreekumar, A., Laxman, B., Rhodes, D.R., Bhagavathula, S., Harwood, J., Giacherio, D., Ghosh, D., Sanda, M.G., Rubin, M.A., and Chinnaiyan, A.M., 2004. Humoral immune response to α-methylacyl-CoA racemase and prostate cancer. *Journal of the National Cancer Institute*, 96(11), 834-843.

Sylvia, P., Brehm, S.O., and Hoch, H.J.A., 1975. DNA-binding proteins in human serum. *Biochemical and Biophysical Research Communications*, 63(1), 24-31.

Tahir, S.A., Yang, G., Goltsov, A.A., Watanabe, M., Tabata, K.-i., Addai, J., Kadmon, D., and Thompson, T.C., 2008. Tumor Cell–Secreted Caveolin-1 has Proangiogenic Activities in Prostate Cancer. *Cancer Research*, 68(3), 731-739.

Takayama, T.K., Fujikawa, K., and Davie, E.W., 1997. Characterization of the precursor of prostate-specific antigen Activation by trypsin and by human glandular kallikrein. *Journal of Biological Chemistry*, 272(34), 21582-21588.

Thévenot, D.R., Toth, K., Durst, R.A., and Wilson, G.S., 2001. Electrochemical biosensors: recommended definitions and classification. *Biosensors and Bioelectronics*, 16(1), 121-131.

Thompson, I.M., Pauler, D.K., Goodman, P.J., Tangen, C.M., Lucia, M.S., Parnes, H.L., Minasian, L.M., Ford, L.G., Lippman, S.M., and Crawford, E.D., 2004. Prevalence of prostate cancer among men with a prostate-specific antigen level≤ 4.0 ng per milliliter. *New England Journal of Medicine*, 350(22), 2239-2246.

Tombelli, S., Minunni, M., and Mascini, M., 2005. Analytical applications of aptamers. *Biosensors and Bioelectronics*, 20(12), 2424-2434.

Tricoli, J.V., Schoenfeldt, M., and Conley, B.A., 2004. Detection of prostate cancer and predicting progression current and future diagnostic markers. *Clinical Cancer Research,* 10(12), 3943-3953.

Tuerk, C., and Gold, L., 1990. Systematic evolution of ligands by exponential enrichment: RNA ligands to bacteriophage T4 DNA polymerase. *Science,* 249(4968), 505-510.

Uzzo, R.G., Wei, J.T., Waldbaum, R.S., Perlmutter, A.P., Byrne, J.C., and Vaughan, D., 1995. The influence of prostate size on cancer detection. *Urology,* 46(6), 831-836.

Varki, A., Cummings, R., Esko, J., Freeze, H., Stanley, P., and Bertozzi, C., 2009. Glycomics. Essentials of Glycobiology. 2nd edition. *Cold Spring Harbor Laboratory Press, Cold Spring Harbor, NY*.

Velonas, V.M., Woo, H.H., Remedios, C.G.d., and Assinder, S.J., 2013. Current status of biomarkers for prostate cancer. *International Journal of Molecular Sciences,* 14(6), 11034-11060.

Walter, L.C., Bertenthal, D., Lindquist, K., and Konety, B.R., 2006. PSA screening among elderly men with limited life expectancies. *Jama,* 296(19), 2336-2342.

Wang, C., Tao, W., Ni, S., Chen, Q., Zhao, Z., Ma, L., Fu, Y., and Jiao, Z., 2015. Tumor-suppressive microRNA-145 induces growth arrest by targeting SENP1 in human prostate cancer cells. *Cancer Science,* 106(4), 375-382.

Wang, J., 1998. DNA biosensors based on peptide nucleic acid (PNA) recognition layers. A review. *Biosensors and Bioelectronics,* 13(7), 757-762.

Wang, J., 2006. *Analytical electrochemistry*. John Wiley & Sons.

Wang, J., Palecek, E., Nielsen, P.E., Rivas, G., Cai, X., Shiraishi, H., Dontha, N., Luo, D., and Farias, P.A., 1996. Peptide nucleic acid probes for sequence-specific DNA biosensors. *Journal of the American Chemical Society,* 118(33), 7667-7670.

White, N.M., Fatoohi, E., Metias, M., Jung, K., Stephan, C., and Yousef, G.M., 2011. Metastamirs: a stepping stone towards improved cancer management. *Nature Reviews Clinical Oncology* 8(2), 75-84.

Wians, F.H., Cheli, C.D., Balko, J.A., Bruzek, D.J., Chan, D.W., and Sokoll, L.J., 2002. Evaluation of the clinical performance of equimolar-and skewed-response total prostate-specific antigen assays versus complexed and free PSA assays and their ratios in discriminating between benign prostatic hyperplasia and prostate cancer. *Clinica Chimica Acta*, 326(1), 81-95.

Xu, L., Sun, C., Petrovics, G., Makarem, M., Furusato, B., Zhang, W., Sesterhenn, I., McLeod, D., Sun, L., and Moul, J., 2006. Quantitative expression profile of PSGR in prostate cancer. *Prostate Cancer and Prostatic Diseases*, 9(1), 56-61.

Yang, D.-K., Chen, L.-C., Lee, M.-Y., Hsu, C.-H., and Chen, C.-S., 2014. Selection of aptamers for fluorescent detection of alpha-methylacyl-CoA racemase by single-bead SELEX. *Biosensors and Bioelectronics*, 62, 106-112.

Yeh, J.-H., Sidhu, S.S., and Chan, A.C., 2008. Regulation of a late phase of T cell polarity and effector functions by Crtam. *Cell*, 132(5), 846-859.

Zehentner, B.K., Secrist, H., Zhang, X., Hayes, D.C., Ostenson, R., Goodman, G., Xu, J., Kiviat, M., Kiviat, N., and Persing, D.H., 2006. Detection of α-methylacyl-coenzyme-A racemase transcripts in blood and urine samples of prostate cancer patients. *Molecular Diagnosis & Therapy*, 10(6), 397-403.

Zhang, G.-J., Chua, J.H., Chee, R.-E., Agarwal, A., Wong, S.M., Buddharaju, K.D., and Balasubramanian, N., 2008. Highly sensitive measurements of PNA-DNA hybridisation using oxide-etched silicon nanowire biosensors. *Biosensors and Bioelectronics*, 23(11), 1701-1707.

Chapter 2. Materials and Methods

This Chapter will cover technical details about the immobilisation of probes on the electrode surface and physical principles of electrochemical techniques used for both detection as well as characterisation. Furthermore, the main focus is on self-assembled monolayer and polypyrrole surface chemistry along with particular electrochemical techniques (Electrochemical Impedance Spectroscopy and Square wave Voltammetry) used in this work.

2.1 Immobilisation techniques

In order to fabricate a successful biosensor, surface engineering of the sensor transducer plays a key role. Surface chemistry has been demonstrated as a tool to engineer biosensor surfaces and is one of the most crucial aspects for biosensor construction. It is also our very first aspect of the fabrication step where specific oligonucleotide-based probes are immobilised on the electrode surface. The proper control of the immobilisation step is essential in order to have good sensitivity, selectivity and stability of the biosensor (Campuzano *et al.* 2006). There have been many electrode surfaces reported for immobilisation, for example; gold, graphene, glassy carbon, carbon nanotubes, gold nanoparticles, glass, etc. The work in this thesis majorly employs planar gold electrode surface for the biosensor fabrication. Broadly, immobilisation techniques could be divided into physical adsorption, covalent binding, affinity and entrapment. These techniques pose advantages and disadvantages, some of which are listed in Table 2.1.

Table 2.1 Immobilisation techniques

Immobilisation strategy	Type of interaction	Advantages	Disadvantages	References
Physical	Noncovalent interactions like van der Waals, hydrophobic, electrostatic interactions	rapid, simple and low cost	It may result into random orientation of probe followed by instability of layer in different conditions like change in ionic strength of buffer, pH or other reagents	Du *et al.* 2012; Madaboosi *et al.* 2015
Covalent e.g. Self-assembled monolayer (SAM)	chemical bond between the probe and the electrode surface	It ensures good stability (bond can be broken under extreme conditions), results into well-ordered layer, high degree of control and thickness of electrode surface, high sensitivity and orientation	It may need prior modification of probes and linker molecules. It can be slow, irreversible process and expensive	Li *et al.* 2012; Jolly *et al.* 2015
Affinity	Specific interactions like between streptavidin and biotin or avidin and biotin	Appreciable orientation, ensures high functionalisation through specificity and well controlled	It employs use of biocompatible linkers and therefore are expensive	Ma *et al.* 2013; Zhang *et al*. 2013
Entrapment or encapsulation	Involves trapping of probes within a polymer like pyrrole, chitosan, dopamine, acrylamide etc.	Results in high entrapment of probes, high thermal stability, stability against nucleases, no covalent modification needed, well controlled polymer growth	Could result into leaching of probes and reduced binding efficiency.	Prabhakar *et al.* 2007; Jolly *et al.* 2016

This thesis will mainly focus on covalent immobilisation such as self-assembled monolayer (SAM) and polymer chemistry.

2.1.1 Self-assembled monolayer

There are many immobilisation techniques being reported for aptamer attachment to surfaces depending on the electrode surface and application. Specifically for gold electrode surfaces, self-assembled monolayer (SAM) is one of the most highly reported techniques because it results in a highly controlled density of biological probe

and thickness on the transducer surface (Hong *et al.* 1999). The key aspect to take into consideration for the immobilisation of oligonucleotide-based probes on gold surfaces is to have an optimum density (Keighley *et al.* 2008). Thiols, sulphides and disulphides have demonstrated very high affinity towards gold by forming a covalent bond between the sulphur and gold atoms, making alkane thiol-based SAMs very popular (Figure 2.1) (Bain *et al.* 1989; Bain and Whitesides 1989; Love *et al.* 2005).

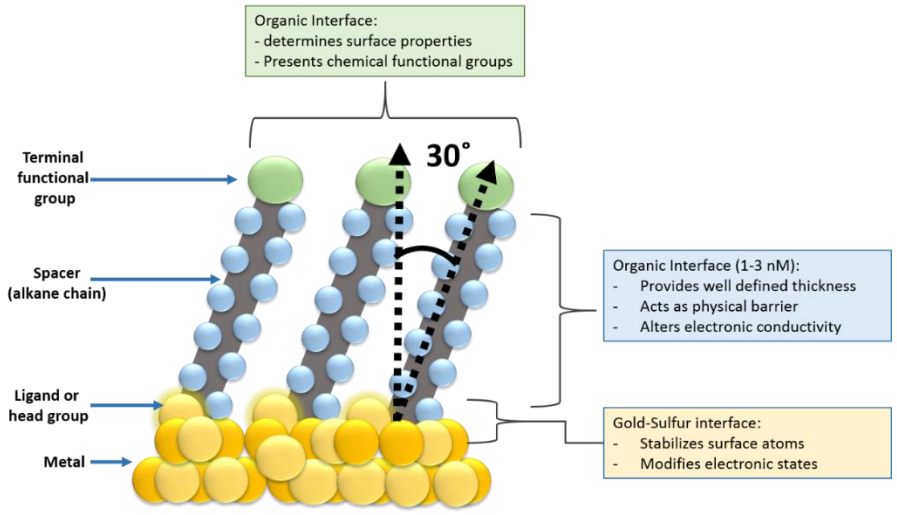

Figure 2.1 SAM formation on gold substrates. Adapted from Love et al. 2005.

Sulphur in the proximity of gold undergoes the following reaction:

$$RSH + Au \Leftrightarrow RS - Au + H^+ + e^-$$

The sulphur-gold reaction is spontaneous with 80%-90% coverage within the first few minutes, but a well organised layer is formed in no less than 12-16 hours (Schreiber 2000). The formation of well organised SAMs depends not only on factors such as presence of contaminants and surface quality (roughness and purity), but also on the length of the alkane thiols (Finklea 1996; Darling *et al.* 2002). In 2005 Love *et al.* determined the maximum density of alkane thiol on gold surfaces to be 4.64 x 10^{14} molecules/cm^2 with a gap of 4.99 Å between two adjacent molecules (Love *et al.* 2005). The time-dependent well organised SAM formation undergoes two main steps where there is spontaneous assembly within the first few minutes. In the early stages, alkane thiols lie flat on the gold electrode surface through physisorption, called the

'lying down' phase (Camillone Iii *et al.* 1994). Thereafter follows a chemisorption process where a semi-crystalline structure is formed due to van der Waals forces resulting in lateral movement until a tilt angle of about 30˚ between the hydrocarbon chains and the electrode surface is achieved (Love *et al.* 2005). It is worth mentioning that the ability of the thiols to move laterally along the gold surface results in the formation of well-ordered layering and healing any defects (Ulman 1996).

In such a process, even the terminal groups of the alkane thiol affect the SAM properties which define its interactions with the biological molecules. For example, a carboxylate group can be used to bind an amine terminated DNA aptamer using ethyl (dimethylaminopropyl) carbodiimide (EDC) and N-hydroxysuccinimide (NHS) activation step (Jolly *et al.* 2015). Sagiv *et al.* (Sagiv 1980) in 1980 demonstrated a chemisorbed monolayer using siloxane chemistry on a silicon surface. Chapter 4 will explain further silane based immobilisation of DNA aptamers on glass substrates.

Since SAM provides the provision of having various functional terminal groups, it permits the researchers to engineer novel and controlled biosensor designs. SAMs have been used to immobilise various molecules from biological (enzymes (Fang *et al.* 2003), DNA aptamers (Jolly *et al.* 2015), peptides (Laurent *et al*. 2008) etc.), chemicals (ferrocene (Mukherjee *et al.* 2013)) to metals (gold nanoparticles (Bertok *et al.* 2013), copper (Nishizawa *et al.* 1997), etc.) and more. Chapter 3 and Chapter 6 will further discuss different types of SAMs on the gold substrate to fabricate biosensors. The tailoring of SAM layers have led to the establishment of mixed SAMs. Keighley *et al.* (Keighley *et al.* 2008) in 2008 demonstrated the effect of DNA probe density using co-immobilised binary SAM on gold electrodes on hybridisation efficiency. In 2010 Wu *et al.* (Wu *et al.* 2010) reported a ternary SAM on screen printed gold electrodes as a potential antifouling SAM for amperometric detection of oligonucleotides. Furthermore, by tuning the composition of mixed SAMs, the number of functional groups can be monitored. In fact, by carefully selecting the spacer molecules, the desired hydrophobicity or hydrophilicity, as well as significant chemical reactivity, could be achieved. Such a strategy could impede non-specific binding and therein improve the electrochemical signals (Herne and Tarlov 1997).

2.1.2 Poly(pyrrole)-based immobilisation

Conducting polymers are organic materials that conduct electricity. The most conductive polymers used for electrochemical biosensor constructions are poly(pyrrole) (PPy), polythiophene and polyaniline (Figure 2.2).

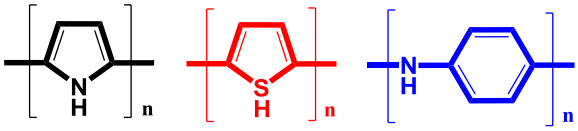

Figure 2.2 Organic conductive polymers: (black) poly(pyrrole); (red) polythiophene; (blue) polyaniline.

Among them, PPy is one of the most extensively used conducting polymers in the design of bioanalytical sensors (Peng *et al.* 2009; Ramanavičius *et al.* 2006). This is due to its copious properties such as redox activity (Han *et al.* 2005), ion-exchange and ion discrimination capacities (Johanson *et al*. 2005; Weidlich et al. 2005), strong absorptive properties (Azioune *et al.* 2005; Chehimi *et al.* 1999), catalytic activity (Khomenko *et al.* 2005) and biocompatibility (Wang *et al.* 2004). PPy as a polymer can be further characterised by its high electrical conductivity, hydrophilic character and high stability in water (Andrade 1985). In fact, its low oxidation potential enables a pyrrole polymer film to be grown from an aqueous solutions which is compatible with most of the biological elements (Asavapiriyanont *et al.* 1984).

2.1.2.1 Synthesis of poly(pyrrole) films

PPy films can be synthesised by either chemical or electrochemical methods. The first method consists of chemical oxidation of pyrrole monomers in aqueous or organic solutions in the presence of a metal catalyst. Rodriguez *et al.* synthesised PPy in the presence of hydrogen peroxide or iron chloride in acetonitrile or water (Rodriguez *et al.* 1997). Chemical synthesis of PPy is limited by a purification step from catalyst and secondary products. Also the composition and structure are not well defined and many defects in the polymer chain can occur resulting in a decrease in conductivity. More often, a PPy film is formed by electro polymerisation of its monomers. This method allows a reproducible well-defined structures and properties of the polymer. As a result

a film is obtained with known thickness. The polymerisation mechanism of the succession of electrochemical and chemical reaction is represented in Figure 2.3.

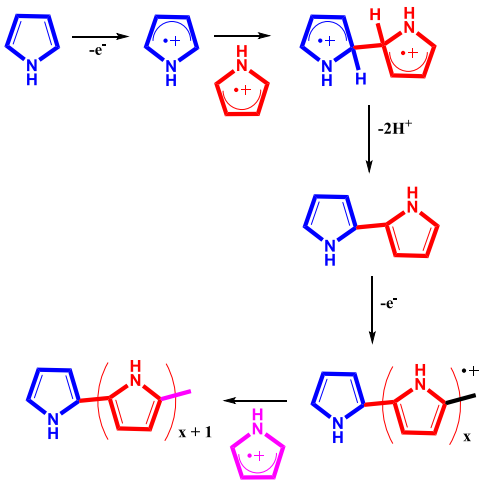

Figure 2.3 Mechanism of electro-polymerisation of PPy.

Electro polymerisation is achieved through a few electrochemical steps. The first step consists of the electrochemical oxidation of monomers to form radical cations. This is followed by dimerization via coupling of radical/radical with the elimination of two protons. Dimers can easily be oxidized because of stabilisation of radical cations. The oxidised dimer can be coupled with another oxidized monomer or dimer. Polymerisation is terminated when a radical cation is no longer reactive or when the last reactive chain is blocked by steric effects.

2.1.2.2 Immobilisation onto poly(pyrrole)

Different strategies are investigated to immobilise biomolecules on PPy. For example, biomolecules can be entrapped in a polymer film during electro polymerisation of monomers. In 1999 Wang *et al.* reported a label-free approach consisting of the introduction of single-strand DNA as doping ions during electro polymerisation of PPy films (Wang *et al.* 1999). DNA hybridisation was monitored by the decrease in current changes of PPy due to the reduction in conduction. A similar approach was reported by Komarova *et al.* in 2005, where an electrochemical DNA sensor was constructed with an ultrathin film of conducting PPy doped with an oligonucleotide

probe (Komarova *et al.* 2005). A low detection limit of 0.16 pM was demonstrated using chronoamperometry measurements. However, such an approach faces certain drawbacks such as possible denaturation of biomolecules (in the case of enzymes), leaching of probes from the polymer or uncontrolled orientation of probes in the polymer layer which can decrease the performance of the sensor.

Another method consists of direct physical adsorption of biomolecules on PPy films as reported in the literature and are mostly for enzymatic biosensors (Ahuja *et al.* 2008; Apetrei and Apetrei 2013), however, changes in the ionic strength or pH can cause the release of biomolecules from the surface, especially during the regeneration step of the sensor by acidic solutions.

The covalent approach to anchor biomolecules on PPy films is also well developed. Biomolecules carrying amine, carboxylic or activated ester groups can be covalently attached to a functionalised polymer film on its nitrogen or carbon positions. For instance, a pyrrole monomer can be modified by chemical groups and then electro polymerised to form a PPy film bearing the function to be able to react with bioreceptors. Pyrrole monomers can be simply modified with carbonyl chain ending with chemical groups, which can then interact with biomolecules. There are some examples of pyrrole modifications, where the pyrrole monomer was modified with propylic acid (Dong *et al.* 2008), 3-aminopropyl (Bisht *et al.* 2005) and activated ester as N-hydroxysuccinimide (Ionescu *et al.* 2006; Ionescu *et al.* 2007) (Figure 2.4).

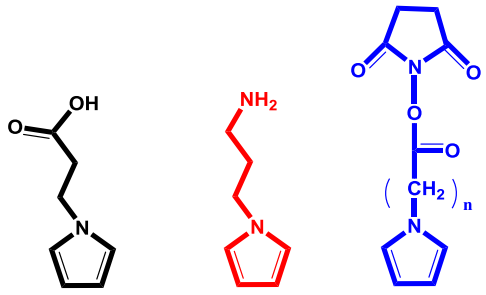

Figure 2.4 Structures of pyrrole derivatives: (black) pyrrole propylic acid, (red) N-3-aminopropylpyrrole, (blue) pyrrole NHS.

In 2002 Rodrígez *et al.*(Rodrígez *et al.* 2002) synthesised pyrrole modified with biotin set apart by a polyethylene glycol chain, which prevented the biosensor from non-specific interactions (Figure 2.5 black). In the literature, the combination of pyrrole

with some redox markers was also described and was used, for example, for the modification of pyrrole with nitrilotriacetic acid (NTA) for complexation of Cu^{2+} ions (Figure 2.5 blue). Such a complexation of Cu^{2+} ions allowed immobilising an histidine modified antibody specific for a herbicide atrazine (Ionescu *et al.* 2010) or histidine modified thrombin aptamers (Xu *et al.* 2013).

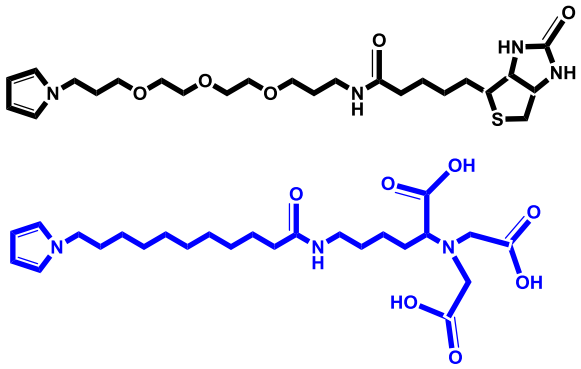

Figure 2.5 Structures of pyrrole monomers functionalised with PEG-biotin (black) and with NTA (blue).

3-substituted PPy has demonstrated an advantage in maintaining its full intrinsic electrical properties compared to N-modification. Modification of pyrrole in the 3' position allows immobilisation of the bioreceptors and a direct measurement of sensing processes. A first example was demonstrated through covalent attachment of bioactive peptides inhibitors of enzymes. The interaction of peptides and enzymes was followed through the electrochemical properties of the PPy layers. This work demonstrated, for the first time, a proven concept that PPy could be used as a molecular wire for transduction of biological events (Garnier *et al.* 1994). Covalent binding of ssDNA probe was demonstrated for the first time in 1997 (Korri-Youssoufi *et al.* 1997a; Korri-Youssoufi *et al*. 1997b). In this case two monomers of pyrrole were substituted by a N-hydroxyphtalamide group and acetic acid group and then electrochemically polymerised. The copolymer film allowed from one side covalent linking of DNA probe to the monomer modified with N-hydroxyphtalamide. This linking was possible by functionalisation of the DNA probe with amine groups which can be attached to the PPy layer via an amide link. The second side modifications of pyrrole by carboxylic groups allowed protecting the surface against non-specific interactions due to electrostatic repulsion of negatively charged DNA (Garnier *et al.*

1999). Since this work, various studies using this copolymer have been published aiming at improving the sensitivity of the detection system (Garnier *et al.* 2007; Korri-Youssoufi and Yassar 2001) and studying the electrical properties of the PPy layers (Tlili *et al.* 2005). For example, Peng *et al.* developed various functionalised pyrrole monomers bearing acid functions for DNA sensors. In a first approach, a monomer pyrrole bearing butanoic acids was synthesised. After electro polymerisation, a ssDNA probe bearing amine group was covalently attached to the PPy via an amide link (Figure 2.6) (Peng *et al*. 2005). Later the group reported modifications of pyrrole with the same function through unsaturated carbon chain of various lengths (Peng *et al.* 2007a; Peng *et al.* 2007b) (Figure 2.6).

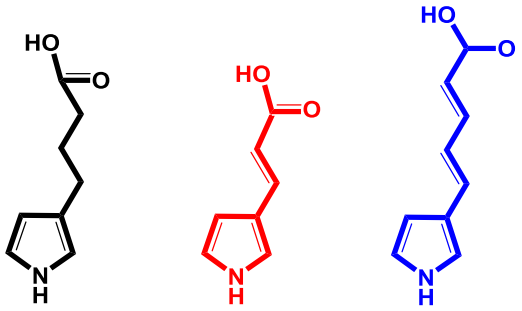

Figure 2.6 Pyrrole derivatives developed by Peng et al.(Peng et al. 2007a; Peng et al. 2007b; Peng et al. 2009) Modifications of pyrrole with (black) butanoic acid; (red) 3-pyrrolylacrylic acid; (blue) 5-(3-pyrrolyl) 2,4-pentadienoic acid.

Various methods have been developed with PPy in biosensor devices throughout the last decade. However, electrochemical modification of PPy is very new and gaining a lot of interest; thanks to its easy one step procedure. Chapter 5 will demonstrate the use of a conducting PPy film on gold surfaces for the development of an electrochemical aptasensor taking into account electrochemical modification procedures.

2.2 Electrochemical techniques

To fully understand the typical setups for an electrochemical measurement, it is crucial to describe the environment around the electrode/solution interface. This section will

further describe the techniques that have been employed for the characterisation and detection of a particular analyte.

2.2.1 Electrochemical interface

Electrochemistry is defined as a study that investigates the correlations between the electrodes (containing electrons) and electrolytes (containing ions) resulting in electrical properties and chemical effects respectively (Bard and Faulkner 1980). In most of the electrochemical studies, the main focus is on the factors that affect the transportation of the charges across the electrode/electrolyte interface. In fact, in an electrochemical cell, generally, the interest is only on the working electrode (WE).

With the help of the voltage applied, one can easily modulate the potential of the WE. When the potential of the WE is pushed to higher negative values, electrons tend to flow from the electrode surface to the electrolyte solution. Such an effect is due to the gain of energy by the electrons to escape the surface and fill the vacant holes of the ions in the electrolyte solution. Such an effect is attributed to a reduction current. Similarly, an oxidation current is created when the potential of the WE is driven to more positive potentials. Such a reaction involving transportation of electrons between the electrode and the electrolyte solution is termed as a Faradaic reaction. A Faradaic reaction follows Faraday's law given by $i=nF$, where the quantity of electricity passed (i) is directly proportional to the rate of reaction and amount of electrons (n) (Bard and Faulkner 2001) and F is Faraday Constant. On the other hand in a non-Faradaic process, there is no flow of electrons involved, leading to accumulation of charges at the electrode/electrolyte interface causing polarisation of electrodes.

In an electrolyte solution, a potential applied to the electrode causes redistribution of the charges leading to changes in surface potential. At a given potential, the electrode/electrolyte interface is in principle characterised by the theory of the electrical double layer (DL); more specifically by the double layer capacitance (Bard and Faulkner 1980). The electrical DL can be simply explained as the rearrangement processes of the charges in the electrolyte in close proximity to the electrode surface in order to counter balance the charge irrespective of the potential of the electrode

(Bard and Faulkner 2001). Electrical DL was best described by Otto Stern in 1924 who suggested combining the theory of Helmholtz model and Gouy-Chapman model (Figure 2.7).

In Stern's model, immersion of the electrode in an electrolyte solution produces a high electric field and presents a row of firmly adsorbed counter ions. It is worth mentioning that this area represents a low relative permittivity. The region established between the electrode surface and the centres of adsorbed ions is called the inner Helmholtz plane (IHP); as we move further away from this region an ionic cloud (diffuse layer) is present. Such an ionic cloud consists of balancing processes occurring between electrostatic and thermodynamic motions. Also, as we move beyond the IHP, the permittivity increases exponentially. Such an arrangement also affects the electrical potential (Ψ) from the electrode surface to the bulk electrolyte. Up to the IHP, the electrical potential decreases quasi-linearly, while it decreases exponentially within the diffuse layer.

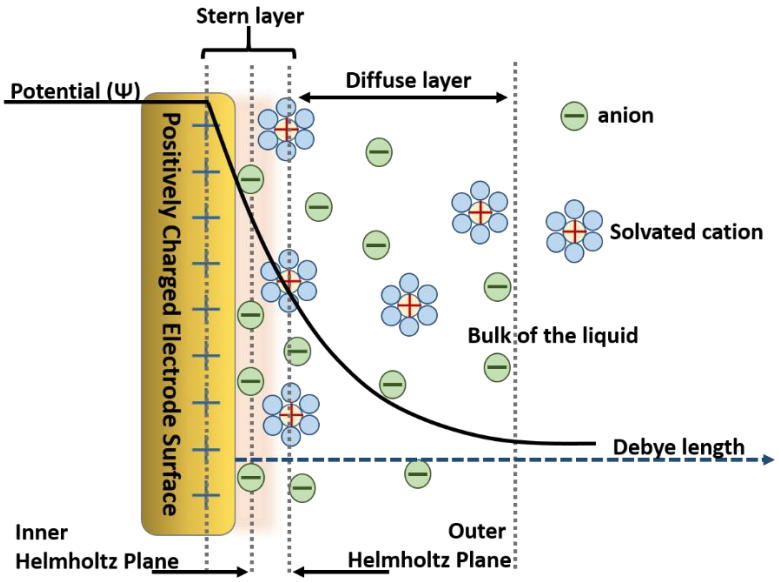

Figure 2.7 Schematics of the electrical double layer by the Gouy–Chapman–Stern model. Adapted from Bard et al. (Bard and Faulkner 2001).

Beyond the IHP, ions approach to the electrode surface due to electrostatic attraction, however, staying distant as non-specifically adsorbed molecules. Such molecules are

solvated and form the outer Helmholtz plane (OHP). Moreover, the two regions formed by the IHP and OHP form the Stern layer. The molecules further away from this layer lack the competency to compensate with the overall charges, thus forming the diffuse layer. Because of these two Helmholtz planes, there is a capacitance due to the DL. It consists of two capacitances in series; one is called the Stern capacitance and the second is the capacitance of the diffuse layer. The distance covered from the OHP to the point where the ions are affected by the electrostatic effect of the surface is defined by the Debye length (thickness of the diffuse layer). In cases like impedimetric and potentiometric biosensors, the limit of detection (LOD) is majorly dependent on the Debye length (λ_D) (Bard and Faulkner 2001). It is imperative to study the ionic effect on the sensitivity of the sensor and is well advised to work within the Debye length range (Figure 2.8). It is also well known that many biomolecules have inherited charges even under physiological conditions. For instance, DNA/RNA molecules are negatively charged due to a sugar-phosphate backbone which can be considered as a cylindrical structure of about 1.5-2 nm in diameter with an estimated length of the nucleotide to be 0.34 nm (Piunno *et al.* 1999). On the other hand, the charge on the proteins is generally dependent on the pH of the solution. The net charge of the protein be calculated by knowing the isoelectric point of the protein. The isoelectric point is characterised by the pH at which the net charge of the protein is zero.

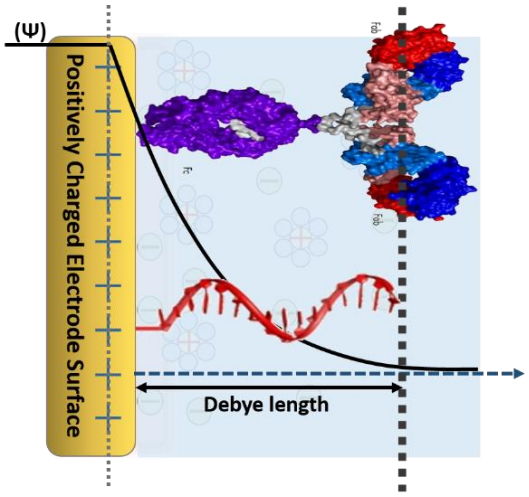

Figure 2.8 Schematic of difference in antibody size and DNA aptamer size with respect to electrical double layer.

Stern *et al.* (Stern *et al.* 2007) demonstrated that the surface of the biomolecules in an electrolyte is surrounded by its counter charges resulting in Debye screening. For an electrolyte solution, Debye length (λ_D) can be expressed as:

$$\lambda_D = \sqrt{\frac{\varepsilon_0 \varepsilon_r kT}{2N_A q^2 I}} \quad (2.1)$$

Where ε_0 and ε_r are the permittivity's of free space and dielectric constant of the solution respectively, k is Boltzmann constant, *T* is temperature, N_A is Avogadro's number, q is the electron charge and *I* is the ionic strength. The ionic strength can be further expressed as:

$$I = \frac{1}{2}\sum_j c_j z_j^2 \quad (2.2)$$

Where c_j is the concentration of ion j and z_j is the charge of the jth ionic species. Therefore, the DL thickness is inversely proportional to the square root of the ionic strength of the electrolyte solution. Although the Debye length is a limiting factor for the sensitivity of a biosensor, researchers have come with alternatives to overcome such a screening effect. Gao *et al.* in 2015 demonstrated the use of polymer chains (like PEG) on the electrode surface to increase the effective screening length resulting in detection of biomolecules in a high ionic strength electrolyte solution (Gao *et al.* 2015). There are other studies that have demonstrated new strategies to work under high ionic strength electrolyte solutions (Jang *et al.* 2015; Kulkarni and Zhong 2012; Stern *et al.* 2010).

2.2.2 Electrochemical impedance spectroscopy

Electrochemical impedance spectroscopy (EIS) is a label-free electrochemical technique that has been widely used as a detection system. It exploits the electrical properties of the molecules to be detected by measuring the changes in the impedance at the electrode/electrolyte interface (Bond and Scholz 2010; Lasia 2002).

EIS measurements are usually based on the measurement of Faradaic processes; employing a redox couple in an equal concentration of reduced and oxidised forms in order to simplify the analysis. A Faradaic process is the charge transferred across the

WE and electrolyte interface as a result of an electrochemical reaction. In EIS, a small AC voltage is superimposed on the formal potential of the respective redox couple.

The resistance of the system is, therefore, mainly a result of how easily the redox couple can reach the electrode surface. The measurement is then scanned on a range of frequencies, typically spanning from 0.1-1 MHz to 0.1-0.01 Hz. For the current study the range used was 100 kHz to 100 mHz. In order to perform such an analysis, a potentiostat with a frequency-response analyser (FRA) is used. Although EIS investigates the full frequency span response, it could be easily implemented in a practical biosensor by possibly selecting a single frequency.

EIS is a measure of the AC current flowing between the electrodes into the bulk electrolyte of the cell. Furthermore, the term "spectroscopy" refers to the measurements recorded by scanning the frequency of the AC signal. A small AC voltage is applied to maintain a certain thermodynamic equilibrium at the electrochemical interface which aids in easy separation of mass transfer and electron transfer. Such a sinusoidal voltage signal can be expressed as a function of time ($V(t)$):

$$V(t) = V_0 \sin(\omega t) \qquad (2.3)$$

Where, V_0 is the amplitude of the voltage signal and ω refers to angular frequency ($\omega = 2\pi f$). f refers to the frequency in Hertz (Hz). As a consequence, an AC current signal ($I(t)$) as a function of time is obtained. $I(t)$ obtained with the same frequency (f) is also referred to current density which is expressed as:

$$I(t) = I_0 \sin(\omega t + \varphi) \qquad (2.4)$$

Where I_o is the current amplitude and φ is the phase angle which depends on the impedance of the respective system. Such a process of applied voltage and current measured can also be represented as shown in Figure 2.9:

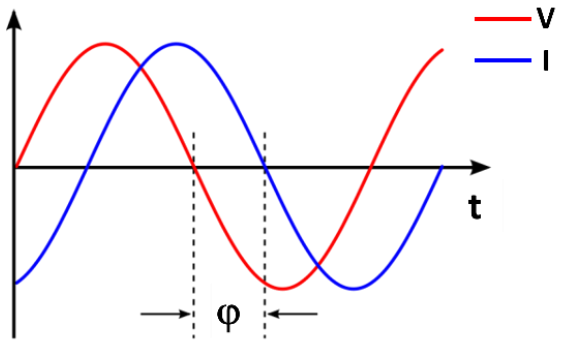

Figure 2.9 AC signal of applied voltage and obtained current response.

The impedance is measured by applying a small AC voltage signal, through which the real and the imaginary part of the impedance are obtained. In principle, the measurement works by applying the potential (V_t) and measuring the current (I_t) at the WE. In general, the impedance (Z) can be determined by Ohms law using equation 2.3 and 2.4:

$$Z = \frac{V_t}{I_t} = \frac{V_0 \sin(\omega t)}{I_0 \sin(\omega t + \varphi)} = Z_0 \frac{\sin(\omega t)}{\sin(\omega t + \varphi)} \quad (2.5)$$

In order to represent a complex impedance, Euler's expression is employed which is expressed as:

$$\exp(j\varphi) = cos\varphi + jsin(\varphi) \quad (2.6)$$

Where j is an imaginary number equal to $(-1)^{1/2}$. Also, equation 2.3 and 2.4 can be further expressed as a function of time:

$$V(t) = V_0 exp(j\omega t) \quad (2.7)$$

$$I(t) = I_0 exp(j\omega t + j\varphi) \quad (2.8)$$

Therefore, impedance can be expressed as a complex number using equations 2.7, 2.8 and 2.6 in equation 2.5

$$Z = \frac{V_t}{I_t} = Z_0 \exp(j\varphi) = Z_0(cos\varphi + jsin\varphi) = Z' + jZ'' \quad (2.9)$$

The real part of impedance (Z') is described as the resistance to the flow of current by the circuit, whereas the electrical energy storage ability by the circuit is reflected by the imaginary part of the impedance (Z''). In other words, the real and imaginary part of impedance are associated with the resistive and capacitive components of the biosensor interface.

The impedance of the electrochemical interface is usually interpreted through biosensor specific equivalent electrical circuits. The most common circuit is the Randles equivalent circuit (Figure 2.10) that includes the solution resistance (R_s), the resistance for electron transfer (R_{ct}), the DL capacitance (C_{dl}) and a Warburg impedance element (W). While the W element gives information about the diffusion of redox couple through the surface layer, the R_s values depend only on the solution along the distance between the WE and RE. Constant phase element (CPE) models the capacitive behaviour of the double layer replacing the infrequently ideal; however, the deviations from an ideal capacitance (n = 1) are reasonably small.

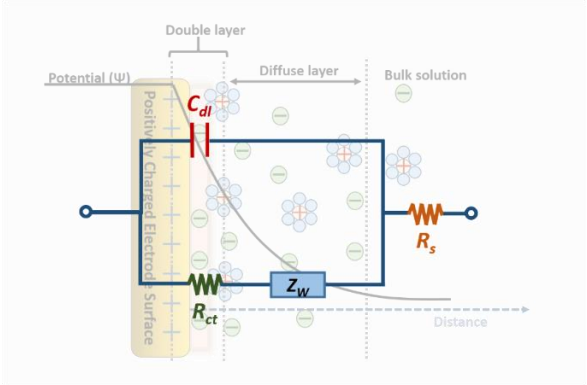

Figure 2.10 Randles equivalent circuit where R_s is the solution resistance, R_{ct} is the charge transfer resistance (impedance), C_{dl} is the double layer capacitance and Z_W is the Warburg element.

The slight modification that was introduced in the Randles equivalent circuit was the replacement of C_{dl} by a CPE. The impedance of CPE is given by equation 2.10:

$$Z_{CPE} = Y_0(j\omega)^{-\alpha} \qquad (2.10)$$

Where, ω is the frequency, Y_0 is the magnitude of admittance, α is an exponent with a value between 0 and 1 (In a CPE, $\alpha \leq 1$). It is important to know that neither Y_0 nor α

are dependent on frequency in Z_{CPE}. From the Z_{CPE}, it is also possible to get an estimation of the C_{dl} using the relationship (Hsu and Mansfeld 2001):

$$C_{dl} = \frac{(Y_o R_{ct})^{1/\alpha}}{R_{ct}} \quad (2.11)$$

In principle, Faradaic currents are affected by diffusion processes. Furthermore, *W* represents the pseudo-impedance due to the mass transfer, which is simply the diffusion of ions from the bulk solution to the electrode surface. *W* at lower frequencies becomes predominant with a phase angle of 45˚ in a diffusion controlled Faradaic process.

The results from an EIS response can be represented in a Nyquist plot (Figure 2.11). This plot enables a direct comparison of the R_{ct} values given by the diameter of the semicircle along the *Z*' axes.

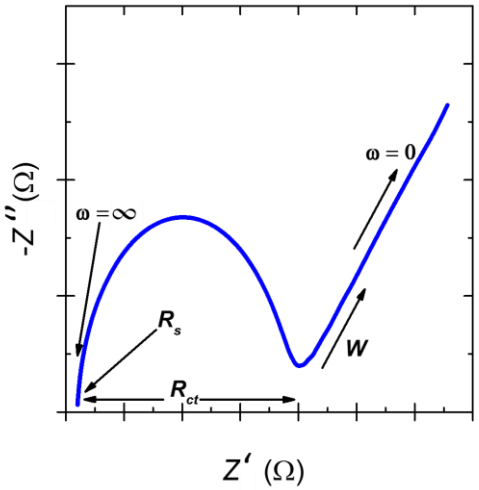

Figure 2.11 Typical Nyquist Plot.

2.2.2.1 Non-Faradaic EIS experiments

A non-Faradaic EIS experiment is performed in the absence of a redox couple. As a consequence, only capacitive changes are monitored. In such a measurement, specific importance is given to the double layer capacitance (C_{dl}) rather than the charge transfer resistance (R_{ct}) of the system (Tsouti *et al.* 2011). One of the common

approaches of calculating capacitance reported in the literature is based on the assumption that the R_{ct} and W contributions can be neglected (Couniot *et al.* 2015). Consequently, a simplified equivalent circuit is obtained, consisting of a resistor in series with a capacitor as shown in Figure 2.12.

Figure 2.12 Equivalent circuit for a non-Faradaic measurements.

As a result, equation 2.9 can be represented as:

$$Z = Z' + jZ'' \cong R_s^* - j\frac{1}{\omega C_{DL}^*} \tag{2.12}$$

Where, the real part of the capacitance can be expressed as:

$$C_{dl}^* = -\frac{1}{\omega Z''} \tag{2.13}$$

Another approach that has been reported includes calculation of a complex capacitance (C*). In such cases, a C^* can be calculated from EIS data using the following relationship (Jolly *et al.* 2015; Jolly *et al*. 2016):

$$C^* = -\frac{Z''}{\omega|Z|^2} - j\frac{Z'}{\omega|Z|^2} = C' + jC'' \tag{2.14}$$

Where C' and C'' are calculated from the measured values of $Z^{''}$ and $Z^{'}$. Furthermore, C* can be plotted as a *Cole-Cole* plot. Figure 2.13 depicts an example of non-Faradaic EIS measurement of the electrode modified with a PNA sequence (left is a Nyquist plot and right is calculated capacitance from EIS data, diameter of the semicircle of which gives an estimate of the capacitance of the system).

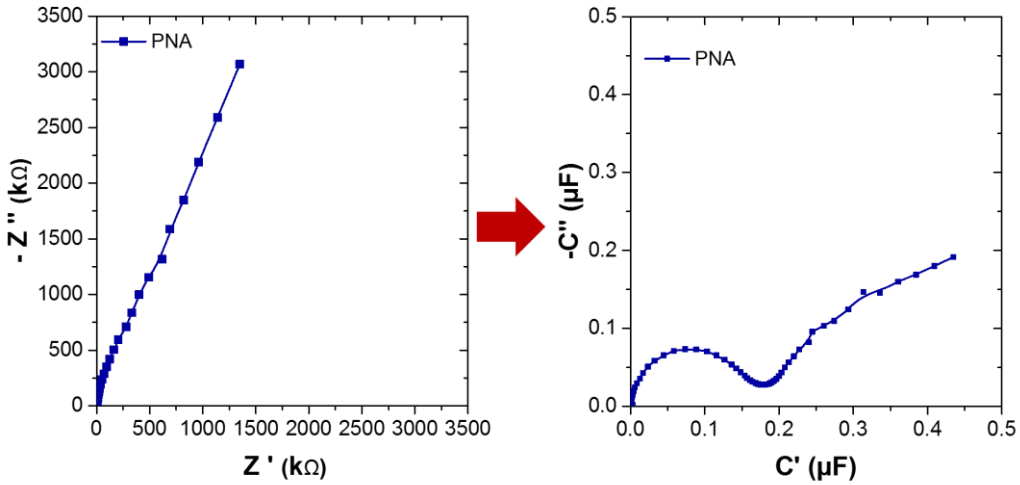

Figure 2.13 Figure showing a Nyquist plot (left) representing the impedance of the system. On the right is a Cole-Cole plot representing the capacitance of the system calculated from impedance data.

There are numerous reports that have demonstrated the development of capacitive sensors (Berggren *et al.* 2001; Tsouti *et al.* 2011). Regardless of the simplicity of measurement, a capacitive sensor based on electrode-electrolyte interfaces needs a compact insulating layer. To address such an issue, in Chapter 5 and Chapter 6, a PEG-based SAM has been employed in order to obtain a compact and defect-free SAM which will prevent leakage currents. Leakage currents are important to exclude as they could result into short-circuiting the metal electrode and solution phases, which in turn may affect the detection of the target (Berggren *et al.* 2001). PEG was employed in the immobilisation procedures because it has been reported that longer linkers form well organised SAMs (Porter *et al.* 1987). Although there are numerous studies on capacitive sensors, many results among them have demonstrated contradictory results (i.e. showing both increment and decrement of capacitance using the same sensor type and target analyte) (Daniels and Pourmand 2007). Rational explanations are given for every specific contradictory result. Nevertheless, no self-contained study has been performed in order to clearly correlate molecular binding events occurring at the electrode surface to EIS signals. As a consequence, the signal changes obtained have been attributed to changes in various factors, for example, dielectric properties, displacement of water molecules, the addition of a metal-like surface, electrostatic

interactions, and the conformation of molecules onto the surface electrodes and so on. Using such an approach, Chapter 6 reports on the development of a capacitive PNA-based biosensor for the detection of miRNAs using AuNPs as an amplification technique.

2.2.3 Amperometric detection

Amperometric biosensors are based on measurement of current produced in a solution due to a chemical reaction when a fixed potential is applied across the electrodes. However, when the current is measured as a function of potential, it is called voltammetry (Grieshaber *et al*. 2008). In principle, either the analyte directly results in a redox reaction at the electrode surface or the current is generated using an electroactive mediator which interacts with the target molecule (Luppa *et al.* 2001). Amperometric techniques are considered some of the most powerful and sensitive techniques, even though most of them often employ redox mediators (Thévenot *et al.* 2001).

On application of a potential in voltammetry experiments, currents are generated as a result of three factors: capacitive currents, Faradaic currents and adsorption effects. Capacitive currents and adsorption currents make up the background current which does not add any information to the analytical information about the electrochemical reaction. It is worth mentioning that such background signal could be a cumulative effect of the redox reaction of impurities present in the solution. On the other hand, the Faradaic current could provide the analytical information about the processes of interest in the electrochemical setup.

2.2.3.1 Cyclic voltammetry

A well established and widely used amperometric technique is cyclic voltammetry (CV). The main aspect of using a CV is to attain a signal in the form of a current from the system under investigation with respect to the constraints responsible for the production of an electrochemical reaction. Such a response occurs by imposing a

varying electrode potential of the WE (potential sweep) between two set potential limits as shown in Figure 2.14 (Bard and Faulkner 1980).

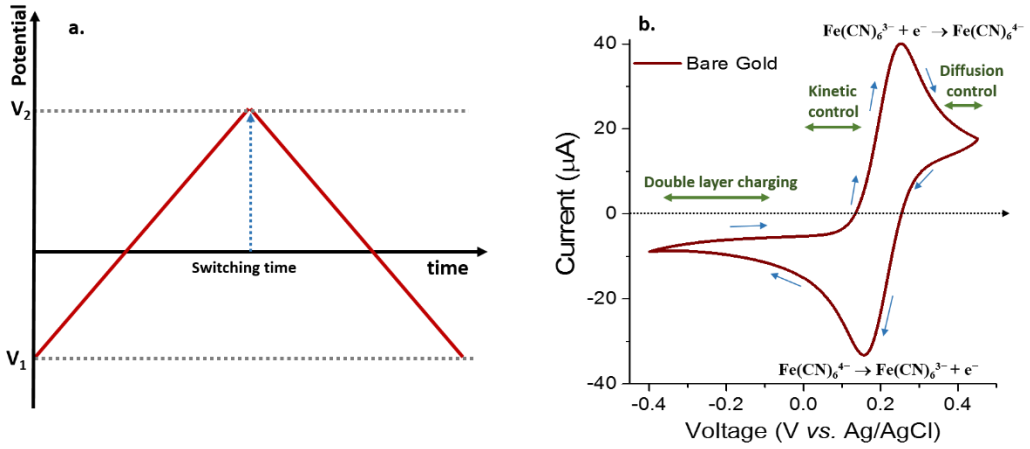

Figure 2.14 Potential plot of a redox reaction diffusing in solution (a); Cyclic voltammetry of a fully reversible redox reaction at the gold working electrode in 10 mM PBS, pH 7.4 containing 10 mM ferro/ferricyanide [Fe(CN)6]3-/4- vs. Ag/AgCl reference electrode (b).

By doing so, if it happens that in the solution, some molecules can lose electrons (oxidation) or gain electrons (reduction), the CV scan will show its respective peaks. This technique allows recognition and quantification of a large number of compounds, and also to study chemical reactions. For example in Figure 2.14, when the voltage applied to the WE increases and reaches closer to the reduction potential of the redox molecule, which in this case is $[Fe(CN)_6]^{3-/4-}$, WE loses an electron which becomes associated with $[Fe(CN)_6]^{3-}$ and in turn becomes reduced. Such a flow of electrons from the electrode to the solution causes the appearance of a reduction peak in the voltammogram. After an initial peak, there is an asymptotical decrease in the Faradaic current with the diffuse layer. The opposite occurring when the electrode potential moves towards the oxidation potential of the redox couple in a reversible process. Such a system can be described by the Randles-Sevčik law which describes the effect of scan rate on the peak current:

$$i_p = 0.4436An^{\frac{3}{2}}\left(\frac{F^3DS}{RT}\right)^{\frac{1}{2}}c \qquad (2.15)$$

Where *A* is the electroactive area of the electrode, *n* is the number of electrons involved in the transfer process, F is Faraday's constant, D is the diffusion coefficient of the redox species, S is the scan rate, T is temperature and c is the bulk concentration of the redox species. In a CV, certain parameters such as the scan rate, can account for the reversibility of some reactions. In other words, the potential scan can produce a peak current for all analytes that can be reduced in the range of the potential sweep. The current (*I)* in the system which is measured either continuously or at specific times, corresponds to the electronic transfer allowing reduction of metal ions on the electrode surface (cathode) and is mainly the sum of Faradaic current, I_f, and non-Faradaic current, I_c.

I_f results from the redox reactions of the analytes at the interface of electrode/electrolyte. I_f constitutes the major component for quantitative analysis of test compounds. I_f can be influenced by the following three factors:

1. The diffusion rate (mass transfer) of the oxidized electroactive species in the electrolyte solution towards the electrode (and vice versa for a reduced species).
2. The electron transfer rate at the electrode/electrolyte interface in case of irreversible reaction.
3. The rate of the chemical reactions preceding or following the electron transfer.

In fact, the current (*I*) is not only a function of the potential (*E*) but also of time, t. On the other hand, I_c is due to the C_{DL} represented by the interface between the surface layer of the electrode and the adjacent layer of the solution given by:

$$I_c = C_{DL} \frac{dv}{dt} \tag{2.16}$$

Where v is the potential applied to the electrode surface. The capacitive current depends on the surface of the electrode, the rate of change of potential with time and the composition of the medium, but not on the concentration of the test compound. It is always suggested to have a reasonable low scan rate since I_c increases linearly with the scan rate. In this dissertation, CV has been employed as a characterisation technique as well as a fabrication technique to perform polymerisation.

2.2.3.2 Square wave voltammetry

CV, as explained in the previous section, produces both Faradaic and non-Faradaic currents and as a result of which the differentiation of analytical peaks from background signal becomes difficult. In order to circumvent the non-Faradaic or capacitive currents, methods like square wave voltammetry (SWV) have been developed (Bard and Faulkner 2001) (Figure 2.15). Such voltage pulsed techniques results in an increase in the ratio of Faradaic current to non-Faradaic current, thus the sensitivity of the measurement.

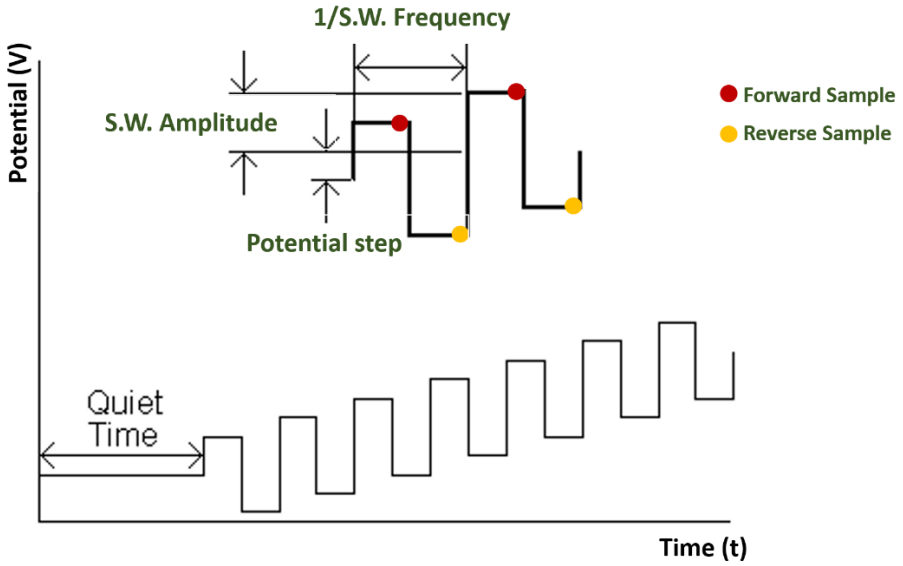

Figure 2.15 Square Wave voltammetry potential variation waveform.

The excitation signal in a SWV measurement consists of a repetitive symmetrical square wave pulse of amplitude V_{sw} superimposed on a staircase wave of potential step height ΔV and with a pulse period t, where the forward pulse of the square wave coincides with the staircase step. The net current, i_{net}, is achieved by taking the difference between the forward current and reverse current ($i_{total} - i_{reverse}$) which is calculated at the end of each half cycle respectively. With such a subtraction, the non-Faradaic current is further suppressed. The peak height obtained from SWV, due to

redox reaction, is directly proportional to the concentration of the electroactive species.

2.3 Other characterisation techniques

Apart from the electrochemical techniques mentioned earlier, surface plasmon resonance (SPR) and Fourier transformation infrared spectroscopy (FT-IR) were also used during the development of specific biosensors reported in this thesis.

2.3.1 Surface Plasmon Resonance

Surface plasmon resonance (SPR) offers a powerful and rapidly developing technique for the study of molecular interactions, where the probes are confined to the surface. It not only offers a label-free detection but also provides real-time quantitative data for the molecular interactions. In general, a SPR technique consists of one probe which is immobilised on the SPR chip (for example DNA aptamers specific to PSA, Figure 2.16) and the analyte in the solution which is flowed over the surface (e.g. PSA). Finally, the binding interactions are measured by monitoring the slight changes in the refractive index (RI) at the sensor surface using optical methods.

SPR is a phenomenon that occurs when a polarized light hits a thin metal film at the interface of media with different RI. The generation of plasmons occurs through proper coupling of incident light to free electrons of the metal. Such a phenomenon can be accomplished by employing an attenuated total reflection technique (ATR). In ATR, plasmons are generated by an induced evanescent wave under total internal reflection conditions. Under total internal reflection conditions, an evanescent wave penetrates into the metal and decays exponentially in the perpendicular to the metal surface into the medium. The depth of the evanescent wave from the sensor surface is within 300 nm depending on the gold thickness and RI of the medium over the metal surface, which is useful for measurements (Van Der Merwe 2001). When a light is directed to the metal film, at a certain incident angle, the light wave vector matches the metal plasmons wave vector resulting in the resonance of the plasmons. During

such a condition, energy from the photons are transferred to plasmons, resulting in a minimum on the reflectance intensity, thus defining the SPR spectrum (Salamon *et al.* 1997). SPR techniques excite and detect collective oscillations of free electrons also known as surface plasmons, via the Kretschmann configuration, in which light is focused onto a metal film through a glass prism and the subsequent reflection is detected (Figure 2.16).

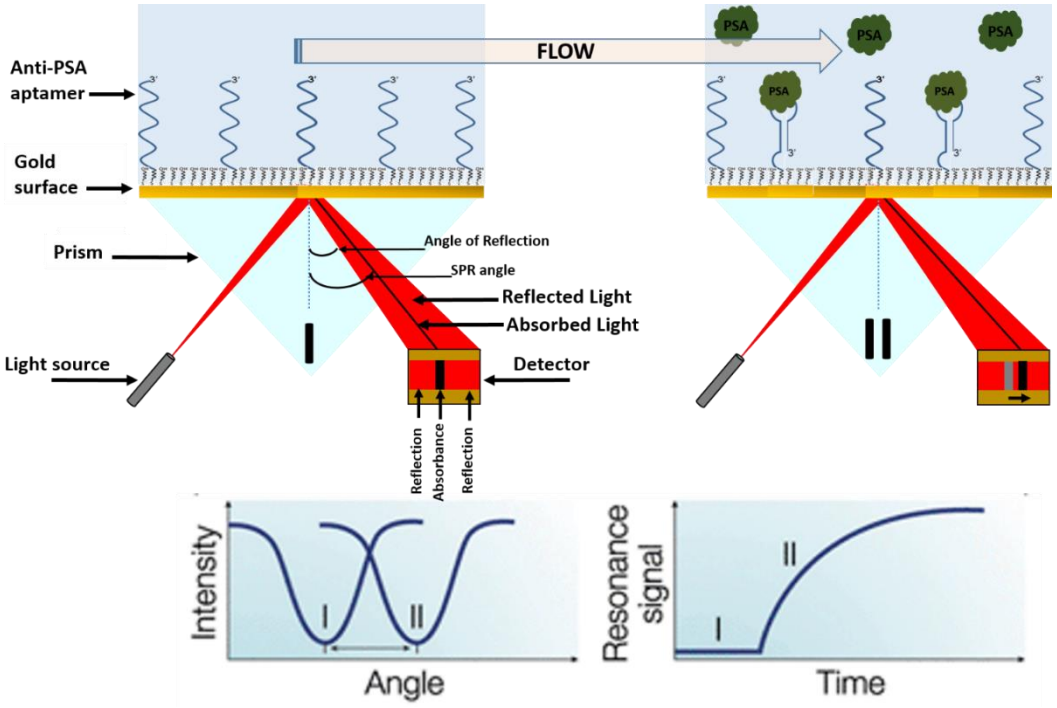

Figure 2.16 Surface Plasmon Resonance schematics (SPR). The excitation of surface plasmons results in a dark line in the reflected beam, and the angular position of the dark line shifts as a molecule-binding event takes place. SPR causes an intensity dip in the reflected light at the sensor surface. A shift in the curve represents molecular binding.

At a certain incident angle, the plasmons are set to resonate with light, resulting in the absorption of light at that particular angle as explained in the previous paragraph. This creates a dark band line in the reflected beam (Figure 2.16). That dark band line can be observed as a dip in SPR reflection intensity. A shift in the reflectivity curve (Figure 2.16) represents a molecular binding event taking place either on or near the metal film, or a conformational change in the molecules bound to the film (like in the case of DNA aptamers). By monitoring this shift *vs.* time, researchers can study molecular binding events.

In this dissertation, SPR is used mostly as a characterisation technique to investigate the binding characteristics of probes when restricted to the electrode surface especially for anti-DNA aptamers for PSA and anti-DNA aptamers for AMACR. SPR has also been used to study the layer by layer formation of polymer films as described in Chapter 5.

2.3.2 Fourier Transform Infrared Spectroscopy

Fourier transform infrared spectroscopy (FT-IR) employs the IR radiation through the sample under study. In such a situation, some of the radiations are absorbed by the sample while some are transmitted. Consequently, a spectrum is generated which represents a molecular fingerprint of the sample under study as a result of absorption and transmission of IR. Absorption peaks represented in the spectrum correspond to the frequencies of vibrations between atom bonds making up the material under study (Alben and Fiamingo 1984; Faix 1992; Stuart 2005). Since no two unique molecular structures produce the same spectrum, FT-IR becomes a useful analytical technique for characterisation.

FT-IR spectrometry was developed in order to simultaneously measure all of the IR frequencies. By employing an interferometer, which is a simple optical device, such a simultaneous measurement could be performed. An interferometer in principle can produce a signal with all the IR frequencies encoded in it. A FT-IR instrument consists of a source, an interferometer, a sample, a detector and a computer. The source is employed to emit an IR energy, the beam produced is passed through an aperture which is used to modulate the amount of energy that will be exposed to the sample under study.

The beam enters the interferometer where the beam is split into two optical beams using a beam splitter. The beams, after passing through their respective mirrors, combine again at the beam splitter producing an interferogram. An interferogram consists of the unique property of each data point which makes up the final signal (about each IR frequency).

The beam later passes through the sample where parts of the beams are reflected or transmitted by the sample giving it the characteristics of that particular sample. The resultant beam is finally passed to the detector for the final measurements. Through a computer, Fourier transformation of the detected spectrum is performed which involves decoding of all the frequencies and converting into a user-friendly spectrum output.

In order to study thin films, powders, polymers or even strongly absorbing materials, Attenuated total reflectance (ATR) technique is used in conjunction with FT-IR spectroscopy. ATR-FTIR is different from other spectroscopic techniques as it depends on total internal reflection along with attenuation of a total reflection.

The ATR crystal simply comprises an IR transparent material with a high RI and polished surfaces as shown in Figure 2.17.

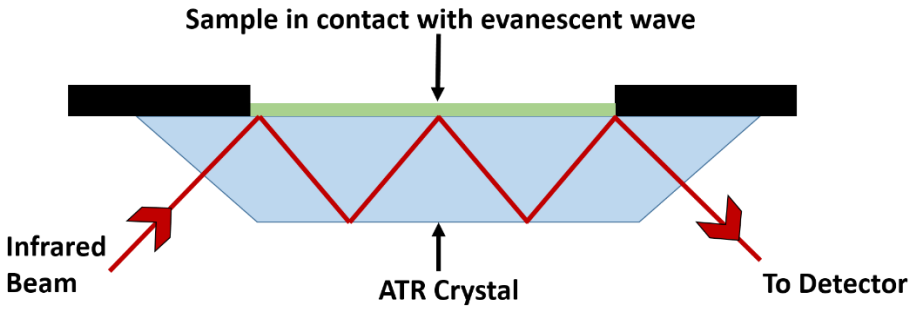

Figure 2.17 Attenuated Total Reflection (ATR) principle.

The IR beam enters the ATR crystal at an incident angle of typically 45° (relative to the crystal surface) and therein is totally reflected at the crystal to sample interface. Because of the wave-like property of the incident beam, the light is reflected by a virtual boundary surface and not directly by the boundary surface. The virtual boundary lies within the optically less dense sample. Such an effect is called the Goos-Hänchen effect. Such an effect refers to the lateral displacement of an incident wave under a total internal reflection effect that occurs at the interface of two mediums with different RI. During ATR, there is a fraction of light that reaches into the sample under study and is known as an evanescent wave. Lateral displacement occurs as a result

from the propagation of an evanescent wave parallel to the interface. The penetration depth of the resultant evanescent wave depends on the wavelength, the RI of the ATR crystal and the sample and angle of the entering light beam. The evanescent wave decays exponentially up to a few microns (ca. 0.5 - 5 μm) from the surface. In the spectral regions of IR, where the sample absorbs only certain energy, the evanescent wave is attenuated and is measured by the detector. After internal reflections, the IR beam exits the crystal and is captured by the IR-detector.

FT-IR in this thesis has been employed to study the surface modification of polypyrrole on gold electrodes. It was used as a validation technique to confirm the electrodeposition of PEG on polypyrrole films as described in Chapter 5.

References

Ahuja, T., Mir, I.A., and Kumar, D., 2008. Potentiometric urea biosensor based on BSA embedded surface modified polypyrrole film. *Sensors and Actuators B: Chemical,* 134(1), 140-145.

Alben, J.O., and Fiamingo, F.G., 1984. Fourier transform infrared spectroscopy. *Optical Techniques in Biological Research*, 133-179.

Andrade, J.D., 1985. Surface and interfacial aspects of biomedical polymers. Vol. 1. Surface chemistry and physics. *Plenum Press,* 470.

Apetrei, I.M., and Apetrei, C., 2013. Amperometric biosensor based on polypyrrole and tyrosinase for the detection of tyramine in food samples. *Sensors and Actuators B: Chemical,* 178, 40-46.

Asavapiriyanont, S., Chandler, G., Gunawardena, G., and Pletcher, D., 1984. The electrodeposition of polypyrrole films from aqueous solutions. *Journal of Electroanalytical Chemistry and Interfacial Electrochemistry*, 177(1), 229-244.

Azioune, A., Siroti, F., Tanguy, J., Jouini, M., Chehimi, M.M., Miksa, B., and Slomkowski, S., 2005. Interactions and conformational changes of human serum albumin at the surface of electrochemically synthesized thin polypyrrole films. *Electrochimica Acta,* 50(7), 1661-1667.

Bain, C.D., Troughton, E.B., Tao, Y.T., Evall, J., Whitesides, G.M., and Nuzzo, R.G., 1989. Formation of monolayer films by the spontaneous assembly of organic thiols from solution onto gold. *Journal of the American Chemical Society,* 111(1), 321-335.

Bain, C.D., and Whitesides, G.M., 1989. Formation of monolayers by the coadsorption of thiols on gold: variation in the length of the alkyl chain. *Journal of the American Chemical Society,* 111(18), 7164-7175.

Bard, A.J., and Faulkner, L.R., 2001. *Electrochemical methods: fundamentals and applications*. 2nd Edn, Wiley New York.

Berggren, C., Bjarnason, B., and Johansson, G., 2001. Capacitive biosensors. *Electroanalysis*, 13(3), 173-180.

Bertok, T., Sediva, A., Katrlik, J., Gemeiner, P., Mikula, M., Nosko, M., and Tkac, J., 2013. Label-free detection of glycoproteins by the lectin biosensor down to attomolar level using gold nanoparticles. *Talanta,* 108, 11-18.

Bisht, V., Takashima, W., and Kaneto, K., 2005. A novel thin film urea biosensor based on copolymer poly (N-3-aminopropylpyrrole-co-pyrrole) film. *Surface and Coatings Technology,* 198(1), 231-236.

Bond, A.M., and Scholz, F., 2010. Electroanalytical methods: guide to experiments and applications. *Springe*r.

Camillone Iii, N., Eisenberger, P., Leung, T., Schwartz, P., Scoles, G., Poirier, G., and Tarlov, M., 1994. New monolayer phases of n-alkane thiols self-assembled on Au (111): Preparation, surface characterization, and imaging. *The Journal of Chemical Physics,* 101(12), 11031-11036.

Campuzano, S., Pedrero, M., Montemayor, C., Fatás, E., and Pingarrón, J.M., 2006. Characterization of alkanethiol-self-assembled monolayers-modified gold electrodes by electrochemical impedance spectroscopy. *Journal of Electroanalytical Chemistry,* 586(1), 112-121.

Chehimi, M.M., Abel, M.-L., Perruchot, C., Delamar, M., Lascelles, S.F., and Armes, S.P., 1999. The determination of the surface energy of conducting polymers by inverse gas chromatography at infinite dilution. *Synthetic Metals,* 104(1), 51-59.

Couniot, N., Afzalian, A., Van Overstraeten-Schlögel, N., Francis, L., and Flandre, D., 2015. Capacitive biosensing of bacterial cells: Analytical model and numerical simulations. *Sensors and Actuators B: Chemical*, 211, 428-438.

Daniels, J.S., and Pourmand, N., 2007. Label-free impedance biosensors: Opportunities and challenges. *Electroanalysis*, 19(12), 1239-1257.

Darling, S., Rosenbaum, A., Wang, Y., and Sibener, S., 2002. Coexistence of the ($23\times\sqrt{3}$) Au (111) Reconstruction and a Striped Phase Self-Assembled Monolayer. *Langmuir,* 18(20), 7462-7468.

Dong, H., Cao, X., Li, C.M., and Hu, W., 2008. An in situ electrochemical surface plasmon resonance immunosensor with polypyrrole propylic acid film: Comparison between SPR and electrochemical responses from polymer formation to protein immunosensing. *Biosensors and Bioelectronics,* 23(7), 1055-1062.

Du, M., Yang, T., Zhao, C., and Jiao, K., 2012. Electrochemical logic aptasensor based on graphene. *Sensors and Actuators B: Chemical,* 169, 255-260.

Faix, O., 1992. Fourier transform infrared spectroscopy. *In Methods in lignin chemistry,* pp. 83-109. Springer Berlin Heidelberg..

Fang, A., Ng, H.T., and Li, S.F.Y., 2003. A high-performance glucose biosensor based on monomolecular layer of glucose oxidase covalently immobilised on indium–tin oxide surface. *Biosensors and Bioelectronics,* 19(1), 43-49.

Finklea, H., 1996. Electrochemistry of organized monolayers of thiols and related molecules on electrodes. *Electroanalytical Chemistry,* 19, 110-335.

Gao, N., Zhou, W., Jiang, X., Hong, G., Fu, T.-M., and Lieber, C.M., 2015. General strategy for biodetection in high ionic strength solutions using transistor-based nanoelectronic sensors. *Nano letters,* 15(3), 2143-2148.

Garnier, F., Bouabdallaoui, B., Srivastava, P., Mandrand, B., and Chaix, C., 2007. Conjugated polymer-based DNA chip with real time access and femtomol detection threshold. *Sensors and Actuators B: Chemical,* 123(1), 13-20.

Garnier, F., Korri-Youssoufi, H., Srivastava, P., Mandrand, B., and Delair, T., 1999. Toward intelligent polymers: DNA sensors based on oligonucleotide-functionalised polypyrroles. *Synthetic Metals,* 100(1), 89-94.

Garnier, F., Youssoufi, H.K., Srivastava, P., and Yassar, A., 1994. Enzyme recognition by polypyrrole functionalised with bioactive peptides. *Journal of the American Chemical Society,* 116(19), 8813-8814.

Grieshaber, D., MacKenzie, R., Voeroes, J., and Reimhult, E., 2008. Electrochemical biosensors-sensor principles and architectures. *Sensors,* 8(3), 1400-1458.

Han, D.-H., Lee, H.J., and Park, S.-M., 2005. Electrochemistry of conductive polymers XXXV: Electrical and morphological characteristics of polypyrrole films prepared in aqueous media studied by current sensing atomic force microscopy. *Electrochimica Acta,* 50(15), 3085-3092.

Herne, T.M., and Tarlov, M.J., 1997. Characterization of DNA probes immobilised on gold surfaces. *Journal of the American Chemical Society,* 119(38), 8916-8920.

Hong, H.S., Kim, S.J., and Lee, K.S., 1999. Long-term oxidation characteristics of oxygen-added modified Zircaloy-4 in 360° C water. *Journal of Nuclear Materials,* 273(2), 177-181.

Hsu, C., and Mansfeld, F., 2001. Technical note: concerning the conversion of the constant phase element parameter Y0 into a capacitance. *Corrosion,* 57(9), 747-748.

Ionescu, R.E., Gondran, C., Bouffier, L., Jaffrezic-Renault, N., Martelet, C., and Cosnier, S., 2010. Label-free impedimetric immunosensor for sensitive detection of atrazine. *Electrochimica Acta,* 55(21), 6228-6232.

Ionescu, R.E., Herrmann, S., Cosnier, S., and Marks, R.S., 2006. A polypyrrole cDNA electrode for the amperometric detection of the West Nile Virus. *Electrochemistry Communications,* 8(11), 1741-1748.

Ionescu, R.E., Jaffrezic-Renault, N., Bouffier, L., Gondran, C., Cosnier, S., Pinacho, D.G., Marco, M.-P., Sánchez-Baeza, F.J., Healy, T., and Martelet, C., 2007. Impedimetric immunosensor for the specific label free detection of ciprofloxacin antibiotic. *Biosensors and Bioelectronics,* 23(4), 549-555.

Jang, H.-J., Ahn, J., Kim, M.-G., Shin, Y.-B., Jeun, M., Cho, W.-J., and Lee, K.H., 2015. Electrical signaling of enzyme-linked immunosorbent assays with an ion-sensitive field-effect transistor. *Biosensors and Bioelectronics,* 64, 318-323.

Johanson, U., Marandi, M., Tamm, T., and Tamm, J., 2005. Comparative study of the behavior of anions in polypyrrole films. *Electrochimica Acta,* 50(7), 1523-1528.

Jolly, P., Formisano, N., Tkáč, J., Kasák, P., Frost, C.G., and Estrela, P., 2015. Label-free impedimetric aptasensor with antifouling surface chemistry: A prostate specific antigen case study. *Sensors and Actuators B: Chemical,* 209, 306-312.

Jolly, P., Tamboli, V., Harniman, R.L., Estrela, P., Allender, C.J., and Bowen, J.L., 2016. Aptamer–MIP hybrid receptor for highly sensitive electrochemical detection of prostate specific antigen. *Biosensors and Bioelectronics*, 75, 188-195.

Keighley, S.D., Li, P., Estrela, P., and Migliorato, P., 2008. Optimization of DNA immobilisation on gold electrodes for label-free detection by electrochemical impedance spectroscopy. *Biosensors and Bioelectronics,* 23(8), 1291-1297.

Khomenko, V., Frackowiak, E., and Beguin, F., 2005. Determination of the specific capacitance of conducting polymer/nanotubes composite electrodes using different cell configurations. *Electrochimica Acta,* 50(12), 2499-2506.

Komarova, E., Aldissi, M., and Bogomolova, A., 2005. Direct electrochemical sensor for fast reagent-free DNA detection. *Biosensors and Bioelectronics,* 21(1), 182-189.

Korri-Youssoufi, H., Garnier, F., Srivastava, P., Godillot, P., and Yassar, A., 1997a. Toward bioelectronics: specific DNA recognition based on an oligonucleotide-functionalised polypyrrole. *Journal of the American Chemical Society,* 119(31), 7388-7389.

Korri-Youssoufi, H., Godillot, P., Srivastava, P., El Kassmi, A., and Garnier, F., 1997b. New method of polypyrrole functionalization toward molecular recognition. *Synthetic Metals,* 84(1), 169-170.

Korri-Youssoufi, H., and Yassar, A., 2001. Electrochemical probing of DNA based on oligonucleotide-functionalised polypyrrole. *Biomacromolecules,* 2(1), 58-64.

Kulkarni, G.S., and Zhong, Z., 2012. Detection beyond the Debye screening length in a high-frequency nanoelectronic biosensor. *Nano letters,* 12(2), 719-723.

Lasia, A., 2002. Electrochemical impedance spectroscopy and its applications. *In Modern aspects of electrochemistry,* pp. 143-248. Springer US.

Laurent, N., Voglmeir, J., Wright, A., Blackburn, J., Pham, N.T., Wong, S.C., Gaskell, S.J., and Flitsch, S.L., 2008. Enzymatic glycosylation of peptide arrays on gold surfaces. *ChemBioChem, 9*(6), 883-887.

Li, Y., Deng, L., Deng, C., Nie, Z., Yang, M., and Si, S., 2012. Simple and sensitive aptasensor based on quantum dot-coated silica nanospheres and the gold screen-printed electrode. *Talanta,* 99, 637-642.

Love, J.C., Estroff, L.A., Kriebel, J.K., Nuzzo, R.G., and Whitesides, G.M., 2005. Self-assembled monolayers of thiolates on metals as a form of nanotechnology. *Chemical Reviews,* 105(4), 1103-1170.

Luppa, P.B., Sokoll, L.J., and Chan, D.W., 2001. Immunosensors—principles and applications to clinical chemistry. *Clinica Chimica Acta*, 314(1), 1-26.

Ma, W., Yin, H., Xu, L., Xu, Z., Kuang, H., Wang, L., and Xu, C., 2013. Femtogram ultrasensitive aptasensor for the detection of OchratoxinA. *Biosensors and Bioelectronics,* 42, 545-549.

Madaboosi, N., Soares, R.R., Chu, V. and Conde, J.P., 2015. A microfluidic immunoassay platform for the detection of free prostate specific antigen: a systematic and quantitative approach. *Analyst*, 140(13), 4423-4433.

Mukherjee, S., Bandyopadhyay, S., and Dey, A., 2013. Tuning the apparent formal potential of covalently attached ferrocene using SAM bearing ionizable COOH groups. *Electrochimica Acta,* 108, 624-633.

Nishizawa, M., Sunagawa, T., and Yoneyama, H., 1997. Underpotential deposition of copper on gold electrodes through self-assembled monolayers of propanethiol. *Langmuir,* 13(20), 5215-5217.

Peng, H., Soeller, C.,and Travas-Sejdic, J., 2007a. Novel conducting polymers for DNA sensing. *Macromolecules,* 40(4), 909-914.

Peng, H., Soeller, C., Vigar, N., Kilmartin, P.A., Cannell, M.B., Bowmaker, G.A., Cooney, R.P., and Travas-Sejdic, J., 2005. Label-free electrochemical DNA sensor

based on functionalised conducting copolymer. *Biosensors and Bioelectronics*, 20(9), 1821-1828.

Peng, H., Soeller, C., Vigar, N.A., Caprio, V., and Travas-Sejdic, J., 2007b. Label-free detection of DNA hybridisation based on a novel functionalised conducting polymer. *Biosensors and Bioelectronics,* 22(9), 1868-1873.

Peng, H., Zhang, L., Soeller, C., and Travas-Sejdic, J., 2009. Conducting polymers for electrochemical DNA sensing. *Biomaterials,* 30(11), 2132-2148.

Piunno, P.A., Watterson, J., Wust, C.C., and Krull, U.J., 1999. Considerations for the quantitative transduction of hybridisation of immobilised DNA. *Analytica Chimica Act*a, 400(1), 73-89.

Porter, M.D., Bright, T.B., Allara, D.L., and Chidsey, C.E., 1987. Spontaneously organized molecular assemblies. 4. Structural characterization of n-alkyl thiol monolayers on gold by optical ellipsometry, infrared spectroscopy, and electrochemistry. *Journal of the American Chemical Society,* 109(12), 3559-3568.

Prabhakar, N., Arora, K., Singh, S.P., Singh, H., and Malhotra, B.D., 2007. DNA entrapped polypyrrole–polyvinyl sulfonate film for application to electrochemical biosensor. *Analytical Biochemistry,* 366(1), 71-79.

Ramanavičius, A., Ramanavičienė, A., and Malinauskas, A., 2006. Electrochemical sensors based on conducting polymer—polypyrrole. *Electrochimica Acta,* 51(27), 6025-6037.

Rodrígez, L.-M.T., Billon, M., Roget, A., and Bidan, G., 2002. Electrosynthesis of a biotinylated polypyrrole film and study of the avidin recognition by QCM. Journal of *Electroanalytical Chemistry,* 523(1), 70-78.

Rodriguez, J., Grande, H., and Otero, T., 1997. Handbook of organic conductive molecules and polymers. *John Wiley & Sons Ltd: New York 2*.

Sagiv, J., 1980. Organized monolayers by adsorption. 1. Formation and structure of oleophobic mixed monolayers on solid surfaces. *Journal of the American Chemical Society,* 102(1), 92-98.

Salamon, Z., Macleod, H.A., and Tollin, G., 1997. Surface plasmon resonance spectroscopy as a tool for investigating the biochemical and biophysical properties of membrane protein systems. II: Applications to biological systems. *Biochimica et Biophysica Acta (BBA)-Reviews on Biomembranes*, 1331(2), 131-152.

Schreiber, F., 2000. Structure and growth of self-assembling monolayers. *Progress in Surface Science*, 65(5), 151-257.

Stern, E., Vacic, A., Li, C., Ishikawa, F.N., Zhou, C., Reed, M.A., and Fahmy, T.M., 2010. A Nanoelectronic Enzyme-Linked Immunosorbent Assay for Detection of Proteins in Physiological Solutions. *Small*, 6(2), 232-238.

Stern, E., Wagner, R., Sigworth, F.J., Breaker, R., Fahmy, T.M., and Reed, M.A., 2007. Importance of the Debye screening length on nanowire field effect transistor sensors. *Nano letters*, 7(11), 3405-3409.

Stuart, B., 2005. *Infrared spectroscopy*.John Wiley & Sons, Inc..

Thévenot, D.R., Toth, K., Durst, R.A., and Wilson, G.S., 2001. Electrochemical biosensors: recommended definitions and classification. *Biosensors and Bioelectronics*, 16(1), 121-131.

Tlili, C., Korri-Youssoufi, H., Ponsonnet, L., Martelet, C., Jaffrezic-Renault, and N.J., 2005. Electrochemical impedance probing of DNA hybridisation on oligonucleotide-functionalised polypyrrole. *Talanta*, 68(1), 131-137.

Tsouti, V., Boutopoulos, C., Zergioti, I., and Chatzandroulis, S., 2011. Capacitive microsystems for biological sensing. *Biosensors and Bioelectronics*, 27(1), 1-11.

Ulman, A., 1996. Formation and structure of self-assembled monolayers. *Chemical Reviews*, 96(4), 1533-1554.

Van Der Merwe, P.A., 2001. Surface plasmon resonance. Protein-Ligand Interactions: Hydrodynamics and Calorimetry, *Oxford University Press*: *New York, NY, USA*, pp.137-170.

Wang, J., Jiang, M., Fortes, A., and Mukherjee, B., 1999. New label-free DNA recognition based on doping nucleic-acid probes within conducting polymer films. *Analytica Chimica Acta,* 402(1), 7-12.

Wang, X., Gu, X., Yuan, C., Chen, S., Zhang, P., Zhang, T., Yao, J., Chen, F., and Chen, G., 2004. Evaluation of biocompatibility of polypyrrole in vitro and in vivo. *Journal of Biomedical Materials Research Part A,* 68(3), 411-422.

Weidlich, C., Mangold, K.-M., and Jüttner, K., 2005. EQCM study of the ion exchange behaviour of polypyrrole with different counterions in different electrolytes. *Electrochimica Acta,* 50(7), 1547-1552.

Wu, J., Campuzano, S., Halford, C., Haake, D.A., and Wang, J., 2010. Ternary surface monolayers for ultrasensitive (zeptomole) amperometric detection of nucleic acid hybridisation without signal amplification. *Analytical Chemistry,* 82(21), 8830-8837.

Xu, H., Gorgy, K., Gondran, C., Le Goff, A., Spinelli, N., Lopez, C., Defrancq, E., and Cosnier, S., 2013. Label-free impedimetric thrombin sensor based on poly (pyrrole-nitrilotriacetic acid)-aptamer film. *Biosensors and Bioelectronics,* 41, 90-95.

Zhang, K., Xie, M., Zhou, B., Hua, Y., Yan, Z., Liu, H., Guo, L.-n., Wu, B., and Huang, B., 2013. A new strategy based on aptasensor to time-resolved fluorescence assay for adenosine deaminase activity. *Biosensors and Bioelectronics,* 41, 123-128.

Chapter 3. Aptamer-based impedimetric sensing of PSA

This Chapter will provide a presentation on the development of an aptasensor for the detection of PSA, which is currently the gold standard for PCa biomarkers. The study will focus on EIS as a detection technique and SPR as a validation tool. The Chapter will highlight the effect of buffer conditions on the EIS signal, the effect of anti-PSA DNA aptamer surface density on PSA binding efficiency, the transition from 6-mercapto-1-hexanol (MCH) to thiol terminated sulfo-betaine based self-assembled monolayer (SAM) for enhanced antifouling properties.

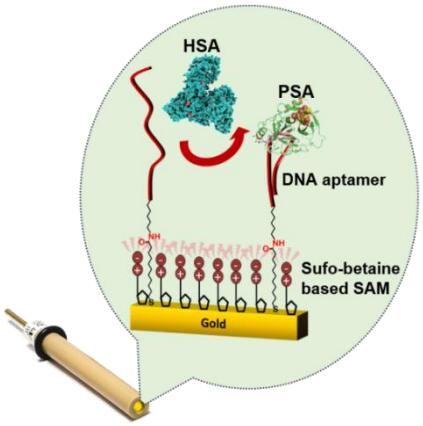

The work presented in this Chapter has been published in Formisano *et al.* (Formisano *et al.* 2015) and Jolly *et al.* (Jolly *et al.* 2015)

3.1 Background

In recent years, a range of assays for PSA such as electrochemical assays (Okuno *et al.* 2007; Panini *et al.* 2008), enzyme-linked immunosorbent assay (Acevedo *et al.* 2002), cantilever assay (Wee *et al.* 2005), and chemiluminescent immunoassay (Albrecht *et al.* 1994; Seto *et al.* 2001) have been developed which are mostly based on antibodies as recognition elements. In this study, instead of using antibodies, an anti-PSA DNA aptamer (Chapter 1, Figure 1.6a) was utilised as a molecular

recognition element to detect PSA. Since the development of an anti-PSA DNA aptamer by Savory *et al*. (Savory *et al*. 2010) in 2010, only one group reported the detection of PSA using anti-PSA DNA aptamers (Liu *et al.* 2012). Gold nanoparticles (AuNPs) were used for the layer by layer construction of a PSA aptasensor. AuNPs were encapsulated by graphitized mesoporous carbon and bovine serum albumin (BSA) was used as a blocking molecule to reduce non-specific binding (Liu *et al.* 2012). Affinity-based immobilisation for DNA aptamer was used for the fabrication process. Amperometric techniques namely, cyclic voltammetry (CV) and differential pulse voltammetry (DPV) were used as measurement techniques with a limit of detection (LOD) of 0.25 ng/mL (or 7.58 pM).

To develop sensitive and selective electrochemical aptasensors, electrode surface chemistry is one of the biggest fields of investigation. Research worldwide is typically focussed on finding the most suitable recognition platform to give a stable organization to the sensor interface leading to optimised binding efficiency and signal outcome (Lee *et al.* 2005; Putzbach and Ronkainen 2013). For sensing applications, shorter thiols are normally preferred to provide partial access to the redox markers to an underlying metal surface. In contrast, such a mechanism might not hold true for every application like the development of aptasensors, where the length of the linker can have an effect on target binding to its respective aptamer (Balamurugan *et al.* 2006).

With the motivation to develop a simple fabrication strategy, a simple and sensitive PSA aptasensor is reported in this Chapter by employing a new type of thiol terminated sulfo-betaine molecules. Furthermore, a demonstration of electrochemical measurement using the constructed PSA aptamer biosensor is given and discussed.

3.2 Bio-functionalisation on gold surface

Prior to bio-functionalisation, gold disk working electrodes with a radius of 1.0 mm (ALS, Japan) were cleaned using mechanical polishing, followed by electrochemical cleaning as described by Keighley *et al*. (Keighley *et al.* 2008b). First, the electrode surfaces were mechanically polished for 2 minutes with 1 μm diamond solution

(Buehler, USA) and thereafter for 5 minutes with 50 nm alumina slurry (Buehler, USA) on respective polishing pads (Buehler, USA). A sonication process for 10 minutes between each step was performed, followed by rinsing with MilliQ water in order to remove any remaining particles. Electrodes were then subjected to electrochemical cleaning in 0.5 M H_2SO_4 (Sigma, UK) by scanning the potential between the oxidation and reduction of gold, −0.05 V and +1.1 V *versus* an Ag/AgCl reference electrode (RE), for 50 cycles until there was no further change observed in the voltammogram. The electrochemical cleaning was performed using a three-electrode cell setup with gold electrodes as WE with a μAUTOLAB III/FRA2 potentiostat (Metrohm Autolab, Netherlands). Ag/AgCl (KCl) was used as a RE (BASi, USA) connected via a salt bridge filled with 10 mM PBS, pH 7.4 (prepared from Tablets, Sigma, UK) and a Pt counter electrode (ALS, Japan). After electrochemical cleaning, electrodes were washed with a surplus amount of MilliQ water to remove any acid residues. Finally, electrodes were cleaned with ethanol and were left to dry in a dustless environment for several minutes.

In this study, two different PSA aptasensors based on thiol surface chemistry are presented. For successful EIS measurement, it is necessary to have a good reliable SAM on the gold electrode surface in order to have a reproducible sensor. One of the most accepted approaches to achieve this goal is by alkanethiol chemistry as described in Chapter 2. Alkanethiols can be easily adsorbed and form a SAM (Love *et al.* 2005) on a clean gold surface through gold-sulphur bonds. For the study, all aqueous solutions were prepared using 18.2 MΩ cm ultra-pure water (MilliQ) with a Pyrogard filter (Millipore, UK) and all other reagents were of analytical grade.

3.2.1 SAM with thiolated anti-PSA DNA aptamers

The first SAM studied comprised of a thiol-terminated anti-PSA DNA aptamer (5′-HS-$(CH_2)_6$-TTT TTA ATT AAA GCT CGC CAT CAA ATA GCT TT-3′ (synthesised by Sigma, UK) and MCH (Sigma, UK) in different ratios, immobilised on clean gold electrodes (Figure 3.1).

Clean gold electrodes were exposed to 150 µL of mixed anti-PSA DNA aptamer/MCH immobilisation solution for 16 hours in a humidity chamber at 4˚C. The DNA immobilisation solution consisted of immobilisation buffer (Table 3.1) with a calculated amount of anti-PSA DNA aptamers and MCH.

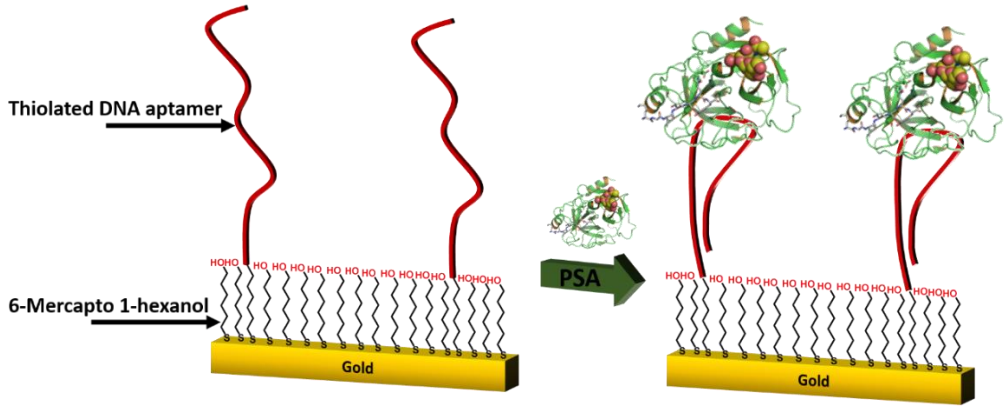

Figure 3.1 Self assembled monolayer (SAM) of co-immobilised thiolated anti-PSA DNA aptamer with 6-mercapto-1-hexanol (MCH) on gold surface (before and after binding of PSA).

A high concentration of MCH (10 mM) was prepared in pure ethanol (HPLC grade, Sigma, UK) which was diluted to working concentration in immobilisation buffer and binding buffer respectively.

Table 3.1 Buffers used and their composition

Buffer	Composition
Immobilisation buffer	10 mM Tris-HCl containing 10 mM KCl, 10 mM $MgCl_2$ (pH7.4)
Binding Buffer	0.1 M phosphate buffer (PB) solution containing 0.1 M KCl and 0.05% Tween20 (pH 7.4)
Measurement buffer	10 mM ferro/ferricyanide $[Fe(CN)_6]^{3-/4-}$ in 0.1 M phosphate buffer (PB) solution containing 0.1 M KCl (pH 7.4)

*All the chemicals used for buffer preparation were purchased from Sigma, UK

Prior to the addition of MCH, anti-PSA DNA aptamers were heated to 95˚ C for 10 minutes followed by gradual cooling over half an hour to room temperature to fold stable structures of aptamers (Savory *et al.* 2010). After immobilisation, electrodes were rinsed with MilliQ water to remove any unattached anti-PSA DNA aptamers and

MCH. In order to ensure complete thiol coverage of the gold surface, the electrodes were thereafter backfilled with 1 mM MCH for 1 hour. Electrodes were then rinsed with MilliQ water and placed in the binding buffer for 1 hour to stabilise the SAM. Anti-PSA DNA aptamer/MCH immobilisation solutions were prepared in the range of ratios from 1:9, 1:49, 1:99, 1:199 and 1:499 to optimise the anti-PSA DNA aptamer surface coverage for maximum binding efficiency.

3.2.2 SAM with amine terminated anti-PSA DNA aptamers

In the second part of the Chapter, a new molecule called thiol terminated sulfo-betaine ((*R*)-3-((2-(5-(1,2-dithiolan-3-yl)pentanamido)ethyl)dimethylammonio)propane-1-sulfonate) has been used for the development of a PSA aptasensor. Thiol terminated sulfo-betaine was synthesised as a 398.60 g/mole molecule according to a previously published method (Bertok *et al.* 2013). It contains both positive and negative charges and acts like a zwitterion (Figure 3.2). It has been previously reported as a potential candidate to reduce non-specific binding and increase the sensitivity of the sensor performance. However, there has been no application with aptamers reported to date.

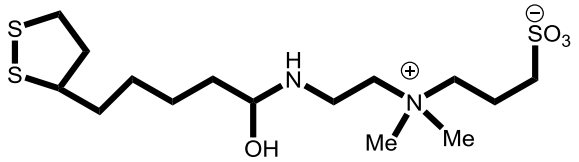

Figure 3.2 Chemical structure of thiol terminated sulfo-betaine.

For the aptasensor fabrication, clean gold electrodes were immersed in a 1 to 99 ratio of two thiols (11-Mercaptoundecanoic acid, MUA (Sigma, UK): thiol terminated sulfo-betaine) and incubated for 16 hours. A stock solution of 10 mM MUA was prepared in pure ethanol (HPLC grade) and a stock solution of thiol terminated sulfo-betaine was prepared in water. All the solutions were prepared fresh before use. These two thiols form the SAM layer as shown in Figure 3.3. The electrodes were rinsed with MilliQ water and prepared for the second step of modification which involved attachment of the bio-recognition element.

Amine terminated anti-PSA DNA aptamer (5′-NH_2-$(CH_2)_6$-TTT TTA ATT AAA GCT CGC CAT CAA ATA GCT TT-3′, synthesised by Sigma, UK) was immobilised using standard amine coupling reaction with the carboxylate groups (Hermanson 2013).

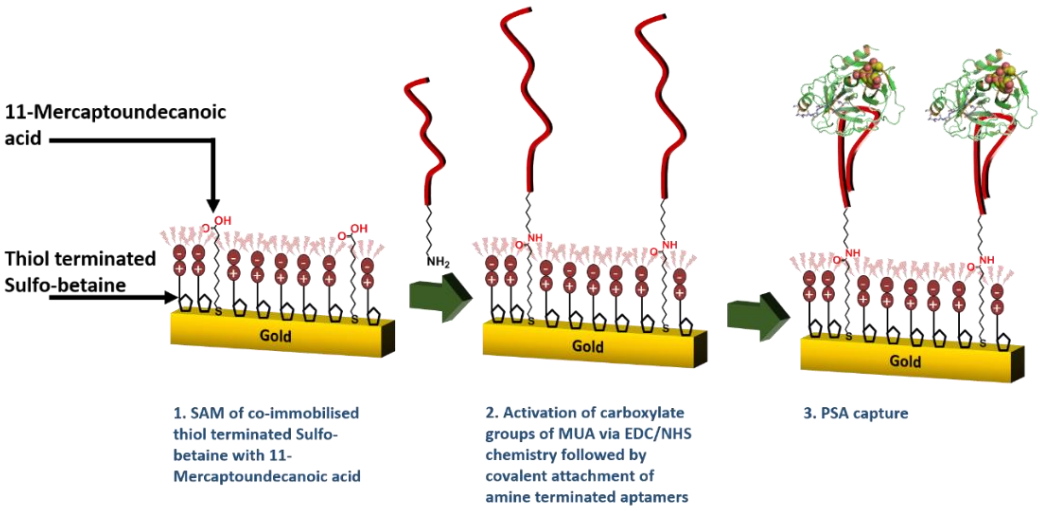

Figure 3.3 Fabrication schematic with amine terminated anti-PSA DNA aptamers.

The carboxylate groups of MUA are activated by a mixture of 0.2 M N-(3-dimethylaminopropyl)-N′-ethylcarbodiimide hydrochloride (EDC, Sigma, UK) and 0.05 M N-hydroxysuccinimide (NHS, Sigma, UK). The reaction follows the conventional coupling principle as shown in Figure 3.4. The carboxylate groups of MUA are activated by a cross-linker (EDC), which forms a highly reactive intermediate called O-acylisourea. Such an intermediate is highly unstable in aqueous solution and undergoes hydrolysis in a few seconds. Yet, this can be overcome by using NHS in the reaction, which reacts with the O-acylisourea and forms another intermediate product with an active ester functional group demonstrating enhanced stability in aqueous media. Finally, in the presence of a primary amine (such as in our case, an amine terminated anti-PSA DNA aptamer), the sulfo-NHS group can be replaced leading to the formation of a stable amide bond.

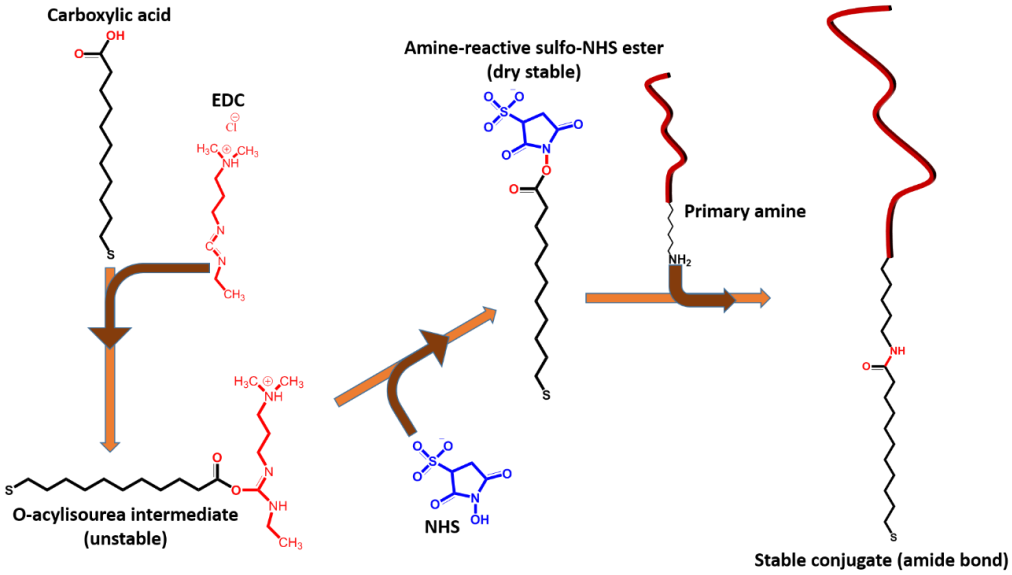

Figure 3.4 Principle of EDC/NHS chemistry on MUA using amine terminated anti-PSA DNA aptamers (adapted from Hermanson et al. 2013).

The electrodes were incubated in a mixture of EDC/NHS for 20 minutes followed by incubation with 1 µM amine-terminated anti-PSA DNA aptamer prepared in binding buffer for 2 hours leading to covalent attachment of aptamers on the activated SAM. Later, the electrodes were washed with MilliQ water and incubated with 1 M ethanolamine (pH 8.5, Sigma, UK) for half an hour to block all the un-reacted sites of MUA. Finally, the electrodes were rinsed with MilliQ water and placed in the binding buffer for stabilization for 1 hour.

3.3 Effect of changing buffers on stability of SAM

Before any investigation on the efficiency of an aptasensor to detect the analyte of interest via EIS measurement, it is important to understand the dynamics of the SAM on the EIS signal itself. Therefore, a study was performed with both types of fabricated PSA aptasensor, namely SAM with MCH and SAM with thiol-terminated sulfo-betaine, to investigate the stability of the SAM when incubated in two different buffers. In order to obtain reliable data from an EIS measurement, it is vital to monitor the stability of the aptasensor. It is often reported in the literature that the binding of

proteins to aptamers is performed in a different buffer from the measurement buffer. Hence, we investigated if the change in R_{ct} values of the fabricated sensor was due to the binding of protein and not because of buffer effects. These samples were tested first of all for stability in 0.1 M PB (pH 7.4) containing 0.1 M KCl. Measurements were then taken in 0.1 M PB (pH 7.4) containing 10 mM $[Fe(CN)_6]^{3-/4-}$ and 0.1 M KCl. Figure 3.5 (left) represents the time that an electrode can take to give stable R_{ct} values without the addition of any protein. It should be noted that the stabilisation time profile depends on the surface chemistry and buffers used. The total time for stabilisation of the sensor can be minimised by careful sensor design and storage conditions. Once a stable R_{ct} has been recorded as shown in Figure 3.5, electrodes were then immersed in 10 mM Tris-HCl (pH 7.4 containing 10 mM KCl, 10mM $MgCl_2$ and 0.05% Tween20 for 30 minutes.

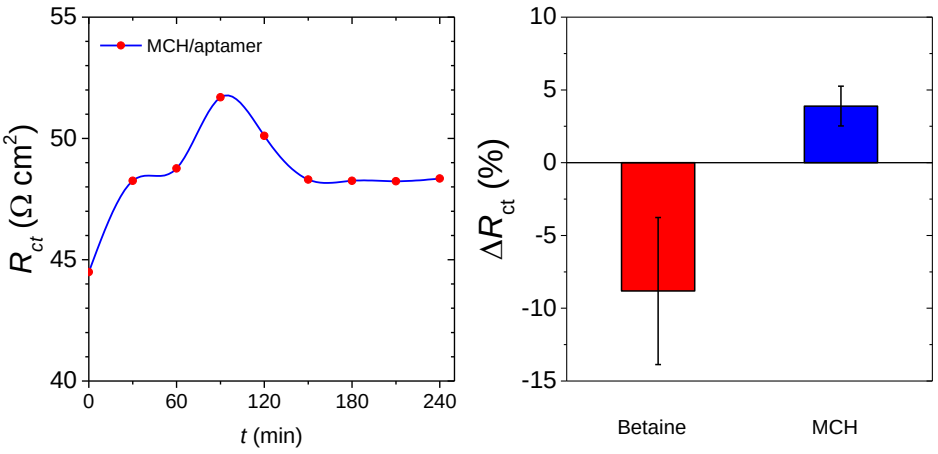

Figure 3.5 Left Graph representing the change in R_{ct} of an electrode over 30 minutes interval time in 0.1 M PB (pH 7.4) containing 10 mM $[Fe(CN)_6]^{3-/4-}$ and 0.1 M KCl (n=1). Right represents effect of change in buffer conditions on SAM stability with MCH functionalised electrodes (left) and Sulfo-betaine functionalised (right)in 0.1 M PB (pH 7.4) containing 10 mM $[Fe(CN)_6]^{3-/4-}$ and 0.1 M KCl. Electrodes were first immersed for 30 minutes in 10mMTris-Hcl (pH7.4 containing 10mMKCl, 10mM $MgCl_2$ and 0.05% Tween20 and then EIS measurement was performed in 0.1 M PB (pH 7.4) containing 10 mM $[Fe(CN)_6]^{3-/4-}$ and 0.1 M KCl. The error bars represent the standard deviation obtained for three samples.

The EIS measurement was again recorded and the results obtained from both aptasensors are represented in the Figure 3.5 (right). It can be clearly seen that regardless of the surface chemistry used, the buffer can cause instability of the SAM which is reflected in the change in R_{ct} of the system. One of the reasons for such

instability could be due to changes in the ionic strength of the buffers used. As indicated, both of the aptasensors were stabilised in 0.1 M PB containing 0.1 M KCl which is a result of equilibrium in dynamics of the SAM in the buffer. However, if the ionic strength is changed, such as in this case by using 10 mM Tris-HCl, there is a change in the dynamics of the SAM. Such a disturbance could be attributed to the rearrangement of the SAM comprising of anti-PSA DNA aptamers. Hence, it is very important to maintain the same buffer conditions throughout the EIS measurement in order to obtain reliable data.

3.4 Effect on R_{ct} on binding of PSA with DNA aptamer

Co-immobilisation of thiol-terminated anti-PSA DNA aptamers and MCH onto gold electrodes was used to fabricate functional electrodes for PSA detection as described in the previous section. The EIS measurements were performed using a μAUTOLAB III potentiostat (Metrohm AG) using a three-electrode cell configuration with SAM functionalised gold electrodes as a WE and a Hg/Hg_2SO_4 and a Platinum wire as RE and CE, respectively. The impedance spectrum was measured in measurement buffer within a frequency range 100 kHz to 100 mHz, with a 10 mV a.c. voltage superimposed on a bias d.c. voltage of 0.195 V *vs.* Hg/Hg_2SO_4 (corresponding to the formal potential of the redox couple). The RE was connected via a salt bridge filled with 0.1 M PB containing 0.1 M KCl (pH 7.4).

With these electrodes, Nyquist plots for the system were recorded in an EIS measurement (see example of typical curve in Figure 3.6), where the R_{ct} of the SAM prepared (co-immobilised DNA aptamer and MCH) was determined by fitting the data to the simple Randles equivalent circuit as described in Chapter 2 (Bard and Faulkner 2001; Keighley *et al.* 2008b).

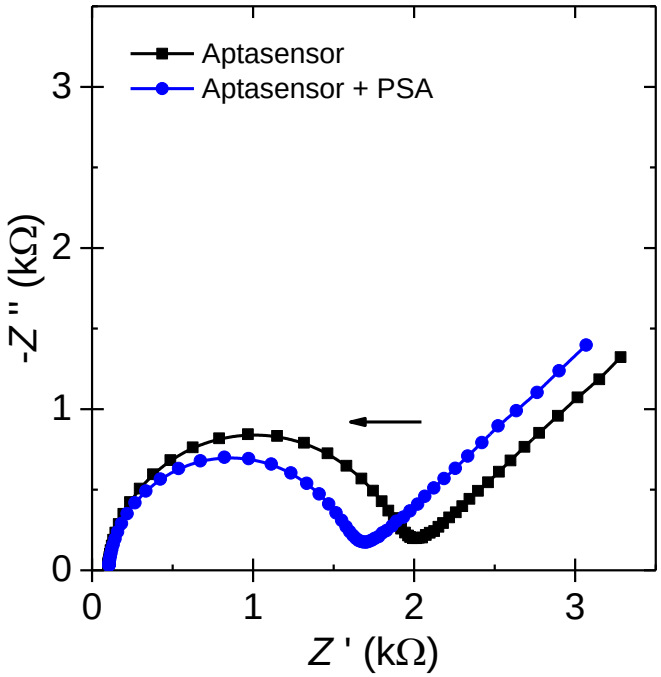

Figure 3.6 EIS characteristics for anti-PSA DNA aptamer/MCH functionalised gold electrodes in 0.1M phosphate buffer (PB) solution containing 0.1 M KCl (pH 7.4) containing 10 mM ferro/ferricyanide $[Fe(CN)_6]^{3-/4-}$. Reduction in R_{ct} was recorded on binding of PSA with anti-PSA DNA aptamer in binding buffer for 30 minutes. The PSA concentration was 10 µg/ml (Jolly et al. 2015).

For binding studies, different concentrations of PSA (Merck Chemicals Ltd., UK) were prepared in the binding buffer using the standard PSA stock solution received from the company. Upon incubation with 10 µg/mL PSA, a reduction of 13% in R_{ct} was observed reflecting binding with anti-PSA DNA aptamers (Figure 3.6). This decrease obtained is contradictory to what has been reported by Liu *et al.* (Liu *et al.* 2012) for PSA where an increase in R_{ct} has been observed. Nevertheless, a reduction of R_{ct} upon aptamer-analyte interactions has also been reported earlier in literature. For example in 2005, Rodriguez *et al.* reported the development of an aptasensor to detect lysozymes, where a decrease in R_{ct} upon binding of the lysozyme to its specific anti-lysozyme DNA aptamer was attributed mainly due to the screening of charges on the DNA aptamer (Rodriguez *et al.* 2005). More recently, Miodek *et al.* in 2015 reported development of a thrombin aptasensor based on a ternary SAM where again

a reduction in R_{ct} upon binding of thrombin was reported at lower analyte concentrations (Miodek *et al.* 2015).

Such a reduction in R_{ct} could be attributed to many factors. Zhang *et al*. in 1995 characterised total PSA from the human seminal fluid, reporting an isoelectric point of PSA between 6.8 and 8 depending on the amount of glycosylation (Wang *et al.* 1981; Zhang *et al.* 1995). Since the measurements were performed in pH 7.4, it is likely that PSA is neutrally charged. However, PSA might screen the charges of the anti-PSA DNA aptamer upon the binding event. Eventually, it could be that more positive charges are exposed outwards because of the protein architecture and the binding itself, which could result in a reduction on the electrostatic barrier to the ferro/ferricyanide anions towards the electrode surface, leading to lowering of the R_{ct} value of the system.

3.5 Effect of Surface coverage on PSA binding

Optimisation of probe density on the electrode surface plays a very crucial role for good biosensor performance. Surface coverage and spacing of probe molecules are dependent on the concentration of the co-immobilised probes with other thiol components. One can assume that there is a dynamic competition between different thiol components until equilibrium is attained. For optimal concentrations of thiol, there is a trade-off between the surface density of the thiolated bioreceptors and the capture efficiency for the analyte, so that the best signal output is achieved. For instance, in DNA detection, as reported in the literature, the maximum percentage change in R_{ct} upon hybridisation with fully complementary target oligonucleotides was obtained with samples functionalised with 20% mole fraction of PNA probes (Keighley *et al.* 2008b). When using DNA probes, the mole fraction reduced to 10% (Keighley *et al.* 2008a). Furthermore, Biogiotii *et al*. in 2012 reported the effect of surface density of ssDNA probes on the nuclease digestion (Biagiotti *et al.* 2012). Therefore, a similar investigation was carried out with PSA aptasensors to better evaluate the aptasensor and the aptamer itself. Dose response with different ratios of DNA aptamers to MCH can be found in Formisano (2015).

It can be assumed that steric hindrance can majorly affect the binding efficiency of PSA to an anti-PSA DNA aptamer when confined to an electrode surface. Because of folding of the DNA aptamers upon binding of PSA, steric hindrance can be a limiting factor and affect binding. Furthermore, steric hindrance can also take place because of the size of the protein (PSA) and also the spacing is needed so that PSA is able to identify the sequence on the anti-PSA DNA aptamer for binding. Hence, a range of anti-PSA DNA aptamer mole fractions were studied.

The variation of the initial R_{ct} of the electrodes, as determined by EIS, with the mole fraction of anti-PSA DNA aptamer to total thiol (DNA aptamer + MCH) in the immobilisation solution is shown in Figure 3.7. EIS measurements show increasing values of initial R_{ct} as the amount of DNA aptamers is increased: 1.06 ± 0.04 kΩ, 0.7 ± 0.15 kΩ, 1.63 ± 0.16 kΩ, 1.86 ± 0.16 kΩ and 11.90 ± 0.17 kΩ for 0.002, 0.005, 0.01, 0.02 and 0.1 mole fraction of DNA aptamer to total thiol respectively. Although it is expected that the lower the DNA aptamer mole fraction, the lower the initial R_{ct}, the results obtained with 0.002 mole fraction were contradictory. The reason could be that at 0.002 DNA aptamer mole fraction, the SAM formed is more homogenous compared to 0.005 mole and thus increases the initial R_{ct}.

These fabricated samples were then studied for their binding efficiency with PSA in terms of change in R_{ct} characterised by EIS. The results are represented in Figure 3.7. PSA concentration of 10 µg/mL was chosen to perform the comparative analysis between the different DNA aptamer mole fraction fabricated sensors. At the highest mole fraction of DNA aptamer studied, i.e. 0.1 DNA aptamer mole fraction, a negligible signal change of 0.9% $\pm$ 1.2 (data not presented in the graph) was recorded mainly because the DNA aptamers were densely packed on the electrode surface leading to steric hindrance. The signal change detected increased when the DNA aptamer concentration was lowered and the best results were recorded with 0.01 DNA aptamer mole fraction with nearly 14% change. 0.002 DNA aptamer mole fraction showed higher signal change compared to 0.005 for the same reason as already explained for initial R_{ct} values. The large standard deviation seen on the bar graph can be attributed to sample to sample variation since at such a low concentration of DNA aptamers, even a slight variation between samples in the number of DNA aptamers

immobilised on the electrode surface can have a significant effect on the number of PSA molecules binding to it.

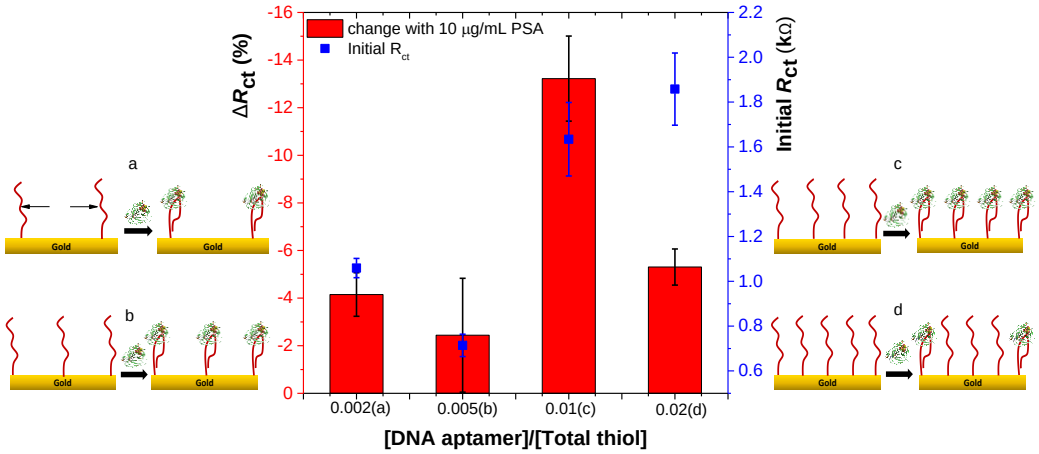

Figure 3.7 Initial R_{ct} of fabricated PSA aptasensor (right axis) over a range of DNA aptamer mole fraction measured in 10 mM ferro/ferricyanide $[Fe(CN)6]^{3-/4-}$ in 0.1M phosphate buffer (PB) solution containing 0.1M KCl (pH 7.4) using EIS . Change in percentage R_{ct} of fabricated PSA aptasensor (left axis) over a range of DNA aptamer mole fraction measured after 30 minutes incubation with 10 ug/ml PSA. The error bars represent the standard deviation obtained for three samples.

The EIS signal recorded is a cumulative effect of many factors such as mass loading, screening of charges, ionic strength, etc. Therefore, a similar study to investigate the effect of DNA aptamer mole fraction for PSA detection was performed by another technique called Quartz Crystal Microbalance with Dissipation mode (QCM-D), which has been reported by Formisano *et al.*(Formisano *et al.* 2015). Experiments with QCMD technique were performed and optimised by Formisano (2015). Unlike EIS, QCM-D measurements are not expected to be affected by conformational changes of the DNA aptamer. The QCM-D response is a result of the change in oscillating frequency that is more dependent on the changes in mass bound to the crystal. Furthermore, QCM-D results confirmed a similar effect of surface density of DNA aptamers on PSA binding. It is worth mentioning that a control protein called human serum albumin (HSA, Sigma, UK) was used to investigate non-specific binding. From the QCM-D data reported by Formisano *et al.* (Formisano *et al.* 2015), the sensor

demonstrated a clear distinction between specific binding of PSA and non-specific binding of HSA up to 400 nM.

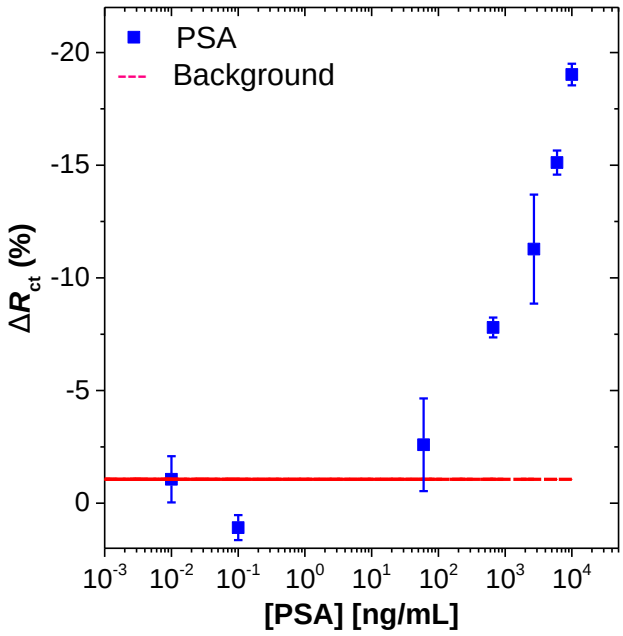

Figure 3.8 Dose response with thiolated anti-PSA aptasensor for different PSA concentrations in 0.1 M PB (pH 7.4) containing 10 mM [Fe (CN) 6]$^{3-/4-}$ and 0.1 M KCl. PSA incubation time was for 30 min. The error bars represent the standard deviation obtained for three samples.

Using 0.01 DNA aptamer mole fraction, a complete dose response was performed using PSA concentrations from a range of 0.01 ng/mL to 10 µg/mL (Figure 3.8). From the dose response, it can be seen that the aptasensor fabricated could potentially detect PSA above the range of 60 ng/mL (or 2 nM), which is 6 times higher than the upper limit of any clinical PSA range in blood.

Although the sensitivity of the sensor was not within the clinical range, it was worth studying the antifouling efficiency of the fabricated aptasensor. The antifouling efficiency depends highly on the composition of the SAM. Therefore, the next stage of the investigation was to use the samples fabricated with optimised DNA aptamer mole fraction for non-specific binding.

HSA, being the most abundant protein found in human blood was used as a suitable candidate as a control protein. Upon exposing the aptasensor to 100 µM HSA, an increase in the R_{ct} value of around 12.5% was recorded (Figure 3.9). Such an effect could be a blocking effect due to occupancy of free MCH spaces on the sensor surface by HSA molecules. With the non-specific attachment of HSA, there is an increased physical barrier to redox couples in the solution to reach the sensor surface and thus increasing the R_{ct} of the system.

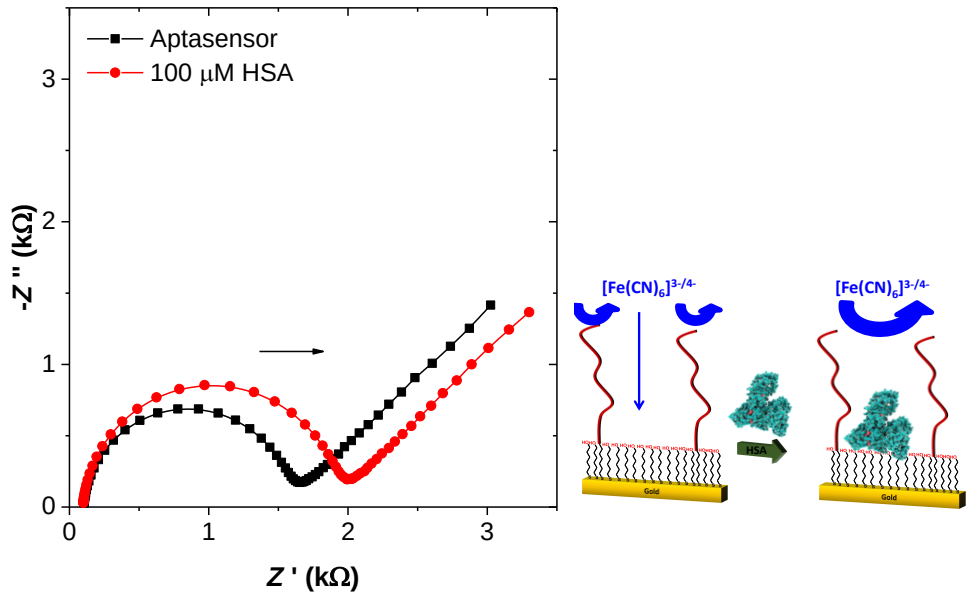

Figure 3.9 EIS characteristics for DNA aptamer/MCH functionalised gold electrodes in 10 mM ferro/ferricyanide $[Fe(CN)6]^{3-/4-}$ in 0.1M phosphate buffer (PB) solution containing 0.1 M KCl (pH 7.4) before (black) and after (red) incubation with 100 µM HSA (red) as a consequence of non-specific binding.

Although it is quite interesting that the PSA aptasensor could potentially differentiate HSA from PSA, in a more complex medium like blood this could lead to decreased sensitivity. Instead, a high concentration of HSA could be used to block the potential sites for non-specific binding and then these samples could be used to detect PSA in real blood samples. Such a step would minimise further binding of non-specific proteins and hence reduce fouling. The possibility of which needs further investigation to discern whether blocking with HSA will decrease binding of PSA with DNA

aptamer or not. However, it is not preferred in an ideal biosensor for clinical applications. In fact, fouling of biosensor surfaces in the form of protein adsorption poses serious challenges which can reduce the sensitivity of the device. To mitigate such a biofouling effect, surfaces can be modified with polymer brushes like PEG, polyzwitterions, polysaccharides and even polypeptoids (Banerjee *et al.* 2011).

3.6 Electrochemical analysis with amine terminated DNA aptamers

The results obtained in the previous section led us to the next step of using a new spacer molecule called thiol terminated sulfo-betaine (sulfo-betaine) which has been reported for its antifouling capabilities (Bertok *et al.* 2013b) . Zwitterionic SAMs are a promising class of antifouling brushes that could be used as an alternative to widely used PEG surfaces (Holmlin *et al.* 2001; Kane *et al.* 2003; Kuang and Messersmith 2012). Various literature has reported the use of sulfo-betaine methacrylate and carboxy-betaine methacrylate, demonstrating enhanced anti-fouling performance comparable or even better than PEG (Yang *et al.* 2008; Zhang *et al.* 2006). In this particular setup, a derivative of sulfo-betaine was used to prepare a mixed SAM with MUA. Finally, amine terminated anti-PSA DNA aptamers were immobilised via conventional EDC/NHS coupling agents through an amide link.

3.6.1 Co-immobilisation of sulfo-betaine with thiolated DNA aptamers

During the course of investigating sulfo-betaine as a possible molecule to fabricate aptasensors with antifouling effects, it was also interesting to determine if sulfo-betaine can be co-immobilised with thiolated DNA aptamers directly on the gold surface. The reason was to ease the immobilisation protocol by excluding multiple steps to just one step fabrication. Also, it would eradicate the effects of rate of diffusion because of different solvents. Samples fabricated in this way were characterised by EIS. A very low initial R_{ct} in the range of 30-60 ohms was recorded. This very low R_{ct} indicates that the SAM formed on the gold surface is not a compact layer, leading to

the non-homogeneous surface. As a consequence, there is easy diffusion of redox couples to the gold surface causing low initial R_{ct} values.

3.6.2 EIS characterisation of aptasensors with amine terminated aptamers

The Nyquist plots obtained with the sulfo-betaine system do not follow the conventional Randles equivalent circuit (Figure 3.11). Instead, two semi-circles are observed, which can be represented by the equivalent circuit in Figure 3.10. The reasons for dual semi-circles could be explained by the processes happening during the immobilisation step. The sulfo-betaine solution was prepared in MilliQ water and MUA in pure ethanol. When these two solutions were mixed together to prepare the immobilisation solution, the efficiency of immobilised molecules on the surface was governed by the diffusion factor. As such there could be areas on the gold surface confined to sulfo-betaine and also areas confined to MUA causing the presence of two semi-circles in the Nyquist plots.

For the study, 1% MUA mole fraction was used to prepare the first SAM layer based on the results from section 3.5. However, it should be noted that the final concentration of DNA aptamers will be less than 1% depending on the efficiency of covalent coupling via EDC/NHS. An attempt to optimise the surface coverage was performed by changing the ratio of MUA to sulfo-betaine, however, the outcome proved it to be challenging. It was assumed that the different diffusion rates of MUA and sulfo-betaine, and the flexibility of the sulfo-betaine chain, were the main factors affecting the density of DNA aptamer on the surface. Adding to this, the efficiency of the EDC/NHS coupling reaction also plays a vital role. As a consequence, there was a large difference in the initial R_{ct} from sample to sample.

Nevertheless, these functionalised electrodes were used to detect PSA. The R_{ct} of the SAM prepared with amine terminated DNA aptamers was determined by fitting data to a modified Randles equivalent circuit shown in Figure 3.10. We assume the first SAM layer to be constant, which is reflected by the semi-circle of a higher frequency range while the R_{ct} was obtained from the second semi-circle at lower frequencies, which can be attributed to a SAM layer that changes with PSA binding.

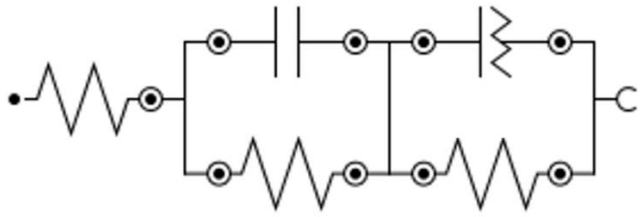

Figure 3.10 Modified Randles equivalent circuit to represent SAM prepared with amine terminated DNA aptamers.

For better evaluation of the PSA aptasensor, a complex capacitance was also defined, as explained in Chapter 2. Figure 3.11b represents a *Cole-Cole* capacitance plot using EIS data obtained at high frequencies before and after PSA binding. A fast capacitive process is observed at high frequencies represented by a semi-circle, followed by an ultra-slow process represented by a larger semicircle (Roling *et al.* 2012). Such a phenomenon is typical of impedance based sensors using redox couples in the electrolyte (Fernandes *et al.* 2014). Assuming that the impedance of the system is dominated by the electrostatic potential barrier of the DNA aptamer layer towards the negatively charged redox marker in the electrolyte, the increase of conductive paths upon binding with PSA could be attributed to the reduction in the net charge of the biolayer and, therefore, consistent with the hypothesis of DNA charge screening by PSA.

3.6.3 Dose response with sulfo-betaine/MUA surface chemistry

Electrodes functionalised with amine-terminated anti-PSA DNA aptamers via EDC/NHS coupling on a mixed SAM layer of MUA and sulfo-betaine were used for the dose response study with different concentrations of PSA. The EIS characteristics recorded for different PSA concentrations are represented in Figure 3.11. Generally, two semicircles are observed in the Nyquist plot, a small semicircle, and larger semicircle at high and low frequencies respectively. The small semicircle obtained at high frequencies, could have been due to relaxation effects of the SAM (Fernandes *et al.* 2014). The R_{ct} recorded from the first semicircle remains relatively constant (ΔR_{ct}

< 5%) throughout the experiments. As with the aptasensor in section 3.4, again a negative signal change was recorded on binding with PSA.

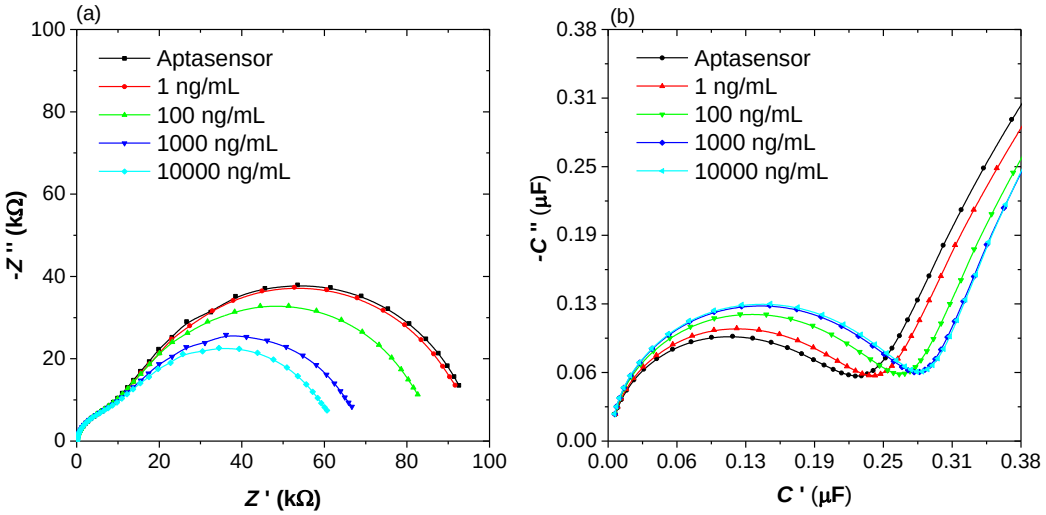

Figure 3.11 Left graph representing EIS characteristics for amine terminated functionalised gold electrodes (blue) in 10 mM ferro/ferricyanide $[Fe(CN)6]^{3-/4-}$ in 0.1M phosphate buffer (PB) solution containing 0.1 M KCl (pH 7.4).A decrease in R_{ct} on incubation with different PSA concentration was recorded. Right graph representing the Cole-Cole capacitance plots for higher frequencies. Incubation of functionalised sensor with PSA concentration was 30minutes.

Since, sulfo-betaine and MUA are considerably longer than MCH, we observe significantly higher values of R_{ct} than what has been reported in section 3.5. A dose response curve with different concentrations of PSA is shown in Figure 3.12. The binding curve obtained follows a Freundlich-type of equation ($\Delta R_{ct}/R_{ct} \propto [PSA]^n$) until 1000 ng/ml, after which it slowly tends to saturation. With this configuration, the sensitivity was increased and it was possible to detect PSA concentrations lower than 1 ng/mL (around 33 pM). By increasing the linker size from C6 spacer to C17 spacer (MUA+C6), it is possible that we have also increased the binding efficiency of the aptasensor (Balamurugan *et al.* 2006). However, the signal change recorded at lower PSA concentrations was relatively small. The reason for such a small signal change could be the net effect of different processes happening at the molecular level. The first dominating event happening is the change in the conformation of DNA aptamers on binding with PSA which should result in an increase in R_{ct}.

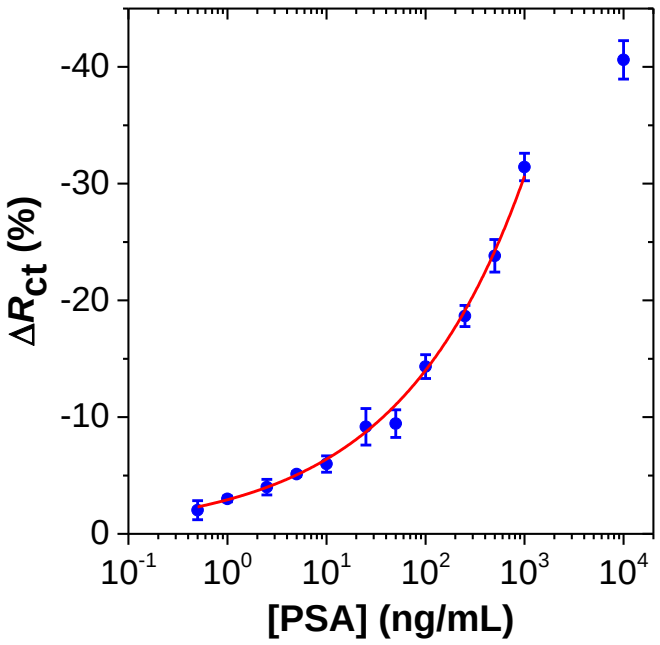

Figure 3.12 Dose response for amine terminated functionalised gold electrodes with different PSA concentrations in 0.1 M PB (pH 7.4) containing 10 mM $[Fe(CN)_6]^{3-/4-}$ and 0.1 M KCl. The error bars represent the standard deviation obtained for four samples.

Our assumption is that at such low concentrations of DNA aptamer, it is likely that all the aptamers are already in their stable folded conformation and hence leading to the effect of DNA aptamer conformational changes on R_{ct} is no longer observed. In addition, there is the screening of negative charges of DNA aptamers upon binding with PSA resulting into reduction in R_{ct}. On the other hand, a competitive effect might be observed to the binding of PSA molecules resulting into a further passivation of the electrode, which can hinder the access of the redox probes to a close distance of the electrode and hence increase in R_{ct}. The charges of protein also add on to R_{ct} values, which may be on either direction depending on the protein surface charge. Consequently, the net R_{ct} of the system depends on the combination of all the factors. Nevertheless, when compared with MCH chemistry, a 60 fold increase in the sensitivity was achieved with sulfo-betaine surface chemistry.

3.6.4 Dose response using surface plasmon resonance

Surface plasmon resonance (SPR) experiments were carried out in a dual-channel SPR7000DC from Reichert Technologies (USA). Gold coated SPR sensors were immobilised *in situ* with the anti-PSA DNA aptamer as per the described method in section 3.2.2, using thiol-terminated sulfo-betaine. Measurements were carried out in 10 mM PBS with 0.05% Tween 20 under flow conditions at 25 °C. The flow rate was kept constant at 25 µl/min upon injection of different protein concentrations, allowing 20 minutes for binding followed by 5 minutes for dissociation of unbound protein.

The binding of the aptamer with PSA was validated by means of SPR data. Using the same surface immobilisation process as for the sulfo-betaine impedimetric aptasensors, the SPR signal was monitored upon injection of different concentrations of PSA. Figure 3.13 shows the SPR equilibrium response values for each PSA concentration. A typical hyperbolic dose response is observed: $y = y_{max} * c/(K_d+c)$ where c is the concentration and K_d the affinity constant.

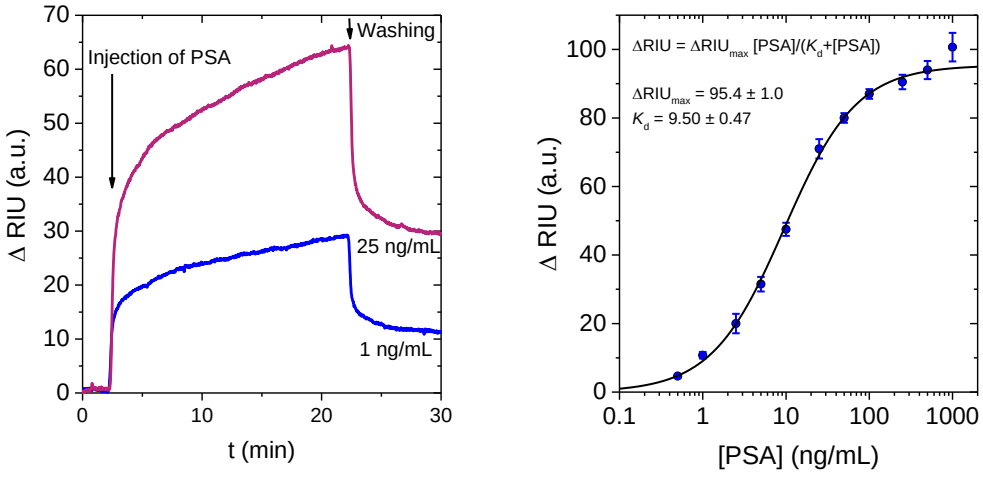

Figure 3.13 Left shows an example of characteristic SPR curves with 1 ng/mL and 25 ng/mL of PSA. Right shows the variation in the equilibrium SPR signals with respect to the baseline for different concentrations of PSA. Measurements were carried out in 10 mM PBS with 0.05% Tween 20. The line is a fit of the data to a hyperbolic dose response equation. The error bars represent the standard deviation obtained for three samples.

Fitting the data yields an affinity constant of $K_d = 9.50 \pm 0.47$ ng/ml (or 0.29 nM) with a root mean square (RMS) value of 0.99. To the best of the author's knowledge, this is the first time that a value of K_d was calculated by any research group. After this

work was published, many research groups have reported the K_d value of anti-PSA DNA aptamer which lies in nM range depending on the immobilisation and detection techniques (see Table 3.2 and Table 4.4).

3.6.5 Antifouling properties of sulfo-betaine surface chemistry

After successful sensitive detection of PSA, electrodes with sulfo-betaine surface chemistry were studied for non-specific adsorption. Again 100 µM HSA (circa 67 µg/mL) was used as a control protein. HSA was incubated with amine-terminated DNA aptamers functionalised electrodes and the results were compared with electrodes modified with thiolated DNA aptamers (Figure 3.14).

The results clearly indicate a significant difference in R_{ct} change between SAM prepared with sulfo-betaine and SAM prepared with MCH. Furthermore, a negligible signal change (< 1%) was recorded where sulfo-betaine was used to prepare the SAM, as compared to a high R_{ct} change with the SAM composed of MCH. Such an enhanced antifouling effect could be predominantly due to the creation of a hydration layer by sulfo-betaine moieties since zwitterions bind strongly to water (Figure 3.15). Such a hydration layer prevents proteins to penetrate through the water layer and adsorb on the surface (Tegoulia *et al.* 2001; White and Jiang 2010).

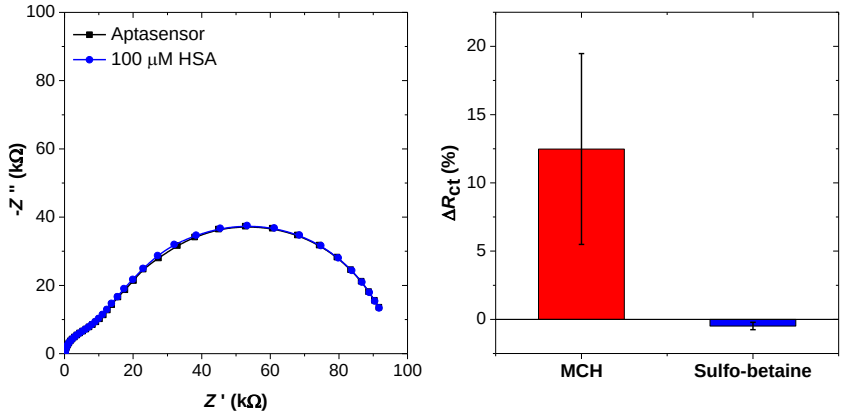

Figure 3.14 Change in R_{ct} on incubation with HSA with functionalised electrodes with amine terminated DNA aptamers (left) and thiolated DNA aptamers (right) in 0.1 M PB (pH 7.4) containing 10 mM $[Fe(CN)_6]^{3-/4-}$ and 0.1 M KCl. 100 µM HSA was used with 30 minutes incubation time. Number of samples per data point: 4

Furthermore, the aptasensor was also challenged with hK2 protein as a control. hK2 was chosen as a control protein candidate, since it shows the most stringent conditions, sharing 80% homology with PSA in protein sequence. Upon incubation with 10 ng/ml and 100 ng/ml of hK2, R_{ct} decreases by -1.1% and -1.6%, respectively (Figure 3.16).

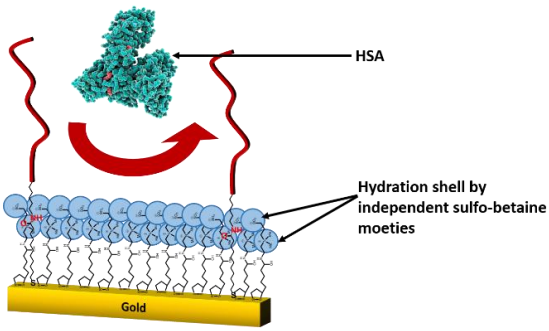

Figure 3.15 Thiol terminated sulfo-betaine based SAM representing formation of hydration layer to prevent non-specific binding.

For comparison, decreases of -6.0% and -14.3% were observed for similar concentrations of PSA. These results indicate that not only that the sulfo-betaine moiety effectively prevents non-specific interactions, but the aptamer is also highly selective towards PSA.

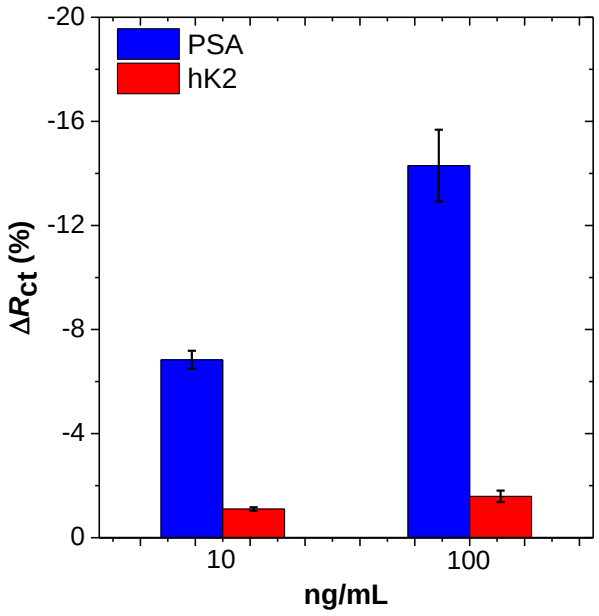

Figure 3.16 Aptamer selectivity test with human Kallikrein II (hK2) protein.

3.7 Summary

This Chapter reports a development of a PSA aptasensor with enhanced antifouling chemistry to detect the biomarker of interest in complex samples. The Chapter presented and discussed the incorporation of molecules like MCH or thiol terminated sulfo-betaine to enable optimization of the sensor surface for increased sensitivity and reduced non-specific binding.

This Chapter reports the use of thiol terminated sulfo-betaine with DNA aptamers as a promising spacer molecule. Although the optimization of surface density was a challenge, the fabricated aptasensors could potentially be used to detect PSA levels lower than 1 ng/ml (around 30 pM), which falls within the clinical range found in blood (1-10 ng/ml). The Chapter also demonstrated how important it is to perform stability tests of the fabricated aptasensors in order to obtain reliable data.

Since this experimental work was performed and published, a handful of other research groups have reported the development of PSA aptasensors based on electrochemical detection techniques as listed in Table 3.2. Many of the PSA aptasensor developments is either based on the use of complex polymer composites or with amplification steps. For instance, Kavosi *et al.* reported a triple amplification strategy for the detection of PSA (Kavosi *et al.* 2015). The group developed the system by modifying the surface of glassy carbon electrode with graphene oxide and chitosan composite to covalently attach anti-PSA antibodies and thionine as redox probes. Finally, Dendrimers modified with AuNPs were used to immobilise thiolated anti-PSA DNA aptamers and HRP linked aptamers to complete the sandwich assay with the primary antibodies on the polymer films. Such a system was used to capture PSA and a LOD of 0.15 pM was achieved using EIS. Tahmasebi and Noorbakhsh reported the development of a PSA aptasensor based on chitosan and carboxylated carbon nanotubes composites on glassy carbon electrodes with a limit of detection of 0.75 ng/mL (Tahmasebi and Noorbakhsh 2016). Although groups have reported better sensitivity than what has been presented in this Chapter, the simplicity of our approach to detect PSA within the clinical range sets our strategy apart.

Table 3.2 Comparison with existing state of art related to electrochemical PSA aptasensor

Detection principle	Electrode	Strategy	LOD/ K_d	Reference
DPV & CV	GCE	AuNPs encapsulated in graphitised mesoporous carbons deposited on GCE followed by immobilisation of streptavidin which was used to bind biotinylated DNA aptamers	LOD: 7.58 pM	Liu *et al.* 2012
EIS & SPR	**GE**	**SAM with thiol terminated sulfo-betaine**	**LOD: 30.3 pM K_d from SPR: 0.29 nM**	**Jolly *et al.* 2015**
EIS & QCMD	**GE**	**SAM with 6-mercapto 1-hexanol**	**K_d: 37 nM**	**Formisano *et al.* 2015**
EIS	GE	SAM of DNA probes which are partially complementary to DNA aptamer was used to capture DNA aptamer/PSA complex.	LOD in fM range	Yang *et al.* 2015
DPV/EIS	GCE	Graphene chitosan composite deposited on GCE followed by immobilisation of antibodies and thionine to capture PSA. AuNPs–PAMAM functionalised with mixture of PSA aptamer and biotinylated-PSA aptamer was used for completing the sandwich type immunoreaction. (Horseradish peroxidase) HRP–streptavidin was used as an electrochemical label that specifically bind to biotinylated aptamers	LOD from DPV: 0.3 fM LOD from EIS: 0.15 pM	Kavosi *et al.* 2015
SWV	GCE	Deposition of Quinone based polymer followed by covalent grafting of amine terminated DNA aptamers	K_d: 2.6 nM LOD in pM range	Souada *et al.* 2015
EIS	GE	Hybrid of DNA aptamer and Molecularly imprinted polymer	LOD: 30 fM	Jolly *et al.* 2016
CV/EIS/DPV	GCE	Carboxylated carbon nanotubes (CNTs) mixed with chitosan was physically adsorbed on the electrode surface. Amine terminated DNA aptamers were covalently attached to carboxylic groups	LOD: 0.75 ng/mL (22 pM)	Tahmasebi and Noorbakhsh 2016

*DPV: Differential Pulse Voltammetry
*CV: Cyclic Voltammetry
*GCE: Glassy Carbon Electrode
*AuNPs: Gold nanoparticles
*GE: Gold Electrode
*EIS: Electrochemical Impedance Spectroscopy
*SPR: Surface Plasmon Resonance
*QCMD: Quartz Crystal Microbalance with Dissipation Signals

References

Acevedo, B., Perera, Y., Ruiz, M., Rojas, G., Benítez, J., Ayala, M., and Gavilondo, J., 2002. Development and validation of a quantitative ELISA for the measurement of PSA concentration. *Clinica Chimica Acta*, 317(1-2), 55-63.

Albrecht, S., Brandl, H., Steinke, M., and Freidt, T., 1994. Chemiluminescent enzyme immunoassay of prostate-specific antigen based on indoxyl phosphate substrate. *Clinical Chemistry*, 40(10), 1970-1971.

Balamurugan, S., Obubuafo, A., Soper, S.A., McCarley, R.L., and Spivak, D.A., 2006. Designing highly specific biosensing surfaces using aptamer monolayers on gold. *Langmuir*, 22(14), 6446-6453.

Banerjee, I., Pangule, R.C., and Kane, R.S., 2011. Antifouling coatings: recent developments in the design of surfaces that prevent fouling by proteins, bacteria, and marine organisms. *Advanced Materials*, 23(6), 690-718.

Bard, A.J., Faulkner, L.R., Leddy, J. and Zoski, C.G., 2001. *Electrochemical methods: fundamentals and applications*, (Vol. 2). New York: Wiley.

Bertok, T., Klukova, L., Sediva, A., Kasak, P., Semak, V., Micusik, M., Omastova, M., Chovanová, L., Vlček, M., and Imrich, R., 2013. Ultrasensitive impedimetric lectin biosensors with efficient antifouling properties applied in glycoprofiling of human serum samples. *Analytical Chemistry*, 85(15), 7324-7332.

Biagiotti, V., Porchetta, A., Desiderati, S., Plaxco, K.W., Palleschi, G., and Ricci, F., 2012. Probe accessibility effects on the performance of electrochemical biosensors employing DNA monolayers. *Analytical and Bioanalytical Chemistry*, 402(1), 413-421.

Fernandes, F.C., Santos, A., Martins, D.C., Goes, M.S., and Bueno, P.R., 2014. Comparing label free electrochemical impedimetric and capacitive biosensing architectures. *Biosensors and Bioelectronics*, 57, 96-102.

Formisano N. (2015). A study on the optimisation of electrochemical impedance spectroscopy biosensors (Doctoral dissertation, University of Bath).

Formisano, N., Jolly, P., Bhalla, N., Cromhout, M., Flanagan, S.P., Fogel, R., Limson, J.L., and Estrela, P., 2015. Optimisation of an electrochemical impedance spectroscopy aptasensor by exploiting quartz crystal microbalance with dissipation signals. *Sensors and Actuators B: Chemical*, 22-, 369-375.

Hermanson, G.T., 2013. *Bioconjugate techniques*. Academic press.

Herne, T.M., and Tarlov, M.J., 1997. Characterization of DNA probes immobilised on gold surfaces. *Journal of the American Chemical Society,* 119(38), 8916-8920.

Holmlin, R.E., Chen, X., Chapman, R.G., Takayama, S., and Whitesides, G.M., 2001. Zwitterionic SAMs that resist nonspecific adsorption of protein from aqueous buffer. *Langmuir,* 17(9), 2841-2850.

Jolly, P., Formisano, N., Tkáč, J., Kasák, P., Frost, C.G., and Estrela, P., 2015. Label-free impedimetric aptasensor with antifouling surface chemistry: A prostate specific antigen case study. *Sensors and Actuators B: Chemical*, 209, 306-312.

Jolly, P., Tamboli, V., Harniman, R.L., Estrela, P., Allender, C.J., and Bowen, J.L., 2016. Aptamer–MIP hybrid receptor for highly sensitive electrochemical detection of prostate specific antigen. *Biosensors and Bioelectronics*, 75, 188-195.

Kane, R.S., Deschatelets, P., and Whitesides, G.M., 2003. Kosmotropes form the basis of protein-resistant surfaces. *Langmuir,* 19(6), 2388-2391.

Kavosi, B., Salimi, A., Hallaj, R., and Moradi, F., 2015. Ultrasensitive electrochemical immunosensor for PSA biomarker detection in prostate cancer cells using gold nanoparticles/PAMAM dendrimer loaded with enzyme linked aptamer as integrated triple signal amplification strategy. *Biosensors and Bioelectronics*, 74, 915-923.

Keighley, S.D., Estrela, P., Li, P., and Migliorato, P., 2008a. Optimization of label-free DNA detection with electrochemical impedance spectroscopy using PNA probes. *Biosensors and Bioelectronics,* 24(4), 906-911.

Keighley, S.D., Li, P., Estrela, P., and Migliorato, P., 2008b. Optimization of DNA immobilisation on gold electrodes for label-free detection by electrochemical impedance spectroscopy. *Biosensors and Bioelectronics,* 23(8), 1291-1297.

Kuang, J., and Messersmith, P.B., 2012. Universal surface-initiated polymerization of antifouling zwitterionic brushes using a mussel-mimetic peptide initiator. *Langmuir*, 28(18), 7258-7266.

Lee, J.W., Sim, S.J., Cho, S.M., and Lee, J., 2005. Characterization of a self-assembled monolayer of thiol on a gold surface and the fabrication of a biosensor chip based on surface plasmon resonance for detecting anti-GAD antibody. *Biosensors and Bioelectronics*, 20(7), 1422-1427.

Liu, B., Lu, L., Hua, E., Jiang, S., and Xie, G., 2012. Detection of the human prostate-specific antigen using an aptasensor with gold nanoparticles encapsulated by graphitized mesoporous carbon. *Microchimica Acta*, 178(1-2), 163-170.

Love, J.C., Estroff, L.A., Kriebel, J.K., Nuzzo, R.G., and Whitesides, G.M., 2005. Self-assembled monolayers of thiolates on metals as a form of nanotechnology. *Chemical Reviews*, 105(4), 1103-1170.

Miodek, A., Regan, E.M., Bhalla, N., Hopkins, N.A., Goodchild, S.A., and Estrela, P., 2015. Optimisation and Characterisation of Anti-Fouling Ternary SAM Layers for Impedance-Based Aptasensors. *Sensors*, 15(10), 25015-25032.

Okuno, J., Maehashi, K., Kerman, K., Takamura, Y., Matsumoto, K., and Tamiya, E., 2007. Label-free immunosensor for prostate-specific antigen based on single-walled carbon nanotube array-modified microelectrodes. *Biosensors and Bioelectronics*, 22(9-10), 2377-2381.

Panini, N.V., Messina, G.A., Salinas, E., Fernández, H., and Raba, J., 2008. Integrated microfluidic systems with an immunosensor modified with carbon nanotubes for detection of prostate specific antigen (PSA) in human serum samples. *Biosensors and Bioelectronics*, 23(7), 1145-1151.

Putzbach, W., and Ronkainen, N.J., 2013. Immobilisation Techniques in the Fabrication of Nanomaterial-Based Electrochemical Biosensors: A Review. *Sensors*, 13(4), 4811-4840.

Rodriguez, M.C., Kawde, A.-N., and Wang, J., 2005. Aptamer biosensor for label-free impedance spectroscopy detection of proteins based on recognition-induced switching of the surface charge. *Chemical Communications,* (34), 4267-4269.

Roling, B., Drüschler, M., and Huber, B., 2012. Slow and fast capacitive process taking place at the ionic liquid/electrode interface. *Faraday Discussions,* 154, 303-311.

Savory, N., Abe, K., Sode, K., and Ikebukuro, K., 2010. Selection of DNA aptamer against prostate specific antigen using a genetic algorithm and application to sensing. *Biosensors and Bioelectronics,* 26(4), 1386-1391.

Seto, Y., Iba, T., and Abe, K., 2001. Development of ultra-high sensitivity bioluminescent enzyme immunoassay for prostate-specific antigen (PSA) using firefly luciferase. *Luminescence,* 16(4), 285-290.

Souada, M., Piro, B., Reisberg, S., Anquetin, G., Noël, V., and Pham, M., 2015. Label-free electrochemical detection of prostate-specific antigen based on nucleic acid aptamer. *Biosensors and Bioelectronics,* 68, 49-54.

Tahmasebi, F., and Noorbakhsh, A., 2016. Sensitive Electrochemical Prostate Specific Antigen Aptasensor: Effect of Carboxylic Acid Functionalised Carbon Nanotube and Glutaraldehyde Linker. *Electroanalysis*.

Tegoulia, V.A., Rao, W., Kalambur, A.T., Rabolt, J.F., and Cooper, S.L., 2001. Surface properties, fibrinogen adsorption, and cellular interactions of a novel phosphorylcholine-containing self-assembled monolayer on gold. *Langmuir,* 17(14), 4396-4404.

Wang, M., Papsidero, L., Kuriyama, M., Valenzuela, L., Murphy, G., and Chu, T., 1981. Prostate antigen: a new potential marker for prostatic cancer. *The Prostate,* 2(1), 89-96.

Wee, K.W., Kang, G.Y., Park, J., Kang, J.Y., Yoon, D.S., Park, J.H., and Kim, T.S., 2005. Novel electrical detection of label-free disease marker proteins using

piezoresistive self-sensing micro-cantilevers. *Biosensors and Bioelectronics*, 20(10 SPEC. ISS.), 1932-1938.

White, A., and Jiang, S., 2010. Local and bulk hydration of zwitterionic glycine and its analogues through molecular simulations. *The Journal of Physical Chemistry B* 115(4), 660-667.

Yang, W., Chen, S., Cheng, G., Vaisocherová, H., Xue, H., Li, W., Zhang, J., and Jiang, S., 2008. Film thickness dependence of protein adsorption from blood serum and plasma onto poly (sulfobetaine)-grafted surfaces. *Langmuir*, 24(17), 9211-9214.

Yang, Z., Kasprzyk-Hordern, B., Goggins, S., Frost, C.G., and Estrela, P., 2015. A novel immobilisation strategy for electrochemical detection of cancer biomarkers: DNA-directed immobilisation of aptamer sensors for sensitive detection of prostate specific antigens. *Analyst*, 140(8), 2628-2633.

Zhang, W.-M., Leinonen, J., Kalkkinen, N., Dowell, B., and Stenman, U.-H., 1995. Purification and characterization of different molecular forms of prostate-specific antigen in human seminal fluid. *Clinical Chemistry*, 41(11), 1567-1573.

Zhang, Z., Chao, T., Chen, S., and Jiang, S., 2006. Superlow fouling sulfobetaine and carboxybetaine polymers on glass slides. *Langmuir*, 22(24), 10072-10077.

Chapter 4. Aptasensors for both quantification and multi-glycan profiling of PSA

Since PSA alone does not fulfil the requirements to discriminate between different stages of PCa, this Chapter will present the development of a dual biomarker detection, namely the amount of PSA and glycoprofiling of PSA. Deviating from the usual electrochemical techniques, such an assay development was studied using optical methods. Two novel sandwich-based immunoassays for PSA detection are reported, in which the capture antibody is replaced by an anti-PSA DNA aptamer. A detector molecule (antibody or a lectin) is used to quantify PSA along with glycoprofiling by a chemiluminescence approach.

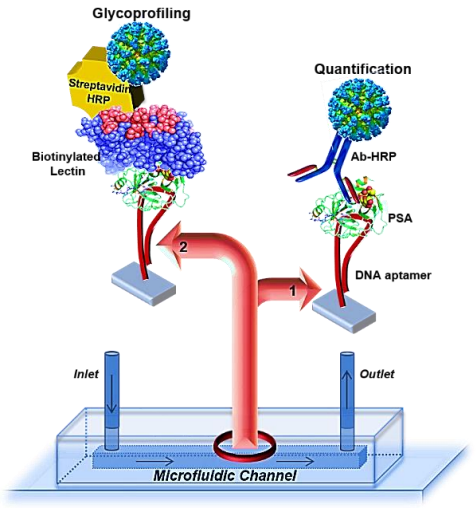

The work presented in this Chapter has been published in Jolly *et al*. (Jolly *et al.* 2016)

4.1 Background

Replacing the antibodies in a classical ELISA configuration has enabled the development of sophisticated assays which are more robust, reproducible and economical (Tennico *et al.* 2010; Toh *et al.* 2015). Such reformed ELISA methods

have also been validated in a microfluidic setup, which holds great promise as a potential point-of-care (PoC) device. For instance, Su *et al*. recently reported a lab-on-paper cyto-device to demonstrate detection of cancer cells together with multi-glycans profiling on living cancer cells (Su *et al.* 2015). In 2011, an aptamer-based ELISA approach was reported by Liu *et al.* for the detection of rare cells using chemiluminescence (Liu *et al.* 2011). Chemiluminescence is a phenomenon of emission of light as a result of a chemical reaction. It is a type of luminescence where light is emitted from a substance as a consequence of the transition from an electronically excited state to the ground state. It is distinct from photoluminescence, which is also referred as fluorescence, where the phenomenon is initiated by the light of a particular wavelength. In this Chapter, enhanced chemiluminescence is being employed for the detection of the analytes. Anti-PSA antibody or streptavidin-tethered with the enzyme horseradish peroxidase (HRP) are used for quantification or glycoprofiling studies, respectively. Such an enzyme catalyzes the substrate having chemiluminescent characteristics like luminol (3-Aminophthalhydrazide). Such a reaction of luminol oxidation is carried out in the presence of HRP and hydrogen peroxide (H_2O_2) as an oxidant, to generate excited state intermediates. The excited intermediated produced during the reaction returns to the ground state by emitting light at a wavelength of 425 nm.

This Chapter reports the development of aptamer-based ELISA for quantification of free prostate specific antigen (fPSA) in a microfluidic device. Along with the quantification of fPSA, glycoprofiling could effectively serve as a complementary procedure for enhanced diagnosis and monitoring of PCa and potentially reduce the levels of false positives through blood tests. Thus, this Chapter also reports multi-glycan profiling of fPSA using an aptamer-based sandwich assay in a microfluidic chemiluminescence sensor. Since PSA is a glycoprotein with various glycoforms (Isono *et al.* 2002; Végvári *et al.* 2012; Vermassen *et al.* 2012), the determination of cancer-associated glycoforms of PSA might help to improve early-stage clinical diagnosis of PCa (Meany and Chan 2011).

4.2 Materials and Methods

4.2.1 List of reagents

Table 4.1 lists the reagents used for the development of the sensor. The antibodies were diluted in 10 mM PBS (pH7.4) and filtered using a 0.4 µm syringe filter to remove any un-dissolved salt crystals and impurities. All aqueous solutions were prepared using MilliQ water and filtered before use. Table 4.2 lists the accessories used to perform the microfluidic assay.

Table 4.1 List of reagents

Catalog No.	Reagent	Purpose/Reaction	Source
Anti-PSA DNA aptamer	5'-H_3N-$(CH_2)_6$-TTT TTA ATT AAA GCT CGC CAT CAA ATA GCT TT-3'	To Capture PSA (as a primary antibody)	Sigma, UK
Anti-PSA DNA aptamer	5'-H_3N-$(CH_2)_6$-TTT TTA ATT AAA GCT CGC CAT CAA ATA GCT TT-Cy5-3'	PSA specific DNA aptamer labelled with Cyanine3 for nanodrop experiments	Sigma, UK
Random DNA sequence non-specific to PSA	(5'-H_3N-$(CH_2)_6$-AAA AAT TAA TTT CGA GCG GTA GTT TAT CGA AA-3'	Control sequence	Sigma, UK
30C-CP1017	f-PSA	Antigen (target)	Fitzgerald, UK
Label	Streptavidin-HRP	Bio-affinity, labelled	Invitrogen Life Technologies (USA)
B-1305	Biotinylated SNA (*Sambucus nigra* agglutinin)	Detector molecule	VectorLab, UK
B-1265	Biotinylated MAA II (*Maackia amurensis* lectin)	Detector molecule	VectorLab, UK
Ab24466	Anti-equimolar total PSA-HRP antibody	Detector Ab for chemiluminescent studies	Abcam, UK

Ab178776	Anti-equimolar total PSA-FITC antibody	Detector Ab for fluorescent studies	Abcam, UK
Super Signal West Femto	Pierce (Supersignal® West Femto Substrate Trial Kit – 34094 and Supersignal West Pico – 35065)	Substrate for HRP enzyme	Thermo Scientific, Portugal
440167	(3-Glycidyloxypropyl)trimethoxysilane (GOPTS)	Immobilisation	Sigma Aldrich, UK
411000	Ethanolamine	Blocking agent to avoid non-specific binding	Sigma Aldrich, UK

Table 4.2 List of microfluidic accessories

Material	Source
Syringe tips LS20	Instech Laboratories, Inc., USA
Polyethylene tubing BTPE-90	Instech Laboratories, Inc., USA
Tubing adaptors SC 20/15	Instech Laboratories, Inc., USA
Microtube Eppendorf tubes (1.5 mL)	Sigma, UK
Syringes 1 mL	CODAN Medical ApS, DK
Syringe Pump NE-300	New Era Pump Sustems, Inc, USA

4.2.2 Fabrication of PDMS microchannel structures

A patterned SU-8 mould was supplied by INESC Microsistemas e Nanotecnologias (Portugal). Several microfabrication steps are performed in order to obtain a well-defined microchannel in a polydimethylsiloxane (PDMS) structure. Briefly, the fabrication of the PDMS microchannels was performed using soft lithography. Fabrication of hard mask, SU-8 mould, and PDMS devices were adapted from

literature as described by Novo *et al* (Novo *et al.* 2013) and Soares *et al.* (Soares *et al.* 2014). The process can be divided into three main categories, namely the aluminium (Al) mask fabrication, SU-8 mould fabrication and microchannel fabrication (Figure 4.1).

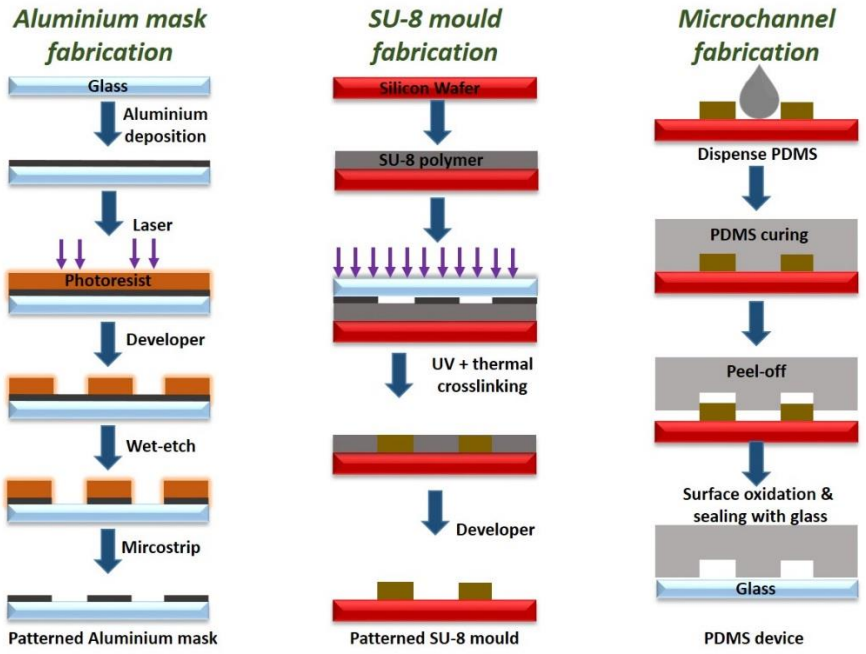

Figure 4.1 Microfabrication steps. (Aluminium mask fabrication) A clean glass substrate is coated with an aluminium layer and a positive photoresist followed by exposure of the photoresist by mask less lithography and developing of the photoresist. An aluminium wet etchant removes the uncovered aluminium and the remaining photoresist is stripped off. (SU-8 mould fabrication) A clean silicon substrate is coated with a negative photoresist and exposed to UV light, using the aluminium mask produced. The photoresist is developed and the unexposed areas are removed. (Microchannel fabrication) PDMS is poured on top of the silicon substrate with pattern, cured in a baking step and removed from the mould. After surface oxidation of both surfaces, the patterned PDMS device is sealed to a clean glass to produce micro channel devices.

Briefly, for the fabrication of the Al mask, a thin and homogeneous layer of Al is deposited on a clean glass substrate by reactive magnetron sputtering. In sputtering, argon atoms are in-fluxed into a vacuum chamber containing both the Al target and the glass substrate. With the application of a DC voltage between the Al target and the glass substrate, a discharge plasma is created for the ionization of the argon atoms. The highly energetic positive ions produced undergo a collision with the target cathode, which removes surface atoms of the target (Al) and emits secondary electrons of the target (Arvinte 2011). The energy released as a consequence of the collision

corresponds to the voltage drop between Al target and plasma. Specifically in a magnetron sputtering, a strong magnetic field is created near the target area to increase the efficiency. Due to the induced magnetic field, there is a higher attraction of the electrons to the target instead of the substrate. Such an attraction results in a longer traveling distance of the electrons and hence a higher chance to ionize further argon atoms. As a consequence, a stable plasma is created containing a high ion concentration. The formation of the required design of the microchannels on the Al layer can be realised by photolithography based on light-sensitive photoresists. A photoresist that dissolves in a specific solvent, when exposed to light is called a positive resist, whereas a negative resist does not dissolve due to cross-linking interaction because of light (Madou 2002). Although there are different ways to expose a specific pattern on a photoresist, but a simple technique is to place an optical opaque mask with the required features on top of the positive resist. Such a step will cover the areas of interest. In a direct write lithography (DWL), usually, a laser beam is integrated into a programmable machine and scans the photoresist line by line, using a computer aided software. Such a process comes under mask-less lithography, which is usually more time-consuming compared to traditional mask lithography. Later, the substrate is washed with a specific solvent to remove the area of photoresist which was exposed to the laser beam. The exposed layer of Al can be chemically etched and the remaining resist is stripped off using a photoresist-strip solution. The mask obtained can be used to create an inverse replica mould of the desired features.

For the SU-8 (Microchem, USA) mould fabrication, a negative photoresist is spin coated on a clean silicon substrate. Later, the Al mask created in the previous steps is mounted on the photoresist. Finally, the resist is exposed to UV radiation. The mould is then developed in propylene glycol monomethyl ether acetate (Sigma-Aldrich, Portugal) (Soares *et al.* 2014b).

Later, the mould patterns were transferred to polydimethylsiloxane (PDMS) to obtain the microfluidic devices for the experiments. PDMS is composed of repeating units of silicon atoms attached to one oxygen and two methyl groups. PDMS is used in this study because of varied advantages like optical transparency in the wavelength from 240 to 1100 nm enabling easy optical detection using chemiluminescence and

impermeable to liquid (McDonald and Whitesides 2002). The PDMS devices consisting of microchannels with width, w = 200 µm, height, h = 20 µm and length, l = 1 cm were sealed to a cleaned glass substrate via an UV-ozone treatment for 6 min at 28-32 mW/cm^2 (UVO cleaner 144AX, Jelight Company Inc., USA) for surface oxidation. The surface oxidised PDMS and glass substrates were then brought together and gently pressed to ensure bonding. After 1 day, these microfluidic devices are permanently sealed and ready for the experiments.

4.2.3 Optical image acquisition and analysis

The fluorescence signal from the microchannel was recorded using a fluorescence microscope (Leica DMLM) connected to a digital camera (Leica DFC300FX). The chemiluminescent signal was acquired using a microscope after flowing luminol, with an exposure time of 10 sec and 10x optical gain, all in a dark background. The acquired images were later analysed using ImageJ software (National Institutes of Health, USA). The values presented here after correspond to the background normalised average measurements from three independent experiments, each with three regions of interest along the microchannel.

4.3 Microfluidic Aptamer Assays

Surface functionalisation of aptamers for both fPSA quantification and glycoprofiling studies were performed according to the steps listed in Table 4.3. The following steps for quantification and glycoprofiling were always performed immediately after the surface functionalisation procedure. New microfluidic structures were used in each experiment.

Figure 4.2 represents the microfluidic device setup. The microfluidic channel is connected via tubing to the syringe tubes. Syringe tubes are placed on a multi-channel syringe pump to control the flow rates and perform a multiplexed assay. On the right, a magnified image of the PDMS structure containing microfluidic channel is shown. It consists of inlet channels connected to the syringe tubes and the outlet channels for

waste. All the tubings were connected carefully in order to avoid any dead space that could lead to entrapment of air.

Table 4.3 Microfluidic assay protocol

Step No.	Purpose	Reagent	Flow Rate (µl/min)	Incubation Time (min)	Concentration	Remarks
1	Silanisation	GOPTS	0.3	15	5%, 10%, 25%, 50% and 100%	Dilutions in water
2	Washing	Water	5	5	Milli-Q water	Rigorous to remove all non-specifically bound silane molecules
3	DNA aptamers	1X PBS	0.4	5, 10, 15, 30	10 µM	Activation needed
4	Washing	1X PBS	5	2	Milli-Q water	Rigorous to remove all non-specifically bound molecules
5	Ethanolamine blocking	1X PBS	0.5	15	10 mM, pH 8.5	To block all unreacted sites of silane
6	Washing	1X PBS	5	2	Milli-Q water	Rigorous
7	a. Antibody FITC/HRP b. Biotinylated Lectin	1X PBS	0.5	10	Both at 100 µg/ml	Detector molecule
8	Washing	1X PBS	5	1	Milli-Q water	To remove unbound molecules
9	Streptavidin HRP	1X PBS	0.5	10	100 µg/ml	Only in case of 11b
10	Washing	1X PBS	5	1	Milli-Q water	Final wash – stringent
11	Detection Substrate	Luminol	5	Until blue colour is seen	Directly from the provider	Only for HRP

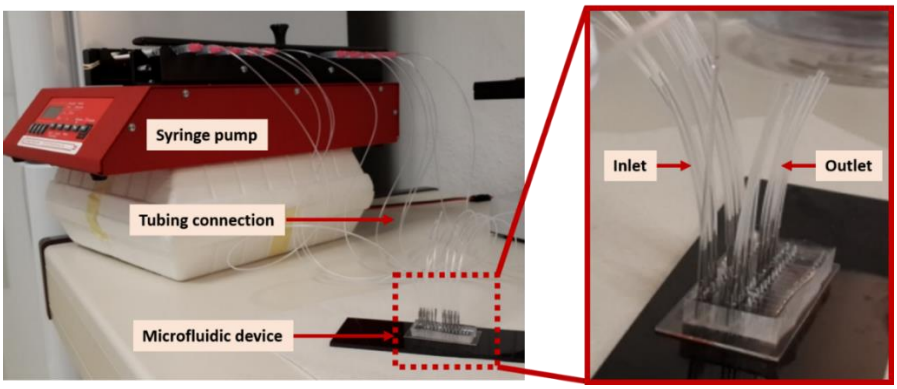

Figure 4.2 Microfluidic assay setup. Left shows the connection of microfluidic structure to the syringe pump via tubing. Right represent the microfluidic device magnified view with inlets and outlets

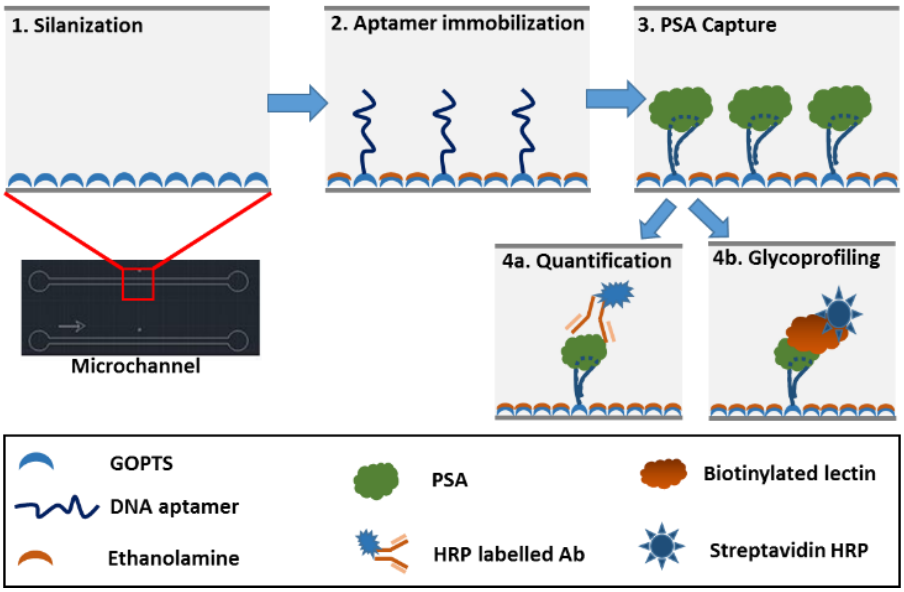

Figure 4.3 Schematic of microfluidic channel functionalisation for assay experiments.

Furthermore, the immobilisation steps listed in Table 4.3 can be represented as a schematic shown in Figure 4.3. For the control experiment, the second step of aptamer immobilisation was replaced by using a random DNA sequence of the same length and modification as that for PSA specific DNA aptamer.

4.4 Effect of DNA aptamer surface coverage on the chemiluminescence signal

With the aim of developing a sensitive microfluidic assay for fPSA detection, various optimisation steps were performed. Since the mode of immobilisation proposed was covalent grafting of DNA aptamers, GOPTS silane was used to minimise the steps. GOPTS is an epoxy organosilane which has the coupling reactivity with several nucleophiles including primary amines (Bañuls *et al.* 2013). Therefore, such a silane can be used to attach antibodies or amine modified oligonucleotides by an epoxide ring opening (Figure 4.4) (Ramachandran *et al.* 2008).

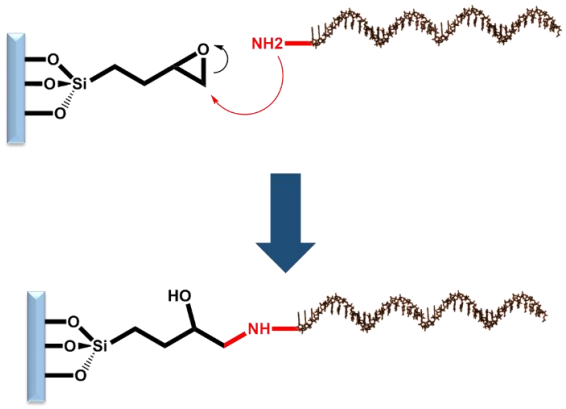

Figure 4.4 Scheme of bio conjugation procedure for GOPTS via oxidative ring opening based using primary amine (ideal case).

Anti-PSA antibody with FITC label was used to optimise the concentration of GOPTS used for silanisation. Briefly, GOPTS with the different concentration ranging from 5%, 10%, 50% and 100% in water was used to silanise the microfluidic channel. After washing steps, anti-PSA Ab labelled with FITC was flowed for 15 minutes. After washing away non-specifically bound antibodies, the channel was visualized using a fluorescence microscope with a compatible filter to the applied fluorophore (Olympus Microscope CHX41, blue excitation filter).

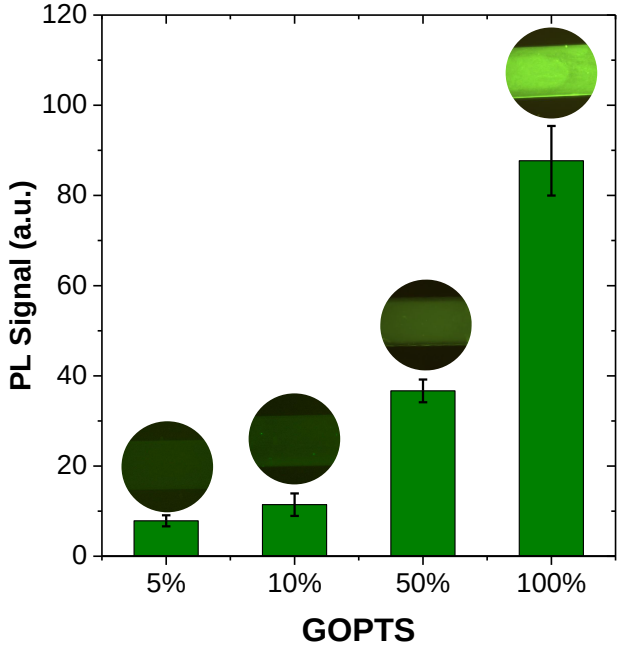

Figure 4.5 Optimisation of concentration of GOPTS for immobilisation of probes. Photoluminescence (PL) signal presented is by using only Ab labelled with FITC as a case study.

Figure 4.5 represents the photo luminescence (PL) signal also called fluorescence signal, obtained with the different concentration of GOPTS. A low fluorescence signal with both 5% and 10% GOPTS is observed. The probable reason could be low coupling efficiency of antibodies to free epoxide rings and/or poor coverage of GOPTS on the surface. Nevertheless, the signal increased drastically with 50% and maximum signal with 100% GOPTS demonstrating an intense fluorescence signal as a result of enhanced coupling on the surface. Therefore, for further optimisation steps, 100% GOPTS was used to silanise the microfluidic channel.

For the development of the sensors, it is imperative to optimise both the physical and chemical aspects of the microfluidic biosensor, namely the dimensions of the microchannel, flow-rates, and probe immobilisation strategies. The first two parameters were previously optimised at INESC-MN and validated with an antibody-based ELISA system to detect fPSA and the optimised steps were used in the present study without further modification (Madaboosi *et al.* 2015).

However, this Chapter reports the use of anti-PSA DNA aptamer as a capture antibody and hence it is crucial to optimise the surface coverage of the probe. The surface density of probes, in particular, plays a vital role in fabricating an efficient biosensor irrespective of the detection technique used as reported by different research groups (Jolly *et al.* 2015; Keighley *et al.* 2008a; Keighley *et al.* 2008b; Madaboosi *et al.* 2015). Also, as demonstrated in Chapter 3, an optimum spacing between the aptamers on the surface allows minimal steric hindrance effects in order to successfully capture the target and undergo conformational changes. For efficient binding of fPSA in the microfluidic channel via anti-PSA DNA aptamers, the immobilisation time of anti-PSA DNA aptamers was investigated. The optimisation was performed after fPSA capture using anti-PSA DNA aptamers, followed by detection with an anti-fPSA antibody labeled with the reporter enzyme horseradish peroxidase (anti-fPSA Ab-HRP). A fixed concentration of DNA aptamer equal to 10 µM in 10 mM PBS (pH 7.4) was flowed for different time intervals and a fixed fPSA concentration of 10 ng/mL was chosen for the experiment. From Figure 4.6, it can be seen that as we increase the time of immobilisation of DNA aptamers from 5 min to 15 min, an increase in the chemiluminescence signal was observed. The signal increased from 12.5 $\pm$ 1.6 a.u. with 5 min incubation to 55.5 $\pm$ 6.9 a.u. with 15 minutes.

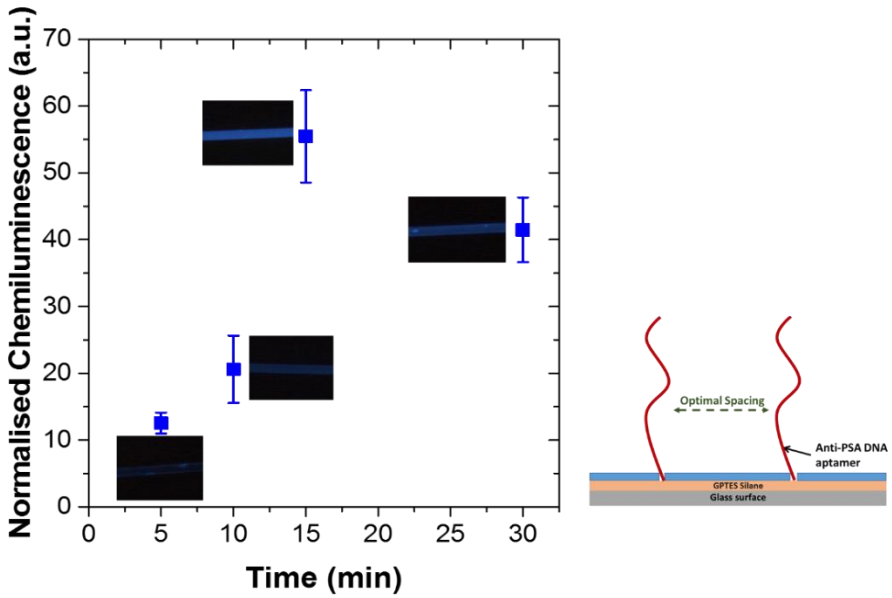

Figure 4.6 Chemiluminescence signal with different time periods of DNA aptamer immobilisation upon PSA binding, detected by anti-fPSA Ab-HRP.

However, as the time was further increased to 30 min, the chemiluminescence signal was reduced to 41.5 ± 4.8 a.u. Such a decrease could be attributed to the presence of high density of the anti-PSA DNA aptamer on the surface. As a result of too densely packed anti-PSA DNA aptamer, there is a decrease in PSA binding due to steric hindrance effects as also seen in Chapter 3 (Formisano *et al.* 2015). Thus, to achieve an effective PSA detection in the described microfluidic channel, 15 min was chosen as the immobilisation time for all the subsequent experiments.

4.5 Estimation of DNA aptamer surface coverage on the microfluidic channel

Nano spotting experiments were performed to estimate the surface coverage of anti-PSA DNA aptamers. For the experiments, anti-PSA DNA aptamers modified with a C-6 amine at the 5' end and labelled with a Cyanine3 on the 3' were spotted on the surface of the thin film of PDMS following the procedure reported by Novo *et al*. (Novo *et al.* 2011). A non-contact nano-spotter (Nanoplotter NP2.1, GeSiM, Germany) was used to spot anti-PSA DNA aptamer solutions with a piezoelectric pipette (Pico tip with a capacity to dispense single droplets with volumes down to ~56 pL) mounted on a computer controlled stage (Novo *et al.* 2011). Different concentrations of anti-PSA DNA aptamer solutions ranging from 1 µM, 3 µM, 5 µM, 8 µM and 10 µM were used to prepare the calibration curve. The total number of times a droplet solution was dispensed and the degree of hydrophilicity of the ozone treated PDMS film at a particular location determines the diameter and amount of DNA aptamers at that spot. The temperature was fixed at 16 °C and humidity was adjusted to near the dew point to increase the evaporation time of the droplets, ensuring homogeneous drying.

The nano-spotting method allows a precise and robust deposition of the solution with controlled volume of anti-PSA DNA aptamers onto a surface using a computer-aided micro-spotter (Novo *et al.* 2011). In the experiment, the aptamer solution is filled in a Pico tip that enables spots on the surface by dispensing the anti-PSA DNA aptamer solution in a non-contact mode (50 drops per spot). Known volumes from 50 droplets

of varied concentrations of anti-PSA DNA aptamer-Cy3 were spotted on a specific location on the PDMS film. The photoluminescence (PL) signal was measured from each deposited spot on the PDMS film. Fluorescence was obtained as a result of adsorbed anti-PSA DNA aptamer-Cy3 and the total number of anti-PSA DNA aptamers adsorbed per unit area was calculated. Each DNA aptamer occupies an area of 6.16×10^{-6} μm^2 assuming that all the DNA aptamers are in their single-stranded state and lying perpendicular to the surface, where a single stranded DNA has a hydrodynamic radius of 1.4 nm.

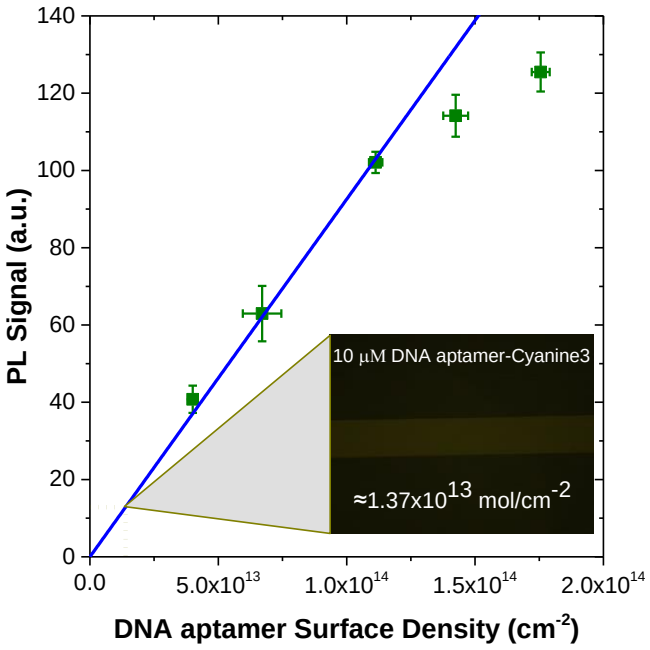

Figure 4.7 Nano-spotting of DNA aptamer labelled with Cy3 to estimate the surface density. The inset image shows the optical micrograph of DNA aptamers labelled with Cy3 covalently immobilised in the microchannel.

The data obtained can be used to make a correlation between the total number of anti-PSA DNA aptamer-Cy3 in the spot and the fluorescence intensity from the spot (Figure 4.7). The curve obtained was then used for determining the surface density of the immobilised anti-PSA DNA aptamers in the microfluidic channel at a known concentration. The inset in Figure 4.7 shows the PL signal of a typical relative surface coverage when anti-PSA DNA aptamers are immobilised in a microfluidic channel. By correlating the data obtained from the microchannel with the calibration curve, a

surface coverage of 1.37×10^{13} molecules/cm^2 was estimated from the obtained PL signal in the microchannel (PL signal: 12.80 $\pm$ 1.68 a.u.) with the covalently grafted anti-PSA DNA aptamer-Cy3.

4.6 Selectivity study using the microfluidic aptamer-based ELISA sensor

The development of a reliable biosensor depends on various factors including the resolution to differentiate between specific and non-specific binding. The selectivity of the sensor was investigated with various control experiments to confirm that the signals obtained with fPSA were due to the specific capture of fPSA by the anti-PSA DNA aptamers immobilised in the microfluidic channel. It is an essential step in a biosensor development procedure to be sure that the signal monitored is due to the capture of the target. Particularly in a sandwich-type of assay, the probability of false positives increases, as it employs two levels of capture. Therefore, stringent control experiments are required in order to develop a reliable sandwich assay.

As this Chapter is a demonstration of the prospective of an aptamer-based ELISA assay in a microfluidic channel, the role of anti-PSA DNA aptamers as a probe to capture fPSA was tested by using two rigid control experiments (Figure 4.8). In the first control experiment, the channel was first silanised and then blocked with ethanolamine without any immobilisation of anti-PSA DNA aptamers (Figure 4.8, #3). In the second control study, a random DNA sequence of the same length as of the ant-PSA DNA aptamer was immobilised on the microfluidic channel (Figure 4.8, #4) following the same protocol as described in the method section. Such a study was performed in order to confirm the role of DNA aptamer as a replacement of primary antibody as a capture probe. When the channels from the control experiments were observed under the microscope, a negligible change of less than 2 a.u. when compared with blank measurement was noticed. Whereas, the signal obtained from micro channels functionalized with anti-PSA DNA aptamers were as high as 55.5 $\pm$ 6.9 a.u. when compared with blank measurement. The results obtained assures the specific

binding of fPSA to anti-PSA DNA aptamers and subsequent sandwich based detection using anti-fPSA Ab labelled with HRP.

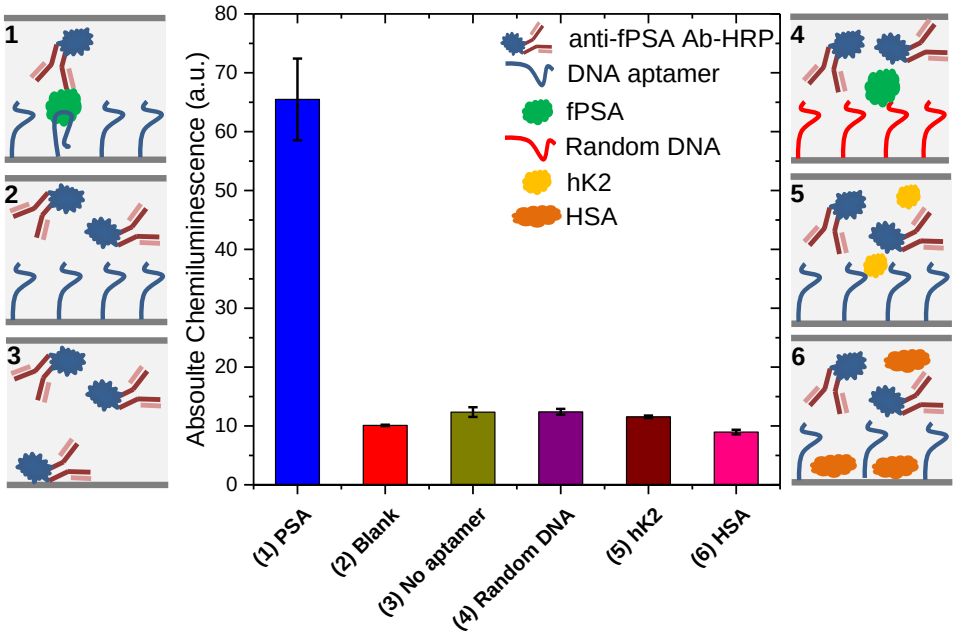

Figure 4.8 Selectivity studies with aptamer-based ELISA. (1) Specific detection of fPSA (10 ng/mL) by anti-PSA DNA aptamers and thereafter, detected by anti-fPSA labelled with HRP. (2) Signal obtained when no fPSA (0 ng/mL) was flowed. (3) Signal change when no aptamer was immobilised in the microchannel and 10 ng/mL fPSA was flowed. (4) When a random DNA sequence as a control was used and 10 ng/mL fPSA was flowed (5) Signal change with 10 ng/mL hK2. (6) Signal change with 4% HSA.

The microfluidic biosensor developed was also challenged with two control proteins using human Kallikrein 2 (hK2) (10 ng/mL) (Figure 4.8, #5) and human serum albumin (HSA) (40 mg/mL) (Figure 4.8, #6). hK2 as described in Chapter 1 is another serine protease from the same kallikrein family as fPSA. It was chosen as a control protein candidate of interest since it shares 80% structural homology with the fPSA. Although the levels of hK2 are 100 fold lower than that of PSA in clinical samples, this protein was stringently chosen since it served as an appropriate control to evaluate the aptamer-based approach over an antibody-based approach using ELISA (Hong 2014; Vaisanen *et al.* 2006). With an aptamer-based ELISA system, an appreciable differentiation in signal change between hK2 and PSA was monitored; the former, when compared with blank, showed a difference of less than 2 a.u. only (Figure 4.8,

#5). This can be distinctively differentiated from 10 ng/mL PSA (Figure 4.8, #1) with a difference of 55 a.u.

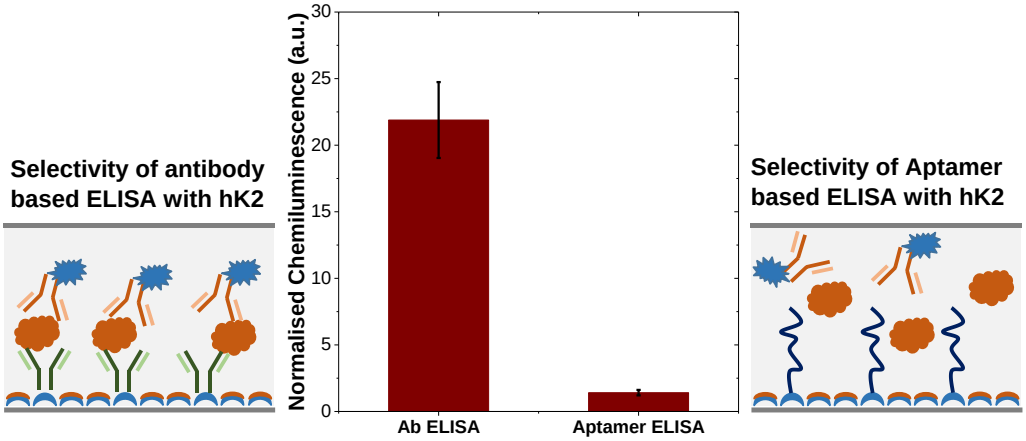

Figure 4.9 Comparison of antibody based ELISA with aptamer based ELISA on cross-reactivity with homologous proteins.

To make a stronger point, classical ELISA was performed by adsorption of capture antibodies in the microfluidic channel and followed by the flow of 10 ng/mL hK2 protein, and finally, a detector antibody labeled with HRP. The channel was then analyzed under a microscope. The results show a high level of cross reactivity of up to 20 a.u. and the inability of the antibodies to differentiate hK2 from PSA (Figure 4.9). The high cross reactivity could be due to the fact that most of the antibodies raised against PSA exhibit certain cross-reactivity with the hk2 due to similar epitopic regions. As another control protein, 4% HSA was used to test matrix interference effects and a slight decrease in chemiluminescence signal (~1 a.u.) was observed (Figure 4.8 #6). This could be attributed to the blocking effect of HSA, leading to decreased non-specific binding of detector antibodies.

4.7 Quantification of fPSA using the microfluidic biosensor

With established enhanced selectivity of the aptamer-based ELISA, aptamer functionalised microfluidic channels were used for the quantification of fPSA. The

aim of the study was to investigate the sensitivity of the developed biosensor. For quantification analysis, the assay was based on a sandwich ELISA format, where anti-fPSA antibodies labeled with HRP were used to detect the fPSA captured by the immobilised DNA aptamers (Aptamer-Antibody Assay). A wide working range of fPSA concentrations ranging from 0.01 ng/mL to 50 ng/mL were used in the current study. It is important to highlight that each assay was performed in a new microchannel immediately after immobilisation since PDMS structures with such small footprint can be easily produced in large numbers and disposability avoids the use of complex generation procedures and potential accumulation of non-specific binding. As seen from Figure 4.10, a significant increase in the chemiluminescence signals is observed between 1 ng/mL and 25 ng/mL of fPSA concentrations, which lies within the cutoff range (gray area) of PSA in blood. It can be immediately observed that the background signal is not limiting the detection sensitivity at the clinically relevant concentrations while still being detectable using the CCD camera of the microscope. This confirms that the ethanolamine blocking works effectively in providing a fit-for-purpose level of non-specificity.

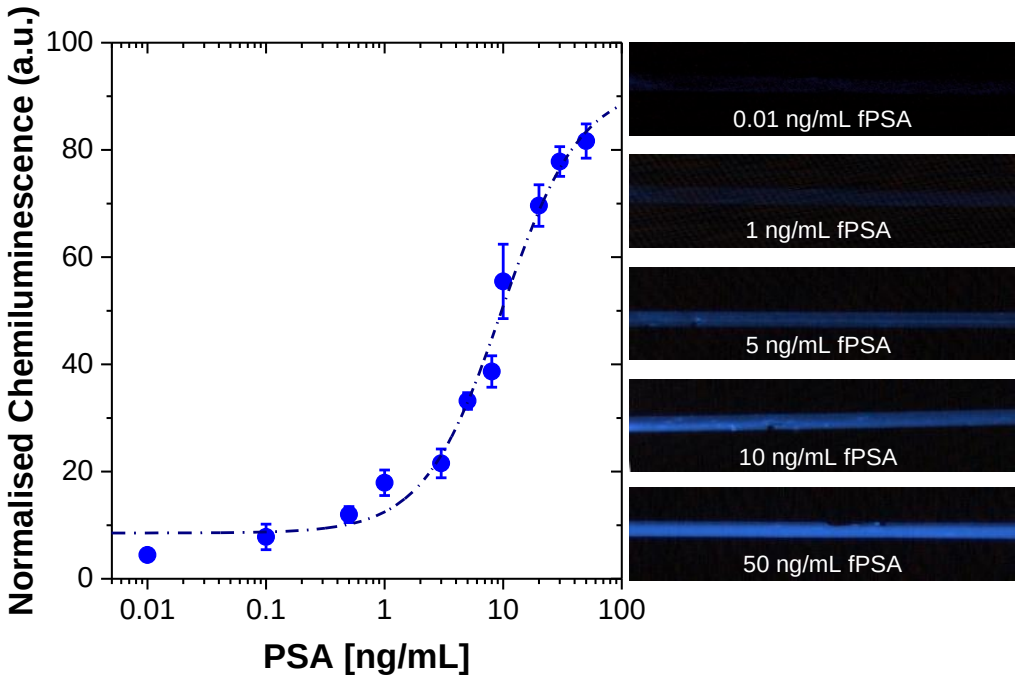

Figure 4.10 Quantification of fPSA using anti-fPSA Ab-HRP. Images represent the chemiluminescence signals from microscopy.

The response obtained for fPSA quantification follows a Hill dose-response equation of the type $y = y_0 + (y_{max} - y_0)\, c^n / (K_d^n + c^n)$ where c is the concentration. The dissociation constant (K_d) for the dose response was calculated as 9.82 ng/mL with a root mean square (RMS) value of 0.98. The value of y_{max}, which is the end value calculated from the fitting was 92.17 a.u., and n = 1.32. The fabricated biosensor could potentially differentiate 0.5 ng/mL of fPSA with a chemiluminescence value of 11.90 $\pm$ 1.49 a.u., which is higher than the y_0 value (8.5 a.u.) calculated from the fitting.

4.8 Multi-glycoprofiling of fPSA

The change in a carbohydrate linkage of particular carbohydrate moieties, such as sialic acid plays a major role in glycoprofiling of PSA. As explained in Chapter 1, glycoprofiling can indicate not only the type of pathological process but, more importantly, in some cases also its stage. There are direct and indirect methods to perform protein glycoprofiling after the release of glycans from intact glycoproteins. Various analytical techniques such as HPLC, capillary electrophoresis, and mass spectroscopy, can be used to further analyse the glycans. However, these techniques are both laborious and expensive (Adamczyk *et al.* 2014; Domann *et al.* 2007; Thaysen-Andersen and Packer 2014).

It is worth mentioning that direct glycoprofiling methods that have been reported in the literature are based on recognition elements such as lectins (Katrlik *et al.* 2010), anti-carbohydrate antibodies (Smith and Cummings 2010) or other glycan binding proteins. Since these bio recognition elements are specific to glycans and not a particular protein, they are capable of recognizing specific glycan structures irrespective of the molecule. Such an approach based on the use of proteins (antibodies, lectins) have a major limitation such as cross-reactivity of the recognition element with other components present in the sample resulting in false positives. Moreover, using antibodies for diagnostic applications have drawbacks such as high costs, poor stability over time and difficulty in engineering them to suit the sensing platforms (Haupt and Mosbach 2000). Also, the protein itself can have its glycoforms

and increases false positives. One alternate promising class of receptor that can address this major issue with current detection platforms are aptamers. Thus, a similar aptamer-based assay design was also used for fPSA glycoprofiling, utilizing lectins as glyco-recognition elements (Aptamer-Lectin Assay). This is demonstrated by profiling the fPSA carbohydrate content using two biotinylated lectins specific for sialic acid: (i) *Sambucus nigra* lectin (SNA) binding preferentially to sialic acid attached to terminal galactose in α-2,6 linked sialic acid and (ii) *Maackia amurensis* lectin II (MAA II), a lectin recognizing terminal α-2,3 sialylation of PSA. The increase of α-2,3 linked sialic acid is highly presented in PCa patients (Ohyama *et al.* 2004).

Since we employed commercial fPSA obtained from healthy donors, no interaction with MAA II lectin was expected. Thus, MAA II lectin was used as a negative control for a commercial non-malignant fPSA. The fabricated biosensor using lectins was able to distinguish between α-2,6 linked sialic acid and α-2,3 linked sialic acid as shown in Figure 4.11. This finding is in agreement with published studies (Saldova *et al.* 2011). The working range is slightly shifted when compared to quantification experiments, the concentrations ranging from 3 ng/mL to 50 ng/mL fPSA. As seen from Figure 4.11, the fabricated biosensor could potentially differentiate 3 ng/mL fPSA from the blank measurement with a difference of 5.64 $\pm$ 0.50 a.u. using chemiluminescence. However, a significant increase in the chemiluminescence signal was observed between 5 ng/mL of PSA to 50 ng/mL of PSA concentration which lies within the cut-off range (grey zone) of PSA in the blood. Nevertheless, here the major focus was on the potential occurrence of sialic acid with different linkages on PSA surface in a multiglycan profiling approach, thus establishing the difference between the two lectin forms using an aptamer-based ELISA.

Again, a dose response fitting was performed using the same Hill equation that was used with quantification of PSA in Figure 4.11, on the data points obtained with SNA lectin. A K_d of 12.5 ng/mL of PSA with a root mean square value of 0.99 was obtained. The value of y_{max} which is the end value calculated from the fitting was 72.08 a.u., and n = 1.96.

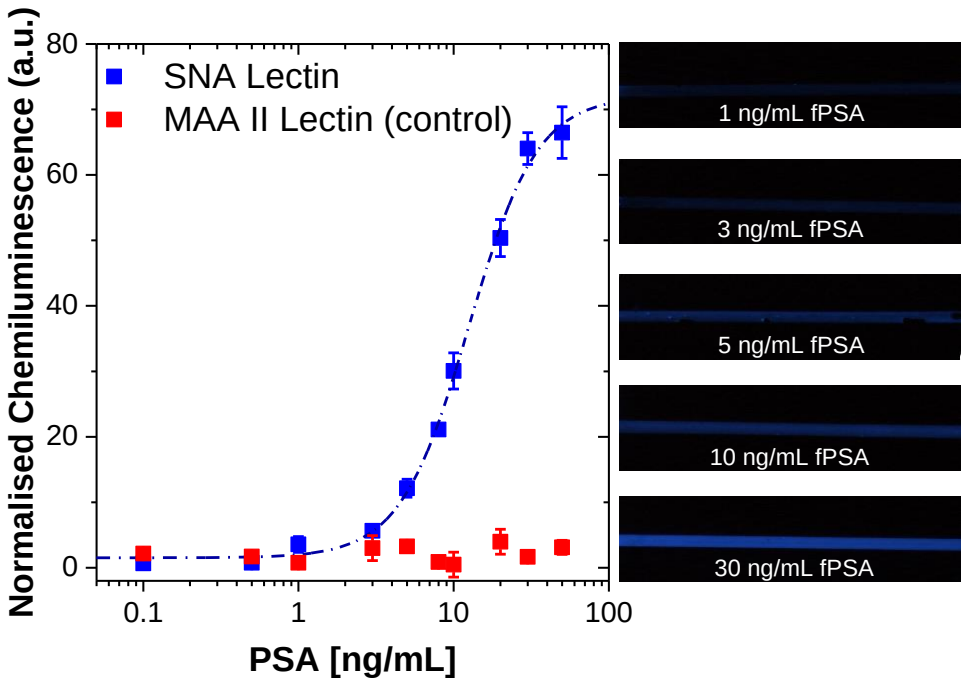

Figure 4.11 Multi-glycan profiling for fPSA detection. Blue data points were obtained using a SNA lectin whereas, red data points were obtained using an MAA II (control) lectin. Images represent the chemiluminescence signals from microscopy for SNA lectin at different concentrations of PSA.

Considering the y_0 value calculated to be 1.53 a.u. from the fitting, the fabricated biosensor could differentiate 3 ng/mL of fPSA with chemiluminescence value of 12.20 $\pm$ 1.36 a.u. In the control experiments, MAA II lectin did not show any binding to PSA in the whole concentration range studied. The differentiation in signal from the two lectins could be observed for fPSA concentrations above 3 ng/mL.

4.9 Summary

This Chapter presents a simple novel aptamer-based microfluidic ELISA assay for the optical detection of fPSA in the clinical range with high sensitivity. The integration of quantification of PSA with multi-glycan profiling of fPSA could serve as a potential platform for PoC devices in PCa diagnosis. A sensitive quantification of PSA of 0.5 ng/mL and multi-glycan profiling where the specific lectin (SNA) could differentiate a response from the control lectin (MAA II) at fPSA concentration down to 3 ng/mL

is demonstrated. Table 4.4 presents a list of reported state of art technologies for the optical detection of PSA. It can be seen the LOD obtained with the presented biosensor is lower or comparable to the reported technologies.

Table 4.4 Comparison of state of art technologies

Method	**Electrode surface**	**Strategy employed**	**Limit of Detection (LOD)**	**Reference**
Chemiluminescent	magnetic Fe_3O_4 graphene oxide nanoparticles	DNA aptamers conjugated with fluorescent dye were immobilised on nanoparticles via π–π stacking	0.5 ng/mL	Choi and Lee 2013
Chemiluminescent resonance energy transfer (CRET)	Fe_3O_4 MWCNTs (multi-walled carbon nanotubes)	DNA aptamer modified with fluorophore and Guanine rich region	1 ng/mL	Cha *et al.* 2014
Fluorescence	MoS_2nanosheet	DNA aptamer modified with fluorophore	0.2 ng/mL	Kong *et al.* 2015
Love-wave sensor	Gold surface on Silicon dioxide/Lithium tantalite wafers	DNA aptamers were immobilised on gold surfaces	<10 ng/mL	Zhang *et al.* 2015
Chemiluminescent	**Glass/PDMS**	**DNA aptamers immobilised in a microfluidic channel**	**0.5 ng/mL** **K_d: 9.82 ng/mL with Ab-HRP and 12.5 ng/mL with Lectins**	**Jolly *et al.* 2015a**

The study addresses how the use of aptamers could be an effective methodology to handle the current antibody limitations with cross-reactivity issues in glycoprofiling. It also shows how aptamers could be used as a potential tool for multi-glycan profiling of biomarkers with high sensitivity and selectivity in a simple microfluidic channel. This approach can be easily extended to a wide range of other biomarkers available for PCa, a step towards multiplexing, which is of great interest for PCa diagnosis. The simultaneous detection of protein cancer biomarkers together with their levels of glycosylation provides enhanced diagnosis and prognosis of the disease.

References

Adamczyk, B., Tharmalingam-Jaikaran, T., Schomberg, M., Szekrenyes, A., Kelly, R.M., Karlsson, N.G., Guttman, A., and Rudd, P.M., 2014. Comparison of separation techniques for the elucidation of IgG N-glycans pooled from healthy mammalian species. *Carbohydrate Research,* 389, 174-185.

Arvinte, R., 2011. Characterization of the electrical and optical properties of the CrNxOy and AlNxOy thin films.

Bañuls, M.-J., Puchades, R., and Maquieira, Á., 2013. Chemical surface modifications for the development of silicon-based label-free integrated optical (IO) biosensors: A review. *Analytica Chimica Acta*, 777, 1-16.

Cha, T., Cho, S., Kim, Y.T., and Lee, J.H., 2014. Rapid aptasensor capable of simply diagnosing prostate cancer. *Biosensors and Bioelectronics,* 62, 31-37.

Choi, H.K., Lee, J.H., 2013. Role of magnetic Fe_3O_4 graphene oxide in chemiluminescent aptasensors capable of sensing tumor markers in human serum. *Analytical Methods,* 5(24), 6964-6968.

Domann, P.J., Pardos-Pardos, A.C., Fernandes, D.L., Spencer, D.I., Radcliffe, C.M., Royle, L., Dwek, R.A., and Rudd, P.M., 2007. Separation-based glycoprofiling approaches using fluorescent labels. *Proteomics 7 Suppl,* 1, 70-76.

Formisano, N., Jolly, P., Bhalla, N., Cromhout, M., Flanagan, S.P., Fogel, R., Limson, J.L., and Estrela, P., 2015. Optimisation of an electrochemical impedance spectroscopy aptasensor by exploiting quartz crystal microbalance with dissipation signals. *Sensors and Actuators B: Chemical,* 220(0), 369-375.

Haupt, K., and Mosbach, K., 2000. Molecularly imprinted polymers and their use in biomimetic sensors. *Chemical Reviews,* 100(7), 2495-2504.

Hong, S.K., 2014. Kallikreins as biomarkers for prostate cancer. *Biomed Research International,* 2014, 526341.

Isono, T., Tanaka, T., Kageyama, S., and Yoshiki, T., 2002. Structural diversity of cancer-related and non-cancer-related prostate-specific antigen. *Clinical Chemistry,* 48(12), 2187-2194.

Jolly, P., Damborsky, P., Madaboosi, N., Soares, R.R., Chu, V., Conde, J.P., Katrlik, J., and Estrela, P., 2016. DNA aptamer-based sandwich microfluidic assays for dual quantification and multi-glycan profiling of cancer biomarkers. *Biosensors and Bioelectronics,* 79, 313-319.

Jolly, P., Formisano, N., Tkáč, J., Kasák, P., Frost, C.G., and Estrela, P., 2015. Label-free impedimetric aptasensor with antifouling surface chemistry: A prostate specific antigen case study. *Sensors and Actuators B: Chemical,* 209(0), 306-312.

Katrlik, J., Svitel, J., Gemeiner, P., Kozar, T., and Tkac, J., 2010. Glycan and lectin microarrays for glycomics and medicinal applications. *Medicinal Research Reviews,* 30, 394 - 418.

Keighley, S.D., Estrela, P., Li, P., and Migliorato, P., 2008a. Optimization of label-free DNA detection with electrochemical impedance spectroscopy using PNA probes. *Biosensors and Bioelectronics,* 24(4), 906-911.

Keighley, S.D., Li, P., Estrela, P., and Migliorato, P., 2008b. Optimization of DNA immobilization on gold electrodes for label-free detection by electrochemical impedance spectroscopy. *Biosensors and Bioelectronics,* 23(8), 1291-1297.

Kong, R.-M., Ding, L., Wang, Z., You, J., and Qu, F., 2015. A novel aptamer-functionalized MoS2 nanosheet fluorescent biosensor for sensitive detection of prostate specific antigen. *Analytical and Bioanalytical Chemistry,* 407(2), 369-377.

Liu, W., Wei, H., Lin, Z., Mao, S., and Lin, J.M., 2011. Rare cell chemiluminescence detection based on aptamer-specific capture in microfluidic channels. *Biosensors & Bioelectronics,* 28(1), 438-442.

Madaboosi, N., Soares, R.R., Chu, V., and Conde, J.P., 2015. A microfluidic immunoassay platform for the detection of free prostate specific antigen: a systematic and quantitative approach. *Analyst,* 140(13), 4423-4433.

Madou, M.J., 2002. *Fundamentals of microfabrication: the science of miniaturization.* CRC press.

McDonald, J.C., and Whitesides, G.M., 2002. Poly (dimethylsiloxane) as a material for fabricating microfluidic devices. *Accounts of Chemical Research,* 35(7), 491-499.

Meany, D., and Chan, D., 2011. Aberrant glycosylation associated with enzymes as cancer biomarkers. *Clinical Proteomics,* 8, 7.

Novo, P., Moulas, G., Prazeres, D.M.F., Chu, V., and Conde, J.P., 2013. Detection of ochratoxin A in wine and beer by chemiluminescence-based ELISA in microfluidics with integrated photodiodes. *Sensors and Actuators B: Chemical,* 176, 232-240.

Novo, P., Prazeres, D.M., Chu, V., and Conde, J.P., 2011. Microspot-based ELISA in microfluidics: chemiluminescence and colorimetry detection using integrated thin-film hydrogenated amorphous silicon photodiodes. *Lab on a Chip,* 11(23), 4063-4071.

Ohyama, C., Hosono, M., Nitta, K., Oh-eda, M., Yoshikawa, K., Habuchi, T., Arai, Y., and Fukuda, M., 2004. Carbohydrate structure and differential binding of prostate specific antigen to Maackia amurensis lectin between prostate cancer and benign prostate hypertrophy. *Glycobiology,* 14(8), 671-679.

Ramachandran, A., Wang, S., Clarke, J., Ja, S., Goad, D., Wald, L., Flood, E., Knobbe, E., Hryniewicz, J., and Chu, S., 2008. A universal biosensing platform based on optical micro-ring resonators. *Biosensors and Bioelectronics,* 23(7), 939-944.

Saldova, R., Fan, Y., Fitzpatrick, J.M., Watson, R.W.G., and Rudd, P.M., 2011. Core fucosylation and α2-3 sialylation in serum N-glycome is significantly increased in prostate cancer comparing to benign prostate hyperplasia. *Glycobiology,* 21(2), 195-205.

Smith, D.F., and Cummings, R.D., 2010. Glycan-binding proteins and glycan microarrays. *Handbook of Glycomics, Elsevier, Amsterdam,* 137-160.

Soares, R., Novo, P., Azevedo, A., Fernandes, P., Aires-Barros, M., Chu, V., and Conde, J., 2014. On-chip sample preparation and analyte quantification using a

microfluidic aqueous two-phase extraction coupled with an immunoassay. *Lab on a Chip,* 14(21), 4284-4294.

Su, M., Ge, L., Kong, Q., Zheng, X., Ge, S., Li, N., Yu, J., and Yan, M., 2015. Cyto-sensing in electrochemical lab-on-paper cyto-device for in-situ evaluation of multi-glycan expressions on cancer cells. *Biosensors & Bioelectronics,* 63, 232-239.

Tennico, Y.H., Hutanu, D., Koesdjojo, M.T., Bartel, C.M., and Remcho, V.T., 2010. On-Chip Aptamer-Based Sandwich Assay for Thrombin Detection Employing Magnetic Beads and Quantum Dots. *Analytical Chemistry,* 82(13), 5591-5597.

Thaysen-Andersen, M., and Packer, N.H., 2014. Advances in LC–MS/MS-based glycoproteomics: Getting closer to system-wide site-specific mapping of the N-and O-glycoproteome. *Biochimica et Biophysica Acta (BBA)-Proteins and Proteomics*, 1844(9), 1437-1452.

Toh, S.Y., Citartan, M., Gopinath, S.C.B., and Tang, T.-H., 2015. Aptamers as a replacement for antibodies in enzyme-linked immunosorbent assay. *Biosensors and Bioelectronics*, 64(0), 392-403.

Vaisanen, V., Peltola, M.T., Lilja, H., Nurmi, M., and Pettersson, K., 2006. Intact free prostate-specific antigen and free and total human glandular kallikrein 2. Elimination of assay interference by enzymatic digestion of antibodies to F(ab')2 fragments. *Analytical Chemistry,* 78(22), 7809-7815.

Végvári, Á., Rezeli, M., Sihlbom, C., Häkkinen, J., Carlsohn, E., Malm, J., Lilja, H., Laurell, T., and Marko-Varga, G., 2012. Molecular microheterogeneity of prostate specific antigen in seminal fluid by mass spectrometry. *Clinical Biochemistry,* 45(4–5), 331-338.

Vermassen, T., Speeckaert, M.M., Lumen, N., Rottey, S., and Delanghe, J.R., 2012. Glycosylation of prostate specific antigen and its potential diagnostic applications. *Clinical Chimica Acta,* 413(19-20), 1500-1505.

Zhang, F., Li, S., Cao, K., Wang, P., Su, Y., Zhu, X., and Wan, Y., 2015. A Microfluidic Love-Wave Biosensing Device for PSA Detection Based on an Aptamer Beacon Probe. *Sensors*, 15(6), 13839-13850.

Chapter 5. Polymer-based electrochemical sensing of AMACR

This Chapter reports on the development of a sensitive aptasensor based on a poly(pyrrole) (PPy) – polyethylene glycol (PEG) platform for the detection of α-methylacyl-CoA racemase (AMACR; P504S), an upcoming biomarker for prostate cancer. The work demonstrates a simple strategy of covalent modification of PPy films formed on the electrodes by using PEG derivatives, without prior need of chemical functionalisation of the pyrrole monomer. Square Wave Voltammetry (SWV) was utilised to characterise the aptasensor and surface plasmon resonance (SPR) as a validation tool. The Chapter also presents the successful application of the aptasensor with human plasma samples.

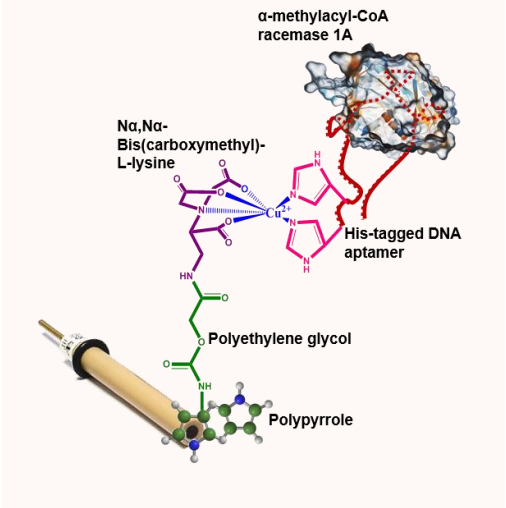

The work presented in this chapter has been submitted for publishing.

5.1 Background

Recently, several research groups have tried to develop biosensors for AMACR detection. However, most of them employ antibodies as a probe for detection (Lin *et al.* 2012; Maraldo *et al.* 2007; Wang and Yau 2014). In 2014, Yang *et al.* (Yang *et al.* 2014) first reported an anti-AMACR DNA aptamer (AMC51) and demonstrated a fluorescent enzyme-linked aptamer assay (ELAA) for AMACR detection, which

featured a low detection limit of 0.44 nM. In this work, we present the development of an electrochemical AMACR aptasensor based on electro-patterned polyethylene glycol (PEG) on polypyrrole (PPy) film. PEG as a polymer has been widely used to develop biosensors, due to its anti-fouling properties (Nogues *et al.* 2012; Rodriguez Emmenegger *et al.* 2009; Sharma *et al.* 2004; Statz *et al.* 2005). However, it becomes very difficult to employ PEG in an electrochemical platform since it is also an insulating polymer. Nevertheless, several research groups have demonstrated the use of PEG on an electrochemical platform. Estrela *et al*. (Estrela *et al.* 2010) developed an electrochemical biosensor for cyclin-dependent kinase protein detection using peptide aptamers and PEG. Kjallman *et al*. (Kjällman *et al.* 2008) reported a DNA-based biosensor using PEG. In 2013, Hayat *et al*. (Hayat *et al.* 2013) demonstrated a design of PEG-aptamer for detection of ochratoxin A; however, the strategy employs the modification of aptamers with PEG. In order to overcome the shortcomings of directly using PEG, we propose the use of organic conducting polymers such as PPy as a foundation of grafting PEG onto a surface.

PPy has attracted a lot of attention in the past decades from those developing biosensors because of its redox properties (Han *et al.* 2005) and high electrical conductivity (Andrade 1985) along with being a suitable interface for bioreceptors association (Azioune *et al.* 2005; Kausaite-Minkstimiene *et al.* 2011; Raoof *et al.* 2004). PPy has been used to immobilise various types of biomolecules through various methods as described in Chapter 2. Miodek *et al*. (Miodek *et al.* 2015) developed an E-DNA sensor for *Mycobacterium tuberculosis* based on an electrochemical method to directly modify the CNTs coated by an un-functionalised PPy film with the macromolecular polymer–dendrimer hybrids. This was done by electro-oxidation of the amine groups of dendrimers that can bind to CNTs as well as to the PPy surface.

In this work, we design an aptasensor specific for human recombinant AMACR 1A protein based on PEG (PEG derivative) electro-patterned on PPy layer and associated with an ANTA/Cu^{2+} complex. Modification of the PPy film by PEG molecules can lead to minimised non-specific binding. On the other, hand association of redox molecules such as copper complexes with PPy can enhance the electrical properties of

the film and improve the sensitivity of detection (Chebil *et al.* 2010; Chebil *et al.* 2013).

5.2 Fabrication of functional AMACR aptasensor

Gold disk working electrodes with a radius of 1.0 mm were cleaned as detailed in Chapter 3. An additional step of chemical cleaning was included with piranha solution (3 parts of concentrated H_2SO_4 with 1 part of H_2O_2 (Sigma, UK)) for 5 minutes, between the mechanical polishing and the electrochemical cleaning. Figure 5.1 represents a schematic of the fabrication strategy (1-6).

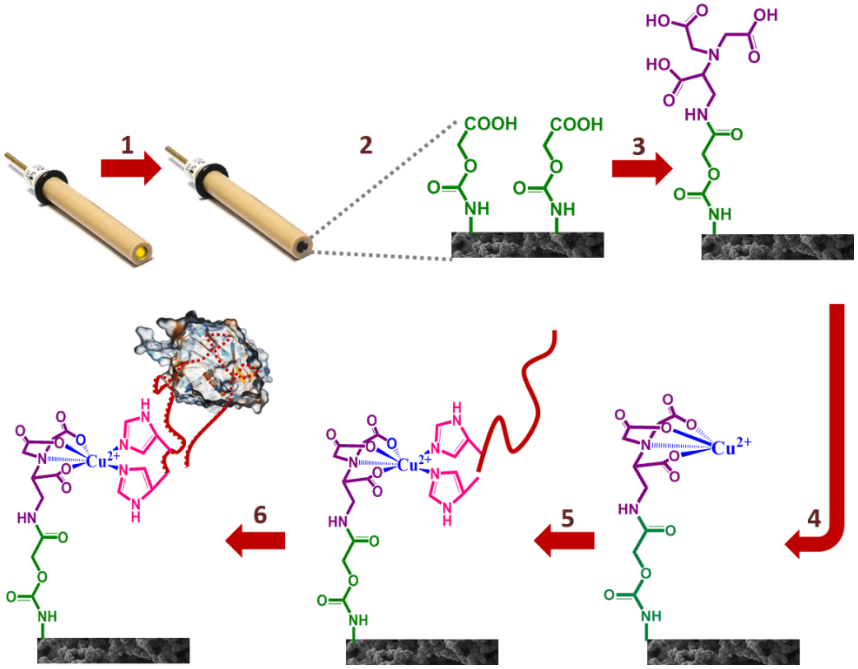

Figure 5.1 Schematic representation of aptasensor manufacture:(1) Electro-deposition of pyrrole on gold electrodes;(2) subsequent electro-patterning of PEG molecules using its amines present on one of terminus; (3) Attachment of ANTA to carboxyl end of PEG via covalent bonding with EDC/NHS coupling agents; (4) Immobilization of copper ions; (5) Immobilization of His-tagged DNA aptamers; (6) detection of AMACR.

A clean gold electrode surface was modified with PPy (1) followed by electrochemical immobilisation of poly(ethylene glycol) 2-aminoethyl ether acetic acid (PEG, Sigma, UK) molecules (2). The free carboxylate groups of PEG were used to covalently attach Nα,Nα-Bis(carboxymethyl)-L-lysine hydrate (ANTA, Sigma, UK) via an amido link

(3). Immobilised ANTA was later used to attach copper molecules via coordinate chemistry (4). Finally, a Histidine tagged AMACR specific DNA aptamer [5'$(His)_6$TTT TTT CCC TAC GGC GCT AAC CCA TGC TAC GAA TTC GTT GTT AAA CAA TAG GCC ACC GTG CTA CAA-3'] (Eurogentec, UK) was immobilised onto the PPy-PEG backbone through the ANTA/Cu^{2+} complex (5). The fabricated aptasensor was then used to detect AMACR protein (6).

5.2.1 Selection of anti-AMACR DNA aptamer

To fabricate a successful aptasensor, it is crucial to fully characterise the aptamer to be used for it. The performance of the aptasensor is majorly dependent on the biological recognition unit. For AMACR, two types of DNA aptamers have been developed. The first aptamer was developed by Base Pair Biotechnologies (AM-310_2) as a 32 nucleotide long DNA aptamer. More recently, Yang *et al*. reported a 60 nucleotide long DNA aptamer (AMC51) for AMACR detection (Yang *et al.* 2014). To perform surface characterisation, classical binary SAM layer was utilised using thiol modified DNA aptamers from both the sources. 0.01 total DNA aptamer mole fraction was used, similar to what is described in Chapter 3. Such a characterisation was performed using surface plasmon resonance technique (SPR).

A pre-treatment step for aptamer activation was performed where the aptamers were heated to 95˚C for 5 minutes followed by gradual cooling to room temperature (Yang *et al.* 2014). 50 nm gold coated SPR gold chips, supplied from Reichert Technologies were used for studying the reaction on SPR. Prior to their modification, the chips were cleaned using piranha solution (3:1 H_2SO_4:H_2O_2) for 20 seconds and rinsed thoroughly with Milli-Q water and dried using nitrogen gas. All buffers were filtered through 0.2 μm filters and degassed for 2 hours by sonication prior to the experiment. The mixed SAM was immobilised on the SPR chip following to protocol previously described. Different concentrations of AMACR were prepared in 10 mM PBS (pH 7.4). Human recombinant AMACR 1A was expressed and purified as reported by Darley *et al*. (Darley *et al.* 2009) and Yevglevskis *et al*. (Yevglevskis *et al.* 2014a; Yevglevskis *et al.* 2014b).

The results from SPR are shown in Figure 5.2. From binding studies, a significant distinction in the binding efficiency can be observed between the two aptamers. Clearly, DNA aptamer (AMC-51) reported by Yang *et al.* showed enhanced binding capabilities as compared to AM-310_2 from Base Pair Biotechnologies. Such a significant difference could be attributed to their respective reported dissociation constant values (K_d). It could be assumed that as the AM-310_2 aptamer has a high dissociation constant of around 480 nM, there is a quick detachment of the protein after binding. On the other hand, AMC51 has nearly a 10 fold lower K_d value of 49 nM. Therefore, from the results obtained, this Chapter will focus on the employment of AMC51 for the fabrication of an electrochemical aptasensor.

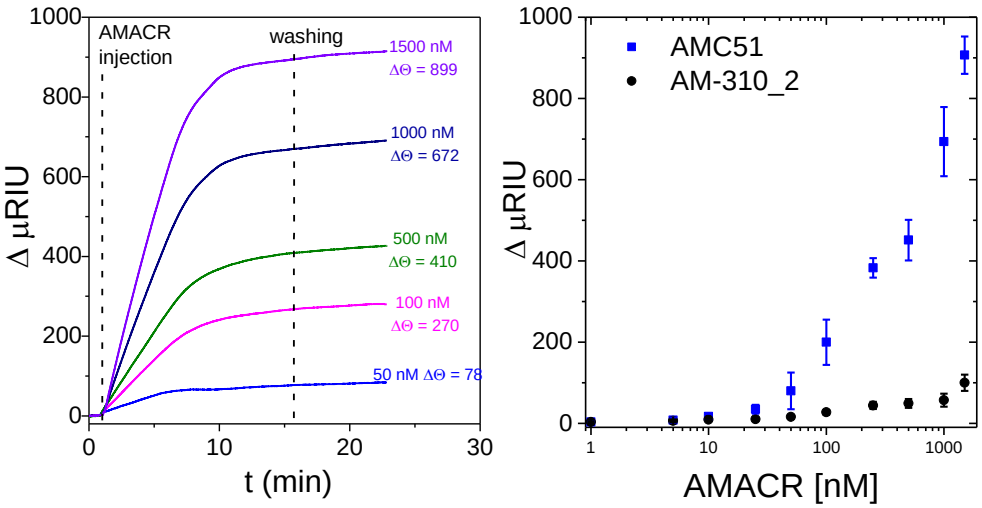

Figure 5.2 Real time SPR curves obtained with different concentrations of AMACR using AMC51 aptamer (left). Right graph shows the SPR response with anti-AMACR DNA aptamers from two sources; AM-310_2 from Base Pair Biotechnologies (black) and AMC51 from Taiwan National University (blue). Error bars represent standard deviation obtained from three independent samples.

5.2.2 Optimisation of polymerisation and PEG deposition

The optimal conditions of polymerisation and PEG association were performed by investigating different parameters such as the thickness of the PPy layer and the potential range of electro-deposition. Such steps were practiced to engineer an intense oxidation peak of ANTA/Cu^{2+} redox complex and efficient AMACR detection. The thickness of the PPy layer strictly depends upon conditions of polymerisation such as

range of potential, number of cycles and concentration of pyrrole monomer. The range of potential and concentration of pyrrole monomer were chosen based on previous literature while number of cycles were varied in this study (Appendix I.3). Initially, three cycles of pyrrole electro-deposition were chosen to optimise the electro-oxidation of PEG. However, the optimal parameters of PEG deposition should also be chosen based on the efficiency of further steps such as ANTA and copper attachment. Covalent grafting of ANTA on PPy-PEG via EDC/NHS chemistry and copper immobilisation were fixed to 30 minutes each.

Electrochemical impedance spectroscopy (EIS) was used to evaluate the different optimisation steps. EIS measurements were performed using a µAUTOLAB III / FRA2 potentiostat apparatus, using a three-electrode cell setup with an Ag/AgCl reference electrode and a Pt counter electrode. The impedance spectrum was measured in 10 mM PBS measurement buffer (pH 7.4) with a 10 mV a.c. voltage superimposed on a bias d.c. voltage of 0.17 V *vs*. Ag/AgCl. Briefly, a clean gold electrode surface was modified with PPy by scanning the potential from -0.4 V to 0.9 V *vs*. Ag/AgCl with a scan rate of 100 $mV.s^{-1}$ in the presence of 50 mM purified pyrrole monomer (Sigma, UK) dissolved in 0.5 M lithium perchlorate ($LiClO_4$, Sigma, UK) for two cycles. Electro-polymerisation was performed using a three-electrode configuration in a small volume cell (BASi, USA) containing 250 µL of pyrrole monomer. A typical CV characteristic of PPy polymerisation performed with two cycles is shown in Figure 5.3.

Surface characterisation of PPy coated gold SPR chips was performed using a scanning electron microscopy (JSM-6480Jeol, Japan) at 1000X magnification with acceleration voltage of 5 kV to acquire SEM images. The SEM micrograph shows characteristic structures of PPy deposited on gold electrodes (Figure 5.3, right). This morphology is characteristic for PPy growing in water and present initiation of "cauliflower" structures as described in the literature (Miodek *et al.* 2015). After reaction, the electrode was rinsed with Milli-Q water.

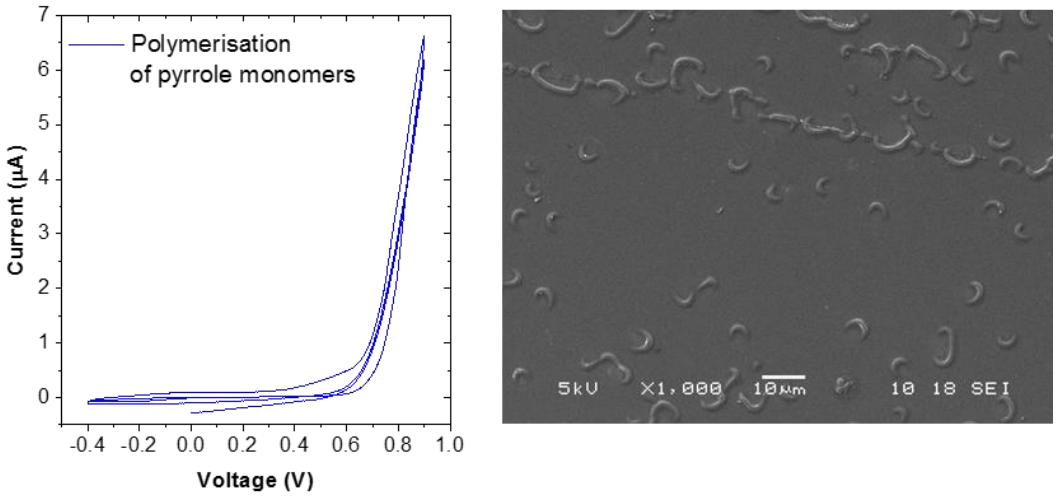

Figure 5.3 Cyclic voltammetry of pyrrole electro polymerisation showing characteristic current peaks that increased with consecutive scans confirming the deposition of a conducting polymer on the surface (left). SEM micrograph showing characteristic structures of polypyrrole deposited on gold electrodes with two cycles (right).

PEG molecules were immobilised on the PPy film by covalent bonding *via* electro-oxidation of amine groups of PEG. In order to modify the generated PPy film with PEG bearing both amine and carboxyl groups, the electrochemical pattering of PEG was performed using the optimised conditions. The modification was realised by the electrochemical oxidation of amine groups of PEG which was again performed in the small volume cell containing 250 µL of 1 mM PEG dissolved in Milli-Q water containing 0.5 M $LiClO_4$ by cycling the potential between 0.0 to 1.1 V vs. Ag/AgCl for 5 cycles (Appendix I.1) with the scan rate of 50 mVs^{-1}.The mechanism of such a reaction assumes formation of radical cations on nitrogen atoms which covalently attach to the nucleophilic groups such as aromatic ring resulting in the rupture of the double bond carbon=carbon and formation of carbon-nitrogen bonds (Adenier *et al.* 2004; Zhang *et al.* 2005).

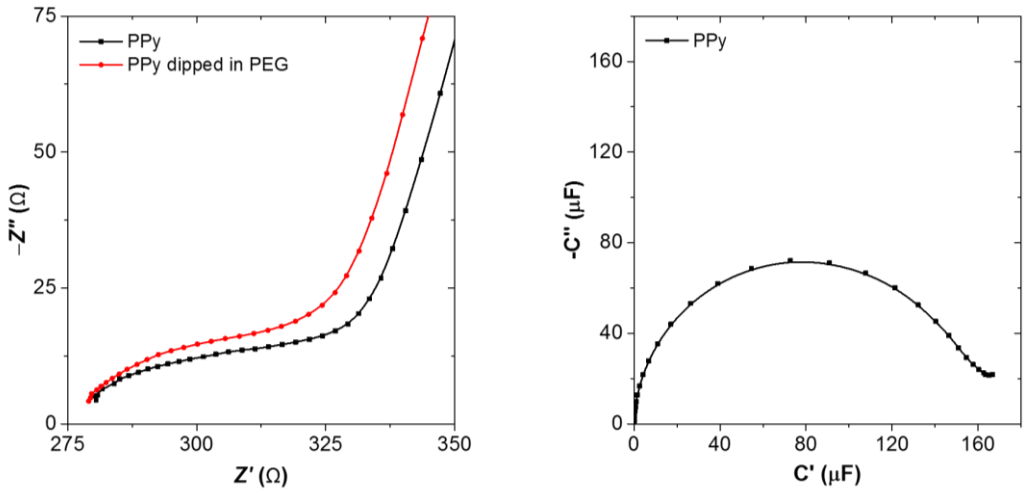

Figure 5.4 Nyquist plot depicting variation in charge transfer resistance of PPy modified gold electrode (black) after dipping it in PEG solution (red without applying the potential) (left). Cole-Cole plot of PPy modified surface (right).

From EIS data, a small R_{ct} for PPy modified gold electrodes was obtained equal to 80 Ω and a large capacitance of around 163 µF (Figure 5.4). Since PEG is an insulating polymer, an increase in the R_{ct} values was expected upon grafting of PEG on a PPy film.

From Figure 5.5 it can be seen that a high R_{ct} of *ca.* 200 kΩ was obtained after electrochemical PEG deposition and the capacitance decreased to nearly 2 µF. The significant decrease in capacitance observed on the attachment of PEG to the PPy film, which decreased further upon attachment of ANTA/Cu^{2+} and the His-tagged DNA aptamer, could be attributed to a series capacitor effect, where the final capacitance decreases upon addition of layers on the same surface. Such a change was compared with a control experiment with electrodes immersed in PEG solution where no electrochemical oxidation was performed and electrodes showed a non-significant change in R_{ct} (Figure 5.5, left), which further validated the electrochemical approach. Such an electrochemical functionalisation has been demonstrated earlier in the case of attachment of aliphatic amines to surfaces such as glassy carbon (Ghanem *et al.* 2008) or CNTs (Adenier *et al.* 2004) and recently on CNTs coated with PPy material (Miodek *et al.* 2015).

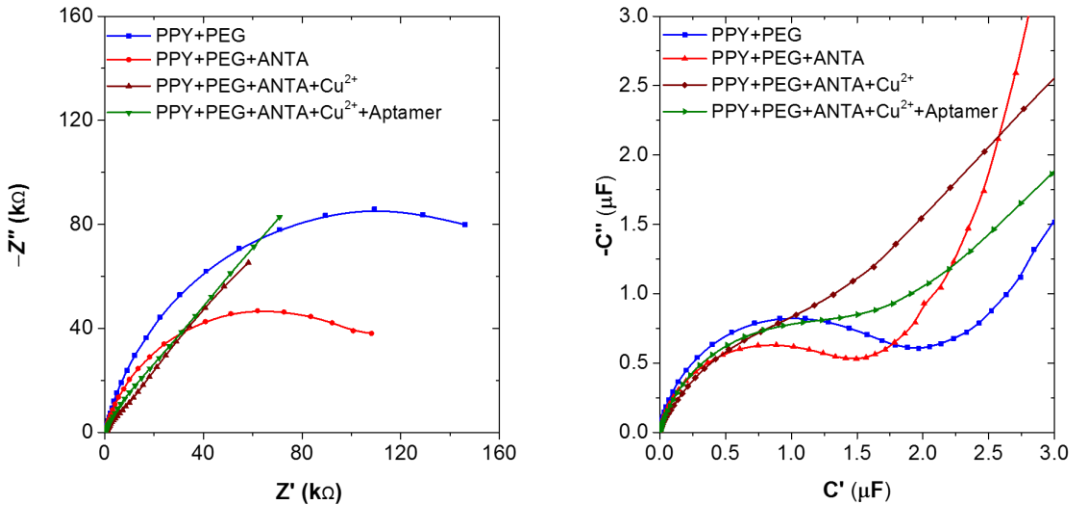

Figure 5.5 Electrochemical impedance spectroscopy characterisation of different layers (left).Cole-Cole plot depicting the changes in capacitance at different layer formation (right).

Immobilisation of ANTA/Cu^{2+} complex and the His-tagged aptamers was performed using the protocol reported by Chebil *et al*. (Chebil *et al.* 2010). The carboxylic acid groups on the free end of the deposited PEG was used to covalently attach ANTA. First, electrodes were subjected to a 2:1 ratio of EDC/NHS (160 mM/80 mM) in water for 20 minutes. Electrodes were then rinsed with Milli-Q water and immersed in 7 mM ANTA dissolved in 10 mM PBS (pH 8.5) for 30 minutes. The electrodes were then rinsed well with Milli-Q water and the unreacted activated carboxylate groups were blocked with 10 mM ethanolamine (pH 8.5, Sigma, UK) for 30 minutes. Finally, the electrodes were immersed in a solution of 3.5 mM copper acetate (Sigma, UK) dissolved in 20 mM acetate buffer (pH 4.6) for 25 minutes. During the process the copper molecules associated with ANTA attached onto the surface *via* coordinate chemistry. The covalent attachment of ANTA onto PPy-PEG showed a reduction in the R_{ct} values. From the *Cole-Cole* plot (Figure 5.5 right) a further reduction in capacitance after PEG deposition was recorded pointing to the deposition of another layer over PEG.

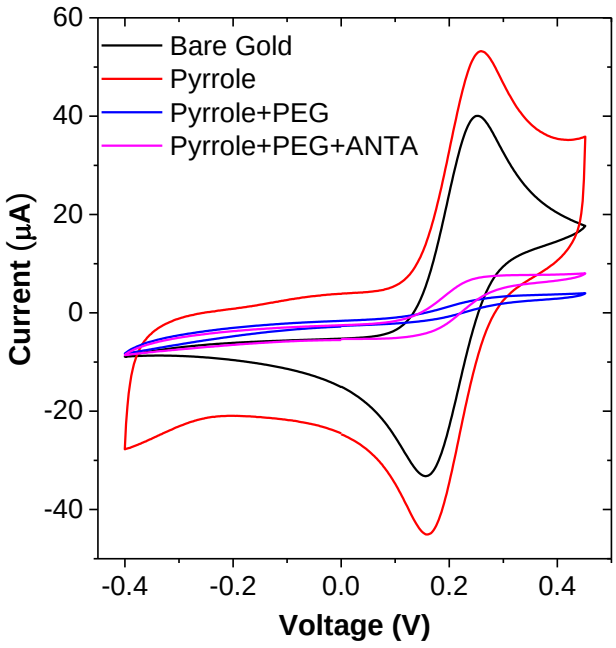

Figure 5.6 Cyclic Voltammetry in 10 mM PBS containing 10 mM ferro/ferricyanide $[Fe(CN)_6]^{3-/4-}$ showing the changes in the current peaks upon modification of gold electrode.

Such an assumption was further studied by cyclic voltammetry (CV) in the presence of a redox couple from -0.4 V to 0.45 V in 10 mM PBS containing 10 mM ferro/ferricyanide $[Fe(CN)_6]^{3-/4-}$ (Figure 5.6). CV showed significant increases in the current of the peak corresponding to the redox reaction after modification of an electrode with PPy (black curve). Electro-deposition of PEG caused a decrease in the current of many folds, which is due to the blocking effect on charge transfer after an association of insulating material such as PEG (blue curve). However, after ANTA attachment, an increase in electrochemical signal was observed (pink curve). This could be attributed to the electrostatic repulsion between the ANTA molecules because of carboxylic acids and possible stabilisation of the whole layer.

5.2.2.1 FT-IR characterisation

The electrochemical grafting of PEG on PPy film was further characterised with Fourier Transform Infrared spectra (FT-IR) and was compared with PEG adsorbed on the gold surface and just PPy film as controls (Figure 5.7). FT-IR was measured using a Spectrum 100 FT-IR spectrometer (PerkinElmer, U.K.) equipped with an attenuated total reflectance (ATR) diamond crystal. For FT-IR, SPR gold chips were used.

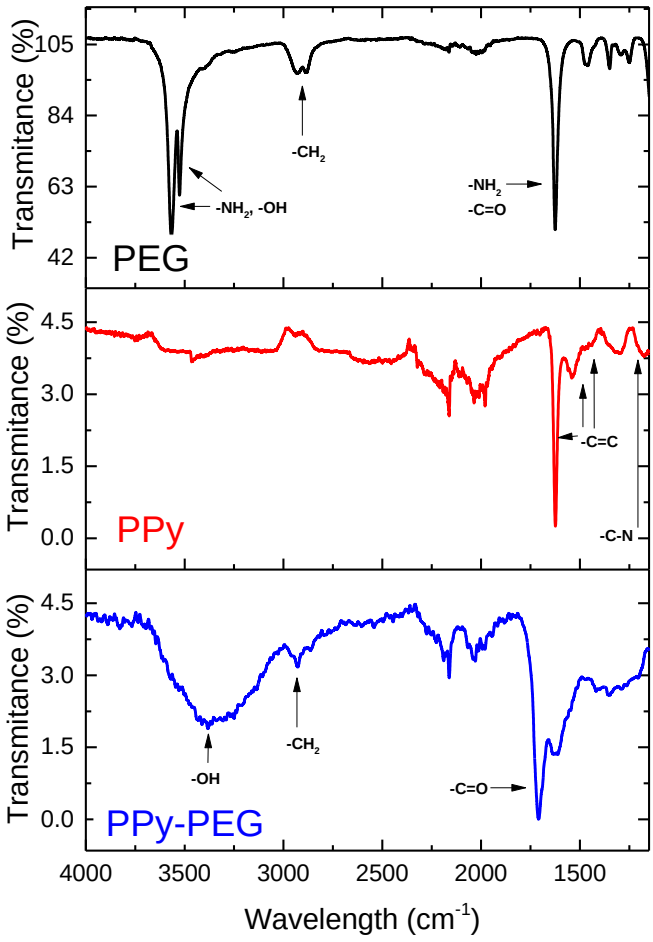

Figure 5.7 FT-IR analysis of PEG adsorbed on gold chip and PPy layer before and after modification with PEG.

From the FT-IR spectrum of PEG, we can see characteristic peaks of primary amine bonds at 3566 cm^{-1} and 1623 cm^{-1}, that can also be assigned to the –OH and C=O

groups. For unmodified PPy, peaks at 1623 cm^{-1}, 1539 cm^{-1} and 1441 cm^{-1} corresponding to C-N and C=C vibrations were observed. Modification of PPy by PEG led to the appearance of -OH and -C=O vibrations at 3364 cm^{-1} and 1709 cm^{-1}, respectively, confirming the presence of carboxylate groups on the surface and modification of the polymer. The presence of PEG`s alkyl chain is confirmed by the peak at 2934 cm^{-1}. Also, a decrease in intensity of C=C bond stretching was observed, which could be attributed to the attachment of PEG to double bonds present in the PPy structure, and confirming the mechanism of the reaction.

5.2.2 Association of anti-AMACR DNA aptamers

In order to provide a different detection mechanism, PPy-PEG material was associated with ANTA/Cu^{2+} complex as a redox marker. Formation of such a complex has been widely studied and is known to be very stable (Khan *et al.* 2006).

The complex between ANTA and a copper ion was formed by the interaction of the metal in sodium acetate buffer, according to the procedure described by Chebil *et al* (Chebil *et al.* 2010). The time for copper ions immobilisation was crucial for this process and was extensively optimised (Appendix I.3). An optimal time of 25 minutes was selected which demonstrated a maximum signal change of *ca.* 30 %. Finally histidine-tagged anti-AMACR DNA aptamers were immobilised on the surface by coordination of copper with two N-imidazole rings of the modified aptamers. For immobilisation, 0.5 µM DNA aptamer solution was used.

The formation of a biolayer was monitored using square wave voltammetry (SWV). SWV was performed in 10 mM PBS (pH 7.4) in the potential range from -0.3 V to 0.4 V with conditioning time of 120 s, modulation amplitude of 20 mV and frequency of 50 Hz. Figure 5.8 shows a characteristic oxidation peak of copper 0.15 V *vs.* Ag/AgCl of copper after attachment on ANTA. This peak can be attributed to the reaction Cu^{2+}/Cu^{+} that occurs on the electrode surface.

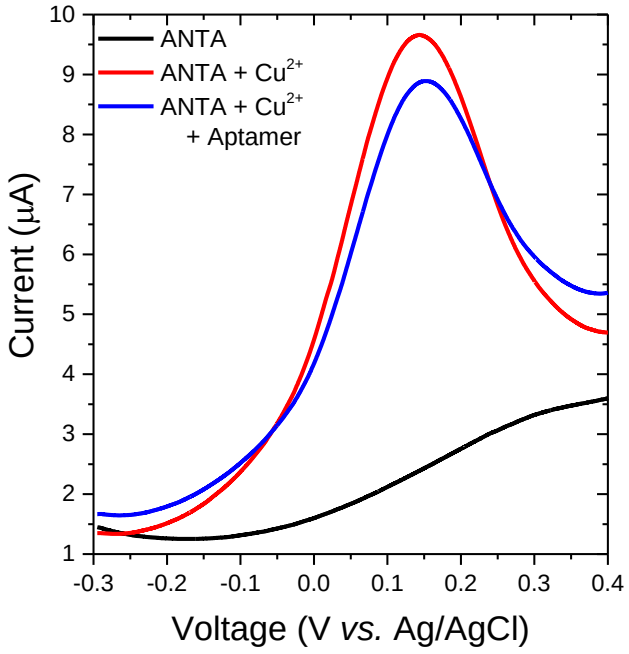

Figure 5.8 SWV characterization of copper ions immobilization followed by immobilization of DNA aptamers measured in PBS pH 7.4.

Copper peaks were also investigated by incubating the electrode at different layer formations, results from which are presented in Appendix I.3. When the PPy modified electrode was dipped in copper acetate, the recorded plot showed an absence of oxidation peaks corresponding to copper. After modification of PPy with PEG, voltammogram showed a small peak of at 0.3V which could be due to a non-specific interaction of copper with the carboxylate (carboxylic acid) groups of PEG. However, an intense copper peak at 0.15 V was observed when the electrode was further modified with ANTA depicting the specific coordination of copper molecules with ANTA molecules.

The charge exchanged during redox process allows calculation of the surface coverage of immobilised copper ions, following the equation:

$$\Gamma = \frac{Q}{nFA} \qquad (5.1)$$

Where, *Q* is the charge under the cathodic or anodic waves, *n* is the number of electrons involved in the redox process, F is the Faraday constant, and *A* is the area of the electrode. Based on the equation (5.1) we calculated the average coverage of the surface as 3.9 $\pm$ 0.4 pmol.cm^{-2}.

A reduction in the current corresponding to this peak was observed after attachment of His-tagged DNA aptamers. This could be related to the low electron transfer to the surface during the redox process due to the attachment of the large molecules such as DNA. Such behaviour was previously observed when PPy was associated with redox markers such as ferrocene (Miodek *et al.* 2015) or copper complex (Chebil *et al.* 2013).

5.3 Anti-fouling properties of PPy-PEG-ANTA/Cu^{2+} complex

In order to evaluate the selectivity performance of the manufactured sensor, it was important to test its cross reactivity and nonspecific binding with other PCa biomarkers with a constant incubation time of 30 min at ambient room temperature. The fabricated aptasensor showed a significant variation of oxidation current peak of Cu^{2+} when it was incubated with 10 nM AMACR in 10 mM PBS, pH 7.4. The DNA aptamer, being specific to AMACR, showed a decrease in copper peak signal of 36.8 $\pm$ 1.6 % of relative current changes measured at 0.15 V *vs.* Ag/AgCl (Figure 5.8). This decrease is due to the blocking effect of electron transfer after attachment of proteins (Khan *et al.* 2006). The sensor was then tested with other biomarkers for PCa such as 10 nM prostate specific antigen (PSA, Fitzgerald, USA), 10 nM PSA-α1-antichymotrypsin (PSA-ACT, Lee Biosolutions, USA) and 10 nM human kallikrein 2 (hK2, R&D systems, UK). The aptasensor showed an efficient selective performance where the signal change was less than 3% in the presence of these other proteins, when compared to PBS alone.

Since the main idea was to demonstrate an improved anti-fouling chemistry, the aptasensor was tested with the most abundant protein present in blood called human serum albumin (HSA). For the same, the electrodes were dipped in a solution containing 4% w/v HSA in buffer and biosensor response was recorded. The

aptasensor demonstrated an excellent antifouling efficiency by showing a signal change of less than 4% (Figure 5.9 left).

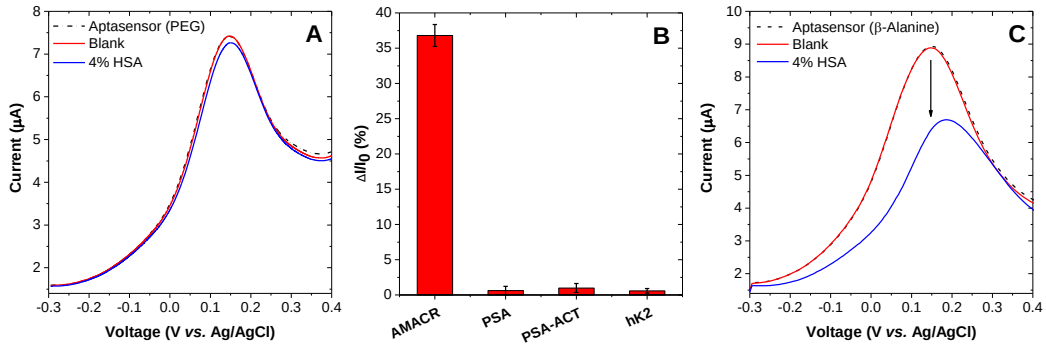

Figure 5.9 Selectivity study with other biomarkers for prostate cancer (bar graph, B). Relative current changes $\Delta I/I_0$, where $\Delta I=(I_0-I)$, where I_0 is the peak current prior addition of the DNA target and I after incubation of the sensor with certain concentration of target. Bars represent mean from 4 independent electrodes with standard deviation. SWV depicting the efficacy of PEG surface (A) over β-Alanine surface (C).

In order to underline the anti-fouling effect of PEG surface, we investigated another molecule such as *β*-alanine ($H_2NCH_2CH_2COOH$) to replace the PEG. *β*-Alanine was deposited onto the PPy layer in the same way that PEG was deposited and an aptasensor was manufactured. This *β*-alanine-based aptasensor was incubated with 4% (w/v) HSA in buffer and the electrochemical signal change was monitored as before (Figure 5.9). A significant relative current variation of up to 25% was recorded, demonstrating a poor anti-fouling efficiency for this aptasensor without PEG.

5.4 Analytical performances of biosensor

A wide range of AMACR concentrations were used from 1, 10, 100 fM; 1, 10, 100 pM; 1, 10 nM in both 10 mM PBS buffer and human plasma spiked samples (1 to 10 dilution in 10 mM PBS, pH 7,4). The concentration of the AMACR stock solutions were determined by UV-visible spectroscopy.

The formation of a biolayer, as well as detection of the target, were also successfully monitored using the SWV method by measuring the Cu^{2+}/Cu^{+} redox signal variation at 0.15 V *vs.* Ag/AgCl. The PEG aptasensor was initially tested with a wide range of

AMACR concentrations from 1 fM – 10 nM in 10 mM PBS pH 7.4, where a decrease in redox signal was observed with increasing AMACR concentrations. After 30 minutes incubation with each concentration, the variation in current of oxidation peak of ANTA/Cu^{2+} was observed. This variation was proportional to the amount of protein captured by aptamers. Based on the variation of current corresponding to ANTA/Cu^{2+} redox signal, a calibration curve was obtained as a function of AMACR concentration (Figure 5.10). The aptasensor demonstrated an excellent response. The sensor could potentially detect AMACR concentrations down to 5 fM. Limit of detection (LOD) of 0.15 fM was calculated using 5 independent samples using the method described by Armbruster *et al*. (Armbruster and Pry 2008).

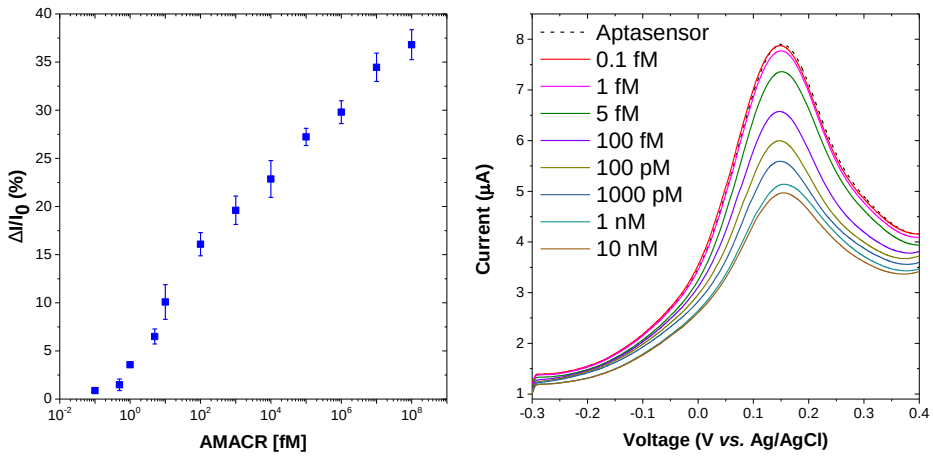

Figure 5.10 Dose response obtained using square wave voltammetry with different concentration of AMACR in 10 mM PBS, pH 7.4 buffer. Relative current changes $\Delta I/I_0$, where $\Delta I=(I_0-I)$, where I_0 is the peak current prior addition of the DNA target and I after incubation of the sensor with certain concentration of target.

After successful testing in buffer, the aptasensor was tested with human plasma samples. The electrodes were initially stabilised in 1 to 10 dilution of human plasma in 10 mM PBS buffer without AMACR protein until stable copper peaks were obtained. Upon stabilisation, human plasma samples spiked with AMACR were tested. The recorded signal after stabilisation was used as a reference to calculate relative changes in current during detection of protein. Again a wide range of AMACR concentrations was tested from 1 fM – 10 nM.

A dose response curve is plotted in Figure 5.11. A reduction in signal change was observed when human plasma was used, which can be attributed to the blocking effect by the histidine residues present in human plasma proteins (Jones *et al.* 2005). Nevertheless, the sensor demonstrated a good response down to concentrations of 5 fM with a LOD of 1.4 fM. The dose response curve is represented with a logarithmic scale in order to demonstrate the large dynamic range of detection and exhibits a linear response between 1 fM and 1 nM.

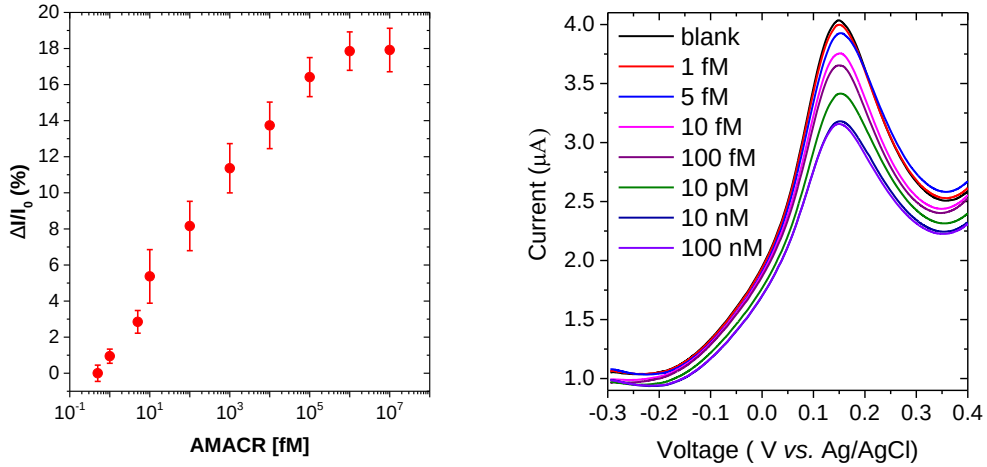

Figure 5.11 Calibration curve in AMACR spiked human plasma samples using SWV delta current. The plot of the relative changes of the current peak vs. concentration of DNA target measured at 0.15 V. Relative current changes $\Delta I/I_0$, where $\Delta I=(I_0-I)$, where I_0 is the peak current prior addition of the DNA target and I after incubation of the sensor with certain concentration of target.

Figure 5.11 (right) shows the SWV curves obtained with different concentrations of AMACR in human plasma. The sensor starts saturating at around 10 nM. These measurements were highly reproducible with standard deviations variation from of 0.3-1.2 % for 5 independent repeats. Furthermore, the efficiency of the sensor could be further improved by replacing copper ions with ferrocene (Miodek *et al.* 2015).

5.5 Surface plasmon resonance as a validation technique

Surface plasmon resonance (SPR) technique was also used to study the biolayer formation and the corresponding binding. For the study, 10 mM pyrrole solution was

prepared in water containing 0.5 M $LiClO_4$. Two cycles of pyrrole polymerisation as explained in section 5.2 was performed on the SPR chip in order to retain the SPR signal. Finally, 5 cycles of PEG deposition were performed on the modified SPR chip with PPy. Polymerisation and PEG deposition was performed outside the SPR cell using µAUTOLAB III / FRA2 potentiostat as described in section 5.2. Such a polymerisation caused an increase in the RI of the gold layer due to deposition of the PPy layer (Appendix I.5). All the steps after PEG deposition were performed using SPR. Figure 5.12 shows the µRIU (refractive index unit) changes at different association steps.

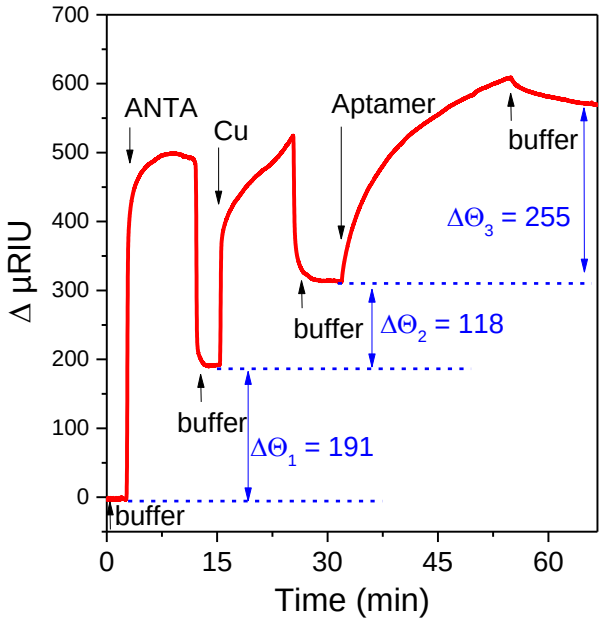

Figure 5.12 SPR curve showing association of different molecules on modified PPy film

After activation by EDC/NHS reaction for 5 minutes, ANTA was immobilised using 7 mM ANTA in 10 mM PBS (pH 8.5) for 10 min at a flow rate of 25 µL/min. A change of 191 µRIU was observed. Followed by ANTA immobilisation, copper was immobilised using 3.5 mM copper acetate dissolved in 20 mM acetate buffer (pH 4.6) for 10 min at the same flow rate as above. A change of 118 µRIU was observed after copper immobilisation. Finally after washing with 10 mM PBS, excess copper was

removed. Activated His-tagged DNA aptamers as described in the method section were immobilised by flowing 0.5 μM DNA aptamers in 10 mM PBS (pH 7.4) for 20 min at the same flow rate as above. DNA aptamers showed a change of 225 μRIU in the SPR signal.

After the immobilisation of the DNA aptamers, the chip was left in the 10 mM PBS (pH 7.4) buffer until stable. Once stable different concentrations of AMACR were flowed. Real time SPR response curves were obtained as shown in Figure 5.13.

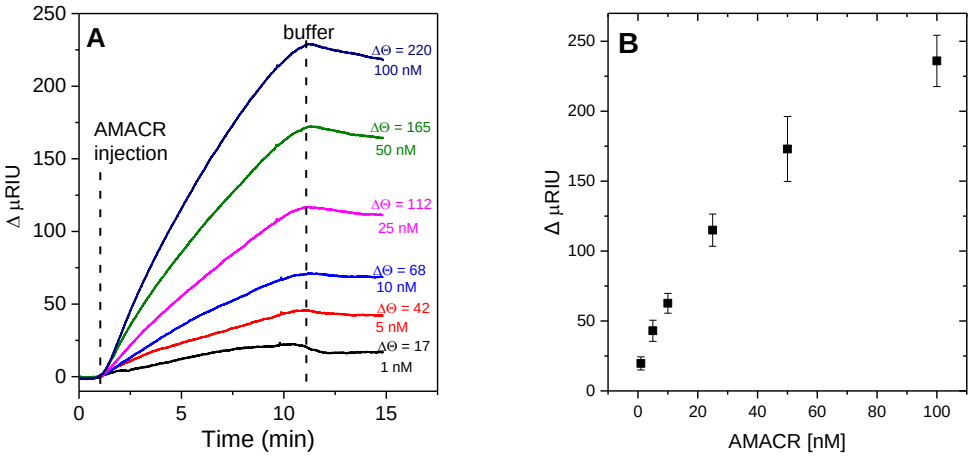

Figure 5.13 Real time SPR curves obtained with different concentrations of AMACR (A). Dose response obtained with different concentrations of AMACR (B). Data points represent mean value from three independent samples with standard deviation.

The dose response obtained from 3 samples is shown in Figure 5.13. The graph obtained shows an appreciable association of target from 1 nM and almost reaching saturation phase at 100 nM. The low sensitivity observed could be attributed to the limit of SPR detection and also added by the thickness of the biolayer on the bare gold SPR chip. Nevertheless, SPR data confirms the layer by layer formation of the biosensor strategy proposed in this Chapter with successful detection of AMACR.

5.6 Summary

This Chapter has presented a simple method of manufacturing a highly sensitive electrochemical aptasensor for detection of AMACR. It was also demonstrated that by electro-engineering PEG on the surface of a PPy film, anti-fouling properties can be significantly enhanced without loss of electrical properties because of PPy. The modified PPy film with PEG-NTA/Cu^{2+}-Aptamer was successfully used to detect AMACR in both spiked buffer and human plasma samples. A low sensitivity of 5 fM was attained with a LOD of 0.15 fM in buffer and 1.4 fM in human plasma respectively. The sensor also demonstrated good selectivity when challenged with other prostate cancer biomarkers and HSA. This approach can be easily extended to a wide range of other biomarkers, by employing their specific aptamer probes.

References

Adenier, A., Chehimi, M.M., Gallardo, I., Pinson, J., and Vila, N., 2004. Electrochemical oxidation of aliphatic amines and their attachment to carbon and metal surfaces. *Langmuir,* 20(19), 8243-8253.

Andrade, J.D., 1985. Surface and interfacial aspects of biomedical polymers. Vol. 1. Surface chemistry and physics. *Plenum Press*, 470.

Armbruster, D.A., and Pry, T., 2008. Limit of blank, limit of detection and limit of quantitation. *Clin Biochem Rev,* 29(Suppl 1), S49-52.

Azioune, A., Siroti, F., Tanguy, J., Jouini, M., Chehimi, M.M., Miksa, B., and Slomkowski, S., 2005. Interactions and conformational changes of human serum albumin at the surface of electrochemically synthesized thin polypyrrole films. *Electrochimica Acta,* 50(7), 1661-1667.

Chebil, S., Hafaiedh, I., Sauriat-Dorizon, H., Jaffrezic-Renault, N., Errachid, A., Ali, Z., and Korri-Youssoufi, H., 2010. Electrochemical detection of d-dimer as deep vein thrombosis marker using single-chain d-dimer antibody immobilised on functionalized polypyrrole. *Biosensors and Bioelectronics*, 26(2), 736-742.

Chebil, S., Miodek, A., Ambike, V., Sauriat-Dorizon, H., Policar, C., and Korri-Youssoufi, H., 2013. Polypyrrole functionalized with new copper complex as platform for His-tag antibody immobilization and direct antigen detection. *Sensors and Actuators B: Chemical,* 185, 762-770.

Darley, D.J., Butler, D.S., Prideaux, S.J., Thornton, T.W., Wilson, A.D., Woodman, T.J., Threadgill, M.D., and Lloyd, M.D., 2009. Synthesis and use of isotope-labelled substrates for a mechanistic study on human α-methylacyl-CoA racemase 1A (AMACR; P504S). *Organic & Biomolecular Chemistry*, 7(3), 543-552.

Estrela, P., Paul, D., Song, Q., Stadler, L.K., Wang, L., Huq, E., Davis, J.J., Ferrigno, P.K., and Migliorato, P., 2010. Label-free sub-picomolar protein detection with field-effect transistors. *Analytical Chemistry,* 82(9), 3531-3536.

Ghanem, M.A., Chrétien, J.-M., Pinczewska, A., Kilburn, J.D., and Bartlett, P.N., 2008. Covalent modification of glassy carbon surface with organic redox probes through diamine linkers using electrochemical and solid-phase synthesis methodologies. *Journal of Materials Chemistry,* 18(41), 4917-4927.

Han, D.-H., Lee, H.J., and Park, S.-M., 2005. Electrochemistry of conductive polymers XXXV: Electrical and morphological characteristics of polypyrrole films prepared in aqueous media studied by current sensing atomic force microscopy. *Electrochimica Acta,* 50(15), 3085-3092.

Hayat, A., Andreescu, S., and Marty, J.-L., 2013. Design of PEG-aptamer two piece macromolecules as convenient and integrated sensing platform: Application to the label free detection of small size molecules. *Biosensors and Bioelectronics*, 45, 168-173.

Jones, A.L., Hulett, M.D., and Parish, C.R., 2005. Histidine-rich glycoprotein: A novel adaptor protein in plasma that modulates the immune, vascular and coagulation systems. *Immunology and Cell Biology,* 83(2), 106-118.

Kausaite-Minkstimiene, A., Mazeiko, V., Ramanaviciene, A., and Ramanavicius, A., 2011. Evaluation of amperometric glucose biosensors based on glucose oxidase encapsulated within enzymatically synthesized polyaniline and polypyrrole. *Sensors and Actuators B: Chemical,* 158(1), 278-285.

Khan, F., He, M., and Taussig, M.J., 2006. Double-hexahistidine tag with high-affinity binding for protein immobilization, purification, and detection on ni-nitrilotriacetic acid surfaces. *Analytical Chemistry,* 78(9), 3072-3079.

Kjällman, T.H., Peng, H., Soeller, C., and Travas-Sejdic, J., 2008. Effect of probe density and hybridisation temperature on the response of an electrochemical hairpin-DNA sensor. *Analytical Chemistry,* 80(24), 9460-9466.

Lin, P.-Y., Cheng, K.-L., McGuffin-Cawley, J.D., Shieu, F.-S., Samia, A.C., Gupta, S., Cooney, M., Thompson, C.L., and Liu, C.C., 2012. Detection of alpha-methylacyl-CoA racemase (AMACR), a biomarker of prostate cancer, in patient blood samples using a nanoparticle electrochemical biosensor. *Biosensors,* 2(4), 377-387.

Maraldo, D., Garcia, F.U., and Mutharasan, R., 2007. Method for quantification of a prostate cancer biomarker in urine without sample preparation. *Analytical Chemistry*, 79(20), 7683-7690.

Miodek, A., Mejri, N., Gomgnimbou, M., Sola, C., and Korri-Youssoufi, H., 2015. E-DNA Sensor of Mycobacterium tuberculosis Based on Electrochemical Assembly of Nanomaterials (MWCNTs/PPy/PAMAM). *Analytical Chemistry*, 87(18), 9257-9264.

Nogues, C., Leh, H., Lautru, J., Delelis, O., and Buckle, M., 2012. Efficient antifouling surface for quantitative surface plasmon resonance based biosensor analysis. *PloS one*, 7(9), e44287.

Raoof, J.-B., Ojani, R., and Rashid-Nadimi, S., 2004. Preparation of polypyrrole/ferrocyanide films modified carbon paste electrode and its application on the electrocatalytic determination of ascorbic acid. *Electrochimica Acta*, 49(2), 271-280.

Rodriguez Emmenegger, C., Brynda, E., Riedel, T., Sedlakova, Z., Houska, M., and Alles, A.B., 2009. Interaction of blood plasma with antifouling surfaces. *Langmuir*, 25(11), 6328-6333.

Sharma, S., Johnson, R.W., and Desai, T.A., 2004. XPS and AFM analysis of antifouling PEG interfaces for microfabricated silicon biosensors. *Biosensors and Bioelectronics*, 20(2), 227-239.

Statz, A.R., Meagher, R.J., Barron, A.E., and Messersmith, P.B., 2005. New peptidomimetic polymers for antifouling surfaces. *Journal of the American Chemical Society*, 127(22), 7972-7973.

Wang, J., and Yau, S.T., 2014. Detection of α-Methylacyl-CoA Racemase in Serum and Urine Using a Highly Sensitive Electrochemical Immunodetector. *Electroanalysis*, 26(7), 1441-1444.

Yang, D.-K., Chen, L.-C., Lee, M.-Y., Hsu, C.-H., and Chen, C.-S., 2014. Selection of aptamers for fluorescent detection of alpha-methylacyl-CoA racemase by single-bead SELEX. *Biosensors and Bioelectronics*, 62, 106-112.

Yevglevskis, M., Bowskill, C.R., Chan, C.C., Heng, J.H.-J., Threadgill, M.D., Woodman, T.J., and Lloyd, M.D., 2014a. A study on the chiral inversion of mandelic acid in humans. *Organic & Biomolecular Chemistry*, 12(34), 6737-6744.

Yevglevskis, M., Lee, G.L., Threadgill, M.D., Woodman, T.J., and Lloyd, M.D., 2014b. The perils of rational design–unexpected irreversible elimination of fluoride from 3-fluoro-2-methylacyl-CoA esters catalysed by α-methylacyl-CoA racemase (AMACR; P504S). *Chemical Communications*, 50(91), 14164-14166.

Zhang, L., Jiang, X., Wang, E., and Dong, S., 2005. Attachment of gold nanoparticles to glassy carbon electrode and its application for the direct electrochemistry and electrocatalytic behavior of hemoglobin. *Biosensors and Bioelectronics*, 21(2), 337-345.

Chapter 6. Electrochemical sensing of miRNAs

This Chapter reports the development of a sensitive electrochemical platform for the detection of MicroRNAs (miRNAs). The platform was developed using peptide nucleic acids (PNA) as probes on gold electrode surfaces to capture target miRNAs. A simple amplification strategy using gold nanoparticles (AuNPs) has been employed where the inherent charges of the nucleic acids have been exploited. Electrochemical impedance spectroscopy (EIS) was used to monitor the changes in capacitance upon any binding event, without the need for any redox markers. On the same chip, by using thiolated ferrocene, a complementary detection mode was developed where the increasing peaks of ferrocene were recorded using square wave voltammetry (SWV) with increasing miRNA concentration. Thus, giving a dual-mode detection using the same chip.

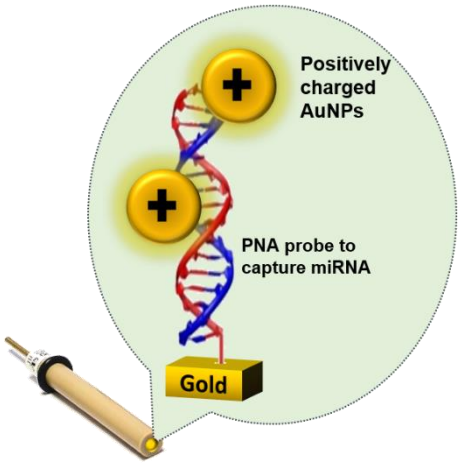

The work is partially published in Jolly *et al*. (Jolly *et al.* 2015) and partly submitted for publishing.

6.1 Background

MicroRNAs (miRNAs) are a class of noncoding genes that are transcribed as a RNA sequence of around 22 nucleotides long (Calin *et al.* 2002). More than twenty years after the first report about miRNA (Chalfie *et al.* 1981; Lee *et al.* 1993), there has been many reports on the miRNAs role in gene expression and regulation. Many reports have shown their importance in various biological processes in the human body including regulation of target genes (Bartel 2004), cellular proliferation and differentiation (Esquela-Kerscher and Slack 2006), cell death (Griffiths-Jones *et al.* 2006), translational and transcriptional regulation of their expression (Zieglschmid *et al.* 2005). It was only in the last decade that miRNAs have shown its significance in human diseases like cancer (He *et al.* 2005; Lu *et al.* 2005; Ramaswamy *et al.* 2001). For instance, miR-155 and miR-21 are up-regulated in breast cancer, but miR-91 has been found to be down-regulated in breast cancer. Other miRNAs can be related to more than one type of cancer. Many recent studies show that miR-145 is a tumour-suppressive miRNA, that is down-regulated in several cancer types, including bladder cancer (Ichimi *et al*. 2009), colon cancer (Akao *et al.* 2007), breast cancer (Spizzo *et al.* 2010), ovarian cancer (Nam *et al.* 2008) and prostate cancer (PCa) (Esquela-Kerscher and Slack 2006).

For PCa, miR-145 is a well-characterised tumour-suppressor with an important regulatory role since it can protect from cancer cell invasion and metastasis (Wang et al. 2015). Since miRNAs have been reported to act like finger prints of a disease including PCa, it therefore, makes them a promising tool as a biomarker. Conventionally, technologies used for miRNA study include Northern blotting (Valoczi *et al.* 2004), *in situ* hybridisation (Catuogno *et al.* 2011), quantitative polymerase-chain reaction (qPCR) (Chen *et al.* 2005) and miRNA microarray. All these techniques are powerful but complex and hence restricted to central laboratories. Consequently, there is a pressing need to develop simple and sensitive techniques to quantify levels of miRNAs in a portable and inexpensive way (Lu *et al.* 2005; Ren *et al.* 2013).

To take up such a challenge, electrochemical biosensors find their right candidature, thanks to their varied advantages such as specificity, portability, and low cost (Wang

2006). There are several reports on detection of miRNAs using electrochemical approaches. EIS has been widely used to quantify target miRNA hybridisation down to femtomolar levels with nanoparticles (Peng and Gao 2011) or with enzyme amplification (Ren *et al.* 2013a). Other electrochemical techniques such as differential pulse voltammetry (DPV), can be applied with EIS for complementary information or use independent and achieve a limit of detection over picomolar level (Kilic *et al.* 2012).

However, the developed biosensors reported lack simplicity in the fabrication process. This Chapter reports the development of a simple and sensitive electrochemical detection platform for miRNA using PNA as probes. PNA was used since it presents many advantages such as neutral charge and higher stability than DNA probes. Furthermore, the PNA/miRNA duplex with mismatches are less stable than a DNA/miRNA duplex with the same mismatches (Demidov et al. 1994; Ray and Norden 2000). A simple amplification strategy using positively charged AuNPs have been employed. For the detection, EIS was used without redox markers to monitor the changes in the dielectric properties of the bilayer through capacitance changes. Exploiting the availability of AuNPs on the surface with PNA/miRNA duplex, thiolated ferrocene was used to provide an amperometric detection using SWV.

6.2 Materials and Methods

6.2.1 Instruments

The experiments were carried out with a CompactStat potentiostat (Ivium Technologies, The Netherlands) and a three-electrode cell system: Ag/AgCl (KCl) reference electrode (BASi, USA) connected via a salt bridge filled with 10 mM phosphate buffer (PB, pH 7.4), Pt counter electrode (ALS, Japan) and gold working electrode (2.0 mm diameter from CH Instruments, USA).

The non-Faradaic impedance spectrum was conducted in 10 mM PB (pH 7.4) measurement buffer over a frequency range from 100 kHz to 100 mHz, with a 10 mV

a.c. voltage superimposed on a bias d.c. voltage of 0 V with respect to the open circuit potential.

The Faradaic impedance spectrum was conducted in 10 mM PB (pH 7.4) measurement buffer containing 10 mM of the ferro/ferricyanide $[Fe(CN)_6]^{3-/4-}$ redox couple (hexacyanoferrate II/III) over a frequency range from 100 kHz to 100 mHz, with a 10 mV a.c. voltage superimposed on a bias d.c. voltage of 0.2 V *vs.* Ag/AgCl (which corresponds to the formal potential of the redox couple).

6.2.2 Oligonucleotides

The HPLC purified synthetic oligonucleotides were purchased from Sigma Aldrich, UK in lyophilized form while PNA probe sequences were purchased from Cambridge Research Biochemical, UK. The sequences are shown in Table 6.1.

Table 6.1 miRNA sequences and PNA probes used in this work. The full complementary sequence in the first row corresponds to mir-145 sequence. AEEA is a glycol linker of nine atoms (8-amino-3,6-dioxaoctanoic acid).

Full comp sequence (miR145)	3'- **UCC CUA AGG ACC CUU** UUU GAC CUG - 5'
Non comp-sequence	3'- **AAA UGC CUA UAG ACC** CUU GAC CUG - 5'
1 mismatch sequence	3'- UCC CUA **U**GG ACC CUU UUU GAC CUG - 5'
2 mismatch sequence	3'- UCC **A**UA AG**C** ACC CUU UUU GAC CUG - 5'
Full comp sequence for PNA probe 1	3'- TCT TCT TCT TCT TCT TCT TCT TCT - 5'
PNA probe1: SH-C6-AEEA-	AGA AGA AGA AGA AGA G
PNA probe2: SH-C6-TTT	AGG GAT TCC TGG
PNA probe3: SH-C6-AEEA-TTT	AGG GAT TCC TGG

6.3 Biosensor Fabrication

Gold disk working electrodes with a radius of 1.0 mm were cleaned as detailed in Chapter 3 and Chapter 4. Clean gold electrodes were then co-immobilised with a thiolated ssPNA probe sequence and MCH in 50% dimethyl sulfoxide (DMSO, Sigma Aldrich, UK), 50% ultra-pure water (v/v) immobilisation solution for 16 hours in a humidity chamber. An optimised ratio of 1:5 was adopted from the literature (Keighley *et al.* 2008). After immobilisation, electrodes were rinsed with surplus MilliQ water to remove any unattached thiols. In order to ensure complete thiol coverage of the gold

surface, the electrodes were thereafter backfilled with 1 mM MCH for 1 hour. Electrodes were then rinsed with MilliQ water and placed in the measurement buffer for 1 hour to stabilise the SAM.

The functionalised surface was then used to capture target miRNA or DNA sequences, which makes the surface negatively charged; finally, positively charged gold nanoparticles were used to electrostatically bind to the PNA-miRNA or PNA-DNA double-strand (Figure 6.1). As the last step, 50 µM thiolated ferrocene (6-(Ferrocenyl)hexanethiol, Sigma, UK) was added to the surface where ferrocene covalently binds to free spaces on the attached AuNPs.

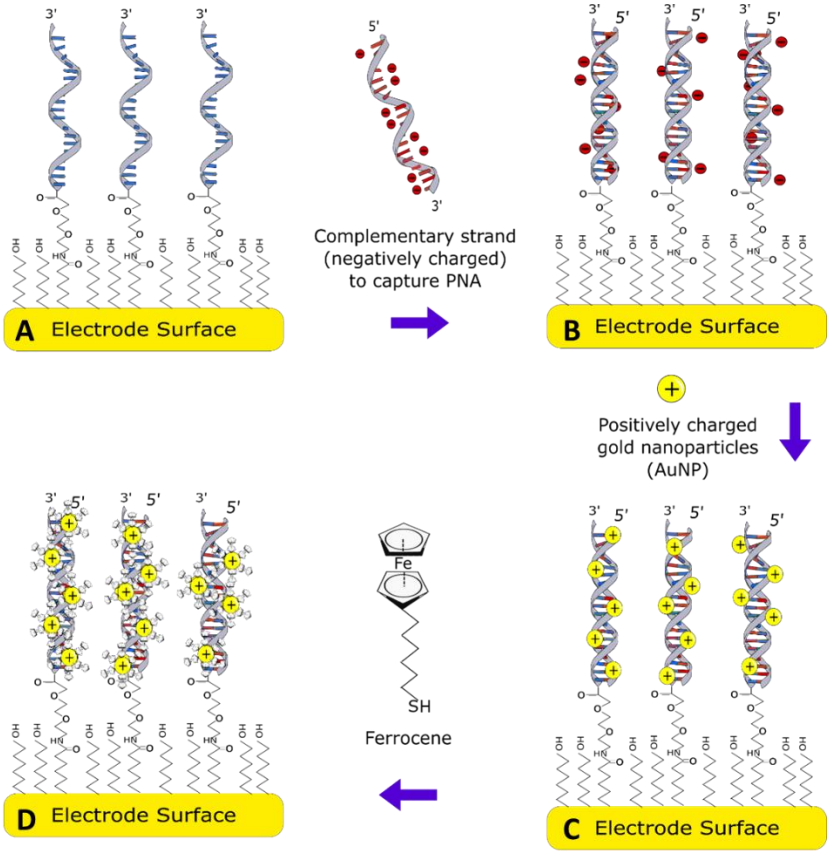

Figure 6.1 Schematic of the biosensor. (a) Immobilised PNA probes. (b) Capture of target oligo (DNA/miRNA). (c) Electrostatic interaction of positively charged AuNPs with PNA/DNA or PNA/miRNA hybrid and finally (d) attachment of thiolated ferrocene to attached AuNPs.

Preparation of positively charged AuNPs was adopted as reported by Kim *et al* (Kim *et al*. 2008). Shortly, an optimised ratio of hydrogen tetrachloroaurate ($HAuCl_4$, Sigma Aldrich, UK) and branched poly-(ethylenimine) (PEI, MW~25 kDa, Sigma Aldrich,

UK) was mixed overnight using vigorous stirring to produce AuNPs. Before experiments, the AuNPs were washed three times using centrifugation and re-dispersion in Milli-Q water.

For the binding studies, different concentrations of target DNA/RNA, non-complementary DNA/RNA and 4% bovine serum album (BSA) were prepared in 10 mM PB, pH 7.4.

The presented work was divided into two aspects. The first aspect includes the study of a PNA sequence with AGA repeats to be tested as a proof of principle. The second study incorporated the use of PNA probe specific to miRNA145 sequence.

6.3 Investigation of strategy using EIS technique

EIS in Faradaic mode was used to investigate different binding steps to evaluate the strategy. The EIS measurements were performed in the presence of 10 mM of the ferro/ferricyanide $[Fe(CN)_6]^{3-/4-}$ redox couple to monitor the application of the strategy. Initially, the PNA immobilised biosensor was tested with positively charged AuNPs to study the nonspecific interactions. From Figure 6.2 (red curve) a negligible change in the R_{ct} of the system is observed. Similar tests were performed with 4% BSA and 100 nM of non-complementary DNA sequence resulting in a signal change of less than 2%.

After successful evaluation of the system with non-specific interactions, the sensor was tested with 100 nM complementary DNA sequence. This interaction resulted in a change of R_{ct} from 1.2 kΩ to 12.8 kΩ (blue curve). This increase could be attributed to the formation of a PNA/DNA duplex, making the electrode surface highly negatively charged. Such a surface provides increased repulsion to the redox ions in the solution to reach the electrode surface and thus, increasing the R_{ct} of the system. Finally, positively charged AuNPs were added, which electrostatically bind to the PNA/DNA duplex only. On binding of AuNPs a decrease in the R_{ct} of the system is observed (pink curve). Such a decrease could be attributed to screening of negative charges of the PNA/DNA duplex with positively charged AuNPs. It is worth

mentioning that the R_{ct} of the system does not return to its initial value. This could be attributed to the fact that although AuNPs are screening the charges, the mass loading effect still causes an increased physical barrier to the redox couple.

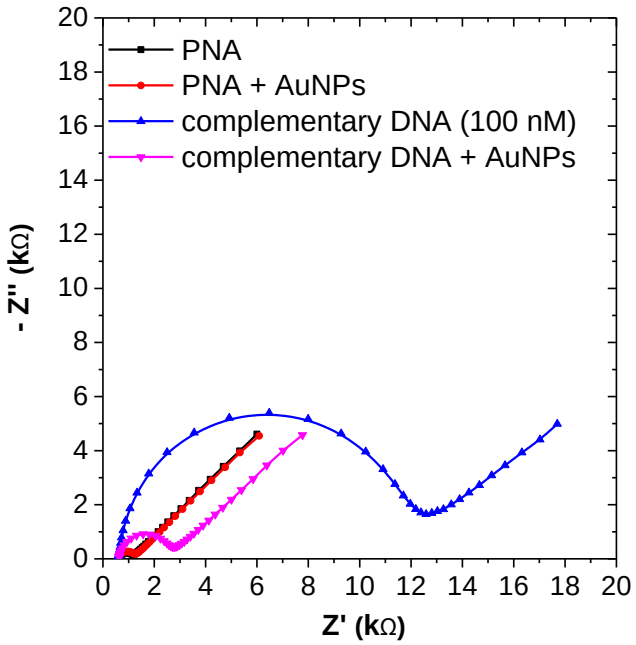

Figure 6.2 EIS Characterisation of binding events using PNA based biosensor. Black curve represents PNA based biosensor. Red curve represents non-specific binding of AuNPs. Blue curve represents the hybridisation of target DNA with PNA probes and finally pink curve represents the electrostatic interaction of AuNPs with PNA/DNA duplex.

6.4 Non-Faradaic EIS Measurement

EIS in Faradaic mode has been used to investigate the applicability of the strategy. However, such a strategy of using positively charged nanoparticles (gold, silver, and zirconium) has been reported earlier. For instance, Zhang *et al.* in 2009 developed an electrochemical based DNA biosensor based on the use of positively charged silver (Ag) nanoparticles (Zhang *et al.* 2009). In the study, PNA based probe was immobilised on the surface of gold electrodes which were used to capture target DNA. On hybridisation, the surface of the electrode becomes negative due to PNA/DNA duplex. Finally, positively charged Ag nanoparticles were added which electrostatically bind to PNA/DNA duplex which is used as a label through a

characteristic solid-state Ag/AgCl reaction. Later in 2010, Kim *et al.* reported the development of naked eye detection platform using PNA probes on glass surfaces and AuNPs as an amplification strategy (Kim *et al.* 2010). In the study, on the hybridisation of DNA to PNA, a negatively charged surface is formed which when incubated with positively charged AuNPs, results in the electrostatic attachment of AuNPs to PNA/DNA duplex. Later, an amplification step was introduced wherein the presence of metal enhancement solution, the AuNPs on the surface of the electrode grow in size resulting into visualisation via an optical scanner or naked eye. In this study, we utilise the same strategy but employing a simplified EIS measurement. EIS was measured in the absence of a redox couple to monitor the changes in capacitance of the system at the electrode/electrolyte interface as a result of the binding event and attachment of positively charged AuNPs. The PNA functionalised electrodes were initially stabilised in 10 mM PB (pH 7.4) before conducting the experiments. After stabilisation, the electrodes were exposed to different concentrations of complementary DNA targets prepared in 10 mM PB buffer (pH 7.4) over an incubation period of 30 minutes. In order to evaluate the capacitance of the system, a complex capacitance was defined as explained in Chapter 2 (Figure 6.3).

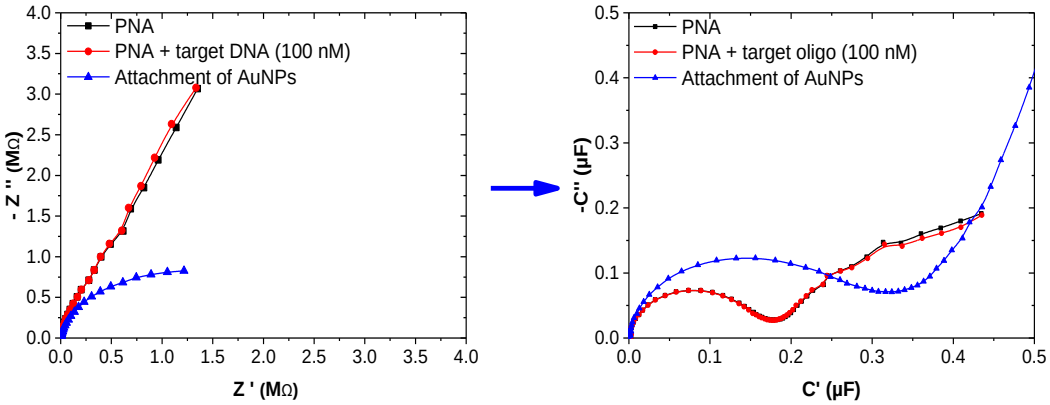

Figure 6.3 Left represents impedance plots of the system while right represents Cole-Cole plot representing capacitance of the system. Black curve shows the capacitance of PNA probe on the surface. Slight decrease in the capacitance is observed with hybridisation of target oligo (red curve) which is significantly increased on binding with AuNPs.

Figure 6.3 (left) shows a typical EIS response when performed in the absence of redox couple. The high impedance values observed are attributed to ultra-slow charge transfer from the solution to the electrode surface. Although nothing constructive can be hypothesised by looking at the Nyquist plot, when the impedance data is converted into its respective capacitance data, *Cole-Cole* capacitance plots can be obtained. With these plots, the capacitance of the system can be estimated by the diameter of the obtained semicircle (Figure 6.3 right). From Figure 6.3 (right), the black curve represents the biosensor. On incubation with 100 nM target DNA over 30 minutes, the red curve was obtained. A very small change of less than 5% decrease in capacitance was observed on binding with target DNA. Such a small signal change could be attributed to the presence of the long linker (AEEA) between the PNA probe and the gold surface. PEG linker (AEEA, $C_{21}H_{23}NO_6$) results in the binding event happening far away from the surface and well above the Debye length of the system, leading to the screening of the DNA charges. Nevertheless, when the sensor was incubated with AuNPs, a huge change in capacitance was observed due to specific electrostatic binding between AuNPs and PNA/DNA duplex. Such a response could be attributed to changes in the dielectric properties of the bio-layer due to the presence of polymer capped AuNPs.

At this point of electrochemical platform development, it was imperative to investigate selectivity studies with stringent controls to prove that the signal change is due to the specific binding event. The fabricated PNA-based sensor was tested with (i) just positively charged AuNPs on the immobilised PNA probes, (ii) 100 nM of non-complementary oligonucleotides and (iv) 4% Bovine Serum Albumin (BSA, Sigma Aldrich, UK). The results demonstrated less than 1% changes in capacitance of the system making it a potential platform for real clinical samples (Figure 6.4).

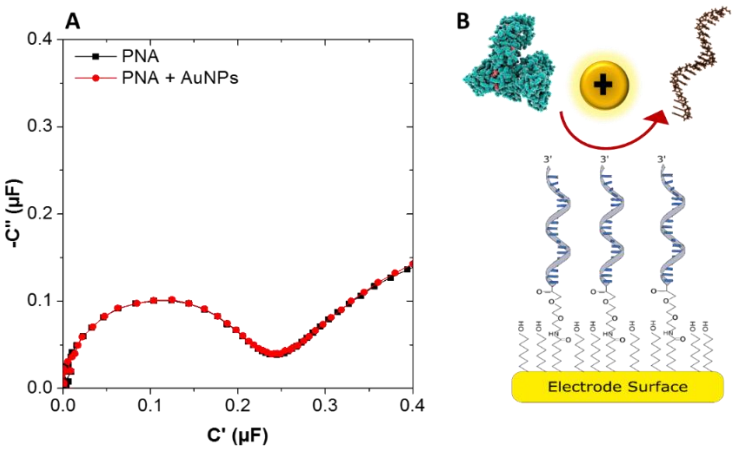

Figure 6.4 (A) Graph representing signal change on incubating the sensor with (B) nonspecific targets like BSA, non-complementary DNA and AuNPs.

After successful selectivity performance of the sensor, a dose response was performed using a wide range of target DNA concentrations. The results are presented in Figure 6.5 with the current detection strategy where a very low detection limit of 1 fM was observed. Again an insignificant change in capacitance was observed on binding with target DNA (black bars) but a clear trend could be observed after the AuNP amplification step shown in red bars.

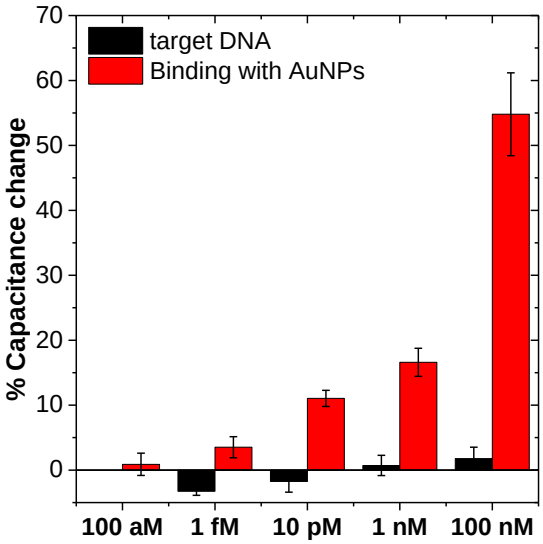

Figure 6.5 Dose response. Black bars represent changes in capacitance on binding with target oligo while red bars represent amplification in capacitance change on binding with AuNPs.

6.5 Open Circuit Potential as an alternative mode of detection technique

Since the strategy employed utilises the change in the net charge on the surface of the electrode, Open Circuit Potential measurements (OCP) were used as another potential technique to monitor changes in potential because of the binding event. OCP measurements and optimisation were performed by Wong (2016). Such a measurement was carried out using a custom made in-house electronic measurement system based on an INA116 ultra low input bias current instrumentation amplifier with a cell (Estrela *et al.* 2008, Formisano *et al.* 2015). The setup used consisted of 1.6 mm diameter gold disc working electrodes (ALS Ltd, Japan), a Hg/Hg_2SO_4 (K_2SO_4) reference electrode placed into a salt bridge, and a platinum wire for grounding the solution in the electrochemical cell. The OCP was measured in real time in a solution of 10 mM PB (pH 7.4). Two working electrodes were measured simultaneously at the same time through two different channels for the small changes in potential due to electrode surface modification, by using a common reference electrode.

By using the OCP technique, slight changes in the electrochemical interface can be picked up by the system. Such changes are attributed to charge change upon DNA hybridisation and attachment of positively charged AuNPs. Figure 6.6 (left) illustrates a typical response curve generated using an OCP setup. After the system reaches a stable value, 1 µM target DNA was injected into the cell. As DNA hybridisation occurs, the potential drops due to the attachment of negatively charged complementary strand DNA to neutrally charged immobilised PNA probes. A stable value from hybridisation is achieved after half an hour and an average change of 4.8 mV is observed. Then, positively charged AuNPs were injected and an average increase of +19.9 mV was achieved. This is attributed to the attraction of the positive charges on the AuNPs to the negative charges on the PNA/DNA layer.

Again, the potential changes monitored upon target DNA hybridisation were lower than expected: less than 5 mV for 1 µM of DNA target which was the highest concentration tested. It is worth mentioning that the experiments were performed without a flow cell and the OCP results in different concentrations are shown in Figure 6.6 right. The likely reason for such small changes could be again due to the presence

of the long linker used for the PNA probe along with the excess of complementary strand DNA that is flowing in the solution, which hinders the potential change due to charge floating in the bulk solution. This possible reason also causes a higher potential change upon injecting AuNPs to the blank test. Although the current results do show that the changes due to attachment of AuNPs are distinguishable between blank and PNA/DNA, a further improvement can be made. To enhance the signal and reduce the background noise an extra rinsing step after each injection, which can rinse away the excessive molecules (DNA/AuNPs), can be incorporated in the measurement strategy. Nevertheless, there is still a clear difference between potential changes on blank and the tested concentrations of target DNA. Additionally, the decrease in the measurement cell volume can significantly decrease the time needed to get a stable signal on a binding event, which would be investigated in our future experiments.

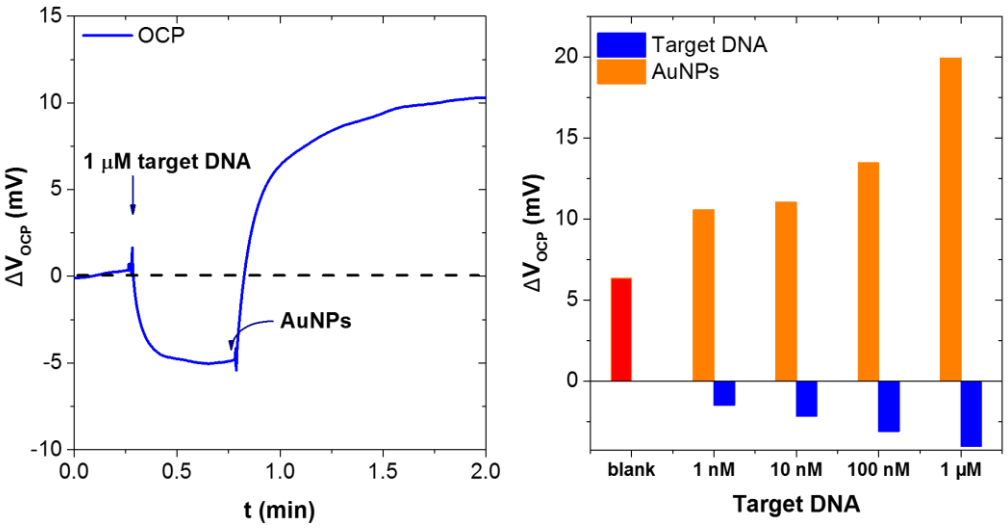

Figure 6.6 Real time OCP signal (left) and Dose response with OCP setup. Bars represents average from two independent electrodes. Blue bars represent binding with target oligo while yellow bars represent AuNPs amplification (right).

6.6 Effect of linker size on non-specific interactions

The size of the PNA linker was also investigated in this study. A C6 thiol linker can be used in place of C6-AEEA linker as a PNA modification that can be co-immobilised on the gold surface. As expected, by reducing the linker length from C6-AEEA to C6,

a significant variation in the capacitance of above 5% was observed upon incubation with the complementary miRNA strand. However, what was more important in this particular electrochemical platform development, was to test its selectivity efficiency. For the same, the biosensor was constructed using both modifications of PNA (C6 and C6-AEEA) with MCH on the gold surface. Electrodes were subsequently tested with just AuNPs without any hybridisation with target DNA. EIS in Faradaic mode as described in section 6.2 was used to monitor the changes in R_{ct}. Figure 6.7 illustrates impedance plots recorded from the EIS experiment. A significant non-specific interaction of around 30% was observed as a result of the reduction in R_{ct} after incubation of PNA based biosensor with C-6 linker with AuNPs. A decrease in R_{ct} is a result of attachment of positively charged AuNPs to the electrode surface which consequently results in a decrease in the resistance to negatively changed redox couple in the solution.

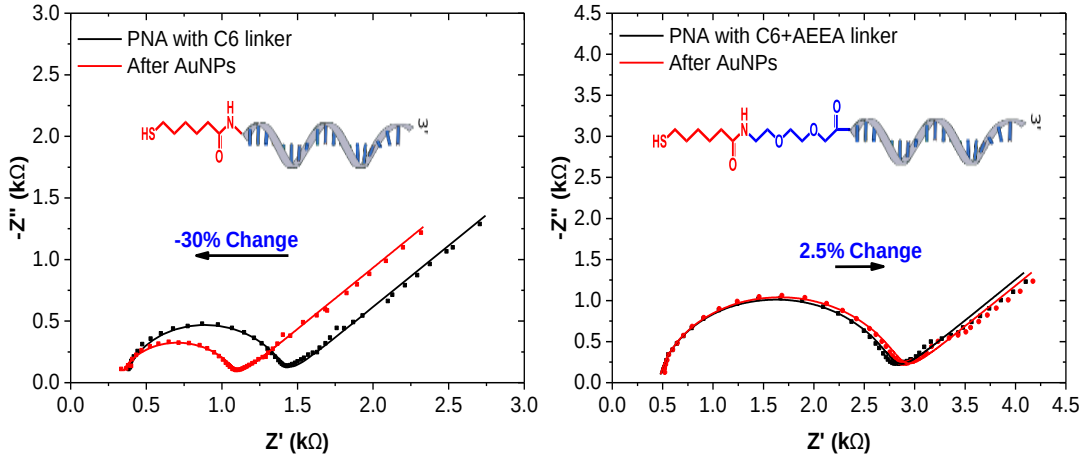

Figure 6.7 Faradaic EIS plots of PNA based biosensor. (Left) Represents C6-Linker modified PNA as a probe for biosensor fabrication and the change in Rct after incubating with AuNPs. (Right) Represents C6-AEEA Linker modified PNA as a probe for biosensor fabrication and the change in Rct after incubating with AuNPs.

Such an observation indicates that the SAM formed on the gold surface is not efficient enough to prevent non-specific interactions. As compared to C6 linker, when a C6-AEEA linker was employed, a significant reduction in the non-specific interaction of less than 3 % was observed showing an enhanced anti-fouling efficiency, thanks to the PEG-like linker. As explained in Chapter 3 and Chapter 5, PEG due to its hydrophilic

nature forms hydration a shell in the solution which helps to prevent non-specific interactions. As a result, for further experiments, only C6-AEEA modification of PNA probe was used to reduce the background noise.

6.7 One chip-dual mode electrochemical platform for detection of mir145

With the successful development of the electrochemical platform for the detection of DNA in the solution, the biosensor was used for the detection of miRNAs. For the study, PNA probe 2 was used which was partially complementary to mir145 taken as a case study. Before going directly to the EIS measurement in non-Faradaic mode, the new PNA sequence was characterised using Faradaic EIS mode. Figure 6.8 represents the impedance curve recorded with PNA probe 2. The black curve represents the initial impedance of the electrode with PNA probe 2.

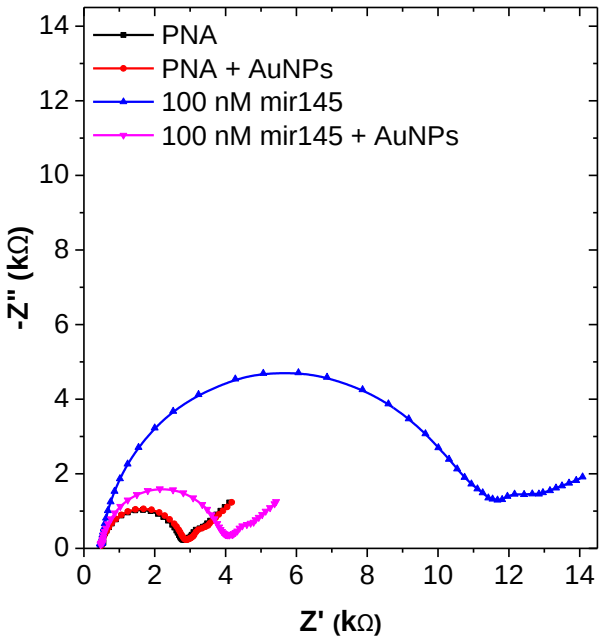

Figure 6.8 EIS Characterisation of binding events using PNA based biosensor. Black curve represents PNA based biosensor. Red curve represents non-specific binding of AuNPs. Blue curve represents the hybridisation of mir145 with PNA probes and finally pink curve represents the electrostatic interaction of AuNPs with PNA/mir145 duplex

The biosensor was tested with just AuNPs for non-specific interactions and the red curve was obtained demonstrating negligible signal change. On incubation with 100 nM mir145 over 30 minutes, a significant change in the R_{ct} from 2.9 kΩ to nearly 12 kΩ occurred (represented by the blue curve). Finally, the electrodes were incubated with positively charged AuNPs and a significant decrease in the R_{ct} from 12 kΩ to 4 kΩ was observed. The observations recorded confirmed the binding events using the previously described strategy.

6.7.1 Capacitive Biosensor

The detection of different concentrations of mir145 was successfully monitored using EIS in non-Faradaic mode by estimating the changes in the capacitance upon a molecular binding event. The PNA-based biosensor was initially tested with a wide range of mir145 concentrations from 1 fM to 100 nM in 10 mM PB pH 7.4, where an increase in the change in the capacitance was observed with increasing miRNA concentrations. After 30 minutes incubation at each concentration, the variation in capacitance was proportional to the amount of captured mir145. Figure 6.9 (right) shows the calculated capacitance from EIS data, diameter of the semicircle of which gives an estimate of the capacitance of the system An initial capacitance of 0.243 µF was observed with PNA-based sensor (C1) which changed to 0.241 µF after incubating with 1fM miR-145 (C2), leading to a change of -0.82%. However, after incubating with AuNPs, the capacitance increased to 0.254 µF (C3), leading to change of +5.4%. Based on the variation of capacitance corresponding to attachment of AuNPs, a calibration curve was plotted as a function of mir145 concentration. The biosensor demonstrated an excellent response (Figure 6.9). The sensor could potentially detect miRNA concentrations down to 1 fM with nearly 6 % change. A LOD of 0.37 fM was calculated using 4 independent samples as described by Armbruster *et al*. (Armbruster and Pry 2008).

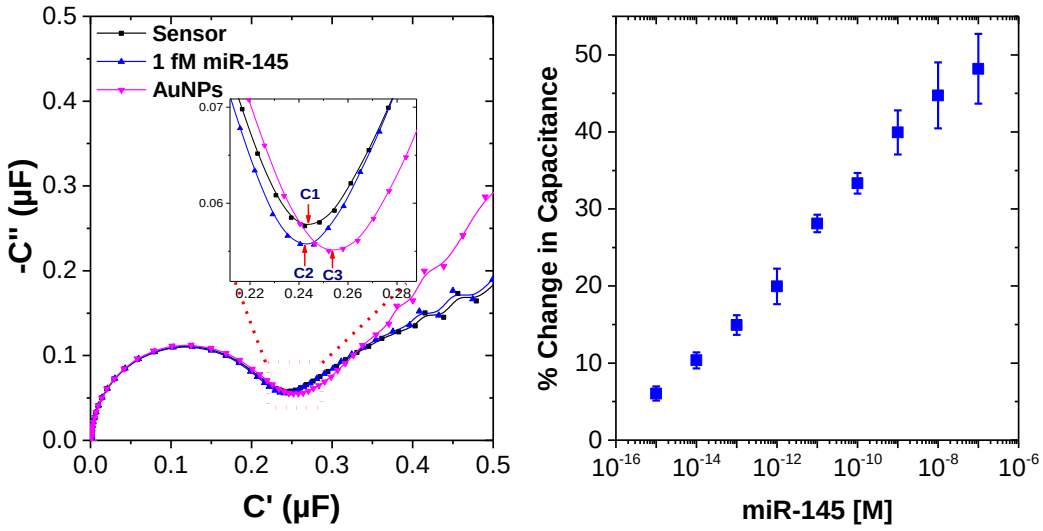

Figure 6.9 Left shows a typical Cole-Cole plot obtained with PNA-based sensor before and after hybridisation with 1 fM miR-145 (black and blue respectively) and AuNP attachment (pink). A zoom-in version of Cole-Cole plot shows the changes in capacitance upon a molecular binding event. Right represents a calibration curve and data points represent average changes in capacitance from a minimum of three independent samples on binding with AuNPs at different concentration of miR-145.

6.7.2 Amperometric Biosensor

With successful application of simple amplification strategy to detect mir145 using capacitance measurements, the setup was explored for additional applications. One such application explored the availability of AuNPs on the surface of the electrode. Formisano *et al.* in 2015 demonstrated the use of AuNPs on the electrode surface as a possible platform to immobilise thiolated ferrocene molecules. Such a modified AuNPs with ferrocene was used as a redox indicator by monitoring the oxidation peaks of ferrocene (Formisano *et al.* 2015). Similarly, in this present strategy, the electrodes were incubated with 50 µM thiolated ferrocene over a period of 30 minutes (Figure 6.10). The square wave voltammetry (SWV) technique was used to monitor the oxidation peaks of ferrocene. SWV was performed in 10 mM PB (pH 7.4) in the potential range from -0.4 V to 0.7 V *vs.* Ag/AgCl with conditioning time of 120 s, modulation amplitude of 20 mV and frequency of 50 Hz.

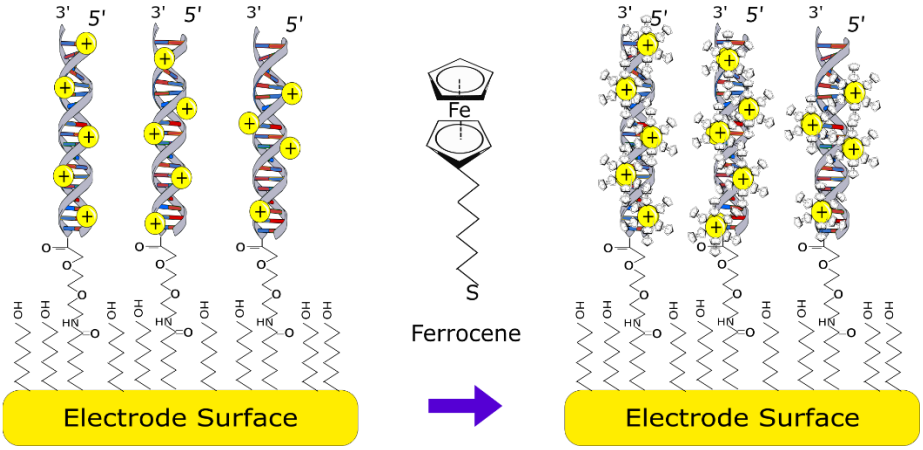

Figure 6.10 Schematic of amperometric detection strategy.

After specific interaction of AuNPs with PNA/mir145 duplex, thiolated ferrocene was flowed through the system, allowing the thiolated ferrocene to covalently bind to the free available spaces of AuNPs. The PNA based biosensor was tested with a wide range of mir145 concentrations from 1 fM to 100 nM in 10 mM PB pH 7.4, where an increasing oxidation peak of ferrocene was observed (Figure 6.11) after the final step of thiolated ferrocene flow.

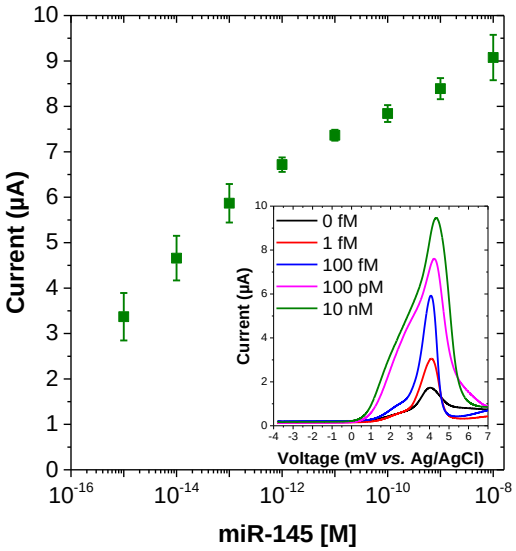

Figure 6.11 Dose response. Data points represent average ferrocene peaks and standard deviation recorded using square wave voltammetry (SWV) from three independent samples on the binding of thiolated ferrocene with AuNPs at different concentration of mir145. Inset represents the SWV curves recorded at different mir145 concentrations.

From Figure 6.11 (left), it can be seen that the peak current increases for increasing miRNA concentrations from 1 fM to 1 pM, after which the peak current start getting saturated resulting in similar peak currents. Such a saturation could be due to aggregation of AuNPs at a higher mir145 concentration resulting in decreased charge transfer. A similar effect could be seen in the SWV recording (right) where as we move toward higher mir145 concentration, a wider ferrocene peak was observed which could be attributed to the non-homogeneous assembly of ferrocene near the electrode surface. It is worth mentioning that a high background current of nearly 1 µA was recorded. Such a current could be due to two probable reasons. Firstly, due to the non-specific interaction of ferrocene to the electrode surface and secondly, due to the presence of even a small amount of AuNPs due to non-specific interaction which could be used as a platform where ferrocene can attach. Nevertheless, when the blank measurement was compared with the lowest mir145 concentration used, a six time higher ferrocene peak current was recorded.

6.7.3 Selectivity Study

The developed PNA based biosensor was challenged with stringent controls in order to investigate the selectivity of the sensor. For the study, 100 nM concentration of mir145 was compared with 100 nM of RNA sequence with 1 mismatch, 2 mismatches and a non-complementary RNA. The results from both capacitance measurement and SWV is presented in Figure 6.12.

In both types of measurements, the signal change observed with 100 nM of RNA sequence with 2 mismatches and a non-complementary RNA showed negligible signal change when compared with 100 nM mir145. However, with 1 mismatch sequence, a significant change in the signal was observed with both the techniques. Such an interaction could be due to the choice of the mismatch. As shown in Table 6.2, the mismatch is in the middle of the sequence, which is the most stable position. Nevertheless, the signal change observed was 50 % lower than what was observed with mir145. The significant non-specific interaction observed could be reduced by adding another parameter of temperature. By using a temperature close to the melting

point of the PNA/mir145 duplex (*ca.* 70.3 °C), the non-specific binding of mismatches can be greatly reduced (Giesen *et al*. 1998).

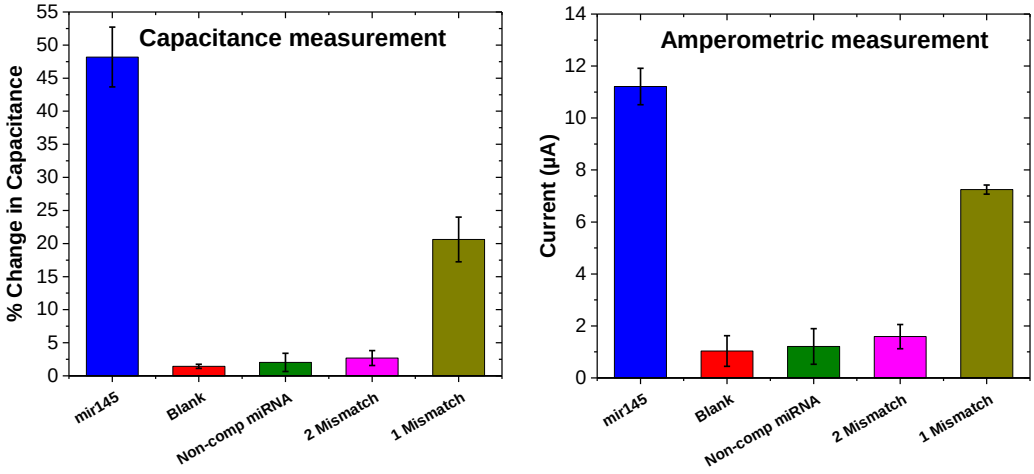

Figure 6.12 Selectivity study. All the oligonucleotide concentration were 100 nM.

6.8 Summary

In this Chapter, a simple electrochemical PNA-based biosensor with AuNPs amplification for the detection of miRNA or DNA was presented. It has been demonstrated how AuNPs can disrupt the dielectric biolayer of the sensor, leading to significant changes in the capacitance of the system. With the current system, a LOD of 0.38 fM was achieved. Table 6.2 lists some of the state of art technologies to detect miRNAs via electrochemical methods. The current technology reported in this Chapter demonstrates a simple amplification strategy with LOD lower or comparable to those reported in the literature.

Table 6.2 List of state of art technologies to detect miRNAs

Detection Method	Electrode	MiRNA	Strategy employed	LOD	Reference
Amperometric (CV and EIS)	Gold electrode	MiR-21	hemin-G-quadruplex complex on AuNPS as the amplification element	3.96 pM	Zhou *et al.* 2012
Amperometric (DPV and EIS)	Gold electrode modified with AuNPs	miR-21	Thiol chemistry	6 fM	Meng *et al.* 2013

Amperometric (CV and DPV)	Gold electrode	miR-21	AuNP as an amplification step	45 fM	Xia *et al.* 2013
Amperometric (DPV and EIS)	Gold electrode modified with AuNPs	miR-159a	Thiol chemistry	3.5 fM	Wang *et al*. 2014b
Amperometric (CV)	Gold electrode	miR-21	AuNPs as an amplification step	3 fM	Liu *et al*. 2014
Amperometric (DPV and EIS)	Gold electrode	let-7a, let-7b, let-7c	AuNPs as an amplification step	99.2 fM	Peng *et al*. 2014
Amperometric (CV, DPV and EIS)	Gold electrode modified with AuNPs	miR-21	Thiol	0.17 fM	Wang *et al*. 2014a
Amperometric (DPV)	Gold electrode modified with AuNPs	miR-139a	Thiol	1.7 fM	Zhou *et al*. 2016
Amperometric (DPV)	Gold electrode modified with AuNPs	miR-21	Thiol	0.36 fM	Li *et al*. 2016
Dual mode EIS and amperometric detection	**Gold Electrode**	**Mir145**	**AuNPs as an amplification step**	**0.37 fM**	**This study**

OCP measurements, as another simple cost effective detection tool, has been demonstrated to detect low levels of target oligonucleotides. Furthermore, a dual-mode detection was developed by using thiolated ferrocene which specifically binds to free spaces of present AuNPs. Such a technique provides a validation data to back up the changes in capacitance. The presented application can be extended to the detection of oligonucleotides specific for various other diseases. Of significant importance is that the detection techniques can easily be expanded into arrays for the parallel screening of panels of DNAs or miRNAs.

References

Akao, Y., Nakagawa, Y., and Naoe, T., 2007. MicroRNA-143 and -145 in colon cancer. *DNA and Cell Biology,* 26(5), 311-320.

Armbruster, D.A., and Pry, T., 2008. Limit of blank, limit of detection and limit of quantitation. *Clin Biochem Rev,* 29(Suppl 1), S49-52.

Bartel, D.P., 2004. MicroRNAs: genomics, biogenesis, mechanism, and function. *Cell,* 116(2), 281-297.

Calin, G.A., Dumitru, C.D., Shimizu, M., Bichi, R., Zupo, S., Noch, E., Aldler, H., Rattan, S., Keating, M., Rai, K., Rassenti, L., Kipps, T., Negrini, M., Bullrich, F., and Croce, C.M., 2002. Frequent deletions and down-regulation of micro- RNA genes miR15 and miR16 at 13q14 in chronic lymphocytic leukemia. *Proceedings of the National Academy of Sciences of the United States of America,* 99(24), 15524-15529.

Catuogno, S., Esposito, C.L., Quintavalle, C., Cerchia, L., Condorelli, G., and De Franciscis, V., 2011. Recent Advance in Biosensors for microRNAs Detection in Cancer. *Cancers,* 3(2), 1877-1898.

Chalfie, M., Horvitz, H.R., and Sulston, J.E., 1981. Mutations that lead to reiterations in the cell lineages of C. elegans. *Cell,* 24(1), 59-69.

Chen, C., Ridzon, D.A., Broomer, A.J., Zhou, Z., Lee, D.H., Nguyen, J.T., Barbisin, M., Xu, N.L., Mahuvakar, V.R., Andersen, M.R., Lao, K.Q., Livak, K.J., and Guegler, K.J., 2005. Real-time quantification of microRNAs by stem-loop RT-PCR. *Nucleic Acids Research,* 33(20), e179.

Demidov, V.V., Potaman, V.N., Frank-Kamenetskii, M.D., Egholm, M., Buchard, O., Sonnichsen, S.H., and Nielsen, P.E., 1994. Stability of peptide nucleic acids in human serum and cellular extracts. *Biochemical Pharmacology,* 48(6), 1310-1313.

Esquela-Kerscher, A., and Slack, F.J., 2006. Oncomirs - microRNAs with a role in cancer. *Nature reviews. Cancer,* 6(4), 259-269.

Estrela, P., Paul, D., Li, P., Keighley, S.D., Migliorato, P., Laurenson, S., and Ferrigno, P.K., 2008. Label-free detection of protein interactions with peptide aptamers by open circuit potential measurement. *Electrochimica Acta*, 53(22), pp.6489-6496.

Formisano, N., Bhalla, N., Wong, L.C., Di Lorenzo, M., Pula, G., and Estrela, P., 2015. Multimodal electrochemical and nanoplasmonic biosensors using ferrocene-crowned nanoparticles for kinase drug discovery applications. *Electrochemistry Communications*, 57, 70-73.

Giesen, U., Kleider, W., Berding, C., Geiger, A., Ørum, H., and Nielsen, P.E., 1998. A formula for thermal stability (Tm) prediction of PNA/DNA duplexes. *Nucleic Acids Research*, 26(21), pp.5004-5006.

Griffiths-Jones, S., Grocock, R.J., van Dongen, S., Bateman, A., and Enright, A.J., 2006. miRBase: microRNA sequences, targets and gene nomenclature. *Nucleic Acids Research*, 34(Database issue), D140-144.

He, L., Thomson, J.M., Hemann, M.T., Hernando-Monge, E., Mu, D., Goodson, S., Powers, S., Cordon-Cardo, C., Lowe, S.W., Hannon, G.J., and Hammond, S.M., 2005. A microRNA polycistron as a potential human oncogene. *Nature*, 435(7043), 828-833.

Ichimi, T., Enokida, H., Okuno, Y., Kunimoto, R., Chiyomaru, T., Kawamoto, K., Kawahara, K., Toki, K., Kawakami, K., Nishiyama, K., Tsujimoto, G., Nakagawa, M., and Seki, N., 2009. Identification of novel microRNA targets based on microRNA signatures in bladder cancer. International journal of cancer. *Journal International du Cancer*, 125(2), 345-352.

Jolly, P., Wong, L., Miodek, A., Lindsay, M.A., and Estrela, P., 2015. A simple and highly sensitive electrochemical platform for detection of MicroRNAs. *SENSORS, 2015 IEEE*, pp. 1-4. IEEE.

Keighley, S.D., Estrela, P., Li, P., and Migliorato, P., 2008. Optimization of label-free DNA detection with electrochemical impedance spectroscopy using PNA probes. *Biosensors and Bioelectronics*, 24(4), 906-911.

Kilic, T., Topkaya, S.N., Ariksoysal, D.O., Ozsoz, M., Ballar, P., Erac, Y., and Gozen, O., 2012. Electrochemical based detection of microRNA, mir21 in breast cancer cells. *Biosensors and Bioelectronics,* 38(1), 195-201.

Kim, K., Lee, H.B., Lee, J.W., Park, H.K., and Shin, K.S., 2008. Self-assembly of poly (ethylenimine)-capped Au nanoparticles at a toluene− water interface for efficient surface-enhanced Raman scattering. *Langmuir,* 24(14), 7178-7183.

Kim, S.K., Cho, H., Jeong, J., Kwon, J.N., Jung, Y., and Chung, B.H., 2010. Label-free and naked eye detection of PNA/DNA hybridisation using enhancement of gold nanoparticles. *Chemical Communications*, 46(19), 3315-3317.

Lee, R.C., Feinbaum, R.L., and Ambros, V., 1993. The C. elegans heterochronic gene lin-4 encodes small RNAs with antisense complementarity to lin-14. *Cell*, 75(5), 843-854.

Li, B., Liu, F., Peng, Y., Zhou, Y., Fan, W., Yin, H., Ai, S., and Zhang, X., 2016. Two-stage cyclic enzymatic amplification method for ultrasensitive electrochemical assay of microRNA-21 in the blood serum of gastric cancer patients. *Biosensors and Bioelectronics*, 79, 307-312.

Liu, L., Xia, N., Liu, H., Kang, X., Liu, X., Xue, C., and He, X., 2014. Highly sensitive and label-free electrochemical detection of microRNAs based on triple signal amplification of multifunctional gold nanoparticles, enzymes and redox-cycling reaction. *Biosensors and Bioelectronics*, 53, 399-405.

Lu, J., Getz, G., Miska, E.A., Alvarez-Saavedra, E., Lamb, J., Peck, D., Sweet-Cordero, A., Ebert, B.L., Mak, R.H., Ferrando, A.A., Downing, J.R., Jacks, T., Horvitz, H.R., and Golub, T.R., 2005. MicroRNA expression profiles classify human cancers. *Nature*, 435(7043), 834-838.

Meng, X., Zhou, Y., Liang, Q., Qu, X., Yang, Q., Yin, H., and Ai, S., 2013. Electrochemical determination of microRNA-21 based on bio bar code and hemin/G-quadruplet DNAenzyme. *Analyst,* 138(12), 3409-3415.

Nam, E.J., Yoon, H., Kim, S.W., Kim, H., Kim, Y.T., Kim, J.H., Kim, J.W., and Kim, S., 2008. MicroRNA expression profiles in serous ovarian carcinoma. *Clinical Cancer Research : an official journal of the American Association for Cancer Research*, 14(9), 2690-2695.

Peng, Y., and Gao, Z., 2011. Amplified detection of microRNA based on ruthenium oxide nanoparticle-initiated deposition of an insulating film. *Analytical Chemistry*, 83(3), 820-827.

Peng, Y., Jiang, J., and Yu, R., 2014. A sensitive electrochemical biosensor for microRNA detection based on streptavidin–gold nanoparticles and enzymatic amplification. *Analytical Methods*, 6(9), 2889-2893.

Ramaswamy, S., Tamayo, P., Rifkin, R., Mukherjee, S., Yeang, C.H., Angelo, M., Ladd, C., Reich, M., Latulippe, E., Mesirov, J.P., Poggio, T., Gerald, W., Loda, M., Lander, E.S., and Golub, T.R., 2001. Multiclass cancer diagnosis using tumor gene expression signatures. *Proceedings of the National Academy of Sciences of the United States of America*, 98(26), 15149-15154.

Ray, A., and Norden, B., 2000. Peptide nucleic acid (PNA): its medical and biotechnical applications and promise for the future. *FASEB journal : official publication of the Federation of American Societies for Experimental Biology*, 14(9), 1041-1060.

Ren, Y., Deng, H., Shen, W., and Gao, Z., 2013. A highly sensitive and selective electrochemical biosensor for direct detection of microRNAs in serum. *Analytical Chemistry*, 85(9), 4784-4789.

Spizzo, R., Nicoloso, M.S., Lupini, L., Lu, Y., Fogarty, J., Rossi, S., Zagatti, B., Fabbri, M., Veronese, A., Liu, X., Davuluri, R., Croce, C.M., Mills, G., Negrini, M., and Calin, G.A., 2010. miR-145 participates with TP53 in a death-promoting regulatory loop and targets estrogen receptor-alpha in human breast cancer cells. *Cell death and Differentiation*, 17(2), 246-254.

Valoczi, A., Hornyik, C., Varga, N., Burgyan, J., Kauppinen, S., and Havelda, Z., 2004. Sensitive and specific detection of microRNAs by northern blot analysis using LNA-modified oligonucleotide probes. *Nucleic Acids Research,* 32(22), e175.

Wang, C., Tao, W., Ni, S., Chen, Q., Zhao, Z., Ma, L., Fu, Y., and Jiao, Z., 2015. Tumor-suppressive microRNA-145 induces growth arrest by targeting SENP1 in human prostate cancer cells. *Cancer Science,* 106(4), 375-382.

Wang, J., 2006. Electrochemical biosensors: towards point-of-care cancer diagnostics. *Biosensors & Bioelectronics,* 21(10), 1887-1892.

Wang, M., Fu, Z., Li, B., Zhou, Y., Yin, H., and Ai, S., 2014a. One-step, ultrasensitive, and electrochemical assay of microRNAs based on T7 exonuclease assisted cyclic enzymatic amplification. *Analytical Chemistry,* 86(12), 5606-5610.

Wang, M., Yin, H., Fu, Z., Guo, Y., Wang, X., Zhou, Y., and Ai, S., 2014b. A label-free electrochemical biosensor for microRNA detection based on apoferritin-encapsulated Cu nanoparticles. *Journal of Solid State Electrochemistry,* 18(10), 2829-2835.

Wong C. (2016). A study of multichannel open circuit potentiometry in biosensor applications (Doctoral dissertation, University of Bath). In preparation.

Xia, N., Zhang, L., Wang, G., Feng, Q., and Liu, L., 2013. Label-free and sensitive strategy for microRNAs detection based on the formation of boronate ester bonds and the dual-amplification of gold nanoparticles. *Biosensors and Bioelectronics*, 47, 461-466.

Zhang, J., Ting, B.P., Jana, N.R., Gao, Z., and Ying, J.Y., 2009. Ultrasensitive Electrochemical DNA Biosensors Based on the Detection of a Highly Characteristic Solid-State Process. *Small,* 5(12), 1414-1417.

Zhou, Y., Wang, M., Meng, X., Yin, H., and Ai, S., 2012. Amplified electrochemical microRNA biosensor using a hemin-G-quadruplex complex as the sensing element. *RSC Advances,* 2(18), 7140-7145.

Zhou, Y., Yin, H., Li, J., Li, B., Li, X., Ai, S., and Zhang, X., 2016. Electrochemical biosensor for microRNA detection based on poly (U) polymerase mediated isothermal signal amplification. *Biosensors and Bioelectronics*, 79, 79-85.

Zieglschmid, V., Hollmann, C., and Bocher, O., 2005. Detection of disseminated tumor cells in peripheral blood. *Critical Reviews in Clinical Laboratory Sciences*, 42(2), 155-196.

Chapter 7. Conclusions and Outlook

With the aim of improving diagnosis in the field of PCa detection, the work in this dissertation is a step towards the development of oligonucleotide-based biosensors for multiple PCa biomarker detections. DNA aptamers represent a challenging and fascinating venue and a possible replacement to antibodies for the development of biosensors. The use of natural and synthetic nucleotides is still developing and paving the way towards advanced biosensor development. It can be seen from the literature how researchers from different fields are coming together to realise high-throughput oligonucleotide-based biosensors for use with complex matrix samples such as clinical or environmental. The ease of manipulation of oligonucleotides, controlled surface chemistry approaches and "straightforward" charge distribution, makes them optimal bioreceptors for biosensing applications.

By combining electrochemical techniques and oligonucleotide-based probes, modern, label-free and robust biosensors can be developed. Such a biosensor using relatively inexpensive electrochemical equipment could denote future low-cost point-of-care (PoC) diagnostic tools. Moreover, the commercialisation of electrochemical biosensors has been fuelled right after the first glucose test in a PoC format. However, the process of commercialisation of oligonucleotide-based biosensors for the detection of PCa biomarkers is still at an early stage and requires further developments. With the aim of exploring the electrochemical techniques coupled with a fine tuning of surface chemistry, in this dissertation several oligonucleotide-based systems of PCa diagnostic interest have been developed in order to provide insightful factors that could be investigated for developing oligonucleotide-based biosensors. Since the strategies to adopt can differ substantially according to the probe and the target, four

types of systems were taken into consideration, exploring different biomarkers for PCa. These consisted of an impedimetric DNA aptamer-based sensing of PSA, an aptasensor for quantification and glycoprofiling of PSA, an AMACR aptasensor based on PPy-PEG surface chemistry and a PNA-based detection of miRNA. Surface chemistry comprises an important part in the development of promising biosensors. Easier fabrication would enable the development of the biosensors for mass-production and would give commercial feasibility. This dissertation has highlighted surface chemistry strategies broadly classified into two categories: SAM-based and polymer-based.

7.1 Summary

Despite the issues including PSA as a reliable PCa biomarker, this biomarker has been chosen for a proof of concept in the project. PSA has been widely used for PCa screening and, to date remains an important biomarker for PCa detection with its various isoforms. However, there is only a very limited number of published reports on PSA detection using DNA aptamers and an even lower number using electrochemical detection techniques with aptamers. In Chapter 3, PSA aptasensor experiments showed that features such as the DNA aptamer coverage density as well as the protein charge effect, are important factors to be optimised. The fine-tuning between these factors has been investigated in the perspective of optimising an aptamer-based impedimetric sensing of PSA. Incorporation of spacer molecules like MCH or sulfo-betaine enables optimisation of the sensor surface for better detection and prevents non-specific binding. The maximum percentage change of R_{ct} upon binding with DNA aptamers was obtained with samples prepared by co-immobilisation of thiolated DNA aptamers and MCH with 1% DNA aptamer mole fraction. Moreover, a negative R_{ct} signal change upon binding of PSA to DNA aptamer has also been reported. This shift is probably indicating that the prevalent effect on R_{ct} is due to the screening of the charges on DNA aptamers by bound PSA. The work also reports for the first time the use of sulfo-betaine with DNA aptamers. Although the optimisation of the surface density was a challenge, the fabricated aptasensor with

sulfo-betaine surface chemistry could potentially be used to detect PSA levels down to 1 ng/mL, which falls in the clinically relevant range (1-10 ng/ml). Whereas, with the MCH based PSA aptasensor the lowest concentration of PSA that could be detected was 60 ng/mL. Both the PSA aptasensor fabrication processes, i.e. with MCH and sulfo-betaine, were compared for their capability to prevent fouling. It was clearly seen that PSA aptasensors with MCH surface chemistry gave a very high non-specific binding with HSA, whereas PSA aptasensor with sulfo-betaine showed negligible non-specific signals. Furthermore, a discussion on the effects of buffer was presented. By changing buffer conditions during the EIS measurements, instability of SAM could take place which can therein result in changes in R_{ct} regardless of having the analyte in the solution. The study showed how important it is to perform stability tests of the fabricated aptasensors in order to obtain reliable data. To the best of the author's knowledge, this was the first report on the buffer effects, which should be taken into consideration on the development of impedimetric oligonucleotide-based biosensors. To address the challenge of direct immobilisation of sulfo-betaine with thiolated DNA aptamers, different surface chemistry strategies could be employed in future work. For example, the combination of ternary SAM with screen-printed gold electrodes (Miodek *et al.* 2015, Campuzano *et al.* 2011) would potentially aid to form a compact SAM with sulfo-betaine and thiolated DNA aptamers since sulfo-betaine has two sulphur groups which can therein form bridges on a rough surface like screen printed electrodes. Then MCH can be used to fill all the free spaces on the gold electrodes.

The second system in this dissertation demonstrates the use of DNA aptamers for parallel sensing of biomarkers in a sandwich-type assays. The resulting assay could not only quantify PSA but also, potentially profile glycoprofiling of PSA in a microfluidic channel. An alternative detection (chemiluminescence) was used with an optical readout system. Replacing the antibodies in a classical ELISA configuration has enabled the development of sophisticated assays which are more robust, reproducible and economical. The integration of quantification of PSA with multi-glycan profiling of fPSA in a microfluidic channel could serve as a potential platform for PoC devices in PCa diagnosis. A sensitive quantification of PSA of 0.5 ng/mL was achieved. Multi-glycan profiling where the specific lectin (SNA) could differentiate a

response from the control lectin (MAA II) at fPSA concentration down to 3 ng/mL was also demonstrated. Although the literature reports many methods for direct glycoprofiling, based on recognition elements such as lectins, anti-carbohydrate antibodies, or other glycan binding proteins, these bio recognition elements are specific to glycans and not a particular protein, leading to cross-reactivity of the recognition element with other components present in the sample, thus leading to false positives. Therefore, the system presented in Chapter 4, where antibodies are replaced with aptamers, could revolutionise the approach to glycoprofiling by decreasing false positives. The assay developed needs further investigation for its application with real clinical samples. Continuing from this, an efficient surface chemistry could be studied (for example PEG-based) in the place of using ethanolamine for enhanced anti-fouling properties. Finally, with advanced microfluidic techniques, the detection area could be further minimised to reduce the reagents used and potentially develop an array-like system.

The sandwich assay developed could be potentially translated to various other sensing platforms, including electrochemical platforms. For example, researchers at the Slovak Academy of Sciences, Slovakia have reported the development of various types of lectin-based biosensors with lectins as the bio-recognition elements (Bertok *et al.* 2013, Kluková *et al.* 2014). More recently, the group reported the development of an antibody-based ELISA-type impedimetric biosensor for the glycoprofiling of PSA with lectin as the detector molecule (Pihikova *et al.* 2016a, Pihikova *et al.* 2016b). However, using such approach with an impedimetric biosensor, there can be a compromise with the signals obtained with the lectins. The reason being that the impedimetric sensing is limited by Debye length; having an antibody (~160 kDa) as the primary recognition layer immobilised over a binary SAM of MUA and MCH takes the biolayer to the upper limit of the Debye length. Furthermore, the immobilised antibodies will also be in a random orientation, resulting in loss of capturing sites for PSA. Consequently, the major part of binding of lectins (~130 kDa) to captured PSA (~30 kDa) will occur way beyond the Debye length and hence cost the signal change due to the screening of charges. To address such an issue, the group is currently working on replacing the primary antibody with DNA aptamers in order to translate

the system presented in Chapter 4 onto electrochemical and SPR platforms to increase the sensitivity of the sensor and reduce the non-specific binding of lectins.

The third system demonstrates the use of polymeric films to develop aptasensors for AMACR detection. It presents a study on the careful selection of DNA aptamers for designing a biosensor. Indeed, the efficiency of the aptamer to capture its target depends largely on the K_d value which was also seen with two different sequences of DNA aptamers for AMACR. DNA aptamer (AMC-51) reported by Yang *et al.* (Yang *et al.* 2014) showed significantly higher binding capabilities as compared to AM-310_2 from Base Pair Biotechnologies. The Chapter also reports a simple strategy to modify PPy films with PEG molecules on gold surfaces through covalent linkage. Such a strategy omits prior modification of pyrrole monomers. An alternative sensing mechanism is being proposed where poly-histidine modified aptamers were immobilised to the surface via a ANTA/Cu^{2+} redox complex covalently attached to the PPy-PEG adduct. Protein/aptamer interactions were monitored through variation of the copper redox signal, using the SWV technique. The Chapter demonstrates that the PPy-PEG-ANTA/Cu^{2+} hybrid material is characterised by enhanced anti-fouling properties and sensitivity. The aptasensor demonstrated an excellent antifouling efficiency by showing a signal change of less than 4%. The PEG surface was further challenged with the β-alanine surface. The β-alanine-based aptasensor showed a significant relative current variation of up to 25%, demonstrating a poor anti-fouling efficiency for this aptasensor without PEG. The aptasensor was able to detect AMACR down to 5 fM both in the buffer and spiked human plasma with a LOD of 0.15 fM and 1.4 fM, respectively. Furthermore, the efficiency of the sensor could be further improved by replacing copper ions with ferrocene as demonstrated in literature (Miodek *et al.* 2015). Also, the system can be further investigated with other metal ions like nickel, lead, zinc, etc in order to perform multiplexing (Johnson *et al.* 2005, Davis *et al.* 1999).

The trend towards the development of aptasensors for PSA and AMACR requires further investigation into their use as an alternative to antibodies. Overall, the development of aptamer-based biosensors for biomarker detection is expected to

attract increasing interest because of its ease of synthesis and the possibilities of multiple modifications.

Developments in biochemistry and molecular biology have led to a deeper understanding of the role of oligonucleotides and showed that the functions they play are far greater than originally expected. This leads to new worlds of biosensing applications, where oligonucleotide-based biosensing approaches can have an unparalleled impact on clinical diagnosis, prognosis, and monitoring. The increasing demand for enhanced efficiency and to overcome some of the drawbacks of using naturally occurring oligonucleotides, has enabled biochemists to come up with synthetic analogues such as PNA, which have further increased the prospects of novel biosensing approaches.

In the fourth system, a sensitive electrochemical platform was developed for the detection of miRNAs and/or DNAs using PNA probes. miRNAs have shown significance in human diseases like cancer and can act as blueprints of the disease. Especially in cancer, miRNA expression levels can potentially give information about the stage of a disease. The Chapter demonstrated the development of a simple detection technique for miRNA using PNA as probes. It exploits the inherent charges of nucleic acids for the development of a powerful amplification strategy with AuNPs. The strategy developed could be easily translated on multiple detection platforms such as non-Faradaic EIS measurements, potentiometric measurements, and amperometric detection. For the detection, EIS was used without redox markers to monitor the changes in the dielectric properties of the bilayer through capacitance changes. Upon molecular interactions near the electrode surface a redistribution of the solvent molecules and of ions is initiated, which causes the changes in the electrochemical double layer. However, such type of systems based on non-Faradaic approach have not been extensively reported in the literature, probably because they are believed to be more complicated in analysing the data and extracting the signals of interest. Nevertheless, such a strategy further simplifies the assay because redox markers are not needed. Also, a dual-mode detection was demonstrated by exploiting the availability of AuNPs on the surface with PNA/miRNA duplex, thiolated ferrocene

was used to provide an amperometric detection using SWV. A dual mode can be used as a validation detection technique to compare the sensor's performance. With the PNA-based system, a LOD of 0.38 fM was achieved. Another simple detection technique based on the measurement of variations of the OCP by employing an ultra-low input bias current instrumentation amplifier circuit. OCP measurement can be recorded in real-time and continuously. In this approach, two working electrodes were measured at the same time through two different channels simultaneously for the potential changes, by using a common reference electrode. Such an instrument allows the provision of future development of an array of sensors. The importance of PEG for the enhanced anti-fouling properties was demonstrated by comparing a PEG-like linker (AEEA) with a non-PEG-like linker (C-6 thiol). By employing AEEA, the non-specific interactions were reduced from 30 % to 2.5 %. The simple dual-mode strategy holds great promise to reduce false positives and can be easily expanded into arrays for the parallel screening of panels of DNAs or miRNAs. Although we used the entire spectrum in EIS measurement, it is possible to measure EIS at a single frequency to accelerate the acquisition of signals.

7.2 Future work

The work presented in this dissertation has fostered several collaborations with other research groups across Europe for extended application of DNA aptamers on various other platforms. Some of the work done, and not presented in this dissertation, include:

7.2.1 Aptamers and molecularly imprinted polymers

As described in Chapter 1, DNA aptamers have some limitations such as *e.g.* nuclease degradation. To prevent this, a novel strategy was developed in collaboration with Cardiff University on the design and evaluation of a new synthetic receptor sensor based on the combination of DNA aptamers and molecular imprinting to overcome some of the challenges faced by both conventional molecular imprinting and DNA aptamers (Figure 7.1, Jolly *et al.* 2016).

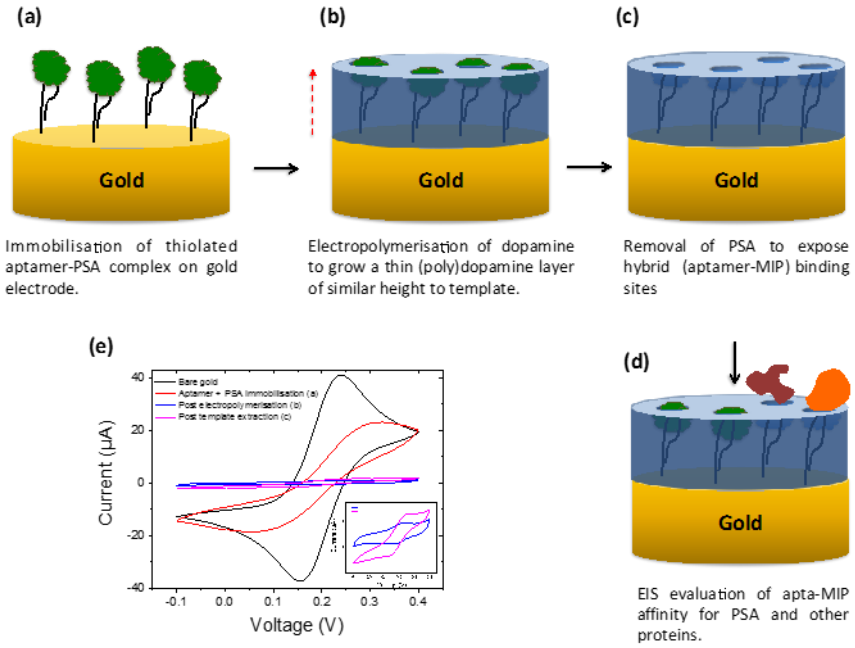

Figure 7.1 Schematic representation of the sensor fabrication. The aptamer-PSA complex is first immobilised on the gold surface utilising thiol chemistry (a) with subsequent electropolymerisation of dopamine around the complex to produce a molecularly imprinted surface (b). Washing of the electrode allows for removal of PSA whilst retaining aptamer-lined, imprinted polymeric cavities, the so-called "apta-MIP" (c). Reintroduction of the template molecule results in rebinding within the imprinted sites (d). Cyclic voltammetry in the presence of redox marker for monitoring of the fabrication process (e) (Jolly et al. 2016).

A thiolated DNA aptamer with established affinity for PSA was complexed with PSA prior to being immobilised on the surface of a gold electrode. Controlled electropolymerisation of dopamine around the complex served to both entrap the complex, holding the aptamer in, or near to, it's binding conformation, and to localise the PSA binding sites at the sensor surface. The PSA was then removed from the template. It was proposed that the molecularly imprinted polymer (MIP) cavity would act synergistically with the embedded aptamer to form a hybrid receptor (apta–MIP), displaying highly selective aptamer pockets to capture the cancer biomarker. Electrochemical impedance spectroscopy was used to evaluate subsequent rebinding of PSA to the apta–MIP surface. The apta–MIP sensor showed high sensitivity with a linear response from 100 pg/ml to 100 ng/ml of PSA and a limit of detection of 1 pg/ml, therefore showing recognition properties superior to that of aptamer alone. The study was further translated to an extended gate MOSFET (metal-oxide-

semiconductor field effect transistor) for the detection of PSA in human serum (Tamboli *et al.* 2016).

7.2.2 Aptamer and memristive devices

DNA aptamers for PSA detection are also being used in the development of a biosensor based on memristive devices in collaboration with the École Polytechnique Fédérale de Lausanne (EPFL), Switzerland. Such an approach is based on the memory effects that are widely appearing in nature (Lehn *et al.* 2007). Pronounced hysteresis in electrical characteristics is a unique signature of memory effects in electronic-based devices (Wu and McCreery 2009). These systems are known as memristive systems or passive systems that fall under the domain of non-linear circuit theory and possess the capability of memory as they can maintain an electronic state. In these structures, the memory effect depends upon charge carriers' rearrangement at the nanoscale level due to external perturbations (Pershin *et al.* 2011). The research group at EPFL earlier demonstrated that two-terminal Schottky-barrier silicon nanowire devices exhibit memristive behaviour of their electrical response when functionalized with antibody films and was used for bio-detection purposes (Carrara *et al.* 2012).

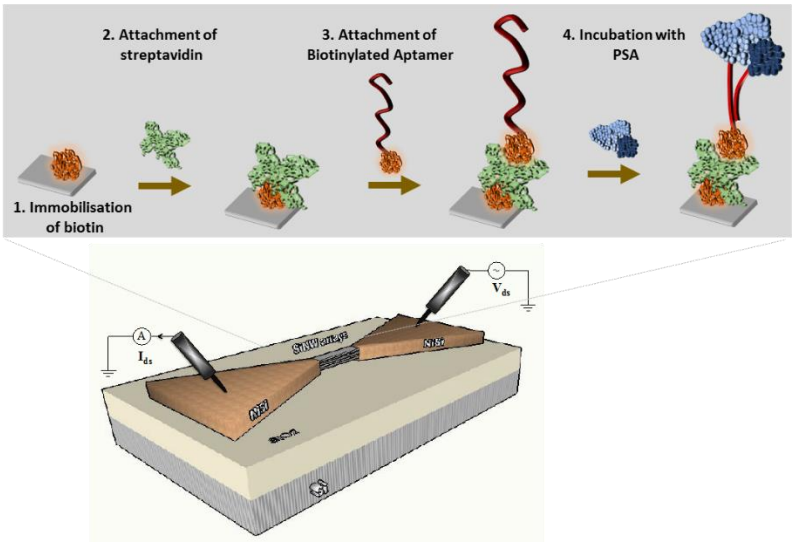

Figure 7.2 Schematic illustrating the affinity based (Physical adsorption) fabrication process of the memristive aptasensor based on silicon nano wire (Tzouvadaki et al. 2016).

In this collaboration, we further investigated the hysteretic properties of memristive silicon nanowires functionalized with DNA aptamers as an alternative application of such devices (Figure 7.2). With this novel approach, PSA is detected with a limit of detection down to 23 aM (Tzouvadaki *et al.* 2016).

7.2.3 One step simple and fast deposition of aptamers

In collaboration with the University of São Paulo, Brazil, the use of the electrochemical grafting protocol to directly immobilise DNA aptamers specific to PSA and Her2 on the polypyrrole film is being investigated (Figure 7.3). Such an approach, if successful, will provide an easy one-step highly controlled immobilisation strategy. Using the EIS technique, a change of 140% in R_{ct} has been observed with 10 µg/mL PSA using PSA specific DNA aptamers, while no signal change was observed with control experiments where a random DNA was immobilised with the same one-step strategy and incubated with 10 µg/mL PSA. The research group would like to see how the sensor behaves in a complex medium and what kind of sensitivity could be attained using the approach.

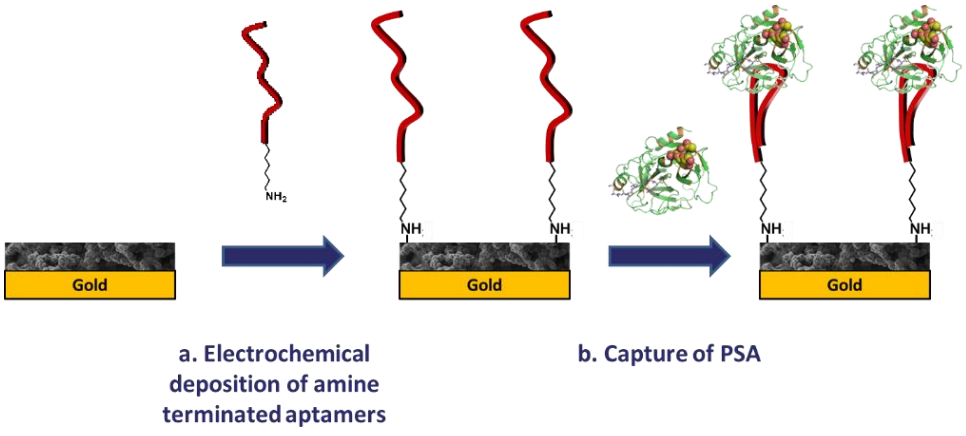

Figure 7.3 Schematic for direct immobilisation of amine terminated DNA aptamers on un-modified poly(pyrrole) films.

7.2.4 Aptamers and nano devices

In collaboration with the University of Applied Sciences Kaiserslautern, Germany, two other biosensor devices have been investigated with the use of DNA aptamers for PSA detection. The first system is based on potentiometric field-effect nanodevices. Amine terminated DNA aptamers were immobilised on silicon nanowire field effect transistors (SiNW FET) using silane chemistry and changes in the threshold voltage of the transistor was monitored upon PSA binding. A detection limit of 1 ng/mL PSA was obtained (Rani *et al.* 2016). In the second system, reduced graphene-oxide thin film transducers have been used to electrochemically deposit AuNPs from gold chloride solutions. Such a modified surface was used to immobilise thiolated DNA aptamers specific to PSA. The fabricated aptasensor was used to detect PSA using the EIS technique where a detection down to 1 pg/mL was achieved (Lu *et al.* 2016). Both these systems are being developed in an array format, so that easy multiplexing can be performed by incorporating multiple receptors for different PCa biomarkers.

7.2.5 Aptamers and real-time drug detection

With the successful use of DNA aptamers for protein detection, DNA aptamers were further investigated to detect small molecules such as cancer drugs. Therapeutic drug monitoring helps patients to maintain the therapeutic concentration of drugs in the circulatory system. A novel biosensor for the monitoring of the small molecule tenofovir (287.2 g/mol, which is an antiretroviral drug) using specific DNA aptamer was developed in collaboration with the École Polytechnique Fédérale de Lausanne, Switzerland. The biosensor (aptaFET) comprises the high selectivity of the aptamer as the recognition element and high sensitivity of field-effect transistors (FET) as a signal transducer (Figure 7.4).

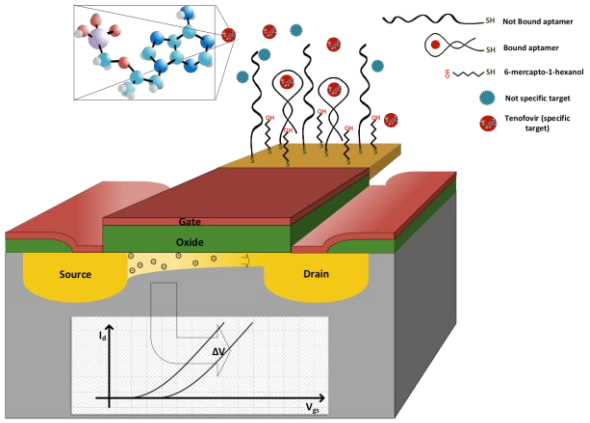

Figure 7.4 Binary SAM of TFV-aptamer and MCH as sensing surface of biosensor. In the inset: chemical structure of TFV with red colour for Oxygen, purple for phosphorus, light blue for carbon, white for hydrogen and dark blue for nitrogen. Schematic of AptaFET. Binding reaction is transformed to electric signal through FET and observed as Id-Vgs shift. TFV is indicated by red circle (Aliakbarinodehi et al. 2016).

The bio-interface of this sensor is a binary self-assembled layer of the specific aptamer for the drug and MCH. A surface chemistry similar to what has been reported in Chapter 3 (section 3.2.1) for the PSA aptamer was used for the DNA aptamer specific to the drug tenofovir. The fabricated aptaFET demonstrated a linear range between 1 nM and 100 nM of tenofovir, and saturation of the surface after 100 nM. The calculated dissociation constant, K_d, is equal to 5.8 ± 0.5 nM, and the calculated LOD is equal to 4.6 nM. Two nonspecific drugs (abiraterone and enzalutamide) and one nonspecific aptamer (aptamer specific to prostate specific antigen) were used as stringent control candidates. Negligible shifts were observed with the controls, when compared to the specific response at similar concentrations (500 nM). The aptaFET was further used in the real-time monitoring of the drug as well as detection in pure human serum (Aliakbarinodehi *et al*. 2016).

In conclusion, the development of oligonucleotide-based biosensor devices is an interdisciplinary field and rely on very distinct aspects such as characterisation of bio-recognition probes with its respective analytes, immobilisation onto electrode surfaces, development of anti-fouling surface chemistries, sensor design, and fabrication, microfluidics, etc. Several oligonucleotide-based systems were analysed and practical applications for different biomarkers for PCa detection have been

demonstrated. By a strategic coupling of different optimisation steps reported in this dissertation, effective and low-cost oligonucleotide-based sensors could be realised and integrated into multiplexed systems. These studies not only demonstrate the enormous potential but how they can be used for a wide range of other biomarkers for various diseases that exploit target/probe features similar to those of the systems here reported. Furthermore, the development of a multiplexed platform for parallel sensing of different biomarkers of PCa would help assist clinicians with deeper information on the pathological and physiological state of the patient (in particular the disease). Such a device could be represented as a point-of-use device that can provide first assessment of the patient's state which would accelerate the diagnosis and or prognosis speed. Not only limiting to diagnosis, the device can be used for surveillance purposes in order to monitor patients at risk or those being treated (either post-surgery or during medication).

References

Aliakbarinodehi, N., Jolly, P., Bhalla, N., Miodek, A., Micheli, G.D., Estrela, P., and Carrara, S., 2016. Label free AptaFET biosensor for drug monitoring in human serum. Submitted to *Scientific Reports*.

Bertok, T., Sediva, A., Katrlik, J., Gemeiner, P., Mikula, M., Nosko, M. and Tkac, J., 2013. Label-free detection of glycoproteins by the lectin biosensor down to attomolar level using gold nanoparticles. *Talanta*, *108*, 11-18

Campuzano, S., Kuralay, F., Lobo-Castañón, M.J., Bartošík, M., Vyavahare, K., Paleček, E., Haake, D.A., and Wang, J., 2011. Ternary monolayers as DNA recognition interfaces for direct and sensitive electrochemical detection in untreated clinical samples. *Biosensors and Bioelectronics*, *26*(8), 3577-3583

Carrara, S., Sacchetto, D., Doucey, M.A., Baj-Rossi, C., De Micheli, G., and Leblebici, Y., 2012. Memristive-biosensors: A new detection method by using nanofabricated memristors. *Sensors and Actuators B: Chemical*, *171*, 449-457.

Davis, J., Glidle, A., Cass, A.E., Zhang, J., and Cooper, J.M., 1999. Spectroscopic evaluation of protein affinity binding at polymeric biosensor films. *Journal of the American Chemical Society*, *121*(17), 4302-4303.

Johnson, D.L., and Martin L.L., 2005. Controlling protein orientation at interfaces using histidine tags: an alternative to Ni/NTA. *Journal of the American Chemical Society*, *127*(7), 2018-2019.

Jolly, P., Tamboli, V., Harniman, R.L., Estrela, P., Allender, C.J., and Bowen, J.L., 2016. Aptamer–MIP hybrid receptor for highly sensitive electrochemical detection of prostate specific antigen. *Biosensors and Bioelectronics*, *75*, 188-195.

Kluková, L., Bertok, T., Kasák, P., and Tkac, J., 2014. Nanoscale-controlled architecture for the development of ultrasensitive lectin biosensors applicable in glycomics. *Analytical Methods*, *6*(14), 4922-4931.

Lehn, J.M., 2007. From supramolecular chemistry towards constitutional dynamic chemistry and adaptive chemistry. *Chemical Society Reviews*, *36*(2), 151-160.

Lu, X., Miodek, A., Jolly, P., Pachauri, V., Estrela, P., and Ingebrandt, S., 2016. Reduced graphene-oxide thin-film transducers as in-line impedimetric biosensors. In preparation

Miodek, A., Mejri, N., Gomgnimbou, M., Sola, C., and Korri-Youssoufi, H., 2015. E-DNA Sensor of Mycobacterium tuberculosis Based on Electrochemical Assembly of Nanomaterials (MWCNTs/PPy/PAMAM). *Analytical Chemistry*, *87*(18), 9257-9264.

Miodek, A., Regan, E.M., Bhalla, N., Hopkins, N.A., Goodchild, S.A., and Estrela, P., 2015. Optimisation and Characterisation of Anti-Fouling Ternary SAM Layers for Impedance-Based Aptasensors. *Sensors*, *15*(10), 25015-25032.

Pershin, Y.V., and Di Ventra, M., 2011. Memory effects in complex materials and nanoscale systems. *Advances in Physics*, *60*(2), 145-227.

Pihikova, D., Pakanova, Z., Nemcovic, M., Barath, P., Belicky, S., Bertok, T., Kasak, P., Mucha, J., and Tkac, J., 2016a. Sweet characterisation of prostate specific antigen using electrochemical lectin-based immunosensor assay and MALDI TOF/TOF analysis: Focus on sialic acid. *Proteomics*. In press.

Pihíková, D., Belicky, Š., Kasák, P., Bertok, T., and Tkac, J., 2016b. Sensitive detection and glycoprofiling of a prostate specific antigen using impedimetric assays. *Analyst*, 141, 1044-1051.

Rani, D., Jolly, P., Pachauri, V., Estrela, P., and Ingebrandt, S., 2016. A new SiNW FET array based aptasensor for electronic and optical detection for PSA. In preparation.

Tamboli, V., Bhalla, N., Jolly, P., Allender, C.J., Bowen, J.L., and Estrela, P., 2016. Apta-MIP hybrid receptors on MOSFET devices for cancer biomarker detection in human serum. Submitted to *Analytical Chemistry*.

Tzouvadaki, I., Jolly, P., Lu, X., Ingebrandt, S., Estrela, P., Micheli, G.D., and Carrara, S., 2016. Label-free ultrasensitive memristive aptasensor. *Nano Letters*, 16 (7), 4472–4476.

Wu, J., and McCreery, R.L., 2009. Solid-state electrochemistry in molecule/TiO_2 molecular heterojunctions as the basis of the TiO_2 "Memristor". *Journal of the Electrochemical Society*, *156*(1), P29-P37.

Yang, D.K., Chen, L.C., Lee, M.Y., Hsu, C.H., and Chen, C.S., 2014. Selection of aptamers for fluorescent detection of alpha-methylacyl-CoA racemase by single-bead SELEX. *Biosensors and Bioelectronics*, *62*, 106-112.

Appendix

I-1. Attachment of PEG to the PPy surface.

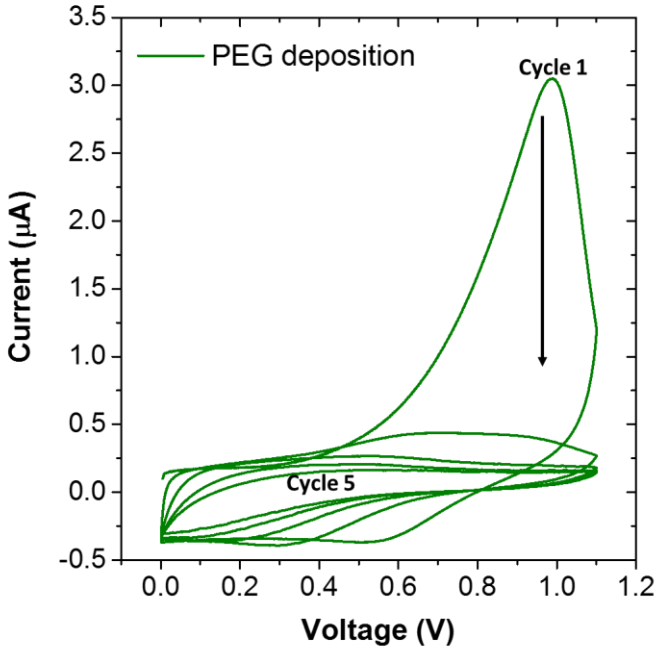

Figure I-1: Electro-oxidation of PEG onto PPy layer performed by cycling the potential between 0.0 and 1.1 V, during 5 cycles, in H_20 containing 0.5 M $LiClO_4$.

The surface of PPy film was modified with PEG. The modification was performed by scanning the potential between 0 and 1.1 V during 5 cycles until saturation of the surface (Figure S-1). During the oxidation of PEG radicals on the amine groups, $–NH^{\bullet+}$ were formed which then interacted with aromatic groups of PPy interrupting its double bonds and resulting in covalent attachment. Figure I-1 shows the presence of a peak at 0.99 V with the current 3.05 µA corresponding to amine groups oxidation. After five cycles of scanning the potential, the current corresponding to this peak decreased to 0.15 µA, which can suggest good attachment of PEG to the surface.

I-2 Optimisation of PEG deposition

In order to obtain an intense oxidation peak of ANTA/Cu^{2+} redox complex and efficient AMACR detection, it was essential to perform various optimisation steps, to optimize the thickness of polypyrrole (PPy) layer, the amount of attached PEG molecules, and the ANTA/Cu^{2+} complex.

In this work, PPy was electro-polymerised on the gold surface using cyclic voltammetry as explained in Chapter 4. Thickness of PPy layer strictly depends from conditions of polymerisation such as range of potential, number of cycles or concentration of pyrrole monomer. The range of potential and concentration of pyrrole monomer were chosen based on literature, while number of cycles should be studied. Initially, three cycles of pyrrole electro-deposition was chosen to optimise the electro-oxidation of PEG. However, the optimal parameters of PEG deposition should also be chosen based on the efficiency of further steps such as ANTA and cooper attachment. Covalent grafting of ANTA on PPy-PEG *via* EDC/NHS chemistry and copper immobilisation were fixed to 30 min for both.

Electrochemical impedance spectroscopy (EIS) was used to evaluate the different optimisation steps. Since PEG is an insulating polymer, it was expected an increase in the charge transfer resistance (R_{ct}) values upon grafting of PEG on a PPy film. In these experiments 1 mM PEG dissolved in water containing 0.5 M $LiClO_4$ was electro-generated on polymer by scanning the potential in different range from 0.0 to 1.0 V, 0.0 to 1.1 V and 0.0 to 1.2 V vs. Ag/AgCl for 1 to 10 cycles. Figure S2a shows the R_{ct} values obtained after PEG deposition in different potential range and for different number of cycles. A significant increase in the R_{ct} was observed by increasing both the number of cycles and the potential range of deposition, signifying higher amount of attached molecules.

The next step of optimisation of PEG deposition was to attach ANTA to the carboxylate groups present on the free end of PEG chain and Figure I2a shows the obtained R_{ct}. From Figure I2a, it was seen that there was not a significant change in the R_{ct} when PEG was attached to the surface for 1 and 2 scanning potential cycles in almost all the potential range chosen.

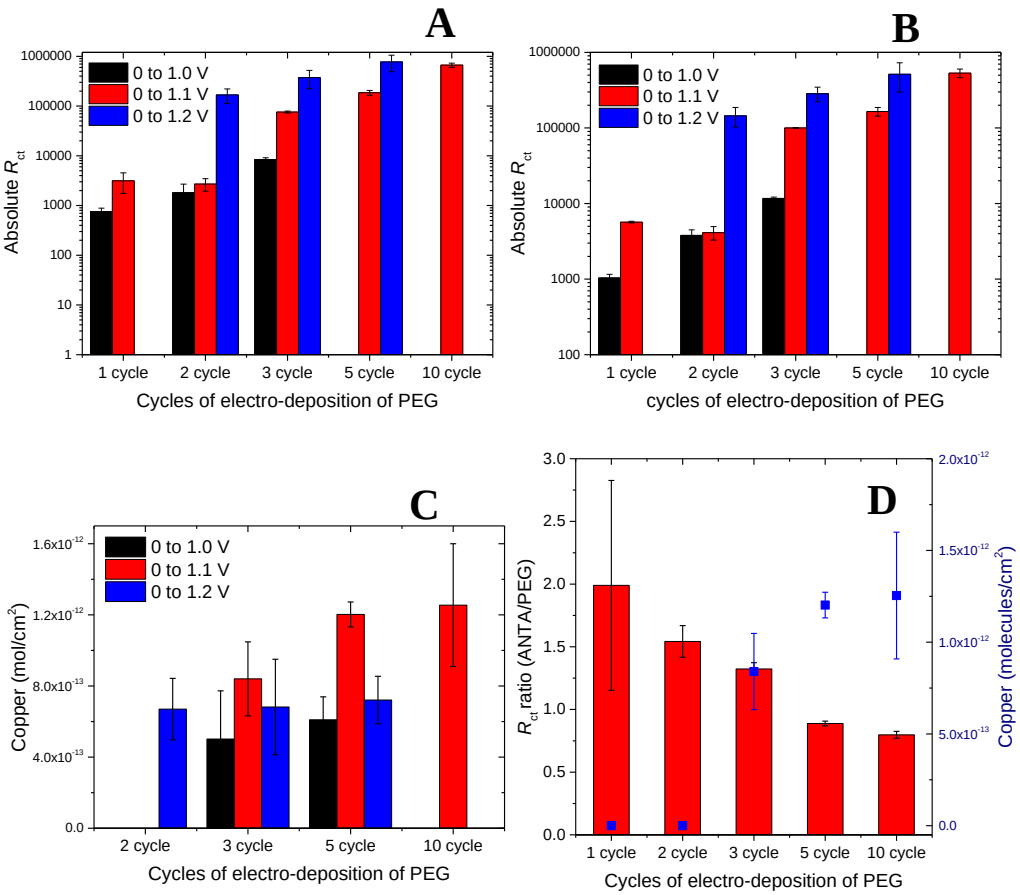

Figure I-2: Charge transfer resistance (R_{ct}) after deposition of PEG using different potentials and cycles (a). R_{ct} obtained after attachment of ANTA to PEG (b). Number of copper molecules immobilised on ANTA at different PEG deposition parameters(c). Correlation of amount of ANTA deposited to number of copper molecules immobilised at PEG deposition potential of 0 to 1.1 V (d).

From Figure I2b, it was seen that there was not a significant change in the R_{ct} when PEG was attached to the surface for 1 and 2 scanning potential cycles in almost all the potential range chosen. For 3, 5 and 10 cycles significant differences in R_{ct} are observed confirming successful attachment of ANTA to the PEG. However, AMACR detection was performed through amperometric signal of ANTA/Cu^{2+} redox complex and all optimum parameters should be determined by studying the electrochemical response of copper ions being immobilised. This was measured by amperometric methods. Electrochemical signal of copper was presented in form of amount of immobilised molecules. The charge exchanged during redox process allows calculation of the surface coverage of immobilised copper ions, following the equation:

$$\Gamma = Q/nFA \qquad (1)$$

Where, Q is the charge under the cathodic or anodic waves, n is number of electrons involved in the redox process, F is the Faraday constant, and A is the area of the electrode(see Figure I2c). Clearly, potential range from 0.0 V to 1.1 V of PEG deposition showed the best result, which has also been reported in literature where electro-grafting of dendrimers PAMAM was performed over a PPy layer (Miodek *et al.* 2015). Saturation of amount of copper was observed after 5 cycles (Figure I-2d) and hence the protocol for PEG deposition was optimised at 5 cycles with a scanning potential in range of 0.0 to 1.1 V *vs.* Ag/AgCl.

I-3 Optimisation of thickness of PPy layer and time for copper immobilisation

After successful optimisation of the deposition of PEG, the effect of thickness of PPy on amount of immobilised ANTA/Cu^{2+} complex was investigated. PPy was grown on the gold surface using cyclic voltammetry (CV) through different number of cycles. After PEG deposition and association of ANTA/Cu^{2+}, the corresponding copper redox signals were recorded and converted to amount of immobilised molecules as described in previous section (see Figure I-3a). It was observed that two cycles of electro-polymerisation gave the best response. The next step was to optimize the time for copper immobilisation, since high quantity of redox molecules might reduce the variation in the signal upon target binding. The time for copper binding was varied between 5 and 30 minutes. After immobilisation of His tagged DNA aptamers for 30 min, the signal change was measured upon binding of 1 nM AMACR to the aptamer.

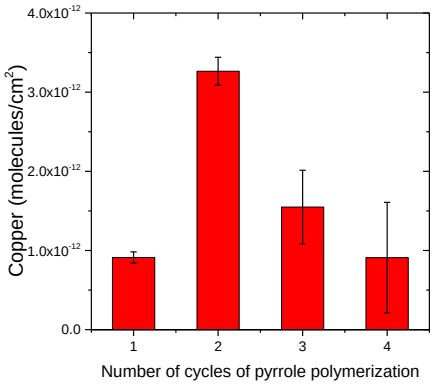

Figure I-3a: Number of copper molecules immobilised on the electrode modified with PPy electro-polymerised by different number of cycles.

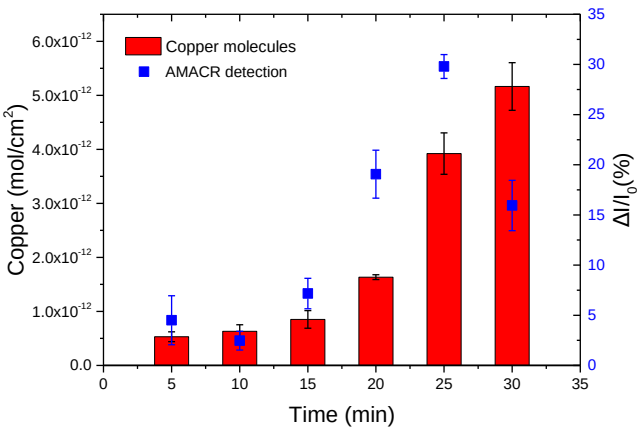

Figure I-3b: Effect of time of copper immobilisation on electrochemical signal changes upon binding of 1 nM AMACR in 10 mM PBS (pH 7.4) with DNA aptamer.

Figure I-3b shows the amount of copper immobilised (red bars) whilst AMACR binding is shown by blue points (by variation of ANTA/Cu^{2+} redox signal using square wave voltammetry (SWV) in 10 mM PBS pH 7.4). Square wave voltammetry was performed in 10 mM PBS (pH 7.4) in the potential range from -0.3 V to 0.4 V with conditioning time of 120 s, modulation amplitude of 20 mV and frequency of 50 Hz. Optimised conditions were at 25 minute copper immobilisation, which maximized the redox signal variation after incubation of electrode with AMACR.

I-4 Characterisation of ANTA/Cu^{2+}electrochemical signal

Immobilization of copper on PPy-PEG-ANTA surface was studied using CV. Cyclic Voltammetry was performed in 10 mM PBS (pH 7.4) in the range from -0.2 V to 0.35 V without redox couple Figure I8a shows apparition of Cu^{2+}/Cu^{+} oxidation peak after incubation of modified electrode in copper acetate solution, confirming efficiency of process (Figure I4a).

The non-specific attachment of copper on electrode surface was also studied. For this purpose electrodes on different steps of fabrication were dipped in solution of copper acetate (CuAc) and analysed using SWV (Figure I4b). When the PPy modified electrode was dipped in CuAc, the recorded plot denotes the absence of oxidation peaks corresponding to copper (black curve). After modification of PPy with PEG,

voltammogram shows a small peak of at 0.3V which could be due to a non-specific interaction of copper with the carboxylate (carboxylic acid) groups of PEG.

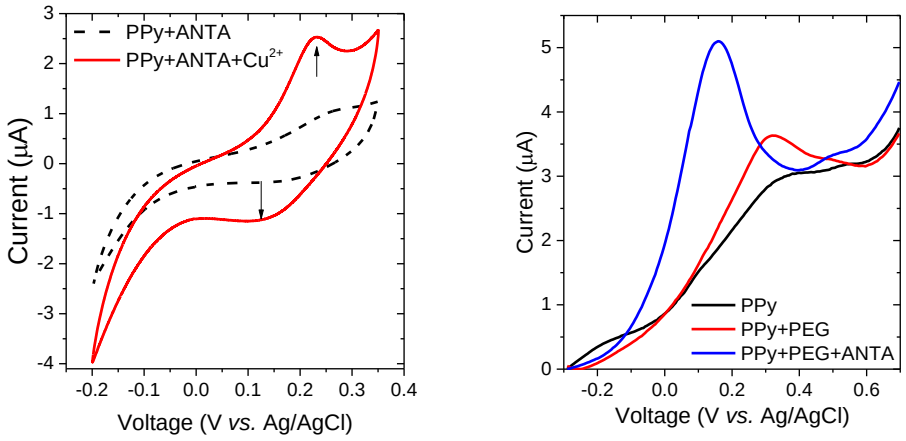

Figure I-4: Cyclic Voltammetry in 10 mM PBS buffer pH 7.4 before and after immobilization of copper on PPy-PEG-ANTA layer (a). Square Wave Voltammetry recorded after dipping electrodes modified on different steps showing non-specific and specific attachment of copper at different layer formation (b).

However, a significant copper peak at 0.15 V was observed when the electrode was further modified with ANTA depicting the specific coordination of copper molecules with ANTA molecules.

I-5 SPR detector scan data

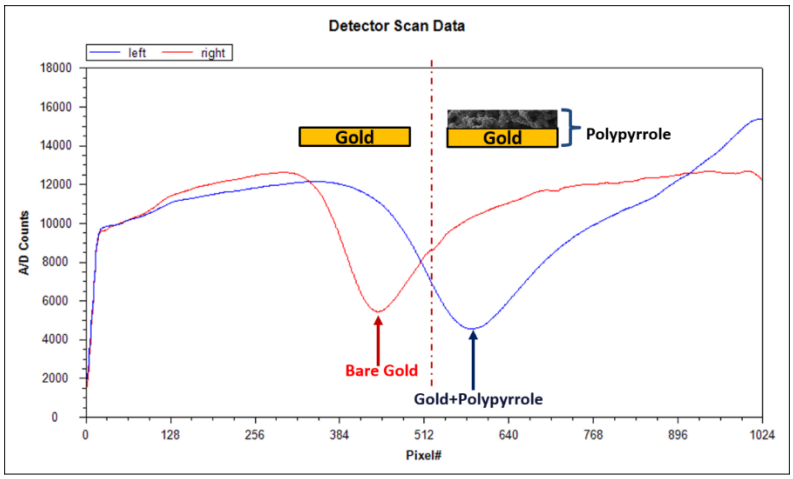

Figure I-5: Detector scan data of gold chip which was partially polymerised to show the comparison between plain gold surface and PPy modified gold surface